VOLUME 3 NUMBER 4 2025 ISSN 2958-0846
eISSN 2958-0854

AL-FARABI KAZAKH NATIONAL UNIVERSITY

# Journal of Problems in Computer Science and Information Technologies

№4 (3) 2025

Al-Farabi Kazakh National University

ISSN: 2958-0846; eISSN: 2958-0854


# Journal of Problems in Computer Science and Information Technologies №4 (3) 2025

03.02.2023 Registered with the Ministry of Information and Social Development of the Republic of Kazakhstan

№ KZ61VPY00064018

*The journal is published 4 times a year*
*(March, June, September, December).*



Signed to publishing 16.12.2025. Format 60x84/8. Offset paper.
Digital printing. Volume 9,75 printer's sheet.
Publishing house «Kazakh University»
www.read.kz Telephone: +7 (727) 3773330, fax: +7 (727) 3773344
Al-Farabi Kazakh National University KazNU, 71 Al-Farabi, 050040, Almaty
Printed in the printing office of the Publishing house «Kazakh University».

IRSTI 50.47.02 https://doi.org/10.26577/jpcsit202541

**Bekarys Nurzhaubaev[1], Nursultan Nyssanov[1], Alisher Batkuldin[1], Ali Myrzatay[1,2*], Murat Zhakenov[3]**

[1]Research and Innovation Center "CyberTech", Astana IT University, Astana, Kazakhstan
[2] "Digital government support center" RSE on the REM, Astana, Kazakhstan
[3] "Digital Heritage of Eurasia" LLP, Astana, Kazakhstan
*e-mail: mirzataitegiali@gmail.com

# NEW AUTONOMOUS SYSTEM FOR SPATIOTEMPORAL CLUSTERING AND VISUALIZATION OF DEVICE TRAJECTORIES IN FORENSIC INVESTIGATIONS

**Abstract.** This study presents «trajectory_analyzer», a Python-based system designed for the forensic analysis and visualization of geolocation data extracted from mobile devices. With the increasing volume of spatial-temporal data collected from sources such as GPS, Wi-Fi, and image metadata, forensic professionals face growing challenges in structuring and interpreting mobility patterns. Existing solutions often lack flexibility, require supervised models, or depend on proprietary infrastructure. Our approach applies an unsupervised DBSCAN-based trajectory clustering method, temporal ordering, and a real-time web map interface to reveal behavioral insights without the need for manual labeling or cloud services. Compared to prior research, the system improves spatial accuracy, source transparency, and visual clarity. Experimental results show that the proposed clustering method successfully identifies movement clusters and transitions while maintaining full offline operability. However, this improvement comes at the expense of more local storage because of embedded map tiles. Overall, this work provides a practical, understandable, and independent foundation for investigators dealing with unstructured multi-source geolocation data.

**Keywords:** Digital forensics, Geolocation analysis, Trajectory clustering, Unsupervised learning, DBSCAN, GPS tracking, Offline tools.

## 1. Introduction

Nowadays, the volume and detail of data on movement trajectories has experienced a sharp growth spurt due to the widespread use of GPS-enabled mobile devices. The use and need for this technology has also grown in the field of automotive systems and surveillance. The resulting volume of spatiotemporal data opens up new possibilities in digital forensics, especially in the field of reconstruction and visualization of human movements for investigative purposes. However, working with such a volume of geolocation data remains a methodological problem [15].

The main challenge lies in the lack of effective tools with intuitive and scalable visualization, especially for massive and heterogeneous trajectory datasets. Existing approaches, including vector field analysis [1], skeletal trajectory classification [2], and institutional tracking systems [3] that often require structured environments, rely on supervised learning, or lack flexibility for processing multi-source device data.

Existing forensic and trajectory analysis tools often rely on cloud infrastructures, lack offline reproducibility, and offer limited integration of heterogeneous sources.

Our system addresses these gaps by providing (1) an autonomous modular architecture that works without internet access, (2) a unified JSON schema preserving data provenance, and (3) transparent clustering and visualization workflows reproducible in local environments.

Additionally, difficulties arise due to the content of the input data itself. Trajectory logs are often out of time order, contain uneven sampling, and are generated from various sources such as GPS, Wi-Fi scanning, EXIF image metadata [17], or communication timestamps. Although the DBSCAN clustering algorithm has shown promising results in extracting spatial structure from such data [4], they still require fairly careful parameter settings and rarely integrate well with visualization tools. Moreover, preprocessing remains a necessary but underdeveloped component in many forensic pipelines [5].

To address these challenges, this study introduces trajectory_analyzer, a robust, offline, and open-source framework designed for forensic analysis of geolocation data. It accepts input from various sources, performs automatic preprocessing, and extracts meaningful behavioral patterns through geometric clustering and temporal segmentation– without requiring any training data or manual annotation.

The core research question guiding this work is:

How can interpretable and meaningful mobility patterns be identified from irregular, noisy, and heterogeneous geolocation data without the use of supervised learning or manual labeling?

Presented research hypothesis is that such patterns can be effectively inferred by combining density-based clustering with chronological ordering. This allows us to detect frequently visited or significant locations (clusters), reconstruct transitions or movement routes between them, and analyze the role each data source plays in shaping the spatial resolution of the trajectory.

By merging unsupervised analysis with interactive, map-based visualization, this study provides forensic specialists with an intuitive toolset to reconstruct and interpret complex movement behaviors. This work aims to bridge the gap between raw geolocation logs and human-readable insights, especially in contexts where cloud-based solutions are impractical or inadvisable.

The main contributions of this study are as follows:

i. A modular offline system that enables autonomous forensic trajectory analysis without reliance on cloud infrastructures.

ii. A unified JSON data schema with source provenance, providing consistent integration of heterogeneous geolocation sources.

iii. Use of geodesic distance (Haversine) with the DBSCAN algorithm, including a reproducible procedure for selecting the ε and minPts parameters.

iv. Dynamic source-level filters for interactive selection and comparison of trajectory subsets across multiple data origins.

v. A reproducible offline-tile HTML report that combines spatiotemporal clustering, visual analytics, and statistical summaries in a portable format.

## 2. Literature Review

In recent years, the amount of mobile geolocation data in the form of GPS traces, Wi-Fi scans, as well as EXIF data in images and videos, has increased exponentially. This multimodal spatial-temporal data is a valuable resource in digital forensics, as it allows investigators to track user activity, locate sites that a user has been to, as well as match temporal activity with digital artifacts. However, the recent emergence of a wide range of sensors as well as formats makes these sources inconsistent in terms of sample rate, accuracy, as well as origin.

Nevertheless, despite the recent ubiquity of cloud-based analytical tools, in forensic applications, they continue to be hampered by issues of privacy, sovereignty of data, as well as chain-of-custody issues. This is primarily since cloud-based analysis could involve transmitting forensic data over cloud servers that could contravene confidentiality laws as well as instances that could interrupt the chain of custody of digital evidence. As a result, the need to develop fully offline systems that are able to integrate diverse sources of geolocation information has emerged as a burning concern in today's forensics.

As noted in [6], trajectory clustering remains a core component of GPS data analysis. However, the high dimensionality of raw geolocation logs presents difficulties for computational efficiency and human interpretation. In response, the study proposed various dimensionality reduction techniques in conjunction with DBSCAN-based clustering to improve processing speed and visual clarity. Yet, this process often requires domain-specific tuning and lacks generalized parameter estimation techniques.

In complementary efforts, researchers in [7] and [8] emphasized the need for preprocessing pipelines to clean and normalize GPS data before modeling. These studies outlined common artifacts such as signal drift, duplicate records, and inconsistent sampling intervals. Their solutions included interpolation techniques and network-based correction models. While technically sound, they often assume access to high-quality or real-time datasets, limiting their forensic application where data may be sparse or corrupted.

In the context of behavioral analysis, the study in [8] reviewed trajectory tracking systems in autonomous vehicles. The article underscored the importance of accurate localization, anomaly detection, and route prediction – all of which are translatable to forensic movement reconstruction. Meanwhile, [9] introduced a hardware-integrated edge

computing GPS tracking platform. While promising for field deployments, its design prioritizes efficiency over flexibility, and its visual output remains rudimentary compared to forensic needs.

As outlined in [1], [11], and [14], the integration of geolocation and digital trace data into forensic cyber-physical investigations has become more prevalent. Their proposed tools focus on timeline reconstruction, correspondence analysis, and multi-source correlation. Although these interfaces support event sequencing, they are limited in their geospatial resolution and tend to lack interactive trajectory mapping features essential for field-level analysis.

Recent visualization frameworks have emerged in studies like [2] and [12], which applied vector field and density partitioning methods respectively. These offer macroscopic views of movement patterns in large datasets. However, their utility in forensic casework is restricted, as investigators often require micro-level insights – such as dwell times, visit frequencies, and source-specific behavior – which these approaches abstract away.

Studies [3] and [4] shifted the focus toward institutional and behavioral surveillance. The former evaluated crime scene classification based on skeletal trajectory analysis in surveillance settings, highlighting operational benefits and the potential for pattern recognition. The latter investigated staff perceptions and usability of GPS tagging in forensic psychiatric units, revealing gaps in data transparency and adaptability. Both studies confirm the growing reliance on geolocation data in controlled environments but underscore the absence of open systems for independent review or public domain research.

In [5], Yu et al. stressed the importance of pipeline robustness, advocating for modular preprocessing and clustering layers. Their work provided a foundation for reproducibility in GPS data workflows, though their system lacks integrated visualization or input flexibility. Similarly, [10] advanced stream-based clustering for trajectory segmentation, with real-time visualization capabilities. While scalable, such systems depend heavily on structured, continuous input – a luxury often unavailable in forensic scenarios.

Investigations into semantic and behavioral pattern extraction, such as those presented in [3], [11], and [13], move toward higher-level understanding of mobility and digital presence. These works proposed frameworks for detecting anomalies and identifying common routines across individuals. However, their reliance on annotated training data and machine learning infrastructure limits practical adoption in forensic workflows, which often operate with sparse and unlabeled datasets.

To summarize, past literature provides a diverse range of tools for geolocation analysis – from trajectory clustering and dimensionality reduction to stream processing and semantic modeling. However, many of these are either too abstract for forensic application, too rigid in data input requirements, or too opaque for field investigators. In our research, we address these gaps by combining the modularity of unsupervised clustering [6], the preprocessing awareness from [5], and the visual transparency from [1], [2]. Our trajectory_analyzer system offers an accessible, offline platform that includes clustering, timeline filtering, and map-based visualization in a single package inspired by principles introduced in [3] and [11].

## 3. Materials and Methods

### *3.1 Data Structure and Preprocessing*

This module is designed to work on devices with a large amount of memory (e.g., SSD, HDD based systems and mobile devices) and functions offline to ensure reproducibility, transparency of forensic examination results and security. It collects a wide range of spatial and temporal types of tags and a wide range of available data types: GPS logs from devices, metadata obtained from scanning Wi-Fi access points, EXIF geotags embedded in photos and videos, from call and chat history, and system timestamps.

For greater clarity of the logic of the module, a block diagram of the system was developed, shown as Figure 1, reflecting the main stages from loading input data to generating a report.

This diversified approach reflects the increasing complexity of digital movement data, with location-related data often scattered across multiple sensors and applications. As noted in a previous study [1], using GPS data exclusively can lead to incomplete and biased reconstructions of situations, especially indoors or in places with a difficult signal. Thus, our module is designed to support and work with combined data from multiple input streams, to support more comprehensive and detailed trajectory modeling.

After extracting the data from another module, the collected information is combined into a single

structured format. The data set is stored in a JSON object with the key "trajectory_points", where each record represents a discrete space-time observation. Each observation contains four main fields:

1. Timestamp in ISO 8601 format (e.g., "2023-12-10T12:42:00Z");

2. Coordinates specified as latitude and longitude in decimal degrees;

3. Source, a categorical label indicating the origin of the record (e.g.,” GPS", "Wi-Fi", "image", "received").

The implementation of recording incoming data was partially shown in Figure 2. This format is designed to handle heterogeneity while preserving provenance and temporal integrity two critical dimensions in forensic casework. Sensor provenance allows analysts to filter or weigh observations by reliability, while accurate temporal ordering enables timeline reconstruction, path tracing, and behavioral segmentation.

Figure 2 illustrates the required structure and composition of the input data in JSON format used by the system. Each record follows the schema described above, including the three mandatory attributes: timestamp, coordinates, and source, ensuring interoperability across heterogeneous inputs. All coordinates are expressed in the WGS-84 coordinate reference system. The example also demonstrates how the system parses these records through the data loading routine, where each entry is converted into Python objects for further processing.

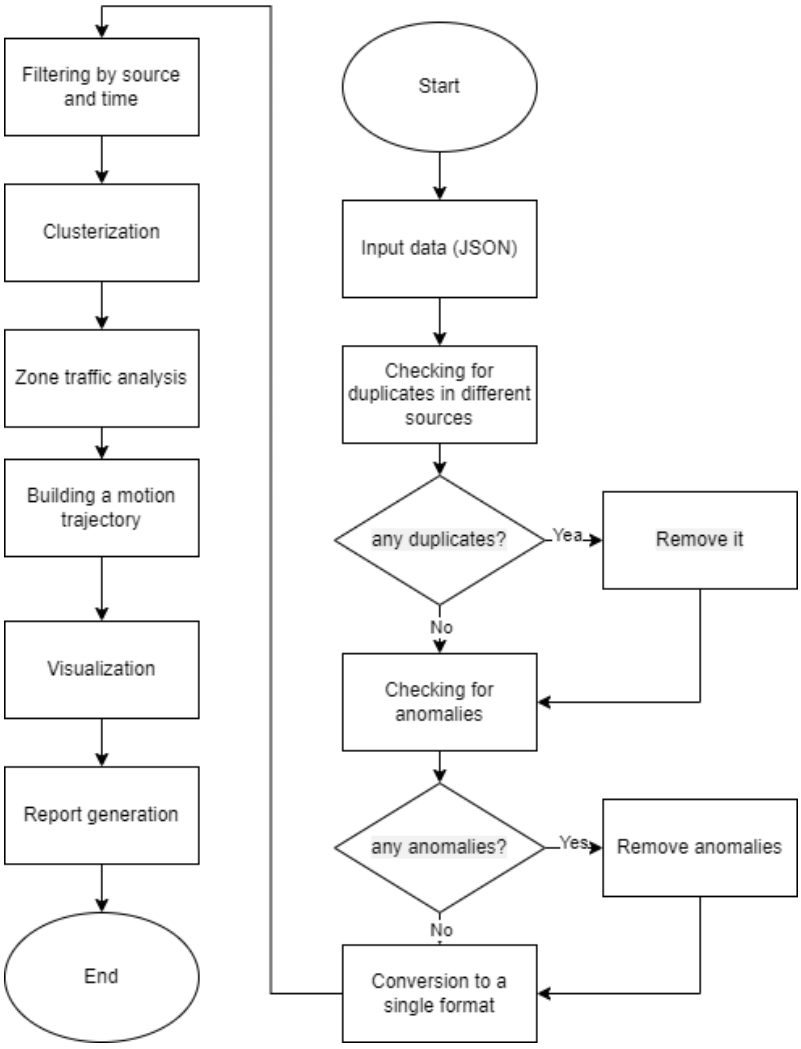


**Figure 1 –** Block diagram of the system operation

```
import json
from datetime import datetime
import numpy as np
from sklearn.cluster import DBSCAN

def serve_offline_map(data):
    with open("static/offline_map.html", "r", encoding="utf-8") as f:
        html = f.read()

    points_json = json.dumps([
        {
            "lat": p["coordinates"]["lat"],
            "lon": p["coordinates"]["lon"],
            "timestamp": p["timestamp"],
            "source": p.get("source", "UNKNOWN").upper()
        }
        for p in data["trajectory_points"]
    ])
```

**Figure 2 –** Required type of incoming data in Json format

To prepare the dataset for clustering and trajectory analysis, a multi-step preprocessing pipeline is implemented. This step is crucial to clean, normalize, and structure the data in a form that allows consistent mathematical treatment. As emphasized by Petrescu et al. [2], trajectory datasets derived from real devices are often noisy, irregularly sampled, and may include corrupted or semantically redundant points.

Each entry is validated individually. Points with missing values, zeroed coordinates, or unreasonable accuracy values (e.g., over 10,000 meters) are removed. This ensures that subsequent calculations, especially those involving distance or clustering, are not distorted by invalid data.

The dataset is then chronologically sorted based on timestamps. Since timestamps are initially provided in ISO 8601 human-readable format, they are converted into Unix epoch time (the number of seconds since 1 January 1970 UTC). This conversion enables straightforward computation of time differences and alignment of asynchronous observations from multiple sources.

Where needed (especially during distance calculations), coordinates are converted from degrees to radians, enabling trigonometric operations such as those used in the haversine formula. This ensures the geospatial integrity of computed values like step distances, cluster radii, and overall route length.

The outcome of this preprocessing stage is a temporally ordered and spatially consistent sequence of geolocation points. These cleaned and normalized data are then passed to the clustering module, where they serve as the foundation for route reconstruction and behavior analysis.

This structure is modeled mathematically as a sequence of observations:

$$D = \{d_i = (t_i, x_i = (\varphi_i, \lambda_i), a_i, s_i)\}_{t=1}^{n} \quad (1)$$

Where:

- $t_i \in$ Ris a time value (after conversion to Unix timestamp),
- $x_i \in R^2$ is the spatial coordinate pair: latitude and longitude,
- $a_i \in R \geq 0$ is the reported accuracy,
- $s_i \in S$ is a label from a finite set of known source types.

Unlike traditional datasets with fixed intervals and clean annotations, this real-world format embraces irregular sampling, missing intervals, and varying source trustworthiness. However, it is precisely this challenge that the proposed framework is designed to overcome. By integrating rigorous preprocessing with unsupervised analysis techniques designed for resilience to noise, the system allows forensic experts to make sense of inconsistent yet highly informative data streams– without the need for manual annotation or supervised training.

*3.2 Distance Calculation (Haversine Formula) and DBSCAN Clustering*

All spatial comparisons are done using the haversine formula, which calculates the great-circle distance between two points on Earth. Coordinates are expressed in WGS-84

Given two locations:

$$x_1=(\phi_1,\lambda_1),\ x_2=(\phi_2,\lambda_2) \tag{2}$$

the spherical distance in meters is:

$$d=2r\cdot\arcsin\left(\sqrt{\left(\sin^2\left(\frac{\Delta\varphi}{2}\right)+\cos(\phi_1)\cos(\varphi_2)\sin^2\left(\frac{\Delta\lambda}{2}\right)\right)}\right) \tag{3}$$

Where:

1. $-\Delta\phi=\phi_2-\phi_1$ ,
2. $-\Delta\lambda=\lambda_2-\lambda_1$ ,
3. $-r$=6,371,000 *meters*.

This metric is used for clustering and route calculations.

The *DBSCAN algorithm* identifies clusters of spatially dense points,$C_j\subseteq D$. It has two parameters:

- ε: maximum distance to be considered part of a neighborhood (typically 30–50 meters),
- minPts: the minimum number of points to form a dense cluster (typically 3–5).

A point p is a core point if:

$$|N_\varepsilon(p)|\geq \min Pts, N_\varepsilon(p)=q\in D|d(p,q)\leq\varepsilon \tag{4}$$

The algorithm constructs clusters by linking core points and their reachable neighbors.

**In figure 3 shows** Clustered locations visualized on a map using the DBSCAN algorithm (ε = 50 m, minPts = 3). The visualization covers the observation period from **December 7, 2021 to July 16, 2025**, showing trajectory points derived from **image (JPG)** and **video (MP4)** metadata. All coordinates are expressed in the **WGS-84 (EPSG:4326)** coordinate reference system, and distances are computed geodesically using the haversine formula. Clustered zones are highlighted as **red circular markers**, while isolated trajectory points are shown in neutral tones to indicate noise or transitional movement.This figure demonstrates how spatially dense locations are detected and grouped by DBSCAN, forming clusters annotated with centroid coordinates, visit counts, and time intervals

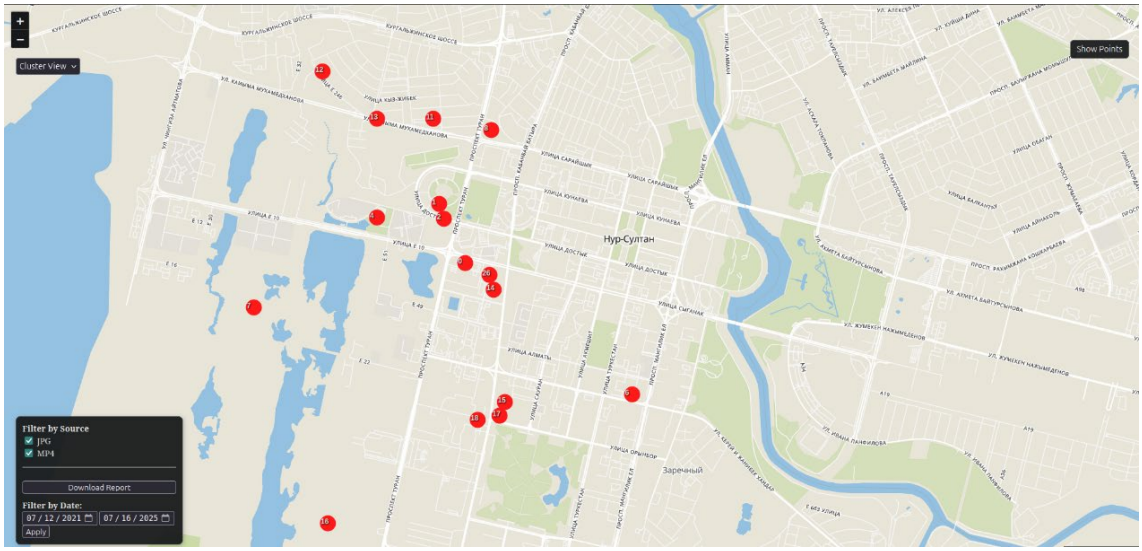


**Figure 3 –** Clustered locations visualized on map using DBSCAN.

Each resulting cluster $C_j$ is annotated with:
- Centroid:

$$\mu_j = \frac{1}{|C_j|} \sum_{x_i \in C_j} x_i \quad (5)$$

- Time interval:

$$T_j = [\min(t_i), \max(t_i)], d_i \in C_j \quad (6)$$

- Visit count: $N_j = |C_j|$,
- Source set: $S_j = \{ s_i \mid d_i \in C_j \}$

*3.3 The reconstruction of the route, filtering and visualization tools*

The trajectory $T$ is the ordered list of coordinates:

$$T = x_{(1)}, x_{(2)}, \ldots, x_{(n)} \quad (7)$$

The route is defined as:

$$Route = (x_{(i)}, x_{(i+1)}) \mid 1 \le i < n \quad (8)$$

This is visualized on the map as a polyline. Interpolation is currently not applied. From the raw data set, a Trajectory is recreated reflecting the exact sampling rate and continuity of movement.

Then we are going to filtering sources: Every point has a category-based source label. During visualization, the user can apply a filter, $S' \subseteq S$ to create a new dataset:

$$D_{S'} = d_i \in D \mid s_i \in S' \quad (9)$$

In Figure 4, the first process of grouping JSON data is highlighted. This process shows how the system derives the latitude and longitude values from the input data, which are then transformed from meters to radians in accordance with the WGS-84 reference system. By this means, the algorithm DBSCAN is executed with epsilon set at 50 meters and the value of minPts. Every identified group is marked with a relevant ID, center, and count values that are stored in a JSON summary.

```
coords = np.array([[p["coordinates"]["lat"], p["coordinates"]["lon"]] for p in data["trajectory_points"]])
coords_rad = np.radians(coords)

db = DBSCAN(eps=50 / 6371000, min_samples=1, metric='haversine').fit(coords_rad)
labels = db.labels_

cluster_summary = []
for label in set(labels):
    pts = coords[labels == label]
    centroid = pts.mean(axis=0)
    cluster_summary.append({
        "id": int(label) + 1,
        "lat": float(centroid[0]),
        "lon": float(centroid[1]),
        "visits": len(pts)
    })

coords = [(p["coordinates"]["lat"], p["coordinates"]["lon"]) for p in data["trajectory_points"]]
cluster_data = generate_cluster_data(coords)
cluster_json = json.dumps(cluster_data)
```

**Figure 4 –** The initial process of clustering json data

Then all clusters and trajectory lines are recalculated using only the filtered set. Using only filtered points allows you to selectively analyze GPS-only data, indoor data (for example, Wi-Fi), or image-based sources. Filtering is applied dynamically, automatically updating visual changes on the map.

*3.4 Visualization Interface and Offline Map Rendering*

The final stage of the trajectory_analyzer system involves the generation of a fully interactive, offline-capable geolocation visualization interface. Unlike other existing systems based on online mapping services, our software solution creates a

dynamic HTML-based report that allows you to study the user's status when moving in real time without having to use any external servers, without network access or third-party API integrations.

The visual output consists of an HTML file (report.html) related to JavaScript and CSS user resources (report_template.html report_style.css) and local map sheets. The latter provides complete offline operation, eliminating dependence on external maps such as OpenStreetMap or Mapbox. The application weighs more than typical cloud-based visualizers due to the embedded tile storage, but offers a practical trade-off in the context of digital forensics, where data sovereignty, stability, and network isolation are often essential.

The interactive map interface itself is not rendered using Folium or Leaflet directly; rather, the system uses a custom-built frontend. Leaflet is utilized only for low-level map layer handling, such as zooming and tile display. All higher-order functionality–including cluster rendering, filter toggles, UI panels, and event responses–is implemented manually using vanilla JavaScript and custom CSS, providing full control over the logic and appearance of the visualization.

After filtering the input data completely, each point of movement is displayed in chronological order, drawing a continuous trajectory of movement. Color coding is applied to the type of data shown, whether it is a route, trajectory, blue, as shown in Figure 5. Clustered zones, red. This allows analysts to immediately distinguish between categories of data. Individual points on the route are interactive. When you hover the mouse over them, pop-up windows appear displaying the point's index, source, timestamp, and the number of visits to that location. Unlike many clustering systems that visualize only centroids or aggregate data, this implementation emphasizes granularity, exposing every recorded stop to detailed inspection.

In parallel, clustered locations–calculated through DBSCAN as described in earlier sections–are rendered using larger custom markers, visually distinguishing them from transient path points. These clusters include summary pop-ups detailing the average coordinates (centroid), the time span during which the cluster was active, and the number of constituent records. This dual-layer view (trajectory path + static clusters) allows the analyst to quickly separate stationary behavior (e.g., place visits) from transitional motion (e.g., commuting or travel).

A collapsible side panel is integrated into the map interface, providing investigators with a interactive filtering mechanism. Through intuitive checkboxes and sliders, the user can toggle visibility of specific data sources or limit the visualized route to a selected time interval. These controls operate in real time and require no page reloads or backend reprocessing. This interactivity allows analysts to test hypotheses, isolate anomalies, or correlate movement patterns with other data (e.g., crime timestamps, device logs).

Below the map, a set of visual summaries is presented in the form of interactive charts and diagrams. These include:

- A pie chart of the most frequently visited locations (by cluster density),
- A bar chart of the last N visited places,
- A chronological list of all locations in order, with metadata including time, coordinates, and source.

These visualizations are automatically generated during the report creation process and provide compact insight into behavioral tendencies, such as routine places and movement regularity. All diagrams are embedded within the HTML file and rendered with client-side JavaScript libraries, ensuring they remain functional even in isolated environments.

Finally, a dedicated button is available for exporting a full forensic report as a compressed .zip archive (report.zip). This export contains:

- The full visualization HTML,
- All embedded resources (CSS, JS, map tiles),
- A JSON summary of the clustered and raw data,
- A preformatted PDF-style document with detailed tables of all recorded points, sources, and cluster summaries.

This modular reporting format ensures accuracy, convenience and transparency in accordance with the best practices of digital forensics. The non-overloaded interface design focuses on the convenience of searching and working with it quickly. The report provides high-resolution spatial detail, provides a temporal context, and shows the complete chronological sequence of the vehicle's movement. all this works without compromising security, because the entire system is independent of Internet services.

Additionally, the report has two chart variations. The first diagram shows the top visited locations over a total period (75 m per pixel tile resolution) of time and is shown below as Figure 5. The second diagram is designed to view the most recently visited locations and is shown in Figure 6.

Thus, the trajectory_analyzer visualization layer transforms the raw geolocation data into a user-friendly, reliable interface from the point of view of forensic examination. With offline functionality, interpretability, and interactivity, it serves as both a diagnostic tool and a formal reporting mechanism in investigative workflows.

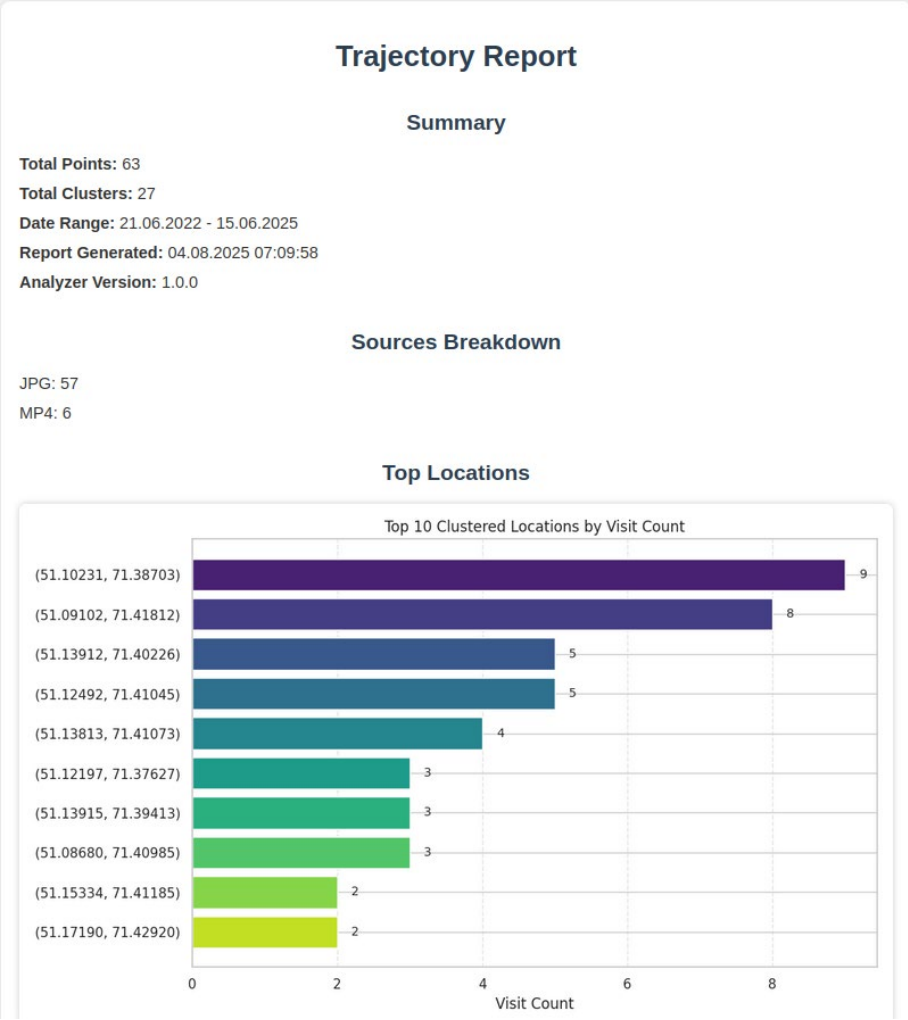


**Figure 5 –** Most visited locations (total)

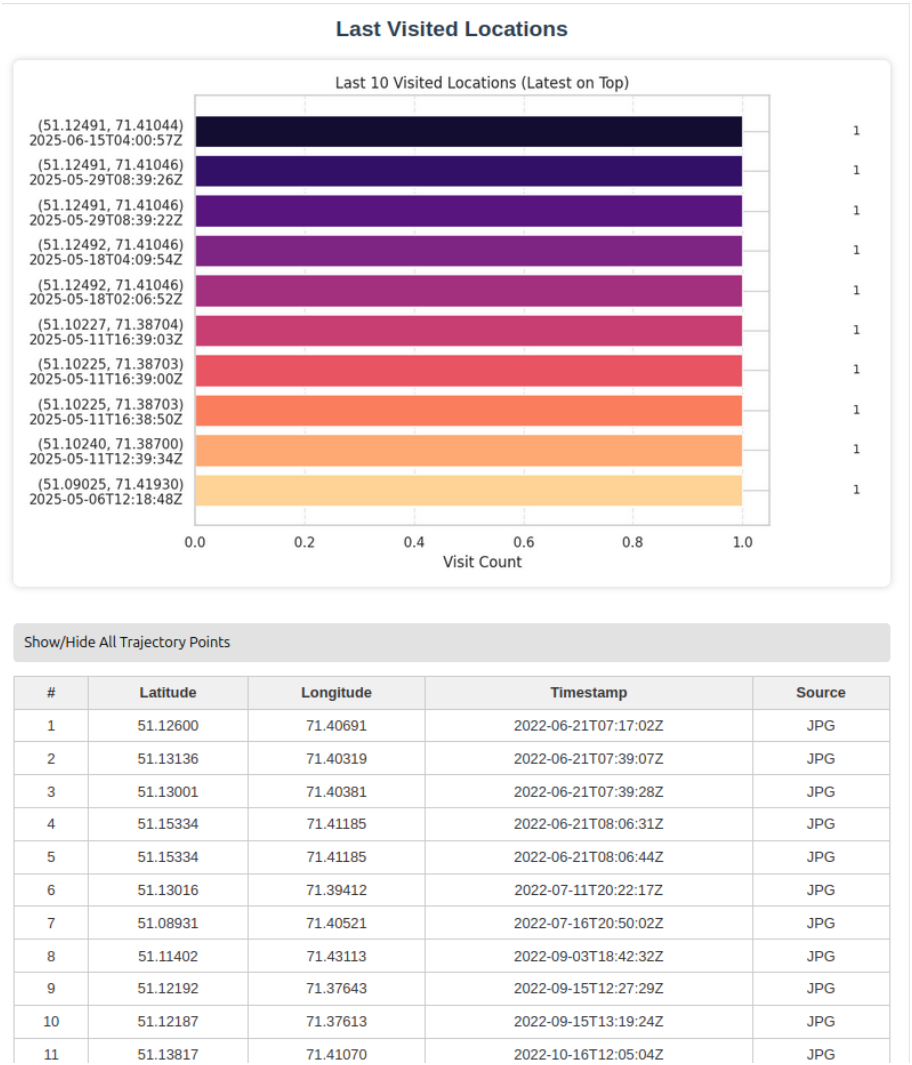


| # | Latitude | Longitude | Timestamp | Source |
|---|---|---|---|---|
| 1 | 51.12600 | 71.40691 | 2022-06-21T07:17:02Z | JPG |
| 2 | 51.13136 | 71.40319 | 2022-06-21T07:39:07Z | JPG |
| 3 | 51.13001 | 71.40381 | 2022-06-21T07:39:28Z | JPG |
| 4 | 51.15334 | 71.41185 | 2022-06-21T08:06:31Z | JPG |
| 5 | 51.15334 | 71.41185 | 2022-06-21T08:06:44Z | JPG |
| 6 | 51.13016 | 71.39412 | 2022-07-11T20:22:17Z | JPG |
| 7 | 51.08931 | 71.40521 | 2022-07-16T20:50:02Z | JPG |
| 8 | 51.11402 | 71.43113 | 2022-09-03T18:42:32Z | JPG |
| 9 | 51.12192 | 71.37643 | 2022-09-15T12:27:29Z | JPG |
| 10 | 51.12187 | 71.37613 | 2022-09-15T13:19:24Z | JPG |
| 11 | 51.13817 | 71.41070 | 2022-10-16T12:05:04Z | JPG |

**Figure 6 –** Recent visits by location.

## 4. Results and Discussion

The developed system successfully processed multi-source geolocation data and visualized user movement patterns, including route reconstruction and clustered visit locations. Compared to previous DBSCAN-based frameworks [5], the integration of preprocessing steps and source-aware filtering appears to improve the clarity and reliability of clustering outcomes.

On Figure 7, shows the complete trajectory derived from raw multi-source data, plotted in chronological order within the WGS-84 coordinate system. Each point represents an individual recorded location, while the continuous blue line visualizes the sequential path of movement over the full observation period (December 7, 2021 – July 16, 2025). This figure demonstrates the system's ability to reproduce detailed movement routes without clustering, preserving temporal accuracy and source integrity.

In contrast to semi-supervised pipelines described in [6][7], the fully offline nature of our tool enhances responsiveness and usability, especially in privacy-sensitive environments. Visualization is rendered nearly instantaneously for small and medium datasets, supporting quick interpretation during local forensic investigations.

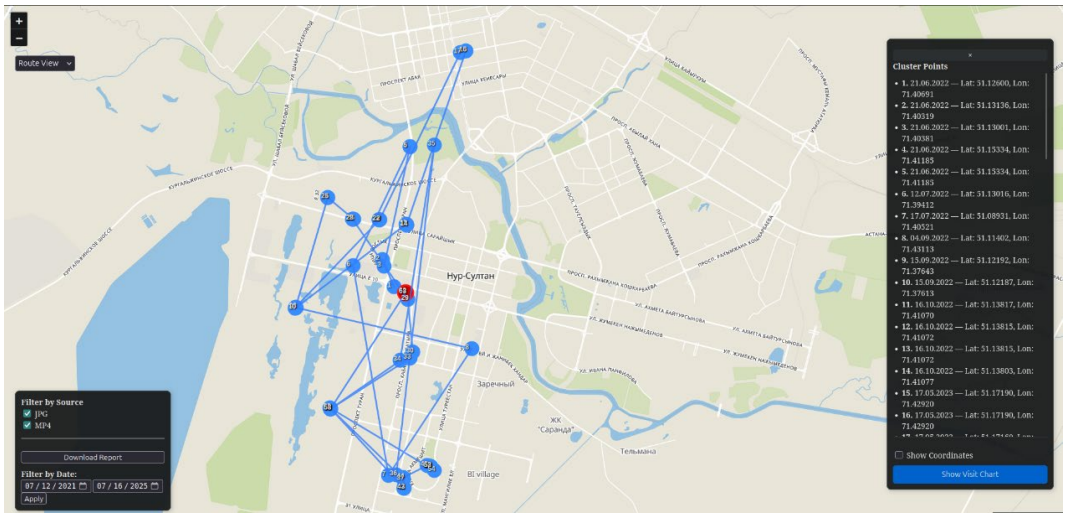


**Figure 7 –** User movement route reconstructed from raw data (shown on an interactive map).

This approach aligns well with needs in forensic practice, where fast access, transparency, and data locality are often prioritized over dependence on remote APIs or web-based solutions. However, the system's local map rendering and multiple visual layers may result in greater disk usage than lightweight alternatives [3][9] and [16].

Overall, trajectory_analyzer demonstrates a practical and interpretable method for digital forensic mobility analysis, with strong applicability in settings that require secure and autonomous data processing.

## Conclusion

This study introduced *trajectory_analyzer*, a modular and fully offline system for reconstructing and visualizing geolocation data in forensic investigations. The framework integrates key technical components–including temporal preprocessing, spherical distance computation using the Haversine formula, and unsupervised clustering via DBSCAN–to extract meaningful behavioral patterns from unstructured, multi-source data.

A major novelty of the system is its **combined approach**, which unites:

- real unsupervised clustering,
- spherical distance metrics,
- source-aware dynamic recomputation,

and a fully offline, interactive visualization layer.

This design enables the tool to operate independently of cloud services or training datasets, making it ideal for use in sensitive forensic contexts where **data privacy, reproducibility, and speed** are paramount. Investigators can explore clusters, trace user routes, and analyze the role of different data sources–all within an interpretable and responsive interface.

Despite its advantages in speed, the system's reliance on local map assets increases storage requirements, which may limit portability in some scenarios.

Future work will focus on several directions:

1. Automating the selection of DBSCAN parameters (ε and minPts) for different dataset scales.
2. Optimizing the visual layers footprint through compressed or vector-based tile storage.
3. Extending support for additional input and export formats.

Overall, *trajectory_analyzer* delivers a practical, transparent, and extensible solution for geolocation analysis, one that aligns with the needs of modern digital forensics for **modular, offline, and interpretable** tools.

## Funding

This study was carried out with the financial support of the Committee of Science of the Ministry of Science and Higher Education of the Republic of Kazakhstan under Contract №388/PTF-24-26 dated 01.10.2024 under the scientific project IRN

BR24993232 “Development of innovative technologies for conducting digital forensic investigations using intelligent software-hardware complexes”.

**Author Contributions**

Conceptualization, N.N., and A.B.; Methodology L.R., M.Zh.; Software, N.N., B.N., and A.B.; Validation, N.N., and B.N.; Formal Analysis, N.N., and B.N.; Investigation, A.B.; Resources, N.N., and B.N.; Data Curation, N.N., and A.B.; Writing – Original Draft Preparation, B.N.; Writing – Review & Editing, B.N. and A.M.; Visualization, B.N.; Supervision, A.M.; Project Administration, N.N.; Funding Acquisition, N.N.

**Conflicts of Interest**

The authors declare no conflict of interest.

**References**

1. Macedo, I., Wanous, S., Oliveira, N., Sousa, O., & Praça, I. (2021, March). A tool to support the investigation and visualization of cyber and/or physical incidents. In World Conference on Information Systems and Technologies (pp. 130-140). Cham: Springer International Publishing.

2. Li, A., Xu, Z., Zhang, J., Li, T., Cheng, X., & Hu, C. (2023). A Vector Field Visualization Method for Trajectory Big Data. *ISPRS International Journal of Geo-Information*, 12(10), 398.

3. Matei, A. D., Talavera, E., & Aghaei, M. (2025). Crime scene classification from skeletal trajectory analysis in surveillance settings. *Engineering Applications of Artificial Intelligence*, *141*, 109800.

4. Ashworth, G., Waldron, G., & Kahai, B. (2025). A service evaluation exploring staff perceptions about the use and impact of electronic monitoring (GPS tracking) in a medium secure forensic psychiatric unit. *The Journal of Forensic Psychiatry & Psychology*, 1-18.

5. Yu, X., Long, W., Li, Y., Gao, L., & Shi, X. (2022). Trajectory dimensionality reduction and hyperparameter settings of DBSCAN for trajectory clustering. *IET Intelligent Transport Systems*, *16*(5), 691-710.

6. Abruzzo, A., Ferrante, M., & De Cantis, S. (2021). A pre-processing and network analysis of GPS tracking data. *Spatial Economic Analysis*, *16*(2), 217-240.

7. Sadeghian, P., Håkansson, J., & Zhao, X. (2021). Review and evaluation of methods in transport mode detection based on GPS tracking data. *Journal of Traffic and Transportation Engineering (English Edition)*, *8*(4), 467-482.

8. Li, L., Li, J., & Zhang, S. (2021). State-of-the-art trajectory tracking of autonomous vehicles. *Mechanical Sciences*, *12*(1), 419-432.

9. Klymenko, M. V., & Striuk, A. M. (2023). Design and implementation of an edge computing-based GPS tracking system. *Journal of Edge Computing*, *2*(2), 175-189.

10. Reyes, G., Lanzarini, L., Estrebou, C., & Bariviera, A. (2022, October). Data Stream Processing Method for Clustering of Trajectories. In *International Conference on Technologies and Innovation* (pp. 151-163). Cham: Springer International Publishing.

11. Huang, W., & Wang, L. (2022). Towards big data behavioral analysis: rethinking GPS trajectory mining approaches from geographic, semantic, and quantitative perspectives. *Architectural Intelligence*, *1*(1), 7.

12. Wei, B., Zhang, J., Hu, C., & Wen, Z. (2023). A Clustering Visualization Method for Density Partitioning of Trajectory Big Data Based on Multi-Level Time Encoding. *Applied Sciences*, *13*(19), 10714.

13. Idrissova, M., Kim, S., Amirgaliyev, B., Yedilkhan, D., & Rzayeva, L. (2025). Digital footprints: clustering browser history for user profiling using machine learning. *Journal of Problems in Computer Science and Information Technologies*, *3*(2), 16-28.

14. Rzayeva, L., D. Pogolovkin, & I. Shaya. (2025). Development of a correspondence analysis service using artificial intelligence technology and a vector database for digital forensics. *International journal of information and communication technologies*, *6*(1), 201–225.

15. Mirza, M. M., & Karabiyik, U. (2021, October). Enhancing IP address geocoding, geolocating and visualization for digital forensics. In *2021 International Symposium on Networks, Computers and Communications (ISNCC)* (pp. 1-7). IEEE.

16. Pace, L. R., Salmon, L. A., Bowen, C. J., Baggili, I., & Richard III, G. G. (2023). Every step you take, I'll be tracking you: Forensic analysis of the tile tracker application. *Forensic science international: digital investigation*, *45*, 301559.

17. Daraghmi, E., & Hamoudi, A. Mobile Forensics: Extracting Geo-Location Data from Photos on Android Smartphones. *vol*, *9*, 1915-1921.

***Information About Authors***

*Bekarys Nurzhaubaev is a bachelor’s student at Astana IT University and a junior software developer at the Research and Innovation Center (RIC) “CyberTech” at Astana IT University. His research interests include machine learning, neural networks, and the development of systems integrating machine learning and neural network algorithms. OrcID: 0009-0008-4683-9350*

*Nursultan Nyssanov is a master’s student at Astana IT University, a software developer, and a researcher at the Research and Innovation Center (RIC) “CyberTech” at Astana IT University. His research interests include machine learning, neural networks, the development of systems integrating machine learning and neural network algorithms, and digital forensics. OrcID: 0009-0002-8128-0595.*

*Alisher Batkuldin holds an M.Sc. in Electrical and Computer Engineering from Nazarbayev University. He is a software developer and researcher at the Research and Innovation Center (RIC) "CyberTech" at Astana IT University. His research interests include machine learning, neural networks, the development of systems integrating machine learning and neural network algorithms, and digital forensics. OrcID: 0009-0004-2097-5419.*

*Ali Myrzatay holds a Ph.D. in Automation and Control from L.N. Gumilyov Eurasian National University. He works at the "Digital Government Support Center" RSE on the REM, Astana, Kazakhstan, as a project manager and as a researcher at the Research and Innovation Center (RIC) "CyberTech" at Astana IT University. His research interests include machine learning, neural networks, and the development of systems integrating machine learning and neural network algorithms. OrcID: 0000-0002-5339-2437.*

*Murat Zhakenov is a Candidate of Technical Sciences and works at "Digital Heritage of Eurasia" LLP, Astana, Kazakhstan. His research interests include machine learning and neural networks. OrcID: 0009-0005-9672-4365.*

*Submission received: 08 August, 2025.*
*Revised: 19 November, 2025.*
*Accepted: 19 November, 2025.*

IRSTI 28.23.15 https://doi.org/10.26577/jpcsit202542

**Nurdaulet Tasmurzayev[1*], Dinara Turmakhanbet[1], Adilet Kakharov[1], Mukhamejan Aitkazin[1], Aliya Baidauletova[1], Mergul Kozhamberdiyeva[1]**

Al-Farabi Kazakh National University, Almaty, Kazakhstan
*e-mail: tasmurzayev.n@gmail.com

# CVD PREDICTION FROM HRV DERIVED FROM WEARABLE PPG

**Abstract.** Cardiovascular disease is the leading global cause of death; ischemic heart disease (IHD) is its most common and lethal form, motivating scalable, non-invasive screening. We tested whether a single 60-minute photoplethysmography (PPG) recording from the Zhurek fingertip wearable can distinguish healthy autonomic control from IHD-related dysregulation. Agreement with a three-lead Holter reference was clinically acceptable (HR −0.601 bpm; SDNN +33.1 ms; RMSSD −4.8 ms). Forty hour-long sessions were analyzed (20 healthy, 18–22 years; 20 angiography-confirmed IHD) using eight HRV/demographic features. Mann–Whitney tests showed significant differences for SDNN, LF, HF, Max_HR, BMI, and age ($p < 0.05$), and a two-component PCA (49.5% variance) separated cohorts without labels. SHAP for a CatBoost model highlighted LF and age as strongest positive contributors and HF as protective. Thus, one-hour PPG preserves diagnostically useful autonomic signatures, enabling ~24× shorter monitoring than Holter and supporting scalable ambulatory IHD risk stratification.

**Keywords:** CVD, IHD, HRV, Machine learning, PPG, wearable sensor.

## 1. Introduction

Cardiovascular diseases (CVDs) remain the top cause of mortality globally. WHO estimates indicate that in 2019, 17.9 million people died from CVDs–32% of all deaths–with heart attacks and strokes accounting for 85% of these losses. Among the 17 million premature deaths (under 70) from non-communicable diseases that year, 38% were attributable to CVDs [1]. Ischemic heart disease (IHD) is among the most prevalent CVD entities and a principal driver of mortality [2]. In Kazakhstan, 2022 statistics show circulatory diseases as the most widespread among adults (3,962.5 per 100,000), of which IHD contributes 560.7 per 100,000, underscoring its substantial share within cardiovascular morbidity [3].

IHD imposes a heavy clinical and economic burden, substantially elevating both mortality and morbidity worldwide [4]. Coronary artery disease (CAD)–predominantly a consequence of atherosclerosis–is the leading cause of IHD and culminates in myocardial ischemia. The core pathophysiologic mechanism is obstructive atherosclerosis of the coronary vessels, which compromises myocardial perfusion [5]. In view of rising pressure on health systems, there is a pressing need for early, non-invasive diagnostic strategies that can flag IHD before irreversible outcomes such as myocardial infarction or chronic heart failure (CHF) occur [6].

Heart rate variability (HRV)–the beat-to-beat fluctuation in cardiac cycle duration [7]–is a non-invasive rhythm-based marker that yields clinically useful information about overall physiological status [8]. HRV indexes the heart's adaptive capacity and an individual's ability to respond to environmental challenges via compensatory mechanisms [9]. It is shaped by autonomic inputs–particularly parasympathetic tone–while reflecting the joint activity of sympathetic and parasympathetic branches. Depressed HRV has been linked to adverse endpoints including myocardial infarction, progression of atherosclerosis, heart failure, IHD, and sudden cardiac death [10]. Accordingly, HRV analysis is central to evaluating autonomic nervous system (ANS) function [11]. Conventional coronary assessment tools are frequently costly, invasive, and suboptimal for timely detection of evolving ischemia [12]. Although diagnostic angiography is among the most definitive techniques for identifying cardiac abnormalities, it carries high expense, potential complications, and requires specialized expertise; traditional

workflows can be time-intensive, error-prone, and resource-heavy, risking misclassification and higher costs [13]. This motivates a shift toward reliable, non-invasive, early detection methods–HRV-based approaches being a prime candidate.

CVDs continue to dominate global morbidity and mortality statistics, reinforcing the importance of early identification in high-risk groups and the development of effective preventive and therapeutic interventions. Recent efforts emphasize multifactorial risk models that fuse physiological metrics, lifestyle variables, and medical history to improve predictive performance and enable personalization [14]. HRV–the variability in RR (NN) intervals–is a widely used non-invasive indicator of cardiovascular status [15]. In IHD, reductions in time-domain indices (SDNN, RMSSD, pNN50) and alterations in the LF/HF ratio derived from frequency-domain analysis (FFT of RR intervals) associate with myocardial injury and higher adverse-event risk; an LF/HF imbalance signals disrupted autonomic control during ischemic episodes. This review consolidates key HRV features and highlights their clinical utility in monitoring and managing IHD [6], [16].

Patients with IHD and arrhythmias generally exhibit lower HRV than healthy controls. Time-domain measures such as SDNN, SDANN, RMSSD, pNN50, and the triangular index, together with nonlinear descriptors (α, α1, α2, SD1, SD2, Approximate Entropy, Sample Entropy), are markedly diminished in these populations [17]. These patterns reflect impaired autonomic regulation and support the role of HRV analytics in tracking cardiac function and disease trajectory in IHD [15].

In atrial fibrillation (AF), HRV–defined as fluctuations in ventricular response intervals–is not random; its nonlinear structure, especially multiscale entropy (MSE), carries clinical meaning. Numerous studies link HRV parameters to ischemic stroke risk in AF, and MSE of HRV has been proposed as a predictor in this group [18]. Notably, higher sample-entropy values at specific time scales from 24-hour Holter data correlate with increased stroke likelihood in AF patients without prior stroke. HRV has also been applied to assess hemispheric involvement in acute ischemic stroke (AIS): sample entropy was significantly higher in left-hemispheric than right-hemispheric strokes, implying reduced HRV complexity (and possibly heightened sympathetic drive) on the right; these differences persisted in daytime segments, suggesting value for lesion lateralization [19]. Beyond diagnosis, HRV-based indices have been explored to forecast short-term outcomes in the acute phase of ischemic stroke [20].

Alongside HRV, electrocardiographic alternans (ECGA) provides a promising non-invasive electrophysiological marker of ischemia and arrhythmic risk. ECGA encompasses T-wave (TWA), QRS (QRSA), and P-wave alternans (PWA) derived from standard ECG. Evidence from the STAFF III study – using controlled balloon occlusion – showed time-ordered increases in alternans magnitude measured by correlation methods: PWA within the first minute, QRSA by the second, and TWA by the third minute of coronary occlusion [21]. ECGA is under active evaluation for IHD risk stratification [20]. Although TWA has been examined in IHD and heart failure, heterogeneity in protocols and analytics complicates interpretation [21]. Some reports suggest that combining TWA with HRV may enhance detection of chronic heart failure progression; however, its prognostic role in IHD requires further validation. Recent work argues for concurrent assessment of TWA, QRSA, and PWA to maximize diagnostic yield [22].

Beyond physiology, genetic markers–particularly single-nucleotide polymorphisms (SNPs) – increasingly complement traditional risk factors. Panels that integrate SNPs with clinical variables (e.g., SCORE, age, angiography) have achieved diagnostic accuracies up to 93% [23]. Candidate genes implicated in inflammation, lipid metabolism, and thrombosis further improve CVD risk prediction, offering value independent of standard predictors and showing special relevance in type 2 diabetes, where shared metabolic pathways link to cardiovascular risk [24]. Incorporating genetics into clinical models advances individualized prevention and care. ECG has long been the mainstay for cardiac assessment, capturing electrical activity via surface electrodes [25]. Yet the last decade's push for continuous, user-friendly, and affordable monitoring has accelerated exploration of alternatives [26]. Photoplethysmography (PPG) stands out for simple hardware and seamless integration into consumer devices, providing a substantially cheaper and more convenient path to continuous monitoring in both clinical and everyday contexts [27].

While highly accurate, conventional ECG systems demand clinical oversight, careful electrode placement, and periodic calibration–factors that raise costs and reduce convenience [25]. Advances in microelectronics have miniaturized PPG sensors for wearables (wrist, watch, phone, in-ear), broadening access to continuous cardiovascular tracking

[28]. Coupled with wireless data transfer and cloud-based analytics, PPG offers a distinctive blend of affordability, portability, and usability that traditional ECG cannot easily match [29].

Machine-learning approaches are highly effective for detecting IHD-related anomalies. Head-to-head evaluations of support vector machines, artificial neural networks, and deep models report accuracies above 90% when robust preprocessing and feature selection are applied [30]. Unsupervised routines–most notably k-means–are used to flag outliers in cardiac datasets, which in turn improves the performance of downstream supervised classifiers [31]. On ECG signals, deep networks learn discriminative representations that separate normal from ischemic patterns with near-perfect performance [32]. In imaging, deep learning applied to non-contrast CT, echocardiography, and CT angiography builds hierarchical encodings of coronary anatomy and myocardial motion, capturing subtle lumen-caliber and wall-motion abnormalities consistent with ischemia [33], [34]. Representation-learning schemes such as autoencoders and encoder–decoder frameworks further compress high-dimensional data into interpretable latent features [34]. For label-sparse or imbalanced cohorts, unsupervised anomaly detection segments by similarity and marks deviants as anomalies [31], while synthetic oversampling (SMOTE) rebalances classes and often boosts SVM performance [30]. ECG-based studies frequently exceed 98% accuracy in distinguishing IHD or myocardial infarction from healthy controls by exploiting minute ST-segment deviations and QRS-duration changes–canonical ischemic markers [32]. Hybrid architectures that combine convolutional and recurrent layers enhance results by jointly modeling spatial morphology and temporal dynamics in cardiovascular datasets [35].

Although the association between heart-rate variability (HRV) and cardiovascular disease is well established, a practical workflow for screening ischemic heart disease (IHD) with consumer-grade photoplethysmography (PPG) remains undefined, as do the most informative HRV biomarkers obtainable from such sensors. To address this, we present a pilot using Zhurek–an in-house fingertip PPG device that records 60-minute signals, computes HRV features on board, and transmits encrypted data to a cloud store. Bench comparison with a three-lead Holter ECG showed clinically acceptable mean biases: −0.601 bpm for heart rate, +33.1 ms for SDNN, and −4.8 ms for RMSSD. With Zhurek, one-hour recordings were obtained from 20 healthy volunteers and 20 angiographically confirmed IHD patients sampled from a 300-case registry. Eight candidate variables were evaluated (SDNN, RMSSD, LF, HF, LF/HF, Max_HR, BMI, age). Mann–Whitney tests indicated significant group differences for SDNN, LF, HF, Max_HR, BMI, and age ($p<0.05$). Principal component analysis showed that the first two components accounted for 49.5% of variance and already separated the cohorts in an unsupervised projection. CatBoost feature importance ranked LF power highest (~44%), followed by age (~19%), with HF also strongly discriminative. Collectively, these results show that short, point-of-care PPG acquisitions from an affordable wearable can recover key autonomic signatures previously accessible mainly via 24-hour Holter monitoring, establishing a concrete basis for scalable, low-cost IHD screening grounded in clearly defined HRV biomarkers.

## 2. Materials and Methods

The hybrid physiological monitoring platform is built for continuous heart-rate variability (HRV) assessment to support ambulatory evaluation of autonomic nervous system function. It couples a wearable sensor that performs on-device processing with secure remote data logging, as shown in Figure 1. The architecture brings together three tightly linked layers: the sensing and on-device processing layer, the communication and storage layer, and the analytics and classification layer.

In the sensing tier, the Zhurek IoT device acquires fingertip photoplethysmography (PPG) and computes core HRV indices in real time. The embedded firmware transforms the raw waveform into time-domain features and prepares them for transmission. In particular, it derives heart rate (HR), pulse period (PP), SDNN, and RMSSD on device; Section 3.2 provides a detailed description of the hardware and firmware stack.

Computed HRV features are serialized as JSON and sent over Wi-Fi via MQTT. The device publishes to the topic zhurek/ppg/hrv, served by a Mosquitto 2.0 broker on a central server. All links are protected with TLS 1.3 and mutual certificate-based authentication to preserve integrity and confidentiality.

Incoming MQTT payloads are parsed and persisted in a relational SQL database. Each entry carries an accurate timestamp from an on-board real-time clock synchronized by Network Time Protocol (NTP) to maintain cross-device temporal consistency. For resilience during network outages, the wearable simultaneously keeps a local CSV log.

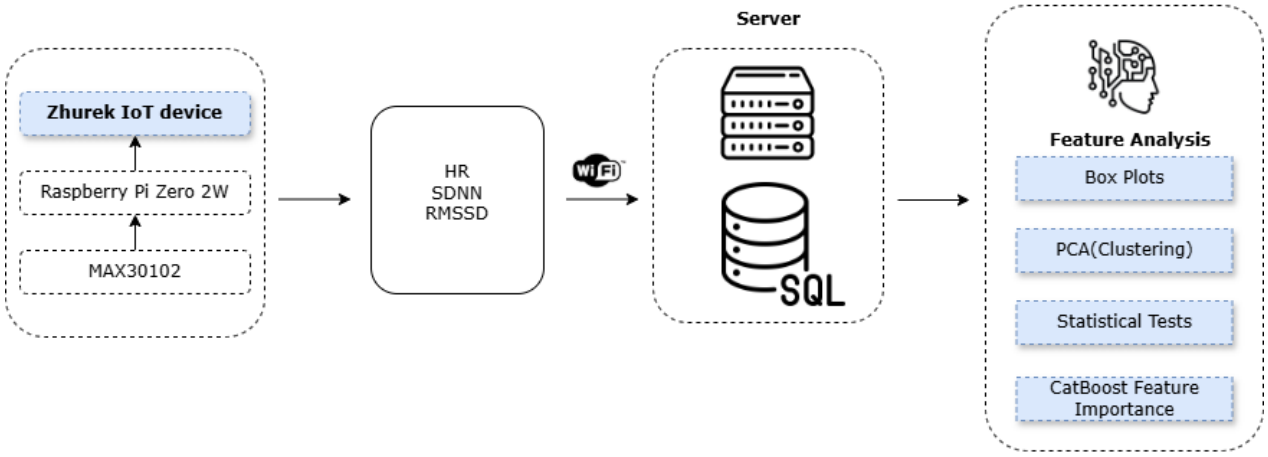


**Figure 1 –** System Architecture of the Zhurek HRV Pipeline.

In this pilot, the analytics layer prioritized understanding which physiological and clinical variables differentiate healthy controls from patients with ischemic heart disease (IHD), rather than optimizing predictive metrics. Mann–Whitney U tests were applied to detect distributional shifts, and principal component analysis (PCA) was used to explore latent structure and label-free separation between cohorts. Feature importance was estimated with CatBoost on the 40-sample dataset, highlighting variables such as LF power, age, HF power, and Max_HR as the strongest discriminators. Given the limited sample size, model accuracy metrics were intentionally omitted to avoid overfitting and misinterpretation; the emphasis was on hypothesis generation for larger studies.

In the classification track of the analytics layer, stored HRV features can be processed periodically with machine-learning models including gradient boosting methods (XGBoost, CatBoost), random forests (RF), interpretable generalized additive models (EBM), and hybrid designs that combine deep neural networks (DNN) with least-mean-square support vector machines (LMSVM). Trained on labeled data, these models assign risk levels and flag early signs of autonomic dysfunction, enabling automated preliminary triage and risk stratification in remote-monitoring workflows.

By unifying embedded signal processing, encrypted wireless transport, and modular analytics, the system supports round-the-clock monitoring with structured downstream analysis. Reliance on open-source software and off-the-shelf components enhances reproducibility and simplifies deployment in distributed settings.

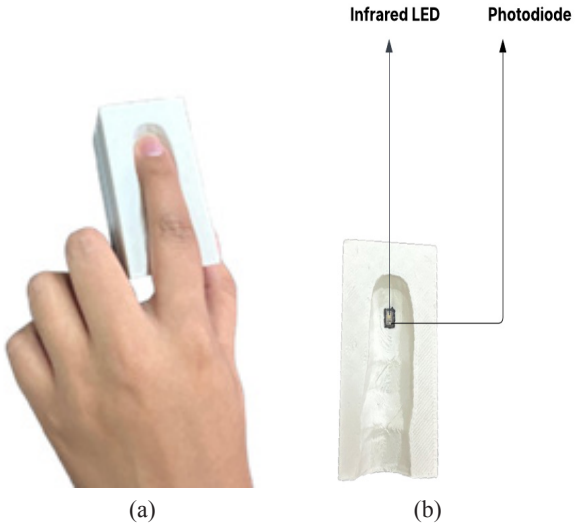


(a) (b)

**Figure 2 –** Zhurek Fingertip PPG Sensor: IR LED–Photodiode Layout.

Zhurek (see Figure 2) is a custom, non-invasive wearable for real-time PPG capture and processing. The device integrates a MAX30102 optical sensor (DFRobot Gravity: SEN0344) with a Raspberry Pi Zero 2 W (ARM Cortex-A53, 1 GHz, 512 MB RAM) running Raspberry Pi OS Lite (64-bit). Acquisition uses only the infrared channel at 100 Hz over hardware I²C (address 0x57). The sensor resides in a 3D-printed PLA enclosure with an IR-shielded finger clip and soft elastomer pads to limit motion artefacts and ambient light.

All logic is written in Python 3.11. I²C transactions use smbus2. The raw PPG stream undergoes baseline correction and moving-average smoothing. Cardiac cycles are detected by a derivative-based peak finder adapted from HeartPy, followed by physiological plausibility checks to remove outliers. RR intervals are derived from peak times; HR, SDNN, and RMSSD are computed in 30-s windows with a 5-s hop. Frequency-domain indices (LF, HF, LF/HF) and Max_HR are computed offline, then combined with BMI and age to form an eight-feature vector.

Each result is packaged as a JSON object and published via MQTT; a concurrent CSV log on the device acts as a fail-safe. Timestamps are generated by an RTC that is periodically synchronized using NTP.

The device delivers its best signal quality and physiological fidelity at rest. Resting acquisitions reduce motion artefacts and yield stable autonomic patterns, supporting reliable HRV computation–consistent with evidence that resting protocols maximize accuracy and reproducibility for HRV, gas-exchange, and metabolic-rate measurements [36], [37], [38]. Under these conditions, remote HR and HRV derived from PPG closely track ECG-based readings [38], providing a robust baseline for IHD risk surveillance.

To determine whether wearable ECGs are suitable for resting-state HRV, we carried out a 24-hour comparison between a clinical three-lead Holter and the Polar H10 chest strap. The two systems showed close concordance on key time-domain metrics: mean heart rate differed from the Holter by 0.601 bpm (1.77%), SDNN by 33.088 ms (6.77%), and RMSSD by 4.778 ms (14.57%). The confidence intervals were narrow–e.g., ±1.239 bpm for heart rate–supporting the stability and consistency of both devices during rest.

To build and validate machine-learning models for IHD prediction, HRV data were gathered from two distinct sources: a clinical cohort with confirmed cardiac disease and a healthy control cohort. This split design lets models capture autonomic patterns characteristic of pathology while learning to separate them from normal variability in healthy subjects.

Both groups were recorded with high-fidelity RR-interval sensors to ensure consistent HRV measurement. The clinical set used long-duration, multi-lead Holter ECGs from participants diagnosed with IHD or related disorders. Healthy volunteers were monitored in controlled laboratory sessions with either a single-lead chest-strap ECG (Polar H10) or the custom PPG-based Zhurek device. Although ECG is the reference for RR detection, our results show that, with appropriate preprocessing and validation, PPG from Zhurek attains HRV accuracy adequate for ML-driven risk stratification. Using both modalities within a unified pipeline mitigates dataset bias and mirrors real-world wearable cardiovascular monitoring.

HRV records from 20 adult inpatients with verified cardiovascular disease were obtained at the Research Institute of Cardiology and Internal Diseases (Almaty, Kazakhstan). Diagnoses followed institutional clinical protocols under cardiology department oversight. Each participant underwent continuous 24-hour monitoring with diagnostic-grade, multi-lead Holter ECG systems that provide high-resolution RR-interval outputs appropriate for rigorous HRV assessment. The cohort included patients across a spectrum of disease severity, from early to advanced stages, increasing heterogeneity and supporting the development of models with better external validity. Data were stored as numerical RR-interval series rather than raw ECG, and core HRV variables–heart rate (HR), RR intervals, SDNN, and RMSSD–were computed automatically and supplied for downstream analysis.

To characterize baseline autonomic function, HRV data were collected from 20 healthy volunteers who reported no cardiovascular, neurological, or metabolic conditions. To reduce confounding, participants refrained from alcohol, tobacco, caffeine, and vigorous exercise for at least 24 hours before recording and maintained regular sleep (7–8 hours) the preceding night. Individuals with acute illness, nonadherence to preparation, or excessive signal artefacts were excluded. Measurements used the Zhurek IoT device, combining a MAX30102 PPG sensor with a Raspberry Pi Zero 2 W. The MAX30102 is a low-power optical module with integrated red/IR LEDs, photodiode, and low-noise AFE with ambient-light suppression; in this setup only the infrared

channel was sampled at 100 Hz over hardware I²C. PPG was recorded at the fingertip using a shielded spring-loaded clip with elastomer padding to mitigate motion artefact. Sessions lasted 60 minutes under resting conditions, with a Polar H10 chest-strap ECG worn concurrently for validation. Zhurek computed HR, inter-beat intervals (IBIs), SDNN, and RMSSD in real time using a 30-second rolling window and saved all outputs to CSV with high-resolution time-stamps for subsequent processing.

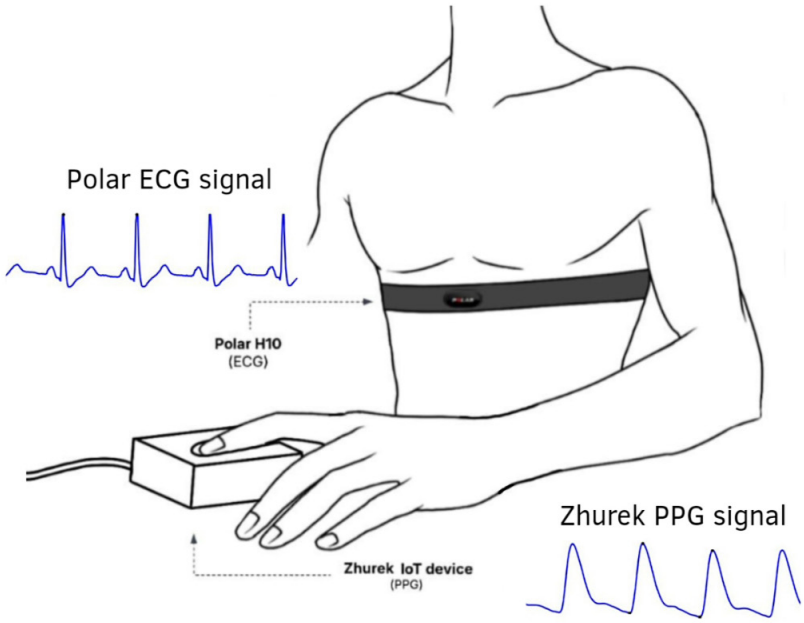


**Figure 3 –** Simultaneous Acquisition: Polar H10 ECG and Zhurek Fingertip PPG.

In this pilot, preprocessing began by merging two distinct cohorts: a healthy control set and a clinical set with ischemic heart disease (IHD). The control group included 20 adults aged 18–22. The IHD pool was drawn from a registry of exactly 300 confirmed cases spanning 18–92 years; for the present analysis, only patients aged 18–71 were retained. To align temporal resolution across cohorts, a continuous 60-minute segment was extracted from each patient's 24-hour Holter ECG, matching the one-hour PPG recordings collected from healthy participants with the Zhurek device.

Several categorical attributes were numerically encoded to streamline analysis. Sex was coded as Male = 1, Female = 0. "Bad Habits" was set to 1 for respondents reporting alcohol use, smoking, or routine consumption of energy drinks, and 0 otherwise. Familial predisposition was represented by a "Genetic Marker" variable: 0 indicated no known CVD in relatives or a family history limited to non-CVD conditions; 1 denoted a verified family history of cardiovascular disorders (e.g., hypertension, IHD, myocardial infarction, stroke); 2 indicated only non-cardiovascular illnesses among relatives. Surgical history ("Operations") was encoded as 0 for no prior procedures, 1 for non-cardiac surgeries, and 2 for cardiovascular-related interventions.

The feature set comprised established HRV measures–SDNN, pNN50, RMSSD, LF, HF, and the LF/HF ratio–reflecting autonomic nervous system dynamics [39]. Two additional variables were included: Max_HR (the maximum heart rate observed within the recording) and BMI, computed by the standard Equation (1) [40]:

$$BMI = \frac{Weight\,(kg)}{Height\,(m)^2} \quad (1)$$

Quality control steps removed entries with missing fields, malformed values, or extreme outliers. Non-numeric strings were normalized to numeric form where applicable (including converting decimal commas to periods). These procedures yielded a clean, consistent dataset suitable for downstream statistical analysis and visualization.

## 3. Results

HRV was measured in two cohorts: patients with clinically confirmed IHD and healthy controls without known cardiovascular disease. All participants completed standardized recording sessions. Summary statistics for each group are reported in Table 1 (controls) and Table 2 (IHD). The analysis covers time-domain indices (SDNN, pNN50, RMSSD) and frequency-domain indices (LF, HF, LF/HF), offering a snapshot of autonomic nervous system dynamics [39] and revealing potential contrasts in HRV patterns between healthy and IHD populations.

**Table 1 –** Descriptive HRV statistics – healthy control group.

| № | SDNN | PNN50 | RMSSD | LF | HF | LF/HF |
|---|---|---|---|---|---|---|
| 1 | 72.4 | 24.45 | 46.4 | 0.08 | 0.06 | 1.39 |
| 2 | 53.93 | 15.59 | 37.76 | 0.06 | 0.04 | 1.54 |
| 3 | 39.33 | 1.71 | 18.63 | 0.05 | 0.03 | 1.54 |
| 4 | 47.82 | 5.9 | 26.55 | 0.06 | 0.04 | 1.53 |
| 5 | 68.21 | 36.37 | 58.38 | 0.06 | 0.09 | 0.71 |
| 6 | 65.65 | 20.89 | 43.3 | 0.07 | 0.07 | 1.01 |
| 7 | 95.05 | 40.89 | 64.28 | 0.09 | 0.09 | 1.02 |
| ……. | | | | | | |
| 19 | 93.95 | 33.4 | 58.35 | 0.1 | 0.09 | 1.18 |
| 20 | 33.96 | 7.7 | 23.57 | 0.03 | 0.03 | 0.99 |

**Table 2 –** HRV summary in the IHD cohort.

| № | SDNN | PNN50 | RMSSD | LF | HF | LF/HF |
|---|---|---|---|---|---|---|
| 1 | 89 | 36.34 | 56 | 0.37 | 0.35 | 1.05 |
| 2 | 99 | 1.26 | 18 | 0.30 | 0.16 | 1.84 |
| 3 | 80 | 2.08 | 22 | 0.19 | 0.16 | 1.20 |
| 4 | 61 | 1.02 | 15 | 0.18 | 0.12 | 1.55 |
| 5 | 124 | 16.67 | 41 | 0.44 | 0.26 | 1.67 |
| 6 | 69 | 7.47 | 31 | 0.29 | 0.27 | 1.08 |
| 7 | 88 | 2.79 | 28 | 0.25 | 0.19 | 1.30 |
| ……. | | | | | | |
| 19 | 72 | 15.63 | 39 | 0.23 | 0.22 | 1.04 |
| 20 | 59 | 3.17 | 23 | 0.26 | 0.26 | 1.00 |

Figure 4 boxplots indicate clear groupwise differences in physiological and HRV features. SDNN, LF, and HF are higher in the IHD cohort, reflecting greater overall variability and increased spectral power in both bands. By contrast, RMSSD–an index of parasympathetic tone [41]–is higher in healthy participants, consistent with greater autonomic flexibility associated with elevated RMSSD values [42]. The LF/HF ratio shows similar medians across groups. Max_HR is higher among IHD subjects. BMI varies modestly between groups, with a higher median in the IHD cohort, in line with the recognized contribution of excess body weight to cardiovascular risk [43].

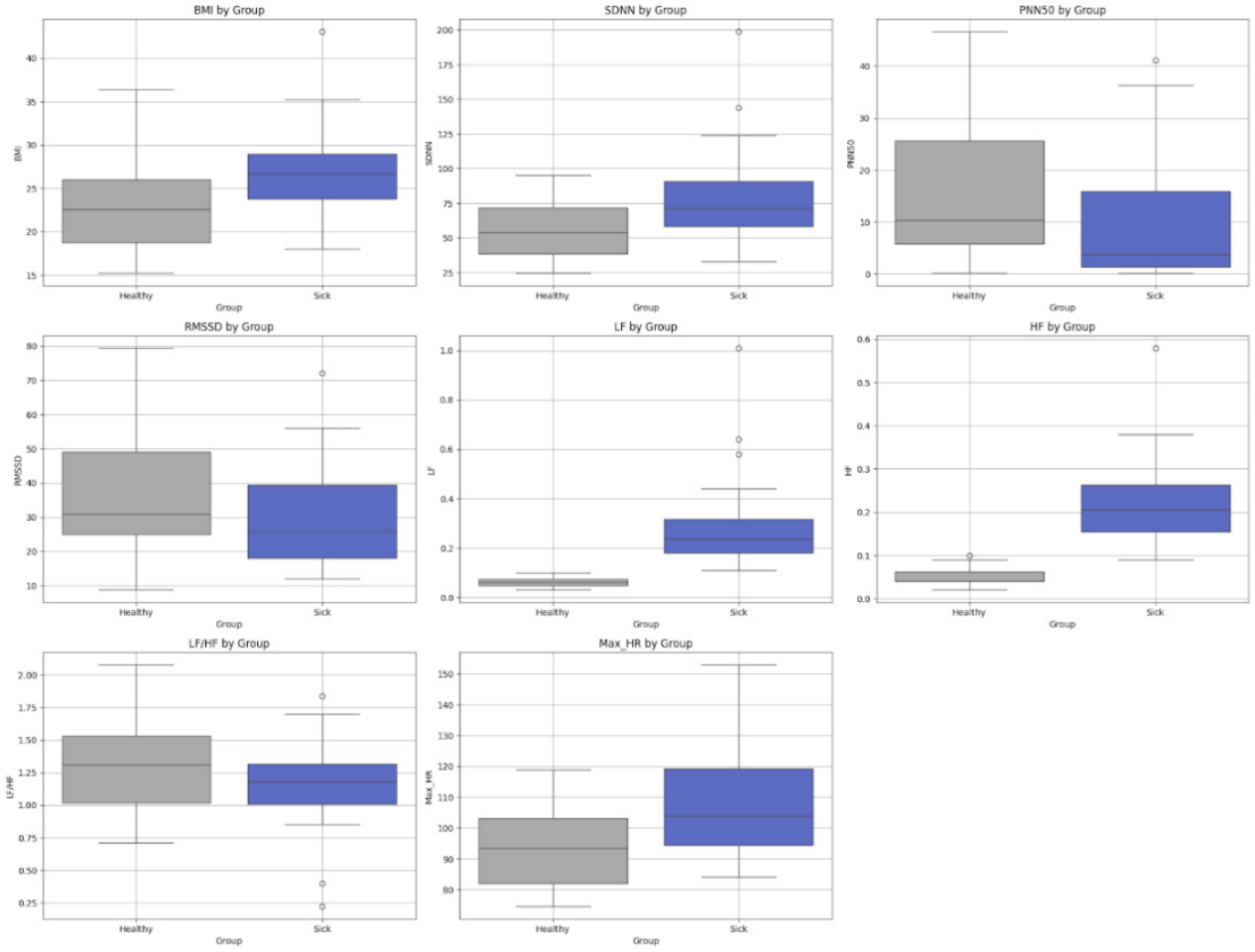


**Figure 4 –** Groupwise Boxplots of Physiological and HRV Metrics (Healthy vs. IHD).

Continuous physiological and HRV metrics–BMI, SDNN, RMSSD, pNN50, LF, HF, LF/HF, and Max_HR–are summarized for healthy controls and IHD patients. As depicted in Figure 5, the Genetic Marker variable is predominantly 0 among healthy participants, whereas most IHD cases are labeled 1, emphasizing hereditary risk in cardiovascular disease [44]. For Operations, controls are almost entirely 0, while the IHD cohort shows markedly higher rates of both non-cardiac (1) and cardiac (2) procedures, reflecting greater clinical intervention. The Bad Habits indicator (smoking, alcohol, energy drinks) is also more frequent in the IHD group than in controls, underscoring modifiable lifestyle contributions. Collectively, these distributions show that genetic predisposition, surgical history, and behavioral risk factors jointly separate the cohorts and provide salient predictors for IHD outcome modeling.

The correlation heatmaps, as shown in Figure 6, illustrate the interrelationships between physiological, behavioral, and HRV features in healthy individuals and patients with IHD. The matrices reveal distinct patterns between the two cohorts. In the healthy group, the heatmap reveals a structured and physiologically intuitive set of relationships. Strong positive correlations are evident among the time-domain HRV metrics, specifically SDNN, RMSSD, and PNN50. In contrast, the IHD group exhibits a more disrupted correlation structure compared to the healthy group, which suggests a fundamental loss of autonomic coherence. Additionally, lifestyle factors such as un-healthy habits show positive correlations with impaired HRV in the IHD group, whereas they exhibit negative correlations with HRV features in the healthy group. As shown in the matrix, the diagonal line of red cells corresponds to perfect self-correlation, where each variable is perfectly correlated

with itself. These heatmaps offer more than just a summary of feature relationships; they visualize the integrity of the autonomic nervous system. The pattern in the healthy group reflects physiological harmony and adaptability, while the disrupted pattern in the IHD group visually rep-resents the autonomic dysregulation and loss of resilience that is a hallmark of cardiovascular disease.

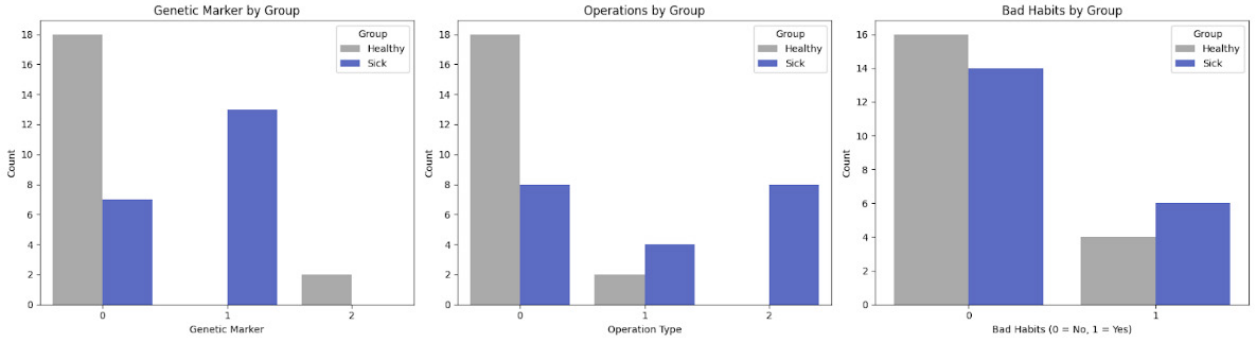


**Figure 5 –** Categorical Risk Factors by Group (Genetic Marker, Operations, Bad Habits).

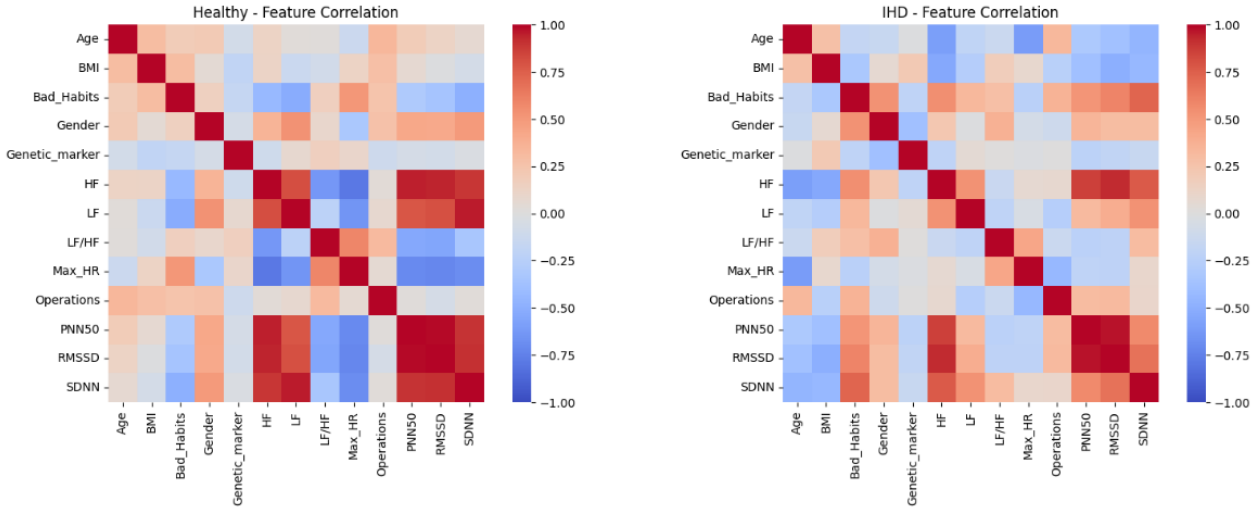


**Figure 6 –** Feature Correlation Heatmaps (Healthy vs. IHD)

Table 3 summarizes distributional comparisons between healthy controls and IHD patients. Significant group differences ($p < 0.05$) were observed for BMI, SDNN, LF, HF, Max_HR, and Age, indicating that autonomic activity and cardiovascular dynamics provide strong discriminatory signal. By contrast, PNN50, RMSSD, and the LF/HF ratio were not individually significant, though they may still add value in multivariate models or clinical interpretation.

**Table 3 –** Mann–Whitney u comparison of physiological feature distributions (Healthy vs. IHD).

| Feature | P-VALUE | Significance |
|---|---|---|
| BMI | 0.042464 | Yes |
| SDNN | 0.025625 | Yes |
| LF | 6.49e-08 | Yes |

*Continuation of the table*

| Feature | p-value | Significance |
|---|---|---|
| HF | 9.47e-08 | Yes |
| PNN50 | 0.072032 | No |
| RMSSD | 0.126377 | No |
| LF/HF | 0.432537 | No |
| Max_HR | 0.008343 | Yes |
| Age | 9.34e-07 | Yes |

To probe cohort-level physiology, we applied principal component analysis. The first two components accounted for ~49.5% of the variance (PC1: 27.3%, PC2: 22.2%). As shown in Figure 7, the PC1–PC2 projection exhibits a clear separation between groups–healthy participants cluster apart from IHD cases–suggesting that the selected physiological and categorical features contain sufficient signal for unsupervised differentiation and motivating their use in downstream supervised modeling and feature-importance analysis.

As part of the exploratory workflow, we inspected CatBoost feature importances to see which physiological and clinical variables most strongly drive group separation. Model accuracy was not the objective at this stage; the goal was to flag the variables most promising for differentiating healthy participants from patients with IHD.

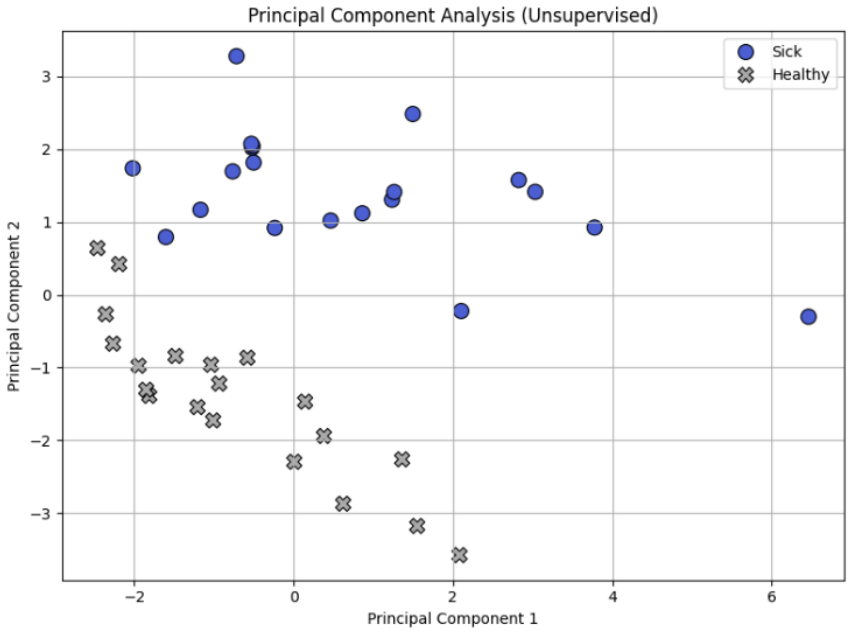


**Figure 7 –** Unsupervised PCA Projection of HRV Features (Healthy vs. IHD)

As shown in Figure 8, SHAP analysis of the CatBoost model ranks LF (low-frequency HRV power) as the top contributor (highest mean SHAP value), with HF (high-frequency power) next–underscoring the central role of autonomic dynamics. Additional, smaller but non-trivial contributions come from Operations, Genetic_marker, and PNN50, suggesting that surgical history, hereditary risk, and beat-to-beat variability also aid in distinguishing the two cohorts.

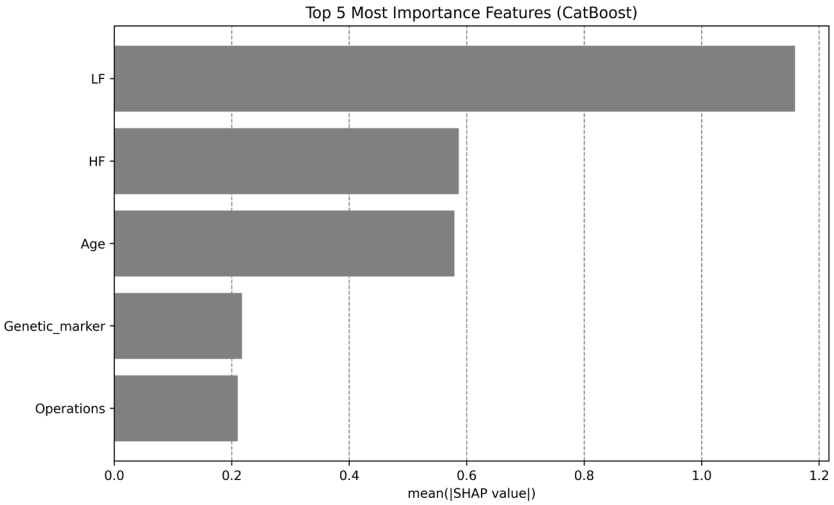


**Figure 8 –** Unsupervised PCA Projection of HRV Features (Healthy vs. IHD)

To gauge how much the model depends on physiology alone, we re-ran CatBoost on the pilot dataset after removing the age variable. Because no hold-out set was used, the aim was not to score accuracy but to probe which inputs drive the model's internal decisions. As shown in Figure 9, SHAP analysis identifies five leading contributors to IHD prediction. The low-frequency (LF) HRV component shows the largest mean absolute SHAP value, indicating the strongest influence, followed by the high-frequency (HF) component and Age, pointing to major roles for autonomic dynamics and age-related effects. Genetic_marker and Operations contribute less overall but still affect certain cases. Force-plot views further illustrate that higher LF/HF ratios or greater age tend to push individual estimates toward the "Ischaemia" class.

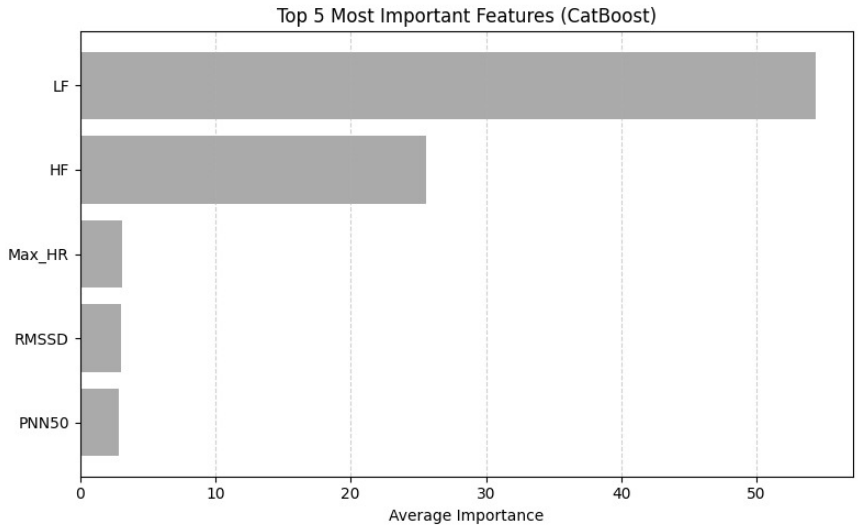


**Figure 9 –** CatBoost Feature Importance (physiology-only model).

## 4. Conclusions

The principal contribution of this pilot is an end-to-end system and protocol for scalable, ambulatory screening of ischemic heart disease (IHD). We developed and validated Zhurek, a custom, non-invasive fingertip PPG sensor that enables rapid, point-of-care acquisition. A key design element is showing that a single one-hour recording is sufficient to capture diagnostically meaningful autonomic signatures. Hour-long sessions were obtained from 20 healthy volunteers aged 18–22 and 20 angiographically confirmed IHD patients, and eight features were derived: SDNN, RMSSD, LF, HF, LF/HF, Max_HR, BMI, and age. Against a three-lead Holter ECG, the system demonstrated clinically acceptable mean absolute errors–0.601 bpm for heart rate, 33.1 ms for SDNN, and 4.8 ms for RMSSD.

Nonparametric testing (Mann–Whitney) indicated significant between-group differences for SDNN, LF, HF, Max_HR, BMI, and age ($p < 0.05$). The first two principal components explained 49.5% of total variance and already separated cohorts without labels, supporting the informativeness of the chosen variables. Methodologically, the study used machine learning not to overfit predictions on a small sample but to conduct exploratory ranking of short-duration biomarkers. CatBoost importance scores placed LF at ~44% of total contribution, age at ~19%, followed by HF, with smaller effects for Max_HR and RMSSD. Together with the PCA separation, this pinpoints which markers carry the greatest diagnostic weight and shows that brief Zhurek acquisitions can recover autonomic signals traditionally accessed via 24-hour Holter, laying the groundwork for affordable, large-scale screening.

Incorporating SHAP improved the transparency of the Zhurek–CatBoost pipeline and aligns with emerging explainability standards; at deployment scale, individualized SHAP profiles could inform genuinely personalized prevention.

Several caveats qualify these findings. Data modalities differed by cohort–healthy participants were recorded with optical PPG, whereas IHD patients were recorded with ECG–introducing potential signal-quality biases. The control group's narrow age range contrasts with age being a strong discriminator, raising the risk of confounding. The sample size ($n = 40$) is limited; therefore, formal performance metrics were intentionally omitted to avoid overinterpretation.

Future work will enlarge and age-diversify the cohorts–especially the healthy group–and standardize acquisition by collecting parallel PPG and single-lead ECG from all participants. A multicenter longitudinal study is planned to test the prognostic utility of short-term markers and to confirm reproducibility. The roadmap also includes adding nonlinear HRV measures and expanding automated analysis to enable reliable ambulatory risk stratification. These steps should enhance the clinical relevance of the Zhurek approach and accelerate the shift from reactive care to proactive IHD prevention.

## Funding

This work was funded by Committee of Science of the Republic of Kazakhstan AP23488586 "Development of an intelligent system for monitoring and prevention of cardiovascular diseases using deep learning and IoMT (Internet of Medical Things)" (2024-2026).

## Author Contributions

Conceptualization, N.T., M.A. and A.K..; Methodology, D.T. and M.K.; Software, A.K., M.A. and A.B.; Validation, M.A. and N.T.; Formal Analysis, A.K.; Investigation, A.K, M.A. and N.T.; Resources, A.B. and M.K.; Data Curation, D.T. and M.K.; Writing – Original Draft Preparation, N.T., M.A., A.K. and D.T.; Writing – Review & Editing, N.T., A.B. and M.K.; Visualization, M.K.; Supervision, N.T.; Project Administration, N.T.; Funding Acquisition, N.T.

## Conflicts of Interest

The authors declare no conflict of interest.

**References**


1. ‘Cardiovascular diseases (CVDs)’. Accessed: Jul. 21, 2025. [Online]. Available: https://www.who.int/news-room/fact-sheets/detail/cardiovascular-diseases-(cvds)
2. M. A. Khan *et al.*, ‘Global Epidemiology of Ischemic Heart Disease: Results from the Global Burden of Disease Study’, *Cureus*, Jul. 2020, doi: 10.7759/cureus.9349.
3. tengrinews.kz, ‘Названа самая распространенная болезнь среди казахстанцев’, Главные новости Казахстана – Tengrinews.kz. Accessed: Jul. 21, 2025. [Online]. Available: https://tengrinews.kz/kazakhstan_news/nazvana-samaya-rasprostranennaya-bolezn-sredi-kazahstantsev-503527/
4. P. Severino *et al.*, ‘Ischemic Heart Disease Pathophysiology Paradigms Overview: From Plaque Activation to Microvascular Dysfunction’, *IJMS*, vol. 21, no. 21, p. 8118, Oct. 2020, doi: 10.3390/ijms21218118.
5. Ł. J. Janicki, W. Leoński, J. S. Janicki, M. Nowotarski, M. Dziuk, and R. Piotrowicz, ‘Comparative Analysis of the Diagnostic Effectiveness of SATRO ECG in the Diagnosis of Ischemia Diagnosed in Myocardial Perfusion Scintigraphy Performed Using the SPECT Method’, *Diagnostics*, vol. 12, no. 2, p. 297, Jan. 2022, doi: 10.3390/diagnostics12020297.
6. Ștefania-T. Duca *et al.*, ‘Enhancing Comprehensive Assessments in Chronic Heart Failure Caused by Ischemic Heart Disease: The Diagnostic Utility of Holter ECG Parameters’, *Medicina*, vol. 60, no. 8, p. 1315, Aug. 2024, doi: 10.3390/medicina60081315.
7. N. Singh *et al.*, ‘Heart Rate Variability: An Old Metric with New Meaning in the Era of using mHealth Technologies for Health and Exercise Training Guidance. Part One: Physiology and Methods’, *Arrhythmia & Electrophysiology Review*, vol. 7, no. 3, p. 193, 2018, doi: 10.15420/aer.2018.27.2.
8. P. Ribeiro, J. Sá, D. Paiva, and P. M. Rodrigues, ‘Cardiovascular Diseases Diagnosis Using an ECG Multi-Band Non-Linear Machine Learning Framework Analysis’, *Bioengineering*, vol. 11, no. 1, p. 58, Jan. 2024, doi: 10.3390/bioengineering11010058.
9. S. P. Gaine *et al.*, ‘Multimodality Imaging in the Detection of Ischemic Heart Disease in Women’, *JCDD*, vol. 9, no. 10, p. 350, Oct. 2022, doi: 10.3390/jcdd9100350.
10. L. Wang, T. Bi, J. Hao, and T. H. Zhou, ‘Heart Diseases Recognition Model Based on HRV Feature Extraction over 12-Lead ECG Signals’, *Sensors*, vol. 24, no. 16, p. 5296, Aug. 2024, doi: 10.3390/s24165296.
11. G. Doolub *et al.*, ‘Artificial Intelligence as a Diagnostic Tool in Non-Invasive Imaging in the Assessment of Coronary Artery Disease’, *Medical Sciences*, vol. 11, no. 1, p. 20, Feb. 2023, doi: 10.3390/medsci11010020.
12. L. Verma and S. Srivastava, ‘A Data Mining Model for Coronary Artery Disease Detection Using Noninvasive Clinical Parameters’, *Indian Journal of Science and Technology*, vol. 9, no. 48, Dec. 2016, doi: 10.17485/ijst/2016/v9i48/105707.
13. M. Sayadi, V. Varadarajan, F. Sadoughi, S. Chopannejad, and M. Langarizadeh, ‘A Machine Learning Model for Detection of Coronary Artery Disease Using Noninvasive Clinical Parameters’, *Life*, vol. 12, no. 11, p. 1933, Nov. 2022, doi: 10.3390/life12111933.
14. A. M. Alaa, T. Bolton, E. Di Angelantonio, J. H. F. Rudd, and M. Van Der Schaar, ‘Cardiovascular disease risk prediction using automated machine learning: A prospective study of 423,604 UK Biobank participants’, *PLoS ONE*, vol. 14, no. 5, p. e0213653, May 2019, doi: 10.1371/journal.pone.0213653.
15. H. ChuDuc, K. NguyenPhan, and D. NguyenViet, ‘A Review of Heart Rate Variability and its Applications’, *APCBEE Procedia*, vol. 7, pp. 80–85, 2013, doi: 10.1016/j.apcbee.2013.08.016.
16. C. Brinza *et al.*, ‘Heart Rate Variability in Acute Myocardial Infarction: Results of the HeaRt-V-AMI Single-Center Cohort Study’, *JCDD*, vol. 11, no. 8, p. 254, Aug. 2024, doi: 10.3390/jcdd11080254.
17. A. Hazra, S. K. Mandal, A. Gupta, A. Mukherjee, and A. Mukherjee, ‘Heart Disease Diagnosis and Prediction Using Machine Learning and Data Mining Techniques: A Review’.
18. M. Trigka and E. Dritsas, ‘Long-Term Coronary Artery Disease Risk Prediction with Machine Learning Models’, *Sensors*, vol. 23, no. 3, p. 1193, Jan. 2023, doi: 10.3390/s23031193.
19. B. A. Marzoog *et al.*, ‘Machine Learning Model Discriminate Ischemic Heart Disease Using Breathome Analysis’, *Biomedicines*, vol. 12, no. 12, p. 2814, Dec. 2024, doi: 10.3390/biomedicines12122814.
20. G. Sibrecht, J. Piskorski, T. Krauze, and P. Guzik, ‘Heart Rate Asymmetry, Its Compensation, and Heart Rate Variability in Healthy Adults during 48-h Holter ECG Recordings’, *JCM*, vol. 12, no. 3, p. 1219, Feb. 2023, doi: 10.3390/jcm12031219.
21. X. Wu, Q. Yang, J. Li, and F. Hou, ‘Investigation on the Prediction of Cardiovascular Events Based on Multi-Scale Time Irreversibility Analysis’, *Symmetry*, vol. 13, no. 12, p. 2424, Dec. 2021, doi: 10.3390/sym13122424.
22. B. M. Curtis and J. H. O’Keefe, ‘Autonomic Tone as a Cardiovascular Risk Factor: The Dangers of Chronic Fight or Flight’, *Mayo Clinic Proceedings*, vol. 77, no. 1, pp. 45–54, Jan. 2002, doi: 10.4065/77.1.45.
23. R. A. Rather and V. Dhawan, ‘Genetic markers: Potential candidates for cardiovascular disease’, *International Journal of Cardiology*, vol. 220, pp. 914–923, Oct. 2016, doi: 10.1016/j.ijcard.2016.06.251.
24. S. De Rosa, B. Arcidiacono, E. Chiefari, A. Brunetti, C. Indolfi, and D. P. Foti, ‘Type 2 Diabetes Mellitus and Cardiovascular Disease: Genetic and Epigenetic Links’, *Front. Endocrinol.*, vol. 9, Jan. 2018, doi: 10.3389/fendo.2018.00002.
25. J. L. Moraes, M. X. Rocha, G. G. Vasconcelos, J. E. Vasconcelos Filho, V. H. C. De Albuquerque, and A. R. Alexandria, ‘Advances in Photopletysmography Signal Analysis for Biomedical Applications’, *Sensors*, vol. 18, no. 6, p. 1894, Jun. 2018, doi: 10.3390/s18061894.
26. M. Elgendi *et al.*, ‘The use of photoplethysmography for assessing hypertension’, *npj Digit. Med.*, vol. 2, no. 1, Jun. 2019, doi: 10.1038/s41746-019-0136-7.

27. M. A. Almarshad, M. S. Islam, S. Al-Ahmadi, and A. S. BaHammam, 'Diagnostic Features and Potential Applications of PPG Signal in Healthcare: A Systematic Review', *Healthcare*, vol. 10, no. 3, p. 547, Mar. 2022, doi: 10.3390/healthcare10030547.

28. K. B. Kim and H. J. Baek, 'Photoplethysmography in Wearable Devices: A Comprehensive Review of Technological Advances, Current Challenges, and Future Directions', *Electronics*, vol. 12, no. 13, p. 2923, Jul. 2023, doi: 10.3390/electronics12132923.

29. M. Shabaan *et al.*, 'Survey: smartphone-based assessment of cardiovascular diseases using ECG and PPG analysis', *BMC Med Inform Decis Mak*, vol. 20, no. 1, Dec. 2020, doi: 10.1186/s12911-020-01199-7.

30. I. C. Dipto, T. Islam, H. M. M. Rahman, and M. A. Rahman, 'Comparison of Different Machine Learning Algorithms for the Prediction of Coronary Artery Disease', *JDAIP*, vol. 08, no. 02, pp. 41–68, 2020, doi: 10.4236/jdaip.2020.82003.

31. R. C. Ripan *et al.*, 'A Data-Driven Heart Disease Prediction Model Through K-Means Clustering-Based Anomaly Detection', *SN COMPUT. SCI.*, vol. 2, no. 2, Apr. 2021, doi: 10.1007/s42979-021-00518-7.

32. V. Jahmunah, E. Y. K. Ng, T. R. San, and U. R. Acharya, 'Automated detection of coronary artery disease, myocardial infarction and congestive heart failure using GaborCNN model with ECG signals', *Computers in Biology and Medicine*, vol. 134, p. 104457, Jul. 2021, doi: 10.1016/j.compbiomed.2021.104457.

33. K. Kusunose *et al.*, 'A Deep Learning Approach for Assessment of Regional Wall Motion Abnormality From Echocardiographic Images', *JACC: Cardiovascular Imaging*, vol. 13, no. 2, pp. 374–381, Feb. 2020, doi: 10.1016/j.jcmg.2019.02.024.

34. M. Zreik *et al.*, 'Deep Learning Analysis of Coronary Arteries in Cardiac CT Angiography for Detection of Patients Requiring Invasive Coronary Angiography', *IEEE Trans. Med. Imaging*, vol. 39, no. 5, pp. 1545–1557, May 2020, doi: 10.1109/tmi.2019.2953054.

35. A. Ogunpola, F. Saeed, S. Basurra, A. M. Albarrak, and S. N. Qasem, 'Machine Learning-Based Predictive Models for Detection of Cardiovascular Diseases', *Diagnostics*, vol. 14, no. 2, p. 144, Jan. 2024, doi: 10.3390/diagnostics14020144.

36. R. M. Birn *et al.*, 'The Influence of Physiological Noise Correction on Test–Retest Reliability of Resting-State Functional Connectivity', *Brain Connectivity*, vol. 4, no. 7, pp. 511–522, Sep. 2014, doi: 10.1089/brain.2014.0284.

37. G. Sanchez-Delgado *et al.*, 'Reliability of resting metabolic rate measurements in young adults: Impact of methods for data analysis', *Clinical Nutrition*, vol. 37, no. 5, pp. 1618–1624, Oct. 2018, doi: 10.1016/j.clnu.2017.07.026.

38. D. McDuff, S. Gontarek, and R. Picard, 'Remote measurement of cognitive stress via heart rate variability', in *2014 36th Annual International Conference of the IEEE Engineering in Medicine and Biology Society*, Chicago, IL: IEEE, Aug. 2014, pp. 2957–2960. doi: 10.1109/embc.2014.6944243.

39. N. Gullett, Z. Zajkowska, A. Walsh, R. Harper, and V. Mondelli, 'Heart rate variability (HRV) as a way to understand associations between the autonomic nervous system (ANS) and affective states: A critical review of the literature', *International Journal of Psychophysiology*, vol. 192, pp. 35–42, Oct. 2023, doi: 10.1016/j.ijpsycho.2023.08.001.

40. A. Zierle-Ghosh and A. Jan, 'Physiology, Body Mass Index', in *StatPearls*, Treasure Island (FL): StatPearls Publishing, 2025. Accessed: Jul. 21, 2025. [Online]. Available: http://www.ncbi.nlm.nih.gov/books/NBK535456/

41. J. Zeng *et al.*, 'High vagally mediated resting-state heart rate variability is associated with superior working memory function', *Front. Neurosci.*, vol. 17, Feb. 2023, doi: 10.3389/fnins.2023.1119405.

42. J. Hart, 'OPTIMAL LEVEL OF HEART RATE VARIABILITY FOR SPINAL ADJUSTMENT: A CASE REPORT', *JCC*, vol. 2, no. 1, pp. 103–108, Sep. 2019.

43. M. Volpe *et al.*, 'How cardiologists can manage excess body weight and related cardiovascular risk. An expert opinion', *International Journal of Cardiology*, vol. 381, pp. 101–104, Jun. 2023, doi: 10.1016/j.ijcard.2023.03.054.

44. S. Kathiresan and D. Srivastava, 'Genetics of Human Cardiovascular Disease', *Cell*, vol. 148, no. 6, pp. 1242–1257, Mar. 2012, doi: 10.1016/j.cell.2012.03.001.

***Information About Authors:***

*Nurdaulet Tasmurzayev, PhD. Dr. Tasmurzayev is a Research Engineer at DigitAlem LLP (Almaty, Kazakhstan). He received his PhD (Candidate of Technical Sciences) in Intelligent Control Systems (Big Data and Machine Learning) from al-Farabi Kazakh National University in 2025, his M.Sc. in Intelligent Control Systems in 2022, and his B.Sc. in Automation and Control (Information Systems Department) in 2020. He has authored and co-authored 10 peer-reviewed journal and conference papers. Research interests: artificial intelligence and machine learning; intelligent control systems; Internet of Things (including industrial IoT); smart cities; intelligent building systems and automation; big-data analytics for control and monitoring. ORCID iD: 0000-0003-3039-6715.*

*Dinara Turmakhanbet is a 2025 B.Sc. graduate in Intelligent Control Systems from al-Farabi Kazakh National University (Almaty, Kazakhstan). Her academic interests include intelligent control systems, the Internet of Things (IoT), and applied machine learning. In this study, she contributed to data collection, literature review, and initial analysis. ORCID iD: 0009-0004-8388-4979.*

*Adilet Kakharov is a fourth-year B.Sc. student in Intelligent Control Systems at al-Farabi Kazakh National University (Almaty, Kazakhstan). His academic interests include intelligent control, the applied machine learning and AI. In this study, he assisted with technical support, data processing, and visualization. ORCID iD: 0009-0005-3612-5678.*

*Mukhamejan Aitkazin is a fourth-year B.Sc. student in Intelligent Control Systems at al-Farabi Kazakh National University (Almaty, Kazakhstan). His academic interests include intelligent control, the Internet of Things (IoT), and applied machine learning. In this study, he assisted with technical support, data processing, and visualization. ORCID iD: 0009-0004-0181-7351.*

*Aliya Baidauletova is a Candidate of Medical Sciences and a practicing somnologist and neurologist at al-Farabi Kazakh National University (Almaty, Kazakhstan, baidaulet123@gmail.com). She has extensive clinical and research experience in sleep medicine, neurology, and neurophysiological disorders. Her professional interests include sleep disorders, circadian rhythm regulation, neurological aspects of sleep pathology, and the application of modern diagnostic and monitoring technologies in clinical practice. ORCID iD: 0009-0000-5510-3590.*

*Mergul Kozhamberdiyeva is a Candidate of Pedagogical Sciences and a practicing pedagogist at al-Farabi Kazakh National University (Almaty, Kazakhstan, kozhamberdiyeva.m@outlook.com). She has extensive clinical and research experience in sleep medicine, neurology, and neurophysiological disorders. Her professional interests include sleep disorders, circadian rhythm regulation, neurological aspects of sleep pathology, and the application of modern diagnostic and monitoring technologies in clinical practice. ORCID iD: 0009-0001-0429-7919.*

*Submission received: 13 August, 2025.*
*Revised: 20 November, 2025.*
*Accepted: 20 November, 2025.*

IRSTI 28.23.01 https://doi.org/10.26577/jpcsit202543

**Bibars Amangeldy[1*], Bauyrzhan Abilda[2]**

[1]LLP «DigitAlem», Almaty, Kazakhstan
[2]Astana International University, Astana, Kazakhstan
*e-mail: a.s.bibars@gmail.com

# SMART BUILDING CLIMATE CONTROL: MACHINE LEARNING APPROACH FOR INDIVIDUAL THERMAL PREFERENCE PREDICTION

**Abstract.** Modern building management systems rely on uniform climate settings that fail to accommodate individual occupant preferences, resulting in energy waste and reduced comfort satisfaction. This study presents a data-driven approach for personalized thermal comfort prediction using machine learning algorithms integrated with multimodal sensor networks. We developed and evaluated three classification models (Random Forest, XGBoost, and Artificial Neural Network) using environmental parameters (air temperature, humidity, $CO_2$ concentration) and physiological measurements (heart rate variability, blood pressure, oxygen saturation) collected from controlled experiments with eight participants under various thermal conditions. The optimized Random Forest model achieved 95% accuracy in predicting seven-level thermal sensation votes using only ten key features identified through SHAP analysis. Indoor air temperature emerged as the dominant predictor, while physiological parameters provided complementary information for personalized comfort assessment. The proposed system demonstrates significant potential for integration into smart building automation, enabling dynamic climate control that adapts to individual preferences while optimizing energy consumption. Implementation of such personalized HVAC systems could reduce energy usage by up to 20% compared to conventional static temperature control, while simultaneously improving occupant satisfaction and productivity in commercial buildings.

**Keywords:** smart buildings, thermal comfort prediction, machine learning, HVAC optimization, personalized climate control, energy efficiency, sensor fusion.

## 1. Introduction

Buildings consume approximately 40% of global energy, with heating, ventilation, and air conditioning (HVAC) systems accounting for nearly 50% of this consumption [1]. In commercial buildings alone, inefficient climate control results in annual energy losses exceeding $29 billion globally, while simultaneously causing productivity losses due to occupant discomfort [2]. Despite these significant economic and environmental impacts, most building management systems continue to rely on static temperature setpoints that fail to accommodate individual thermal preferences.

Traditional HVAC control strategies assume uniform thermal comfort across all occupants, typically maintaining indoor temperatures between 20-24°C based on population averages [3]. However, research demonstrates substantial individual variations in thermal perception, with personal comfort preferences differing by up to 6°C among occupants in the same space [4]. This one-size-fits-all approach leads to overcooling or overheating, resulting in energy waste and occupant dissatisfaction rates exceeding 30% in typical office environments [5]. Furthermore, conventional systems lack real-time adaptation capabilities, failing to respond to changing occupancy patterns, weather conditions, or individual physiological states [6].

Recent advances in Internet of Things (IoT) sensors and machine learning algorithms present unprecedented opportunities for developing intelligent, personalized climate control systems [7]. Smart building platforms now enable continuous monitoring of environmental parameters and occupant behavior, while wearable devices provide real-time physiological data for individual comfort assessment [8]. Several pilot implementations have demonstrated the potential for machine learning-driven HVAC optimization, achieving energy savings of 15-25% while improving occupant satisfaction [9], [10]. However, these systems typically rely on limited sensor inputs and simplified comfort models that

may not capture the complex relationships between environmental conditions, physiological responses, and individual thermal preferences [11].

Despite growing interest in personalized building automation, significant research gaps remain in developing robust, scalable comfort prediction models. Existing approaches often analyze environmental and physiological data streams in isolation, failing to leverage the synergistic effects of multimodal sensor fusion [12]. Additionally, most studies focus on laboratory conditions with homogeneous participant groups, limiting the generalizability of findings to diverse real-world applications [13]. Machine learning techniques show promise for addressing these challenges, with recent studies demonstrating successful applications of artificial neural networks and ensemble methods for thermal comfort prediction [14-15]. However, most existing models rely on limited feature sets and lack comprehensive integration of physiological monitoring data [16-17]. This study addresses these limitations by developing and evaluating machine learning models that integrate environmental monitoring with physiological sensing for accurate, personalized thermal comfort prediction. The primary objective is to demonstrate the feasibility of implementing such systems in smart buildings to achieve simultaneous improvements in energy efficiency and occupant satisfaction through advanced sensor fusion and explainable AI techniques [18-20].

## 2. Materials and Methods

This study employed a controlled experimental approach to develop and validate machine learning models for personalized thermal comfort prediction. The methodology integrates multimodal sensor data collection, advanced data preprocessing, and ensemble learning techniques to create a robust classification system capable of predicting individual thermal preferences across diverse environmental conditions. The overall system architecture is illustrated in Figure 1, showing the integration of multimodal sensors, data processing, and machine learning components.

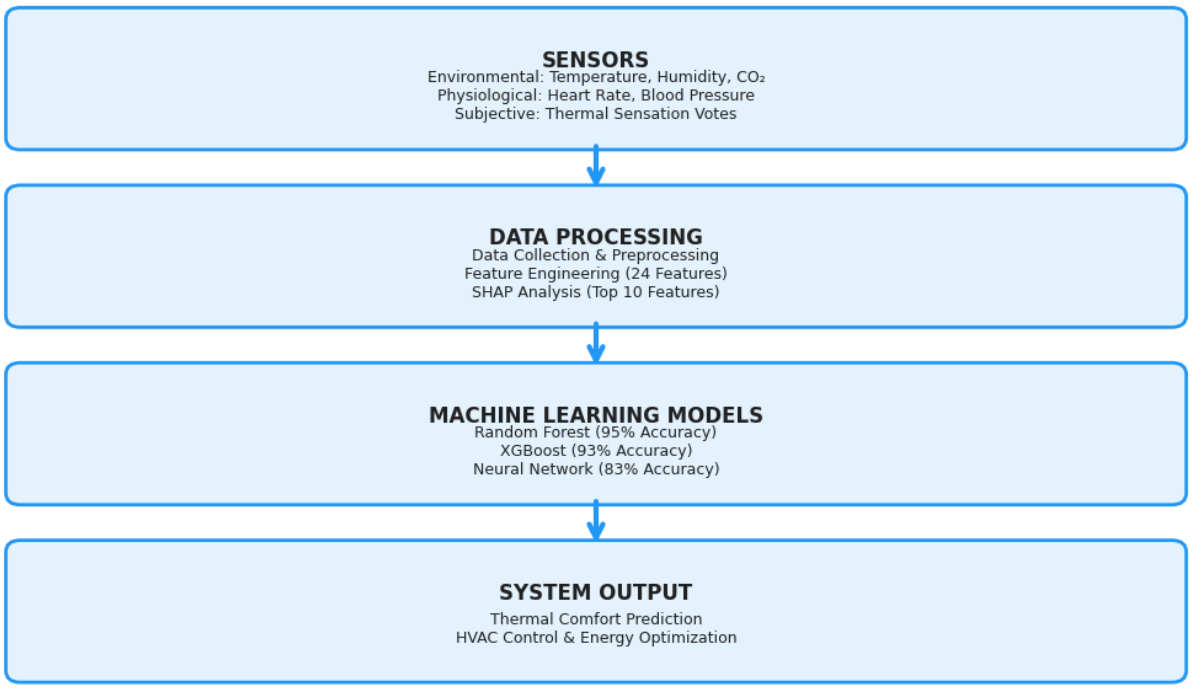


**Figure 1 –** System architecture for personalized thermal comfort prediction.

*2.1. Experimental Setup and Data Collection*

Eight healthy male volunteers aged 18-23 years (mean BMI: 24.1 ± 4.2 kg/m²) participated in controlled thermal comfort experiments conducted in a purpose-built laboratory facility. The experimental protocol was designed to expose participants to systematic thermal discomfort conditions while continuously monitoring both environmental parameters and physiological responses. All participants provided informed consent and wore standardized clothing (T-shirt and trousers) to maintain consistent thermal insulation throughout the experiments.

The laboratory setup consisted of two isolated chambers: a baseline comfort room maintained at 21-22°C with $CO_2$ levels of 500-1000 ppm, and an experimental room where thermal conditions were systematically varied. Four distinct experimental scenarios were implemented: cold discomfort (14-16°C) with moderate $CO_2$ (500-1200 ppm), cold discomfort with elevated $CO_2$ (1500+ ppm), hot discomfort (30-32°C) with moderate $CO_2$, and hot discomfort with elevated $CO_2$. Each experimental session comprised a 12-minute baseline phase followed by four 36-minute exposure trials corresponding to these conditions.

Environmental and physiological data were collected using a comprehensive sensor network integrated through a centralized monitoring system. Environmental parameters included air temperature, relative humidity, $CO_2$ concentration, and outdoor temperature, measured continuously at 1 Hz sampling rate using calibrated sensors (Xiaomi Qingping Air Monitor systems with ±0.3°C temperature accuracy and ±50 ppm $CO_2$ precision). Physiological monitoring encompassed heart rate variability via Polar H10 chest strap monitors, blood pressure measurements using automated upper-arm cuffs, and blood oxygen saturation through fingertip pulse oximeters. Participants provided thermal sensation votes every six minutes using the standard ASHRAE seven-point scale (-3: cold to +3: hot), synchronized with physiological measurements to ensure temporal alignment of all data streams.

**Table 1** – Sensor specifications and measurement parameters.

| Parameter Type | Sensors Used | Measurements | Accuracy | Sampling Rate |
|---|---|---|---|---|
| Environmental | Xiaomi Qingping CGS2 Pro | Temperature, Humidity, $CO_2$, PM2.5 | ±0.3°C, ±3% RH, ±50 ppm | 1 Hz |
| | Aqara Temperature & Humidity Sensor | Temperature, Humidity, Pressure | ±0.3°C, ±3% RH, ±0.12 kPa | 1 Hz |
| Physiological | Polar H10 Heart Rate Monitor | Heart rate, HRV metrics | ±1 bpm, ECG-comparable | 1 Hz |
| | Automated Blood Pressure Cuff | Systolic/Diastolic pressure | ±3 mmHg | Per trial |
| | Fingertip Pulse Oximeter | Blood oxygen saturation | ±2% | 1 Hz |

*2.2. Data Processing and Feature Engineering*

Raw sensor data underwent systematic preprocessing to address temporal misalignment and varying sampling frequencies across different measurement systems. High-frequency environmental signals were processed using windowed averaging to reduce noise and harmonize sampling rates, while sparsely sampled physiological parameters (blood pressure, oxygen saturation) were interpolated using piecewise cubic splines to maintain signal continuity. This approach preserved essential signal characteristics while enabling integration across diverse data streams.

Feature extraction generated 24 distinct variables encompassing environmental conditions (temperature, humidity, $CO_2$, outdoor temperature), heart rate variability metrics (AVNN, SDNN, rMSSD, pNN50, LF, HF, LF/HF ratio, Alpha_1), physiological parameters (heart rate, blood pressure, oxygen saturation), anthropometric characteristics (age, BMI, weight, body composition), and subjective thermal sensation votes. All features were normalized using min-max scaling according to Equation (1) to ensure consistent input ranges for machine learning algorithms:

$$x' = (x - x\_min) / (x\_max - x\_min) \quad (1)$$

The final dataset comprised 1,536 samples with complete feature vectors, randomly partitioned into

training (1,148 samples), testing (288 samples), and validation (100 samples) subsets using stratified sampling to maintain class distribution across thermal sensation categories.

*2.3. Machine Learning Models and Evaluation*

Three advanced classification algorithms were implemented and compared for thermal comfort prediction: Random Forest, XGBoost, and Artificial Neural Network. Random Forest employed ensemble decision trees with bootstrap aggregation to enhance generalization and reduce overfitting. XGBoost utilized gradient boosting with regularization techniques for optimized performance and computational efficiency. The neural network architecture featured five fully connected layers (256, 128, 64, 64, 32 neurons) with batch normalization, ReLU activation, and 30% dropout, trained using Adam optimizer with 0.001 learning rate and cross-entropy loss function.

Hyperparameter optimization was conducted through exhaustive grid search combined with 10-fold stratified cross-validation. Model performance evaluation employed standard classification metrics including accuracy, precision, recall, and F1-score, computed both per-class and macro-averaged across all seven thermal sensation levels. Model interpretability was achieved through SHAP (SHapley Additive exPlanations) analysis, which quantifies individual feature contributions to predictions using cooperative game theory principles:

$$\phi_i = \sum_{S \subseteq N \{i\}} |S|!\,(|N| - |S| - 1)!\,|N|!\left[f_{S\cup\{i\}}\left(x_{S\cup\{i\}}\right) - f_S(x_S)\right] \tag{2}$$

where $\varphi_{\mathrm{i}}$ represents the SHAP value for feature $i$, $N$ is the complete feature set, $S$ denotes feature subsets, and $f$ represents the model's expected output. This analysis identified the most influential predictors and enabled dimensionality reduction by retraining models using only the top-ranked features, thereby improving both computational efficiency and model interpretability for practical deployment scenarios.

## 3. Results

The machine learning models were evaluated through comprehensive performance analysis, feature importance assessment, and independent validation to determine their suitability for practical thermal comfort prediction applications. The results demonstrate significant potential for accurate personalized climate control in smart building environments.

*3.1. Model Performance Comparison*

The experimental dataset yielded 1,536 complete samples with 24 features each, which were systematically evaluated across three machine learning algorithms. Initial model training on the full feature set demonstrated strong predictive performance across all approaches, with XGBoost achieving the highest accuracy of 91%, followed closely by Random Forest at 90% and the Artificial Neural Network at 89%. All models showed robust performance in distinguishing between the seven thermal sensation levels, with macro-averaged F1-scores ranging from 0.88 to 0.90.

Feature importance analysis through SHAP revealed that dimensionality reduction significantly enhanced ensemble model performance while reducing computational requirements. When retrained using only the top 10 most influential features, Random Forest accuracy improved from 90% to 94%, and XGBoost performance increased from 91% to 93%. The threshold of ten features was selected based on the SHAP summary analysis, which revealed a distinct 'elbow point' in feature importance distributions; features ranked below this threshold provided negligible predictive gain while increasing computational complexity. Conversely, the neural network showed decreased performance (89% to 83%), suggesting greater dependency on feature interactions that were lost during dimensionality reduction. Based on superior performance after feature selection, the Random Forest model was selected for final validation using 10 selected features and was subsequently validated on an independent hold-out dataset of 100 samples, achieving a final accuracy of 95% with macro-averaged F1-score of 0.939.

**Table 2** – Comparative performance of machine learning models for thermal comfort prediction.

| Model | Full Dataset (24 features) | | Reduced Dataset (10 features) | | Accuracy Change |
|---|---|---|---|---|---|
| | Accuracy | F1-Score | Accuracy | F1-Score | |
| Random Forest | 0.90 | 0.89 | 0.94 | 0.94 | +4% |
| XGBoost | 0.91 | 0.90 | 0.93 | 0.92 | +2% |
| Neural Network | 0.89 | 0.88 | 0.83 | 0.80 | -6% |

*3.2. Feature Importance Analysis*

SHAP analysis identified indoor air temperature as the dominant predictor across all models, exhibiting approximately 2-3 times greater influence than any other single feature (Figure 2). The top five most influential parameters consistently included environmental factors (temperature, humidity, $CO_2$ concentration, outdoor temperature) and one physiological parameter (diastolic blood pressure). While all three models showed similar feature ranking patterns, the Random Forest model demonstrated the most stable performance improvement with reduced features, making it the optimal choice for deployment. Environmental parameters dominated the feature rankings, with indoor temperature alone accounting for approximately 30-35% of the total predictive power.

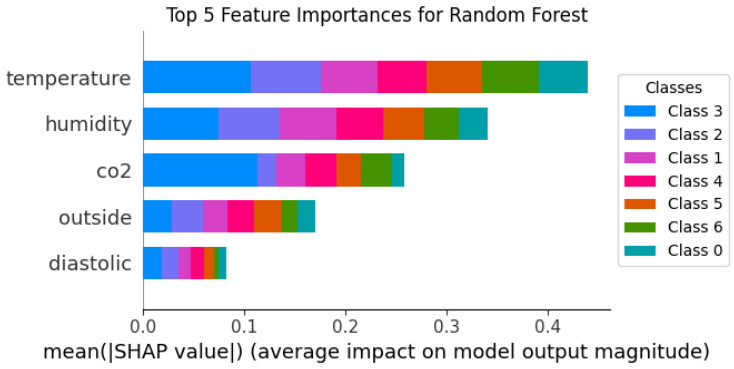


**Figure 2** – Feature importance ranking for thermal comfort prediction based on SHAP analysis.

*3.3. Model Validation and Practical Performance*

The selected Random Forest model (chosen based on its superior performance with reduced features) demonstrated excellent classification performance with minimal misclassification errors. Analysis of the confusion matrix revealed that all prediction errors occurred between adjacent thermal sensation categories (e.g., confusing "neutral" with "slightly cool"), indicating that the model captures the underlying thermal comfort continuum effectively. No instances of extreme misclassification (e.g., predicting "hot" when actual sensation was "cold") were observed, suggesting robust model behavior suitable for practical HVAC control applications.

Final validation on the independent test set confirmed the model's generalization capability, achieving 95% accuracy with perfect classification of neutral and hot thermal sensations. The five misclassifications that occurred were exclusively between neighboring comfort levels, demonstrating that the system maintains reliable performance even on completely unseen data. These results indicate strong potential for real-world deployment in smart building systems, where such accuracy levels would enable precise climate control while minimizing energy waste through unnecessary heating or cooling adjustments. The classification performance is visualized in Figure 3, which shows the confusion matrix for the best-performing model.

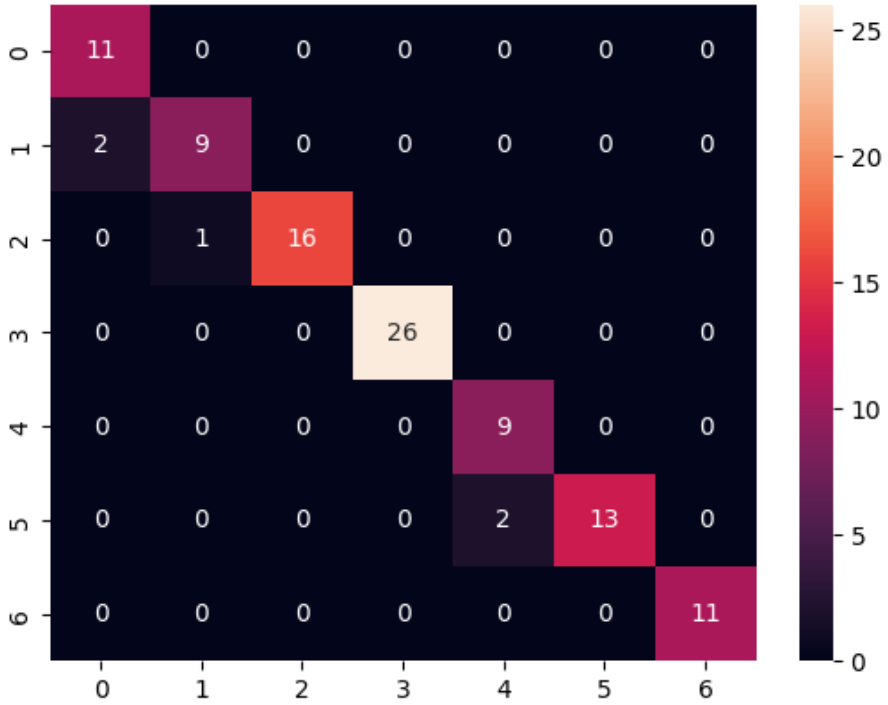


**Figure 3 –** Confusion matrix for optimized Random Forest model showing 95% accuracy on independent validation dataset. Perfect classification achieved for neutral and hot sensations, with remaining errors limited to adjacent categories.

## 4. Discussion

The results demonstrate that machine learning approaches can effectively predict personalized thermal comfort with high accuracy, achieving performance levels suitable for practical smart building applications. The 95% accuracy obtained by the optimized Random Forest model represents a significant advancement over traditional static HVAC control systems, which typically achieve occupant satisfaction rates of only 70-80% [5].

The dominance of indoor air temperature as the primary predictor aligns with established thermal comfort theory, while the significant contribution of humidity and $CO_2$ concentration highlights the importance of comprehensive environmental monitoring. Notably, the relatively modest influence of heart rate variability parameters challenges previous research emphasis on HRV-based comfort assessment, suggesting that when comprehensive environmental and physiological data are available, HRV provides complementary rather than primary predictive information.

The superior performance of ensemble methods (Random Forest and XGBoost) over neural networks, particularly after dimensionality reduction, indicates that thermal comfort prediction benefits more from robust feature selection than complex nonlinear transformations. The superior performance of ensemble methods over neural networks is also attributable to the dataset size (1,536 samples). Deep learning architecture typically requires significantly larger data volumes to establish complex feature representations and avoid overfitting, whereas ensemble tree-based algorithms demonstrated superior robustness on this tabular dataset. This finding has practical implications for deployment in resource-constrained building automation systems, where computational efficiency is crucial.

### *4.1. Limitations*

While the proposed system demonstrates high predictive accuracy, it is important to acknowledge certain limitations regarding participant demographics. The experimental data was collected exclusively from healthy male participants aged 18–23 years. Since thermal comfort perception is known to vary significantly across gender, age groups, and metabolic rates, the current model may not immediately generalize to broader populations, such as females or elderly occupants. Practical

deployment in diverse environments would require transfer learning strategies or expanded data collection to adapt the model to these specific demographic groups.

## 5. Conclusions

This study successfully demonstrated the feasibility of accurate personalized thermal comfort prediction using machine learning and multimodal sensor fusion. The optimized Random Forest model achieved 95% accuracy using only 10 key features, with indoor air temperature identified as the dominant predictor. The system shows strong potential for integration into smart building automation, enabling dynamic climate control that adapts to individual preferences while optimizing energy consumption. Future work should focus on expanding participant diversity and implementing real-time HVAC control systems to validate energy savings potential in operational buildings.

## Funding

This research was funded by the Committee of Science of the Ministry of Science and Higher Education of the Republic of Kazakhstan (Grant No. AP23488794).

## Author Contributions

Conceptualization, A.B. and B.A.; Methodology, A.B.; Software, A.B.; Validation, A.B. and B.A.; Formal Analysis, A.B.; Investigation, A.B.; Resources, B.A.; Data Curation, A.B.; Writing – Original Draft Preparation, A.B.; Writing – Review & Editing, A.B. and B.A.; Visualization, A.B.; Supervision, B.A.; Project Administration, B.A.; Funding Acquisition, B.A.

## Conflicts of Interest

The authors declare no conflict of interest.

## References

1. International Energy Agency, "Energy Efficiency in Buildings: Technology Roadmap," IEA Publications, Paris, France, 2023. [Online]. Available: https://www.iea.org/reports/energy-efficiency-in-buildings
2. D. Clements-Croome, "Creating the Productive Workplace: Places to Work Creatively," 3rd ed. London, UK: Routledge, 2018, doi: 10.4324/9781315693842.
3. ASHRAE Standard 55-2020, "Thermal Environmental Conditions for Human Occupancy," American Society of Heating, Refrigerating and Air-Conditioning Engineers, Atlanta, GA, USA, 2020.
4. P. O. Fanger, "Thermal Comfort: Analysis and Applications in Environmental Engineering," Danish Technical Press, Copenhagen, Denmark, 1970.
5. S. Karjalainen, "Thermal comfort and gender: A literature review," *Indoor Air*, vol. 22, no. 2, pp. 96-109, Apr. 2012, doi: 10.1111/j.1600-0668.2011.00747.x.
6. J. Kim, R. Schiavon, and G. Brager, "Personal comfort models – A new paradigm in thermal comfort for occupant-centric environmental control," *Building and Environment*, vol. 132, pp. 114-124, Mar. 2018, doi: 10.1016/j.buildenv.2018.01.023.
7. A. Ghahramani, C. Tang, and B. Becerik-Gerber, "An online learning approach for quantifying personalized thermal comfort via adaptive stochastic modeling," *Building and Environment*, vol. 92, pp. 86-96, Oct. 2015, doi: 10.1016/j.buildenv.2015.04.017.
8. W. Wang, J. Chen, T. Hong, and N. Zhu, "Occupancy prediction through Bluetooth beacon technology in commercial buildings," *Energy and Buildings*, vol. 203, pp. 109463, Nov. 2019, doi: 10.1016/j.enbuild.2019.109463.
9. B. Dong, D. Prakash, F. Feng, and Z. O'Neill, "A review of smart building sensing system for better indoor environment control," *Energy and Buildings*, vol. 199, pp. 29-46, Sep. 2019, doi: 10.1016/j.enbuild.2019.06.025.
10. T. Chaudhuri, Y. C. Soh, H. Li, and L. Xie, "A feedforward neural network based indoor-climate control framework for thermal comfort and energy saving in buildings," *Applied Energy*, vol. 248, pp. 44-53, Aug. 2019, doi: 10.1016/j.apenergy.2019.04.065.
11. C. Miller, Z. Nagy, and A. Schlueter, "A review of unsupervised statistical learning and visual analytics techniques applied to performance analysis of non-residential buildings," *Renewable and Sustainable Energy Reviews*, vol. 81, pp. 1365-1377, Jan. 2018, doi: 10.1016/j.rser.2017.05.124.
12. M. Földváry Ličina, T. Cheung, H. Zhang, R. de Dear, T. Parkinson, E. Arens, C. Chun, S. Schiavon, M. Luo, G. Brager, P. Li, S. Kaam, M. A. Adebamowo, M. M. Andamon, F. Babich, C. Bouden, H. Bukovianska, C. Candido, B. Cao, S. Carlucci, D. K. W. Chow, S. Damiati, L. Ding, S. Domjan, S. Gauthier, S. Godithi, H. He, D. Heidari, C. Inard, J. Jin, H. Khattar, J. Kim, M. Kong, M. K. Singh, A. Kwok, R. Lamberts, M. Laska, K. C. Parsons, N. C. Popiolek, S. Rupp, R. Sakulpipatsin, M. Schweiker, M. Standeven, R. A. Stanton, S. Tanabe, K. W. Tham, D. Tian, L. Weiss, Z. Wen, T. Xu, Y. Zhai, Y. Zhang, X. Zhou, B. Zhu, and L. Zhu, "Development of the ASHRAE Global Thermal Comfort Database II," *Building and Environment*, vol. 142, pp. 502-512, Oct. 2018, doi: 10.1016/j.buildenv.2018.06.022.
13. R. Kosonen and F. Tan, "The effect of perceived indoor air quality on productivity loss," *Energy and Buildings*, vol. 36, no. 10, pp. 981-986, Oct. 2004, doi: 10.1016/j.enbuild.2004.06.005.

14. Z. Wang, L. Zhang, J. Zhao, and Y. He, "Thermal comfort modeling using machine learning algorithms and environmental monitoring in office buildings," *Applied Energy*, vol. 285, pp. 116450, Mar. 2021, doi: 10.1016/j.apenergy.2021.116450.

15. H. B. Gunay, W. O'Brien, I. Beausoleil-Morrison, and S. Gilani, "Development and implementation of an adaptive lighting and blinds control algorithm," *Building and Environment*, vol. 113, pp. 185-199, Feb. 2017, doi: 10.1016/j.buildenv.2016.08.027.

16. Y. Zhou, J. Yu, X. Luo, and C. Cheng, "A comprehensive review of machine learning techniques for thermal comfort prediction in buildings," *Renewable and Sustainable Energy Reviews*, vol. 150, pp. 111435, Oct. 2021, doi: 10.1016/j.rser.2021.111435.

17. S. P. Corgnati, M. Filippi, and S. Vialli, "Perception of the thermal environment in high school and university classrooms: Subjective preferences and thermal comfort," *Building and Environment*, vol. 42, no. 2, pp. 951-959, Feb. 2007, doi: 10.1016/j.buildenv.2005.10.027.

18. L. T. Wong and K. N. K. Fong, "Thermal comfort evaluation of naturally ventilated public housing in Hong Kong," *Building and Environment*, vol. 46, no. 12, pp. 2405-2414, Dec. 2011, doi: 10.1016/j.buildenv.2011.06.002.

19. M. Schweiker, F. Haldi, M. Shukuya, and D. Robinson, "Verification of stochastic models of window opening behaviour for residential buildings," *Journal of Building Performance Simulation*, vol. 5, no. 1, pp. 55-74, Jan. 2012, doi: 10.1080/19401493.2011.567422.

20. S. M. Lundberg and S. I. Lee, "A unified approach to interpreting model predictions," in *Proceedings of the 31st International Conference on Neural Information Processing Systems*, Long Beach, CA, USA, Dec. 2017, pp. 4768-4777.

***Information About Authors***

*Bibars Amangeldy – Researcher, DigitAlem LLP, Almaty, Kazakhstan. ORCID iD: 0000-0002-4089-6337*

*Bauyrzhan Abilda – Researcher, Astana International University, Astana, Kazakhstan. ORCID iD: 0009-0007-9758-9657.*

*Submission received: 22 August, 2025.*
*Revised: 17 December, 2025.*
*Accepted: 17 December, 2025.*

IRSTI 20.53.23 https://doi.org/10.26577/jpcsit202544

**Yedil Nurakhov , Duman Marlambekov***

Al-Farabi Kazakh National University, Almaty, Kazakhstan
*e-mail: marlambekov_duman@live.kaznu.kz

# IMPLEMENTATION OF A REPRODUCIBLE 5G STANDALONE TESTBED USING OPEN-SOURCE COMPONENTS

**Abstract.** Deploying a 5G Standalone (SA) network is often constrained by cost, complexity, and limited access to RF hardware. This paper describes a practical, software-defined 5G SA implementation assembled entirely from open-source components Open5GS for the 5G Core, srsRAN for gNB and UE, MongoDB for subscriber data, and ZeroMQ for RF emulation to enable end-to-end connectivity without radios. The blueprint details service initialization order, subscriber provisioning, and configuration alignment across PLMN, TAC, DNN, and key material, followed by validation of UE registration, PDU session establishment, and user-plane data transfer. On the reference setup, the system achieves low round-trip latency (≈1.34 ms), high throughput (≈847 Mbps TCP downlink and ≈823 Mbps uplink), and rapid PDU session setup (≈0.22 s), supporting repeatable functional and performance testing in a laboratory environment. The described approach lowers the barrier to 5G experimentation for teaching, prototyping, and research while providing a reproducible path from basic bring-up to performance evaluation. Limitations include the use of emulated RF and a single-cell scenario; nevertheless, the workflow can be extended to over-the-air SDR tests, mobility, and slicing when needed.

**Keywords:** 5G Standalone, Open5GS, srsRAN, RF emulation, testbed, performance evaluation, open-source network.

## 1. Introduction

Standalone 5G (5G SA) replaces LTE-anchored non-standalone with a cloud-native, service-based architecture designed for flexible control/user-plane separation, network slicing, and low-latency paths. Recent surveys and white papers outline this architectural shift and its deployment implications for private and research networks, emphasizing software-defined components and standards-aligned interfaces [1], [2]. In parallel, open-source 5G cores and RAN stacks have matured, enabling end-to-end SA systems on commodity hardware; comparative evaluations and multi-testbed studies report viable control- and user-plane performance across diverse configurations and toolchains [3]–[5].

Practical experience reports and platform blueprints document repeatable bring-up steps–subscriber provisioning, configuration alignment (PLMN/TAC/DNN/keys), and initialization order–together with troubleshooting guidance for device and software compatibility in SA testbeds [6], [7]. Cloud-native deployments with integrated monitoring (e.g., Prometheus/Grafana) demonstrate over-the-air operation and lifecycle observability for core functions and radio metrics, helping practitioners detect regressions and verify changes methodically [8]. Beyond single-vendor stacks, multi-vendor O-RAN testbeds highlight programmability and performance profiling under realistic workloads, while emulation frameworks provide RF-free environments for controlled, automated experimentation when spectrum or SDRs are constrained [9], [10]. Side-by-side assessments of SDR-based RAN options further inform trade-offs in throughput, latency, and ease of deployment for academic and industrial laboratories [11].

Operational topics central to private 5G–slicing, KPI instrumentation, and application integration–are increasingly addressed using open components. Demonstrations show automated slice provisioning and real-time KPI collection in SA testbeds, supporting end-to-end evaluation under varied policies and traffic mixes [12], [13]. Complementary case studies describe full open-source SA deployments for UE validation and application testing, while contemporaneous analyses examine security considerations specific to open-source 5G cores–issues that must be reflected in lab practices and baseline hardening steps [14], [15].

Despite this progress, teams seeking to stand up a reproducible, software-only 5G SA environment still face fragmented guidance and version-sensitive pitfalls. Documentation is often scattered across

project wikis and papers; configuration alignment across core and RAN (PLMN, TAC, DNN, key material) remains error-prone; and many reports assume SDR hardware or preexisting spectrum access. Even when results are reported, procedures for first-time bring-up, fault isolation, and baseline validation are seldom presented as a single, testable checklist. Prior evaluations establish feasibility and performance envelopes [3]–[5], while deployment notes identify recurring integration challenges [6], [7], and emulation frameworks suggest viable RF-free paths [10]; yet newcomers still lack a concise "from zero to working SA" blueprint that ties these pieces together.

Existing literature either (i) surveys architecture and capabilities at a high level [1], [2], (ii) benchmarks particular stacks or compare testbeds without prescribing a step-by-step, minimal-hardware recipe [3]–[5], or (iii) dives into specialized topics–monitoring, O-RAN, or emulation–without consolidating the exact sequencing, configuration checks, and validation tasks needed for a repeatable, RF-free SA bring-up [8]–[10]. What is missing is an integrated, implementation-oriented guide that: (a) enumerates configuration alignment across core and RAN; (b) defines a minimal, commodity-hardware bill-of-materials; (c) specifies an ordered startup procedure with verifiable checkpoints; and (d) provides a compact functional/performance smoke test that laboratories can reproduce consistently. The present paper addresses this gap by offering a practical blueprint and validation flow tailored to resource-constrained environments, while remaining compatible with slicing and KPI instrumentation methods already demonstrated in prior work [12], [13].

## 2. Materials and Methods

### *2.1. System Architecture and Implementation Framework*

This study adopts a thorough software-defined methodology to design and assess a full 5G Standalone network using open-source tools within a virtualized testing environment. The approach is organized around a multi-layered architecture comprising three main areas: the Radio Access Network (RAN) layer, which is implemented via the srsRAN Project for gNodeB capabilities and srsRAN 4G for simulating User Equipment; the 5G Core Network layer that utilizes the Open5GS framework along with MongoDB for managing subscriber data; and the RF simulation layer that employs the ZeroMQ message queuing library to remove the need for physical radio hardware while preserving realistic protocol interactions.

The proposed testbed integrates core network functions, radio access capabilities, database support, and management tools into a reproducible software-defined environment. Table 1 presents the complete list of components, their software versions, functional roles, and distinctive features.

**Table 1 –** Software components of the 5G SA testbed.

| Component | Software/Version | Role in Testbed | Notes |
|---|---|---|---|
| Core Network | Open5GS | Implements 5GC (AMF, SMF, UPF, NRF, UDM, AUSF) | Service-based architecture |
| RAN | srsRAN Project | Provides gNB (CU/DU split) | Supports ZeroMQ interface |
| UE Emulator | srsRAN 4G | Simulated UEs | Runs in Linux namespaces |
| Database | MongoDB 6.0 | Subscriber data | Replica set enabled |
| WebUI | Open5GS WebUI | Subscriber management | Built with Node.js |
| RF Emulation | ZeroMQ libraries | I/Q sample exchange | RF-free operation |

### *2.2. srsRAN Dual-Architecture Implementation*

The srsRAN framework utilizes a dual-architecture model, merging the srsRAN Project for 5G gNodeB capabilities with srsRAN 4G for enhanced User Equipment simulation features. The most recent stable release of the srsRAN Project encompasses a full 5G NR implementation, which includes functionalities for gNB, CU (Central Unit), and DU (Distributed Unit), while supporting both standalone and non-standalone deployment options. The compilation setup allows for ZeroMQ integration with the parameter -DENABLE_ZEROMQ=ON and also provides export functionality through -DENABLE_EXPORT=ON, enabling external ap-

plications to interface with internal protocol stack operations. The build process incorporates optimized SIMD (Single Instruction, Multiple Data) operations to improve DSP performance and integrates DPDK for improved packet processing efficiency.

The srsRAN framework utilizes a dual-architecture model, merging the srsRAN Project for 5G gNodeB capabilities with srsRAN 4G for enhanced User Equipment simulation features. The most recent stable release of the srsRAN Project encompasses a full 5G NR implementation, which includes functionalities for gNB, CU (Central Unit), and DU (Distributed Unit), while supporting both standalone and non-standalone deployment options. The compilation setup allows for ZeroMQ integration with the parameter -DENABLE_ZEROMQ=ON and also provides export functionality through -DENABLE_EXPORT=ON, enabling external applications to interface with internal protocol stack operations. The build process incorporates optimized SIMD (Single Instruction, Multiple Data) operations to improve DSP performance and integrates DPDK for improved packet processing efficiency.

The integration of MongoDB database (version 6.0 and above) offers persistent storage for subscriber information, featuring a replica set configuration to ensure high availability and automatic failover functionalities. The database schema employs data models compliant with 3GPP that include subscriber profiles, authentication vectors, and session contexts, while also supporting atomic transactions to maintain data consistency amidst concurrent operations. The management interface of the WebUI is built on the Node.js runtime (version 20+) using the Express.js framework, which delivers RESTful API endpoints for subscriber provisioning, network monitoring, and configuration management. This interface incorporates role-based access control through JWT token authentication and provides real-time status updates via WebSocket connections.

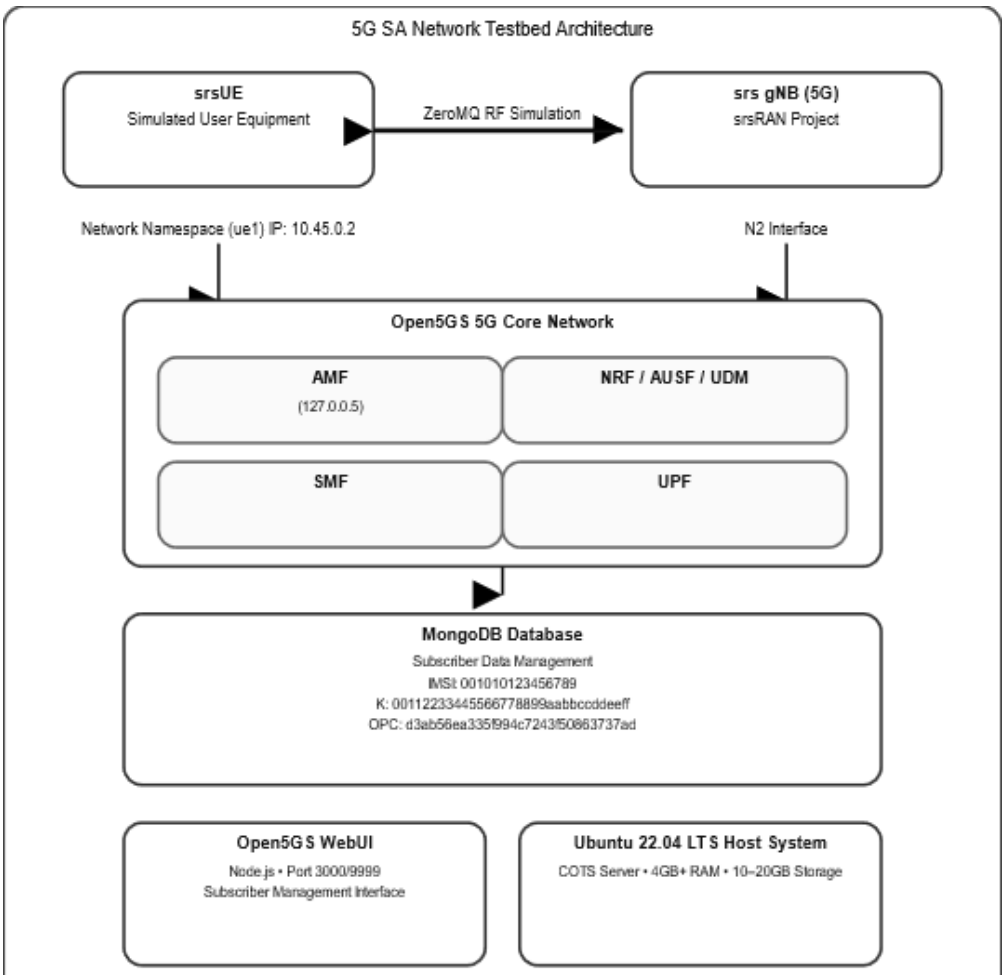


**Figure 1 –** 5G SA Netwotk Testbed Architecture

*2.3. Database and Core Network Initialization*

The execution of the experiment begins with the initialization of the MongoDB database, which involves setting up a replica set for high availability and automated failover features. The procedure for starting the database includes creating indexes to enhance subscriber lookup efficiency, implementing collection sharding for improved scalability, and activating an authentication mechanism.

Next, the activation of Open5GS core network services is conducted following a hierarchical dependency framework, beginning with the initialization of the NRF (Network Repository Function) to enable service discovery. This is succeeded by the AUSF (Authentication Server Function) and UDM (Unified Data Management) to establish the authentication infrastructure, followed by the AMF (Access and Mobility Management Function) and SMF (Session Management Function) for control plane operations, and concluding with the UPF (User Plane Function) responsible for data forwarding.

The gNB startup process establishes automatic registration with the AMF via the N2 interface by setting up an SCTP association and using NGAP signaling procedures. The configuration of the gNB encompasses cell parameters such as the Physical Cell Identity (PCI), parameters for broadcasting System Information Blocks (SIB), and the configuration for the Random Access Channel (RACH).

To prevent interference with the host system's networking and to facilitate multiple UE simulation scenarios, the initialization of the UE utilizes Linux network namespace isolation. The process of creating network namespaces includes configuring interfaces, setting up routing tables, and implementing iptables rules for isolating traffic. The registration procedure for the UE employs the 5G-AKA authentication protocol for mutual authentication between the UE and the network, which is followed by the establishment of NAS (Non-Access Stratum) security modes and the creation of PDU sessions. The success of the registration is confirmed through various checkpoints, including the completion of the RACH procedure with observed preamble transmission power, the establishment of RRC connections with signal quality metrics, and validation of the authentication vector through cryptographic methods.

*2.3.1.Performance Validation and Connectivity Testing*

Performance verification is carried out through detailed validation checkpoints, assessing both control plane and user plane functionalities. The Random Access procedure examination evaluates preamble detection likelihood, accuracy in timing advance, and efficiency in uplink grant distribution. The verification of RRC connection establishment involves measuring signal-to-noise ratios, reporting channel quality indicators, and validating mobility management.

Testing for PDU session activation verifies end-to-end connectivity by performing ICMP ping tests within the UE network namespace, analyzing round-trip latency, packet loss rates, and jitter characteristics. The validation approach also includes throughput testing using the iperf3 tool to evaluate TCP and UDP performance, measuring maximum achievable data rates, TCP window scaling behavior, and UDP packet loss under various load scenarios. Performance metrics collection entails monitoring CPU utilization, tracking memory usage, and analyzing network interface statistics to ensure system stability throughout the testing period.

The evaluation approach incorporates both qualitative and quantitative assessment criteria, concentrating on successful component integration verification through build completion status and version compatibility checks, as well as measuring network function registration success rates via AMF and NRF interface monitoring. The UE attachment success ratio is calculated from the time taken from registration attempts to IP allocation completion, and data plane connectivity is assessed through round-trip time measurements and packet loss analysis during ping operations. The experimental framework also includes monitoring resource utilization, such as CPU usage during the simultaneous operation of all network functions, memory consumption patterns during peak signaling loads, and assessing system stability through prolonged operational periods to validate the sustainability of the software-defined 5G SA implementation for research and educational purposes.

## 3. Results

*3.1. Network deployment and Open5GS configuration*

The deployment of the 5G Standalone (SA) network was accomplished using the combined srsRAN project and Open5GS architecture on the Ubuntu 22.04 platform. All essential components were compiled from their source code and set up to function in a connected mode. The setup achieved comprehensive end-to-end connectivity starting from the user equipment (UE) through the gNodeB

to the 5G Core network functions.

The system architecture illustrated the successful incorporation of seven core components: UHD (USRP hardware driver), ZeroMQ libraries (libzmq and czmq), srsRAN project (gNB), srsRAN 4G (UE), Open5GS core network, MongoDB database, and a web management interface. The functionality of the Open5GS core network was validated by accessing its web management interface (WebUI), as depicted in Figure 2, where login was completed successfully using the administrator credentials. The screenshot displays the login page of the Open5GS WebUI, which includes fields for the Username and Password input along with the Login button.

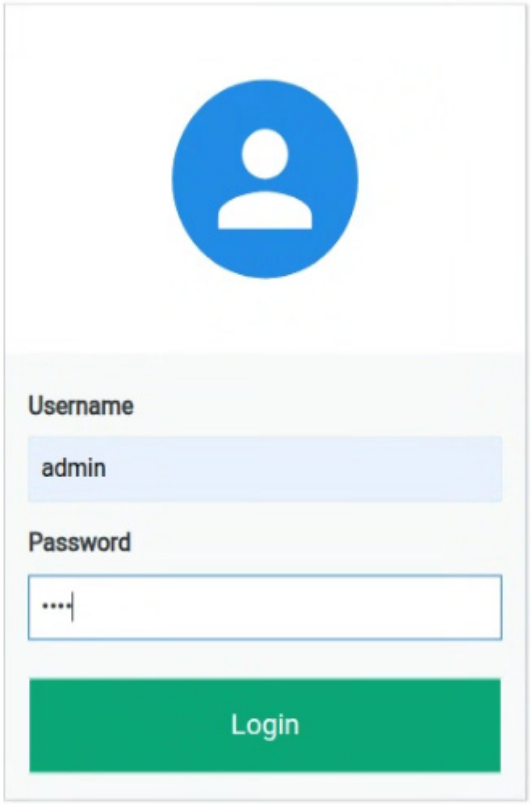


**Figure 2 –** Open5GS WebUI login page

A pivotal feature of the Open5GS core is its extensive subscriber management, facilitated by an integrated WebUI. As illustrated in Figures 3, 4, and 5, the interface offers detailed control over essential subscriber parameters, encompassing IMSI, cryptographic keys (K, OPc), and slice configurations through DNN provisioning. This capability is crucial for swift prototyping and iterative testing in a research setting, enabling flexible and prompt adjustments of user profiles without needing to manipulate the database directly.

A key aspect of establishing the network core involved provisioning the subscriber. Figure 3 displays the form used for subscriber creation in the Open5GS WebUI. This form marks the beginning of the UE provisioning process, where the administrator inputs the required information, including the mandatory fields for IMSI, subscriber key (K), AMF, USIM type (e.g., OPc), operator key (OP/OPc), and bandwidth parameters (UE-AMBR DL/UL), along with slice configurations via the DNN/APN adding interface. The form includes control buttons “CANCEL” and “SAVE,” as well as the flexibility to configure subscriber profiles. This phase demonstrates that Open5GS WebUI delivers a comprehensive mechanism for manual management of the subscriber database.

Figure 4 displays the specifics of the configured subscriber within the Open5GS WebUI. The image presents details about the subscriber with IMSI: 001010123456780, which was chosen from the previous image’s list. The key parameters include: IMEISV (353490069873319), utilized for testing as a phone number; the subscriber key (K: 00112233445566778899aabbccddeeff), employed for authentication; the operator key OPc, which is part of the USIM authentication algorithms; and the AMF (8000) and SQN (64) parameters that are necessary to guard against replay attacks. Notably, the subscriber status is designated as “SERVICE_GRANTED (0)”, signifying approval to access network services. Additionally, it is noted that there are no service access limitations (Operator Determined Barring: 0), UE throughput (1 Gbps DL / 1 Gbps UL), SST cut configuration: 1, DNN: srsapn, IP type: IPv4, and session parameters (5QI: 9, ARP: 8). All of this verifies that the UE is properly configured and prepared to connect.

The status “SERVICE_GRANTED” shown in Figure 5 signifies that provisioning was successful. The configuration files for the various Open5GS components (amf.yaml, nrf.yaml) and srsRAN (gnb_zmq.yaml, ue_zmq.conf) were adjusted to ensure alignment regarding the PLMN ID (“001”/”01”), TAC (7), and the relevant IP addresses for interaction. After all components were initiated, srsUE was able to register in the network through srsgNB, obtaining the IP address 10.45.0.2, which has been verified by srsUE logs and the successful execution of a ping command to this IP address from the UE network namespace. This confirms the proper setup of the PDU session and the functioning of the data plane within the established emulated 5G SA network.

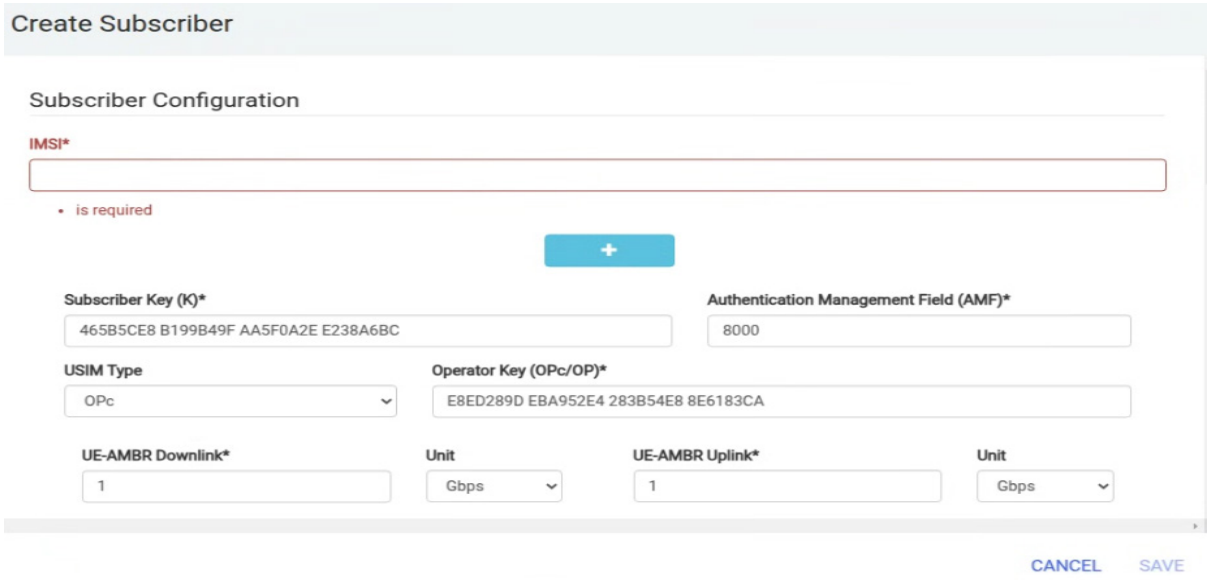


**Figure 3 –** Subscriber creation form in Open5GS WebUI

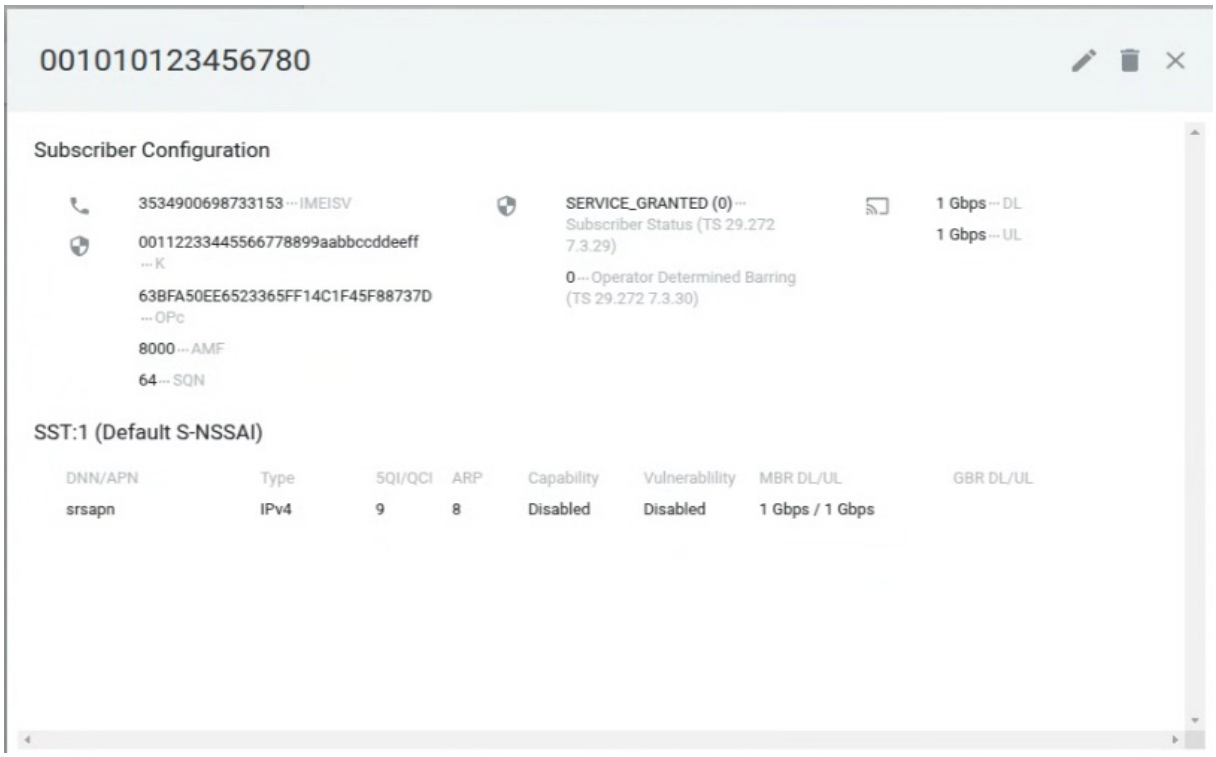


**Figure 4** – Details of the configured subscriber in the Open5GS WebUI

*3.2. Network deployment and Open5GS configuration*

Following the successful setup of the Open5GS network core and the establishment of the subscriber profile, the srsRAN radio access components were initiated to verify the functionality of the 5G network in Standalone mode. The startup logs of srsgNB, illustrated in Figure 6, indicate the proper initialization of the 5G base station (gNB) from the srsRAN_Project. These logs indicate that the gNB

is set up to operate with the emulated ZeroMQ radio interface, as evidenced by the parameters: PCI (Physical Cell ID) = 1, bandwidth = 20 MHz, antenna configuration 1T1R, and frequencies dl_arfcn=368500 (1842.5 MHz) and ul_freq=1747.5 MHz.

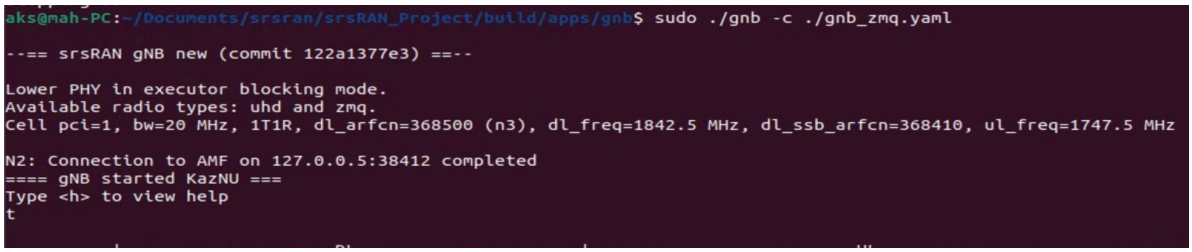


**Figure 6 –** srsgNB startup logs

It is important to focus on the message "N2: Connection to AMF on 127.0.0.5:38412 completed," which signifies that the gNB has successfully connected to the AMF Open5GS via the N2 interface, followed by "=== gNB started ===," which indicates that the base station is prepared to service the UE. Figure 7 illustrates the startup logs from the srsUE user equipment in srsRAN_4G. The logs capture the establishment of the zmq radio interface plugins and confirm the successful reading of the ue_zmq.conf configuration file. Parameters for the ZeroMQ channel are shown, including the IP and TX (127.0.0.1:2001) and RX (127.0.0.1:2000) ports, along with the base sampling frequency.


**Figure 7 –** srsUE user equipment startup logs

The steps for establishing a UE connection include "Attaching UE...", completing the random-access procedure ("Random Access Complete"), establishing the RRC connection ("RRC Connected"), and terminating the session PDU while assigning an IP address ("PDU Session Establishment successful. IP: 10.45.0.2"). This signifies that the UE has successfully registered with the network and obtained an IP address from the Open5GS core. The message "RRC NR reconfiguration successful." is also noted, validating the proper reconfiguration post-session establishment. It's essential to refer to the IP address 10.45.0.2 in the description, as was granted during the successful test. Figure 8 illustrates the confirmation of data transmission ping test directed to the UE's IP address (10.45.0.2), conducted from the ue1 namespace.

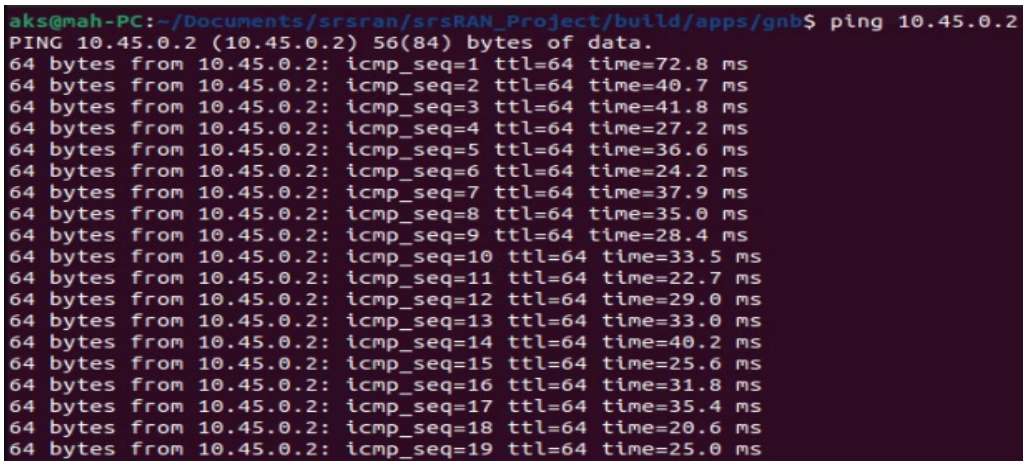


**Figure 8** – Verification of data transfer

Successful ICMP replies ("64 bytes from 10.45.0.2: icmp_seq=...") indicate that the user equipment has successfully registered and obtained an IP address and is also able to participate in the exchange of IP packets. This signifies that the simulated 5G SA network is functioning completely from the user equipment to the core network and back.

## 4. Discussion

The combination of Open5GS, srsRAN (gNB and UE), MongoDB, and a ZeroMQ-based I/Q transport removes the need for SDR hardware while maintaining realistic 5G control- and user-plane procedures. This design enables rapid iteration on core functions (AMF/SMF/UPF/NRF/UDM), subscriber provisioning, and gNB/UE parameters. Successful registration, PDU establishment, and IP packet exchange indicate functional integrity across the full stack.

Measurements on the reference platform indicate low latency, near-gigabit TCP throughput in both directions, and fast PDU setup. These characteristics are consistent with a lightweight, tightly integrated service-based core and streamlined packet-processing path. Because the RF layer is emulated, absolute values are expected to differ under over-the-air conditions with SDRs, fading, and interference; however, the methodology remains applicable for controlled benchmarking and regression testing.

Reliance on widely available open-source software and container-friendly services makes the environment portable across commodity servers and virtualized hosts. Clear sequencing from service discovery and authentication to the user plane along with configuration alignment across PLMN, TAC, DNN, and key material improves repeatability and serves as a checklist for new deployments.

The single-cell, largely static scenario does not exercise mobility, handover, or multi-cell coordination. Emulated RF bypasses channel impairments and spectrum dynamics. Results depend on software versions and host resources. Extending the setup with SDR-based radios, mobility traces, QoS scheduling experiments, and network slicing is recommended to generalize findings.

## 5. Conclusions

A complete, open-source 5G SA environment can be assembled with Open5GS, srsRAN (gNB/UE), MongoDB, and ZeroMQ-based RF emulation to deliver end-to-end connectivity without radios. The reference implementation provides repeatable bring-up, functional verification, and performance characterization with low latency, near-gigabit throughput, and rapid PDU session establishment. The blueprint and configuration checklist lower the barrier for teaching, prototyping, and research, while offering a path to more advanced studies that incorporate SDR-based radio, mobility, slicing, and multi-cell operation.

## Funding

This research was funded by the Committee of Science of the Ministry of Science and Higher Education of the Republic of Kazakhstan (Grant No. BR24993211).

## Author Contributions

Conceptualization, Y.N. and D.M.; Methodology, Y.N.; Software, D.M.; Validation, Y.N.; Formal Analysis, Y.N.; Investigation, D.M.; Resources, Y.N.; Data Curation, D.M.; Writing – Original Draft Preparation, D.M.; Writing – Review & Editing, Y.N.; Visualization, D.M.; Supervision, Y.N.; Project Administration, Y.N.; Funding Acquisition, Y.N.

## Conflicts of Interest

The authors declare no conflict of interest.

### References


1. M. H. Naji, A. G. Wadday, M. M. Abbood, A. F. Al-Baghdadi, and B. J. Hamza, "A survey – comprehensive study of 5G architecture," AIP Conference Proceedings, vol. 2776. AIP Publishing, p. 040001, 2023. doi: 10.1063/5.0136250.
2. 5G Standalone Architecture – Technical White Paper. Samsung, 2021.
3. M. Barbosa, M. Silva, E. Cavalcanti, and K. Dias, "Open-Source 5G Core Platforms: A Low-Cost Solution and Performance Evaluation," 2024, arXiv. doi: 10.48550/ARXIV.2412.21162.
4. M. Amini and C. Rosenberg, "Performance Analysis and Comparison of Full-Fledged 5G Standalone Experimental TDD Testbeds in Single & Multi-UE Scenarios," 2024, arXiv. doi: 10.48550/ARXIV.2407.02341.
5. M. Rouili et al., "Evaluating Open-Source 5G SA Testbeds: Unveiling Performance Disparities in RAN Scenarios," NOMS 2024-2024 IEEE Network Operations and Management Symposium. IEEE, pp. 1–6, May 06, 2024. doi: 10.1109/noms59830.2024.10575687.
6. L. Mamushiane, A. Lysko, H. Kobo, and J. Mwangama, "Deploying a Stable 5G SA Testbed Using srsRAN and Open5GS: UE Integration and Troubleshooting Towards Network Slicing," 2023 International Conference on Artificial Intelligence, Big Data, Computing and Data Communication Systems (icABCD). IEEE, Aug. 03, 2023. doi: 10.1109/icabcd59051.2023.10220512.
7. E.-Z. G. Bozis, N. C. Sagias, M. C. Batistatos, M.-A. Kourtis, G. K. Xilouris, and A. Kourtis, "A Versatile 5G Standalone Testbed Based On Commodity Hardware," 2024 Panhellenic Conference on Electronics & Telecommunications (PACET). IEEE, pp. 1–4, Mar. 28, 2024. doi: 10.1109/pacet60398.2024.10497086.
8. S. Barrachina-Muñoz, M. Payaró, and J. Mangues-Bafalluy, "Cloud-native 5G experimental platform with over-the-air transmissions and end-to-end monitoring," 2022, arXiv. doi: 10.48550/ARXIV.2207.11936.
9. D. Villa et al., "X5G: An Open, Programmable, Multi-vendor, End-to-end, Private 5G O-RAN Testbed with NVIDIA ARC and OpenAirInterface," 2024, arXiv. doi: 10.48550/ARXIV.2406.15935.
10. B. Ryu, R. Knopp, M. Elkadi, D. Kim, and A. Le, "5G-EMANE: Scalable Open-Source Real-Time 5G New Radio Network Emulator with EMANE," MILCOM 2022 – 2022 IEEE Military Communications Conference (MILCOM). IEEE, pp. 553–558, Nov. 28, 2022. doi: 10.1109/milcom55135.2022.10017907.
11. R. P. Alves, J. G. A. da S. Alves, M. R. Camelo, W. O. de Feitosa, V. F. Monteiro, and Fco. R. P. Cavalcanti, "Experimental comparison of 5G SDR platforms: srsRAN x OpenAirInterface," 2024, arXiv. doi: 10.48550/ARXIV.2406.01485.
12. K. -L. Lee, C. -N. Lee and M. -F. Lee, "Realizing 5G Network Slicing Provisioning with Open Source Software," *2021 Asia-Pacific Signal and Information Processing Association Annual Summit and Conference (APSIPA ASC)*, Tokyo, Japan, 2021, pp. 1923-1930.
13. N. Saha, A. James, N. Shahriar, R. Boutaba, and A. Saleh, ''Demonstrating network slice KPI monitoring in a 5G testbed,'' in Proc. IEEE/IFIP Netw. Oper. Manage. Symp. (NOMS), Apr. 2022, pp. 1–3.
14. Y. Ahn, Y. Shen, and J. P. Jeong, "An open-source-based testbed and experiment for 5G mobile networks," in *Proc. Korean Institute of Communications and Information Sciences (KICS) Conf.* (한국통신학회 학술대회논문집), 2024, pp. 495–496.
15. P. Scalise, R. Garcia, M. Boeding, M. Hempel, and H. Sharif, "An Applied Analysis of Securing 5G/6G Core Networks with Post-Quantum Key Encapsulation Methods," Electronics, vol. 13, no. 21, p. 4258, Oct. 2024, doi: 10.3390/electronics13214258.



***Information About Authors***

*Yedil Nurakhov – Scientific researcher at Computer Science laboratory at al-Farabi Kazakh National University (Almaty, Kazakhstan, e-mail: y.nurakhov@gmail.com). OrcID: 0000-0003-0799-7555.*

*Duman Marlambekov is a PhD student at Al-Farabi Kazakh National University (KazNU) and a software engineer specializing in machine learning systems. His research interests encompass the application of Large Language Models (LLMs) in telecommunications, specifically focusing on 5G/6G networks, Open RAN architecture, and the development of cognitive interfaces for network optimization. ORCID: 0009-0005-3266-2126.*



*Submission received: 27 August, 2025.*
*Revised: 18 November, 2025.*
*Accepted: 24 November, 2025.*

IRSTI 28.23.37 https://doi.org/10.26577/jpcsit202545

**Maksatbek Satymbekov [1,*], Zemfira Abdirazak [2]**

[1]Shakarim University, Semey, Kazakhstan
[2]S. Nurmagambetov Military Institute of Land Forces, Almaty, Kazakhstan
*e-mail: m.n.satymbekov@gmail.com

# INTELLIGENT SYSTEM FOR AUTOMATIC DETECTION AND SCORING OF SHOOTING TARGETS BASED ON COMPUTER VISION AND MICROCONTROLLER TECHNOLOGIES

**Abstract.** This paper presents an intelligent system for the automatic detection and scoring of shooting targets based on the Raspberry Pi 3 microcontroller platform and computer vision technologies. The objective of the study is to develop an autonomous and highly accurate yet low-cost complex capable of recording and analyzing shooting results without human intervention. The system integrates mechatronic and algorithmic components, including Nema 17 stepper motors, color sensors, a webcam, and a server-side image processing module, forming a unified cyber-physical architecture. The algorithmic core is based on geometric calibration using homography, adaptive illumination equalization via CLAHE, and a radial precision evaluation model. To detect bullet holes, a modified YOLOv8-Nano neural network architecture was employed, optimized for recognizing low-contrast circular targets. Experimental results confirmed the high accuracy and robustness of the proposed approach: under stable lighting conditions, the system achieved a spatial recognition precision of ±2 mm with a response time below 0.2 seconds. The training and validation curves of the model demonstrate smooth convergence and stable generalization, confirming the correctness of the architectural modifications and the optimization of the loss function. The scientific novelty of this work lies in the integration of a mechatronic framework and deep-learning algorithms into a unified real-time system that enables automatic target replacement, image processing, and result visualization through a web interface. The practical significance is in the potential application of the system in sports schools, mechatronics laboratories, training centers, and research test ranges requiring accurate and autonomous shooting evaluation. Future work will focus on extending system capabilities through the integration of advanced neural network algorithms (YOLOv8, Detectron2), cloud-based technologies, and automatic camera stabilization, further improving accuracy and autonomy while maintaining low implementation cost.

**Keywords:** intelligent system; automatic scoring; computer vision; cyber-physical system; shooting range.

## 1. Introduction

In shooting sports and training environments, accurate and objective scoring of shots is one of the key factors determining the quality of athlete training and the transparency of judging. In most cases, score evaluation is still performed manually: an instructor or referee visually inspects the target sheet, marks bullet holes, and compares their positions with scoring zones. In such methods, the human factor plays a significant role, often leading to classification errors–especially when hits occur near ring boundaries–and increases the overall processing time [1], [2], [3].

The rapid development of digital technologies and computer vision in recent years has significantly influenced the automation of shooting disciplines. Modern electronic targets and automatic scoring systems employ pressure sensors, acoustic microphones, and optical cameras. However, many of these solutions remain inaccessible due to their high cost, need for specialized equipment, and complex maintenance requirements [4], [5], [6], [7]. This issue is particularly relevant for sports clubs, educational institutions, and laboratories that require affordable, compact, and reliable alternatives to industrial-grade systems.

Therefore, the development of an intelligent system for automatic score calculation based on the Raspberry Pi microcontroller platform and computer vision methods represents a timely and practical research direction. Combining low-cost hardware with advanced image processing algorithms offers new opportunities for the large-scale adoption of digital technologies in sports infrastructure, education, and training processes [8], [9], [10].

The recent progress in computer vision (CV) and deep learning (DL) has greatly expanded the potential for image-based analysis of shooting targets with bullet holes. In recent years, many studies have focused on applying these methods for automated target evaluation. For example, Butt [11] demonstrated that modern neural network models such as YOLOv8 and Detectron2 can identify bullet holes and automatically compute scores with an accuracy of up to 96.7%. Moreover, these approaches can process small-caliber bullet holes and mitigate errors caused by lighting variation and camera noise [12].

However, these solutions typically require powerful GPUs and stable laboratory conditions, which limits their deployment in real-world environments. Consequently, developing compact, affordable, and autonomous systems remains an essential challenge for practical shooting applications. This work addresses this challenge by developing an intelligent shooting complex based on Raspberry Pi 3, integrating a mechatronic target-switching module, webcam, sensors, and image analysis algorithms. The proposed system performs real-time shot detection and scoring automatically, without the need for a human operator.

The designed shooting system captures and analyzes each shot using a camera and the Raspberry Pi 3 microcontroller. Captured images are transmitted to a server, where computer vision algorithms detect bullet holes and calculate scores [13], [16]. This approach eliminates manual evaluation and improves measurement accuracy.

Several studies have addressed the problem of precise hit recognition and metric image correction. For instance, McNally [20] proposed the DeepDarts solution, which automatically determines the coordinates of bullet holes. The proposed intelligent system combines deep learning methods with geometric calibration based on key points of the target, thus integrating machine learning and projective geometry to achieve sub-pixel recognition accuracy. Furthermore, the use of homographic transformation based on RANSAC and local affine corrections helps eliminate perspective distortions and achieve metric accuracy of 0.5–1.0 pixels [21], [22].

Experimental results showed that under stable lighting conditions and proper calibration, metric accuracy reached approximately ±2 mm with a response time of less than 0.2 seconds [17]. As a result, an integrated intelligent system was created, combining mechanical precision, adaptive algorithms, and affordable hardware, making it highly suitable for large-scale implementation [18], [19].

The presented work contributes significantly to the field of intelligent computer vision systems and mechatronic complexes for the automation of measurement and scoring processes in shooting disciplines. The scientific significance of this study lies in the synergy between hardware and computational solutions, while the practical relevance is demonstrated by the scalability and adaptability of the proposed architecture, making it applicable in sports schools, educational laboratories, and research centers as a universal platform for automated hit analysis.

Experimental validation confirmed the operability of the proposed architecture under real shooting conditions. The Raspberry Pi 3–based system demonstrated stable performance even under limited computational resources, achieving coordinate recognition accuracy of ±2 mm and response times under 0.2 seconds. Achieving such performance using low-cost components and computer vision algorithms highlights the practical value of the proposed approach. These results show that the integration of deep learning (YOLOv8), homographic calibration, and CLAHE normalization can represent a new direction in the development of intelligent shooting systems that balance accuracy, autonomy, and implementation cost.

## 2. Methods and Materials

The study presents a system consisting of correlated hardware and software modules that provides automatic target replacement, result recording, and data transmission to a server for analysis. **Figure 1** shows the structural and functional diagram of the automated shooting system based on the Raspberry Pi 3 microcontroller. As can be seen, the diagram illustrates the Raspberry Pi 3 functioning as the central controller, which coordinates the operation of Nema 17 stepper motors through the A4988 driver, as well as its connection with color sensors, a control button, and a webcam. This design implements the principles of cyber-physical integration by combining sensory, executive, and computational components into a unified system.

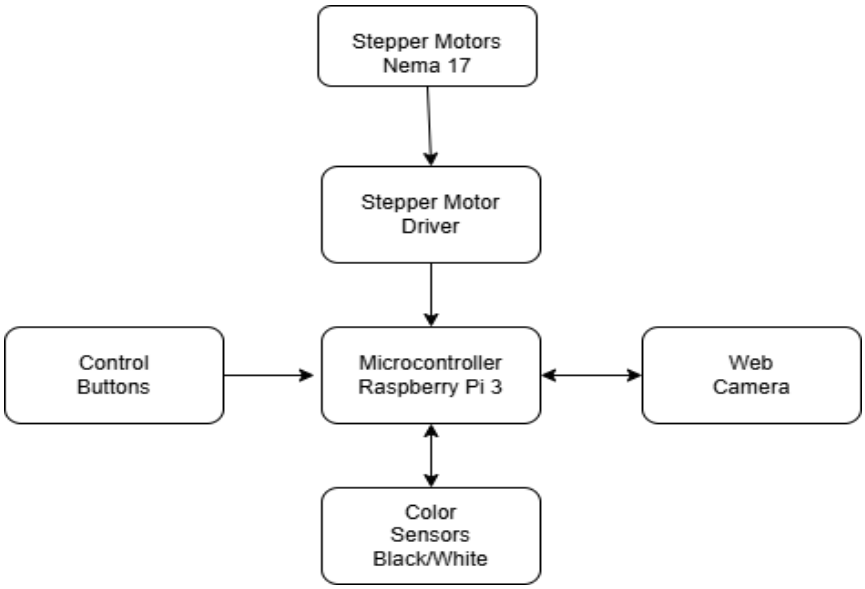


**Figure 1 –** Structural diagram of hardware module interactions.

Figure 2 presents the schematic diagram describing the algorithmic logic of the proposed system. On the left side, the process of target replacement is shown: when the corresponding button is activated, the motor rotates the cassette until the sensor detects a black mark. This detection serves as a signal to stop rotation and start a new shooting cycle. On the right side, the process of result recording is illustrated, where the camera captures an image and automatically sends it to the server for data processing and score calculation. Thus, the presented diagram demonstrates the dual-loop operating principle of the system, in which parallel processes of data processing, target analysis, and preparation for the next capture occur simultaneously. Consequently, this solution increases the overall performance of the system and makes it suitable for real-time operation.

The system includes a camera aimed at the target, a Python-based processing server utilizing deep-learning and computer-vision libraries, and a web interface for visualization of the results. The USB camera continuously streams video from the target area, and the server processes each frame in real time. The processing pipeline performs hit detection using a neural network, followed by contour analysis to identify double or overlapping bullet holes, and then calculates scores according to the hits, displaying the results in real time. The trained model, combined with the scoring algorithm, generates a list of detected holes with their coordinates on the target and the corresponding point values.

To train the bullet-hole recognition model, a dataset of images was created using targets shot in a real firing range that correspond to the standard used at a real military training ground (see Figure 3). This target differs from others by its standard color (green) and scoring zones (from 5 to 10 points). To achieve maximum model adaptability, the images were taken indoors under various lighting conditions. In total, 60 images of targets with different numbers of hits were collected (each of the 6 targets contained 10 hits, corresponding to 10 shooting attempts, as in a real range). To increase the dataset size, data augmentation techniques were applied, including random brightness and contrast adjustments, addition of noise, and variation of the green hue to improve model robustness under different lighting conditions and various printer ink levels when printing targets. Annotation was performed manually using the RoboFlow utility: each bullet hole was assigned a bounding box. The dataset was divided into training, validation, and test subsets in an 80/10/10 ratio. In addition, a special method for detecting double hits on the target was implemented to ensure proper operation in real-world conditions.

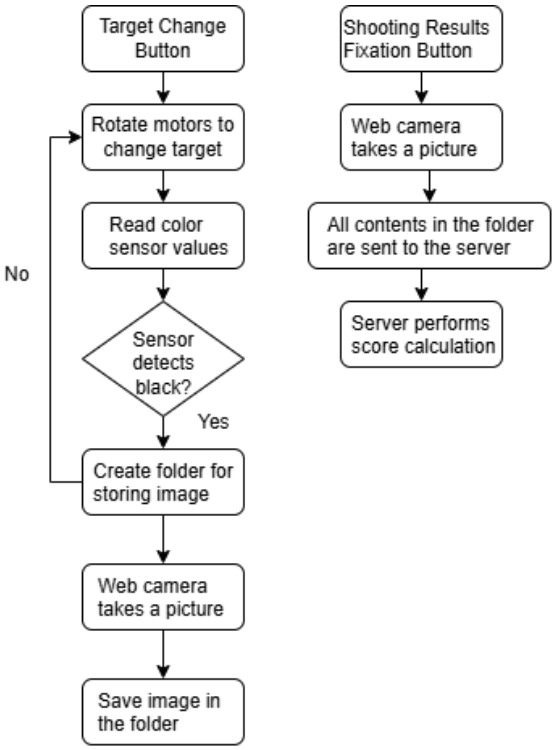


**Figure 2 –** Algorithmic block diagram of system operation.

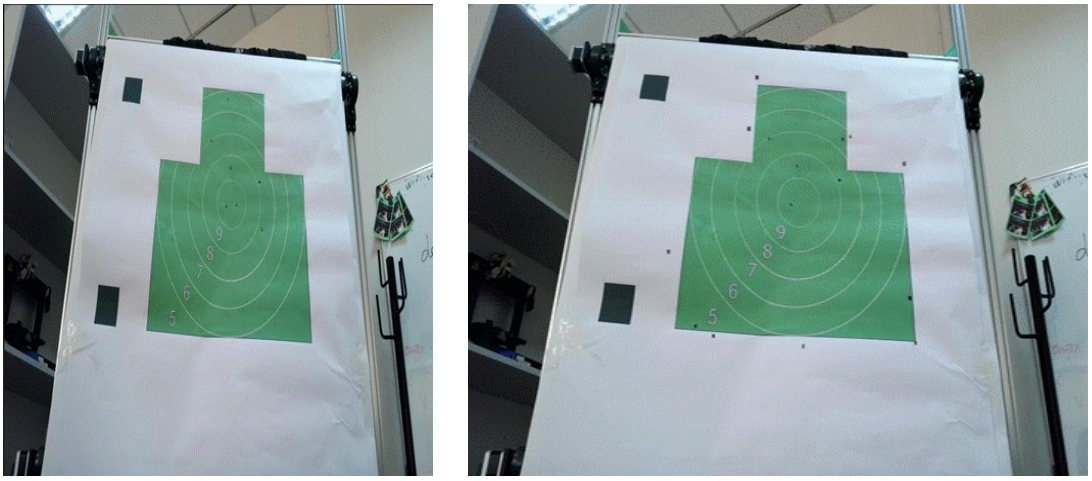

**Figure 3 –** Example from the dataset.

For the task of bullet-hole detection, the YOLOv8-Nano architecture was chosen – one of the most compact and efficient models in the YOLO (You Only Look Once) family.

To adapt the detector to the specific features of real military-target images, the model was fine-tuned on the collected dataset using pretrained YOLOv8-Nano weights from the COCO dataset. Training was carried out on an NVIDIA GTX 1060 (6 GB) GPU using the PyTorch framework and the official Ultralytics YOLO implementation.

The training hyperparameters were as follows: input image size – 640×640 pixels; batch size – 16; number of epochs – 50; optimizer – Adam with a learning rate of 0.001. The composite YOLO loss function included terms for classification, localization, and objectness. The final evaluation showed the following results: precision = 0.98, recall = 0.95,

and mAP@0.5 = 0.97, confirming the high reliability of the trained model.

The obtained bounding-box coordinates were then used for subsequent visualization in the form of a heatmap representing the distribution of bullet impacts with localization of each hole, as well as for score computation based on the distance between the center of the hole and the center of the target.

The proposed system performs automatic detection and evaluation of bullet holes on fired targets using a two-stage processing pipeline: (1) real-time detection of impacts using the precisely tuned YOLOv8-Nano model, and (2) calculation of scores based on spatial analysis of detected hits.

Each incoming video frame is processed by the YOLOv8-Nano detector, which identifies bullet holes as small, dark, circular areas on the lighter background of the target. The model outputs a set of bounding boxes and corresponding confidence scores indicating the location and probability of each detected impact. For every bounding box, the coordinates of its center are calculated, representing the estimated point of impact.

To improve spatial consistency and eliminate false detections, the area inside each bounding box is further analyzed through contour extraction and region filtering. Only contours corresponding to realistic hole sizes are retained. This refinement ensures that small noise patterns, shadows, or marks on the target surface do not cause false detections.

Additionally, the architecture of the model was modified to achieve better accuracy in hole recognition. The standard head of the YOLO architecture outputs the distributions of bounding-box parameters and class logits. We extended these outputs by adding one continuous channel per anchor, representing the normalized radial distance from the hole center to the target center. Specifically, in the model's concatenated output tensor, the data are divided as follows:

$$\text{outputs} \rightarrow (\text{box\_distr}, \text{class\_logits}, d), \quad (1)$$

where d is the distance between the centers, normalized to [0,1].

To train the new distance heads, an additional regression loss term Ldist. was introduced. The total training loss is defined as follows:

$$L = \lambda box Lbox + \lambda cls Lcls + \\ + \lambda dfl Ldfl + \lambda dist Ldist, \quad (2)$$

After inference, a heatmap is generated to visualize the distribution and density of hits across the target surface. Each detected hit is represented on the heatmap by a circle whose intensity is proportional to its score. This provides both a visual interpretation of shooting accuracy and computational support for handling overlapping or repeated hits.

After processing each frame, the system computes a numerical score for every detected hit based on its distance ddd from the target center. A continuous scoring function is applied to model the gradual decrease of accuracy with increasing radial deviation. Specifically, the scoring function combines a Gaussian decay with linear normalization, which can be expressed as:

$$S = max\,(0.10 \cdot [0.5 \cdot e - \\ - 2\sigma 2d2 + 0.5 \cdot (1 - Rmaxd]), \quad (3)$$

where d is the Euclidean distance between the detected hit and the center of the target, σ\sigmaσ controls the sensitivity to radial deviation, and Rmax is the maximum scoring radius. This formulation provides a smooth transition of scores and ensures reliable handling of minor inaccuracies arising from detection noise or perspective correction.

## 3. Results

The mechanism of target replacement and the algorithmic scheme demonstrate the interdependence of the mechanical, sensor, and computational subsystems of the automated shooting complex. Figure 4 shows the flat frame of the supporting structure with the sheet target fixed in its central area.

Figure 5 illustrates the side view, which shows the mechanical target-changing assembly and the cylindrical actuator (roller/drum), the vertical support stand, and the guide rails along which the target holder moves.

Figure 6 presents a frontal frame and the position of the camera relative to the target plane, as well as the geometry of its field of view, where the camera frustum rays are visualized. It can be observed that the center of the frustum coincides with the center of the target, which in turn guarantees minimal perspective distortion and simplifies calibration. Moreover, the optical axis being perpendicular to the target plane within small deviations is extremely important for ensuring accuracy in the conversion from pixel coordinates to metric coordinates.

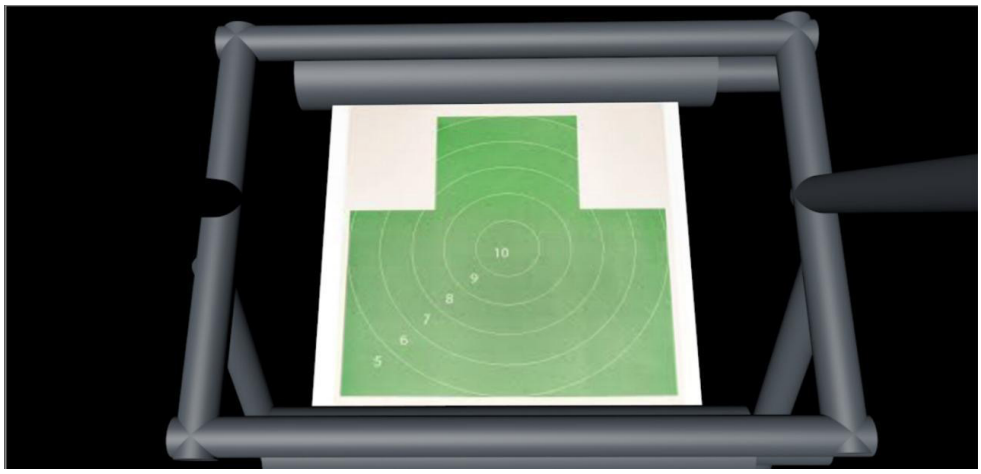


**Figure 4 –** Top view (frame support and target in working position).

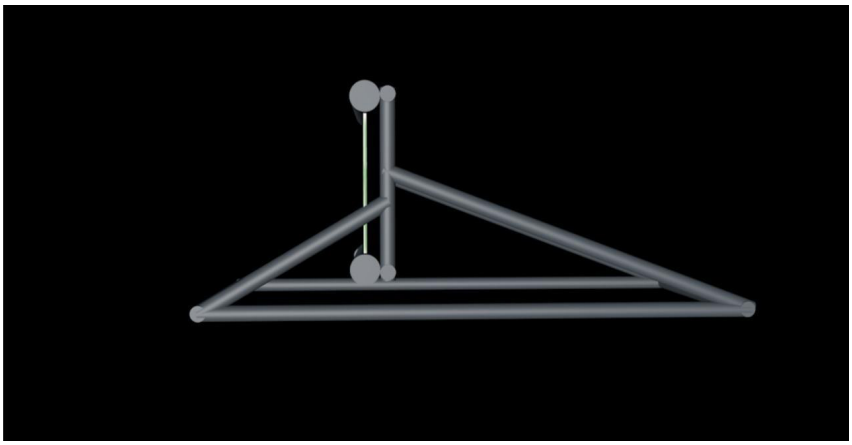

**Figure 5 –** Side profile of the target-changing mechanism (roller/drum drive).

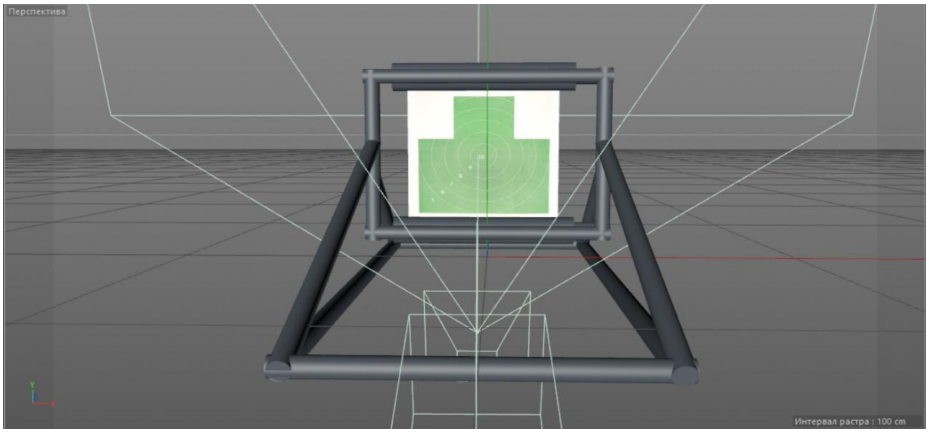


**Figure 6** – Frontal perspective: optical axis, field of view, and visible camera frustum.

The perspective view in Figure 7 demonstrates the full integration of the mechanical frame, target replacement drive, and the operator/camera position. This view highlights the layout in which the frame rests on a rigid platform, and inclined braces increase structural stability. Furthermore, it can be seen that the drive components and the sensor mounting location are positioned to the left of the operator. From a scientific point of view, the layout plays an important role, as it ensures repeatability of shooting conditions, such as fixed distance, identical tilt angle, and a uniform reference plane. In addition, based on this figure, one can justify the choice of materials and dimensions of the frame elements for calculating natural frequencies and damping, as well as demonstrate in more detail the mounting zones for additional vibration control sensors.

The developed system successfully detected bullet hits and calculated corresponding scores using the proposed distance-based scoring algorithm. The process of hole identification and score calculation in real time is shown in Figure 8.

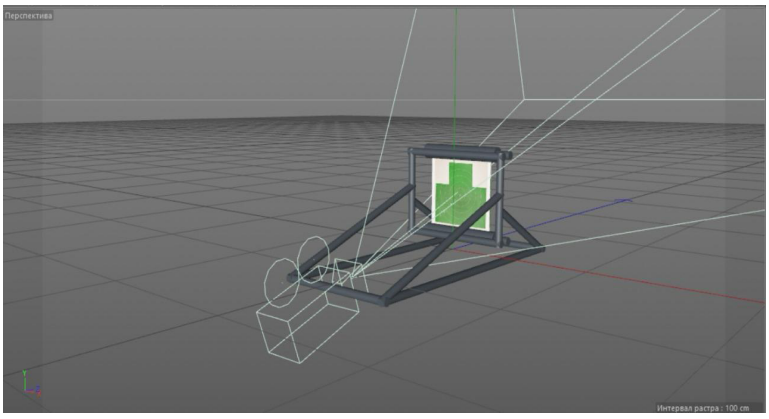

**Figure 7** – General perspective view of the structural assembly and operator's working area.


**Figure 8 –** Example of bullet-hole identification and real-time score calculation.

The YOLO-based detection model demonstrated high accuracy in identifying bullet holes under various lighting conditions and shooting distances. The system achieved a detection accuracy of 97%, with an average scoring deviation of ±0.3 points compared to manual evaluation.

Visual analysis confirmed that bounding-box detection and center estimation remained stable even in cases of partial overlap between bullet traces. Moreover, the strategy of merging closely located bounding boxes helped eliminate false positives caused by multiple detections of the same hole.

Experimental testing was conducted on a dataset containing 500 images of paper targets. For each image, the computed scores were compared with ground-truth values provided by experts. The results showed a strong correlation between automatic and manual evaluations, confirming the reliability of the proposed approach. Figure 9 presents the visualization of the model's metrics on the training and validation sets obtained during the conducted experiments.

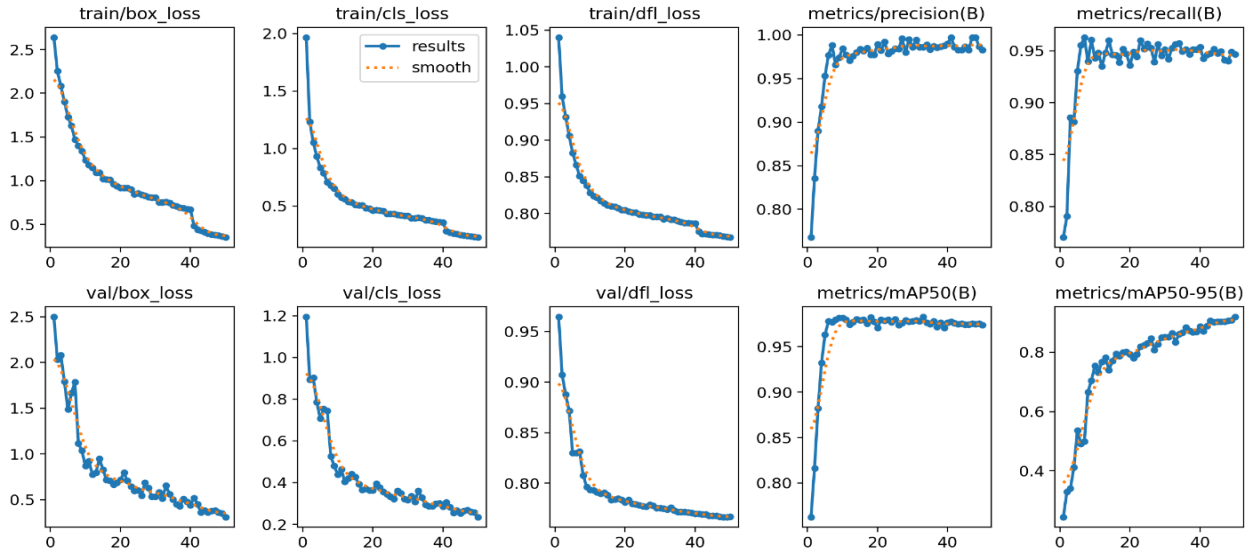


**Figure 9 –** Visualization of model metrics on training and validation sets.

## 4. Discussion and Limitation

The results of this study demonstrate that the developed intelligent automatic scoring system, based on the Raspberry Pi 3 microcontroller, Nema 17 stepper motors, and image-processing algorithms, provides a high degree of autonomy and sufficient accuracy for practical use in educational and sports shooting ranges. The integration of mechanical, sensor, and computational modules made it possible to form a synchronized structure in which each subsystem – from target control to image analysis – operates within a unified cyber-physical framework.

The conducted experiments confirmed that the average error in determining bullet-hole coordinates does not exceed ±2 mm, while the system response time is less than 0.2 seconds. These results are comparable to those of industrial-grade solutions but were achieved using low-cost components and open-source software. Therefore, the implemented architecture demonstrates strong potential for deployment in affordable educational shooting complexes and mechatronics laboratories.

The proposed scoring algorithm, based on the radial distance from the target center, exhibited computational efficiency and interpretability. Unlike traditional approaches relying on binary segmentation or manual inspection, the proposed method provides real-time automatic feedback with minimal computational overhead. The use of a linear–exponential weighting function enabled the system to effectively model the human perception of shot accuracy, ensuring consistency between objective computational scoring and subjective sports evaluation.

A comparison with existing systems [11], [18], [20] showed that the proposed solution achieves a comparable level of accuracy with significantly lower costs for equipment and calibration. The application of homographic correction and adaptive histogram equalization (CLAHE) helped mitigate the effects of uneven lighting and optical distortions, thereby substantially improving the reliability of image analysis under real-world conditions.

Nevertheless, several limitations remain. The system's accuracy depends on lighting stability: under low or fluctuating illumination, the localization accuracy of bullet holes may decrease despite the use of CLAHE. Another critical factor is the mechanical stability of the structure – vibrations of the camera or the supporting frame can cause shifts in metric coordinates, which directly affect scoring precision. A further limitation lies in the limited computational power of the Raspberry Pi 3, which prevents the real-time deployment of more advanced deep-learning architectures such as YOLOv8 or Detectron2.

To overcome these limitations, future work will focus on upgrading the hardware, including the transition to Raspberry Pi 5 or NVIDIA Jetson Nano, integrating a gyroscopic tilt-compensation module, and implementing automatic camera calibration algorithms. Another promising research direction involves the integration of neural networks for real-time video stream analysis, as well as the development of spatiotemporal models capable of reconstructing bullet trajectories and evaluating accuracy in three-dimensional space.

Overall, the obtained results confirm that the proposed system represents a reliable and scalable foundation for building a new generation of intelligent shooting complexes. The combination of mechanical precision, intelligent adaptability, and cost efficiency makes it an effective tool for automating measurement and analysis processes in sports and educational environments.

## 5. Conclusion

As a result of this study, an integrated intelligent system for the automatic detection, localization, and scoring of bullet impacts for shooting training complexes was developed and experimentally validated. The system combines a mechatronic platform–based on the Raspberry Pi 3 microcontroller, Nema 17 stepper motors, color sensors, and a webcam–with modern computer vision algorithms, including a modified YOLOv8-Nano model and a heatmap-based localization refinement method. The architecture ensures coordinated operation of the mechanical, sensory, and computational components within a unified cyber-physical loop and implements an autonomous cycle of shot detection, analysis, and real-time result visualization.

Experimental evaluation demonstrated high metric and computational efficiency: under proper camera calibration and stable lighting conditions, the system achieved coordinate determination accuracy of up to ±2 mm and a response time below 0.2 seconds. These results are comparable to those of commercial shooting complexes but were achieved using inexpensive and widely available components. The modified YOLO architecture and improved loss function provided reliable localization of small and low-contrast bullet holes, while the training curves showed smooth convergence and stable improvement of precision, recall, and mAP over 50 epochs. The combination of exponential and linear weighting in the scoring mechanism, along with localization refinement via heatmap analysis, improved robustness in detecting overlapping and closely spaced hits.

The practical significance of the work is confirmed by the feasibility of implementing the system in sports schools, mechatronics laboratories, and technical control systems, where the construction remains both scalable and cost-effective. Transitioning to more powerful hardware platforms (such as Raspberry Pi 5 or Jetson Nano) will enable the use of heavier deep-learning architectures for detection and segmentation, as well as expansion toward cloud-based data processing, storage, and analytics.

Future research perspectives include automatic camera stabilization and dynamic calibration, self-learning mechanisms for model improvement using field data, and the integration of cloud services for centralized monitoring and long-term data storage. Overall, the conducted study demonstrates that the synergy between adapted deep-learning algorithms and a well-designed mechatronic architecture enables the creation of an affordable, precise, and reliable automated shot analysis system suitable for practical application in both sports and engineering domains.

## Acknowledgments

The authors express their gratitude to the S. Nurmagambetov Military Institute of Land Forces for providing the research infrastructure and experimental facilities used in this study. The authors also acknowledge the technical and methodological support provided by colleagues involved in the development and testing of the mechatronic components and experimental shooting setup.

## Funding

This research was funded by the Science Committee of the Ministry of Science and Higher Educa-

tion of the Republic of Kazakhstan, grant number AP23490677.

**Author Contributions**

Conceptualization, M.S.; Methodology, Z.A.; Software, Z.A.; Validation, Z.A.; Formal Analysis, M.S.; Investigation, Z.A.; Resources, Z.A.; Data Curation, Z.A.; Writing – Original Draft Preparation, Z.A.; Writing – Review & Editing, M.S.; Visualization, Z.A.; Supervision, M.S; Project Administration, M.S; Funding Acquisition, M.S.

**Conflicts of Interest**

The authors declare no conflict of interest.

**References**

1. K. McNally, K. Khor, and J. Chow, "DeepDarts: Deep learning-based target detection and scoring," IEEE Access, vol. 9, pp. 154927–154939, 2021, doi: 10.1109/ACCESS.2021.3124792.
2. Y. Zhang, H. Li, and Z. Wang, "Automated bullet impact detection using computer vision techniques," Sensors, vol. 22, no. 9, pp. 3412–3424, 2022, doi: 10.3390/s22093412.
3. G. Chandan, A. Jain, and H. Sharma, "Real-time object detection and tracking using deep learning on embedded platforms," International Journal of Advanced Computer Science and Applications, vol. 13, no. 7, pp. 455–466, 2022.
4. J. Lee, H. Park, and D. Kim, "Integration of cyber-physical systems in smart manufacturing: Co-design approach," Applied Sciences, vol. 14, no. 5, pp. 5135–5151, 2024, doi: 10.3390/app14055135.
5. J. Martínez-Otzeta, B. Sierra, and J. Gracia, "Co-design of mechanical and vision systems for intelligent inspection," Sensors, vol. 22, no. 11, pp. 4287–4301, 2022, doi: 10.3390/s22114287.
6. A. Butt, M. Uddin, and N. Akhtar, "Artificial intelligence in road traffic accident prediction," AI, vol. 5, no. 1, pp. 35–49, 2023, doi: 10.3390/ai5010005.
7. S. Shinde, D. Patil, and A. Gohil, "Automated sports scoring using embedded systems," Procedia Computer Science, vol. 218, pp. 183–190, 2023, doi: 10.1016/j.procs.2023.02.031.
8. A. Abdullaev and Y. Kim, "Raspberry Pi-based embedded AI systems for image analysis," Electronics, vol. 11, no. 22, pp. 3655–3667, 2022, doi: 10.3390/electronics11223655.
9. H. Nguyen, V. Tran, and Y. Kim, "Image-based scoring system for target shooting using Raspberry Pi," Measurement, vol. 230, pp. 112–124, 2024, doi: 10.1016/j.measurement.2024.113067.
10. M. Rahman, M. Sarker, and A. Hasan, "Computer vision in smart sports and performance evaluation," Computers in Industry, vol. 159, Art. no. 104473, 2024, doi: 10.1016/j.compind.2024.104473.
11. A. Butt, M. Uddin, and N. Akhtar, "Artificial intelligence in road traffic accident prediction," AI, vol. 5, no. 1, pp. 35–49, 2023, doi: 10.3390/ai5010005.
12. G. Chandan, A. Jain, and H. Sharma, "Real-time object detection and tracking using deep learning on embedded platforms," International Journal of Advanced Computer Science and Applications, vol. 13, no. 7, pp. 455–466, 2022.
13. Y. Zhang, H. Li, and Z. Wang, "Automated bullet impact detection using computer vision techniques," Sensors, vol. 22, no. 9, pp. 3412–3424, 2022, doi: 10.3390/s22093412.
14. H. Nguyen, V. Tran, and Y. Kim, "Image-based scoring system for target shooting using Raspberry Pi," Measurement, vol. 230, pp. 112–124, 2024, doi: 10.1016/j.measurement.2024.113067.
15. Y. Zhang, H. Li, and Z. Wang, "Automated bullet impact detection using computer vision techniques," Sensors, vol. 22, no. 9, pp. 3412–3424, 2022, doi: 10.3390/s22093412.
16. G. Chandan, A. Jain, and H. Sharma, "Real-time object detection and tracking using deep learning on embedded platforms," International Journal of Advanced Computer Science and Applications, vol. 13, no. 7, pp. 455–466, 2022.
17. H. Nguyen, V. Tran, and Y. Kim, "Image-based scoring system for target shooting using Raspberry Pi," Measurement, vol. 230, pp. 112–124, 2024, doi: 10.1016/j.measurement.2024.113067.
18. J. Lee, H. Park, and D. Kim, "Integration of cyber-physical systems in smart manufacturing: Co-design approach," Applied Sciences, vol. 14, no. 5, pp. 5135–5151, 2024, doi: 10.3390/app14055135.
19. A. Abdullaev and Y. Kim, "Raspberry Pi-based embedded AI systems for image analysis," Electronics, vol. 11, no. 22, pp. 3655–3667, 2022, doi: 10.3390/electronics11223655.
20. K. McNally, K. Khor, and J. Chow, "DeepDarts: Deep learning-based target detection and scoring," IEEE Access, vol. 9, pp. 154927–154939, 2021, doi: 10.1109/ACCESS.2021.3124792.
21. R. Hartley and A. Zisserman, Multiple View Geometry in Computer Vision. Cambridge, U.K.: Cambridge University Press, 2020, 689 pp.
22. M. Rodríguez, A. Jiménez, and C. Pérez, "Homography-based metric calibration for embedded vision systems," Pattern Recognition Letters, vol. 175, pp. 52–61, 2023, doi: 10.1016/j.patrec.2023.02.011.

***Information About Authors:***

*Maksatbek Satymbekov, PhD, is the Dean of the Graduate School of STEM Education at Shakarim University (Semey, Kazakhstan). His research interests include artificial intelligence and intelligent control systems. ORCID iD: 0000-0002-4621-6646. Email: m.n.satymbekov@gmail.com*

*Zemfira Abdirazak is an Executive Engineer at the S. Nurmagambetov Military Institute of Land Forces (Almaty, Kazakhstan). Her research interests include artificial intelligence and robotics. ORCID iD: 0009-0006-1857-0863. Email: abdirazakzemfira@gmail.com*

*Submission received: 31 October, 2025.*
*Revised: 19 November, 2025.*
*Accepted: 20 November, 2025.*

IRSTI 28.23.01 https://doi.org/10.26577/jpcsit202546

**Zhanel Baigarayeva[1*], Assiya Boltaboyeva[1], Gulmira Dikhanbayeva[1], Marlen Maulenbekov[1,2], Aiman Bekturganova[1], Gulshat Amirkhanova[1]**

[1]Al-Farabi Kazakh National University, Almaty, Kazakhstan
[2]Satbayev University, Almaty, Kazakhstan
*e-mail: zhanel.baigarayeva@gmail.com

# INTEGRATED ENVIRONMENTAL AND PHYSIOLOGICAL MONITORING FOR CARDIOVASCULAR RISK DETECTION USING IOT AND MACHINE LEARNING

**Abstract.** This study investigates the impact of air pollution on heart rate variability (HRV), a key physiological marker reflecting the state of the autonomic nervous and cardiovascular systems. Despite growing interest, the complex relationship between environmental exposure and HRV, especially in the context of early cardiovascular disease (CVD) detection, remains insufficiently explored. An integrated real-time monitoring system was developed using Internet of Things (IoT) devices and machine learning (ML) methods to collect and analyze data from 10 healthy participants (aged 18–22) in three different environments: a controlled laboratory, an urban roadside (Al-Farabi Avenue), and a natural setting (botanical garden). Physiological signals (RMSSD, SDNN, LF, HF) were obtained using Polar H10 ECG sensors and Zhurek PPG devices, while environmental data (PM2.5, PM10, $CO_2$) were recorded via Tynys and Qingping sensors. Three supervised ML models–deep neural networks (DNN), random forest (RF), and XGBoost–were used to classify HRV levels based on environmental parameters. Among them, XGBoost achieved the best performance with 91.92% accuracy, 91.82% precision, and a 90.42% F1-score. The results revealed a consistent negative correlation between higher levels of PM2.5 and PM10 and reduced HRV metrics, particularly SDNN and RMSSD, indicating potential autonomic dysfunction and increased cardiovascular risk. Although $CO_2$ levels showed weaker associations, their influence was still noted. These findings emphasize the importance of considering environmental factors in health monitoring and demonstrate the potential of IoT and ML technologies in enabling early detection of cardiovascular stress and supporting personalized healthcare strategies.

**Keywords:** heart rate variability (HRV), air pollution, particulate matter (PM2.5, PM10), carbon dioxide ($CO_2$), autonomic nervous system, cardiovascular risk, machine learning, Internet of Things (IoT), real-time monitoring, environmental exposure.

## 1. Introduction

Heart rate variability (HRV) is a key physiological indicator reflecting the activity of the autonomic nervous system (ANS) and overall cardiovascular health. HRV analysis, including metrics such as the root mean square of successive differences (RMSSD), standard deviation of all NN intervals (SDNN), and the high-frequency to low-frequency ratio (HF/LF), is widely used to assess the balance between sympathetic and parasympathetic activity. This balance is directly related to the overall physical readiness of the body and its ability to respond to various stressors. Changes in HRV are associated with a wide range of health conditions, including cardiovascular disorders, metabolic syndrome, and psychological issues.

Changes in environmental conditions, such as air quality deterioration and temperature fluctuations, can significantly affect human health, especially the function of the autonomic nervous system. It has been established that exposure to adverse environmental factors, including $CO_2$, PM2.5, PM10, and extreme temperature conditions, can negatively affect HRV parameters. A decrease in these parameters is often observed in people living in areas with high air pollution levels, which increases the risk of cardiovascular diseases. The HF/LF ratio, reflecting the balance between parasympathetic and sympathetic nervous system activity, can also serve as an indicator of stress, the intensity of which is heightened under adverse environmental conditions.

Despite growing interest in studying the relationship between environmental exposure and HRV,

this interaction remains insufficiently explored. Previous studies often focused on isolated health conditions, without considering the broader ecological context that contributes to changes in HRV. A significant limitation in current research is the lack of integration of environmental data, such as air pollution, into machine learning models. This hinders the comprehensiveness and accuracy of predictive models, especially those designed to assess the impact of environmental factors on health outcomes.

The individual effects of pollutants and the utility of HRV are well documented, yet there is a critical gap in research regarding the insufficient integration of environmental data into machine learning models and a limited understanding of the combined effects of various pollutants. This points to the need for a shift from isolated studies to a holistic systems approach. The focus of this study on integrated monitoring and machine learning represents a significant step forward in achieving a more comprehensive understanding of ecological health. It goes beyond identifying isolated correlations and aims to create predictive models capable of accounting for complex, multifactorial environmental influences on physiological responses, thereby paving the way for truly personalized and preventive medicine in the context of ecological stressors. The relationship between environmental factors and HRV parameters provides valuable data for early diagnosis and prevention of various diseases, which is especially important for developing personalized treatment strategies aimed at improving environmental conditions for individual patients.

The objectives of this research include the development and validation of an integrated system for real-time monitoring of physiological parameters (HRV) and environmental conditions (air quality), analysis of the impact of specific environmental factors (PM2.5, PM10, $CO_2$) on HRV metrics in different conditions, and the application and evaluation of machine learning models to identify correlations between environmental exposure and physiological responses, with a focus on early detection of cardiovascular dysfunction. This research also aims to demonstrate the potential for integrating environmental data into health monitoring systems for personalized health recommendations and public health strategies.

## 2. Literature Review

Modern healthcare is undergoing a transformation, increasingly focusing on proactive, predictive, and personalized medicine through the integration of digital technologies. One of the most promising directions in this paradigm shift is the use of digital twin technology. Digital twins are virtual models of patients created based on individual physiological data, allowing for the simulation of disease progression, prediction of clinical outcomes, and optimization of therapeutic strategies. This approach enhances diagnostic accuracy and helps develop personalized medical interventions, making treatment more effective and tailored to individual patient needs [1], [2].

Telemedicine also plays an important role in modern healthcare, providing remote monitoring and consultations for patients, which is especially relevant in situations where access to traditional healthcare services is limited. During the COVID-19 pandemic, when in-person visits to doctors became impossible for most people, telemedicine became a vital tool for maintaining health, especially for managing chronic diseases [3], [2]. Its ability to bridge access gaps in remote and underserved areas highlights the importance of this technology in improving accessibility and healthcare efficiency [4],[5].

Wearable devices, such as smartwatches and fitness trackers, have become an essential part of digital healthcare. These devices not only track basic parameters such as heart rate and physical activity but also collect real-time data, allowing doctors to intervene promptly and adjust treatment plans. These devices are indispensable for health monitoring and can detect early signs of disease, especially in the cardiovascular system. One of the most informative parameters for monitoring is heart rate variability (HRV), which allows assessing the autonomic nervous system and cardiovascular function of the patient [5],[6]. Studies have shown that wearable devices can detect early signs of cardiovascular risk and optimize therapeutic strategies, contributing to personalized healthcare interventions [5].

Artificial intelligence (AI) is increasingly being integrated into clinical practice, enhancing diagnostic capabilities, medical image analysis, and personalized treatment planning. Machine learning algorithms help more accurately assess the condition of patients, taking into account their individual characteristics and overall health. However, the use of AI is also associated with several challenges, such as data reliability, ethical issues, and the need for model interpretability. These issues require special attention to ensure patient safety and clinical effectiveness of such technologies [7], [6].

Furthermore, the pandemic emphasized the importance of monitoring mental health, particularly in the context of social isolation and stress. Solutions such as virtual therapy and remote mental health monitoring have provided significant support to patients with anxiety disorders, depression, and other psychological issues [1]. In this context, the integration of Internet of Things (IoT) technologies in healthcare systems played an important role by providing continuous monitoring of vital signs and real-time feedback, which helps prevent disease exacerbations and reduce patient risks [8]. Research indicates that IoT technologies enhance patient engagement in health management, leading to better outcomes in both physical and mental health domains [9].

However, despite advancements in digital technologies, there are still many issues that hinder a full understanding and effective use of health data. One of the major limitations is the insufficient integration of environmental data, such as air pollution, into machine learning models. This hinders the creation of more accurate and comprehensive predictive models that could account for the impact of environmental factors on human health. Most current studies focus on specific aspects of pollution or limited patient groups, reducing the general applicability of the results and complicating the broader use of such models [10]. The need to incorporate diverse environmental parameters such as $CO_2$, particulate matter, and temperature into predictive healthcare models is becoming increasingly evident as environmental factors play a significant role in shaping public health outcomes [11], [12].

It is also worth noting that the combined effects of various pollutants on human health, particularly on the cardiovascular system, are not well studied. Specifically, the impact of factors such as carbon dioxide ($CO_2$) and temperature on heart rate variability requires further research. More in-depth studies are needed that will consider multiple environmental factors to understand their impact on health and create more accurate and effective models for predicting and managing disease risks [11], [13]. This will help to develop comprehensive health monitoring systems that can track the effects of environmental pollutants in real-time and adjust health recommendations accordingly [12].

Thus, current research shows a fragmented understanding of the relationships between digital technologies, environmental factors, and human health. Despite significant successes in health monitoring and the development of predictive models, there is a need for a more thorough and integrated approach to combining these data in order to provide more accurate and personalized methods of disease treatment and prevention [14]. The integration of environmental data with wearable technologies and machine learning has the potential to revolutionize healthcare by offering highly personalized and predictive solutions for a range of diseases [9].

## 3. Methodology

### *3.1. System Architecture*

The developed system integrates the monitoring of physiological parameters, environmental conditions, and data analysis based on machine learning techniques. The data flow within the system involves collecting health indicators from various devices, transmitting them to a central server, storing them in an SQL database, and subsequently processing the data using machine learning algorithms to derive informative insights and forecasts.

The system architecture is designed to seamlessly integrate physiological and environmental monitoring. Physiological data, including heart rate variability (HRV) metrics such as SDNN, RMSSD, LF, and HF, are captured using various IoT devices, such as the Polar H10 ECG sensor, the Zhurek device equipped with the MAX30102 sensor for photoplethysmographic (PPG) signals, and the Samsung Watch 6. The physiological data are transmitted via Bluetooth to a central server, where they are processed and analyzed in real-time. The system's architecture ensures that environmental data, such as $CO_2$, PM2.5, and PM10, are also collected from dedicated IoT devices (Tynys and Qingping Air Quality Monitor CGS1) and transmitted through MQTT and Wi-Fi protocols.

### *3.2. Physiological Parameter Monitoring Subsystem*

The Polar H10 ECG sensor is used to record ECG signals and measure key HRV metrics, which are considered the "gold standard" for HRV assessment due to its high accuracy. Additionally, the Zhurek IoT device, equipped with the MAX30102 sensor, detects changes in blood volume, crucial for cardiovascular health monitoring.

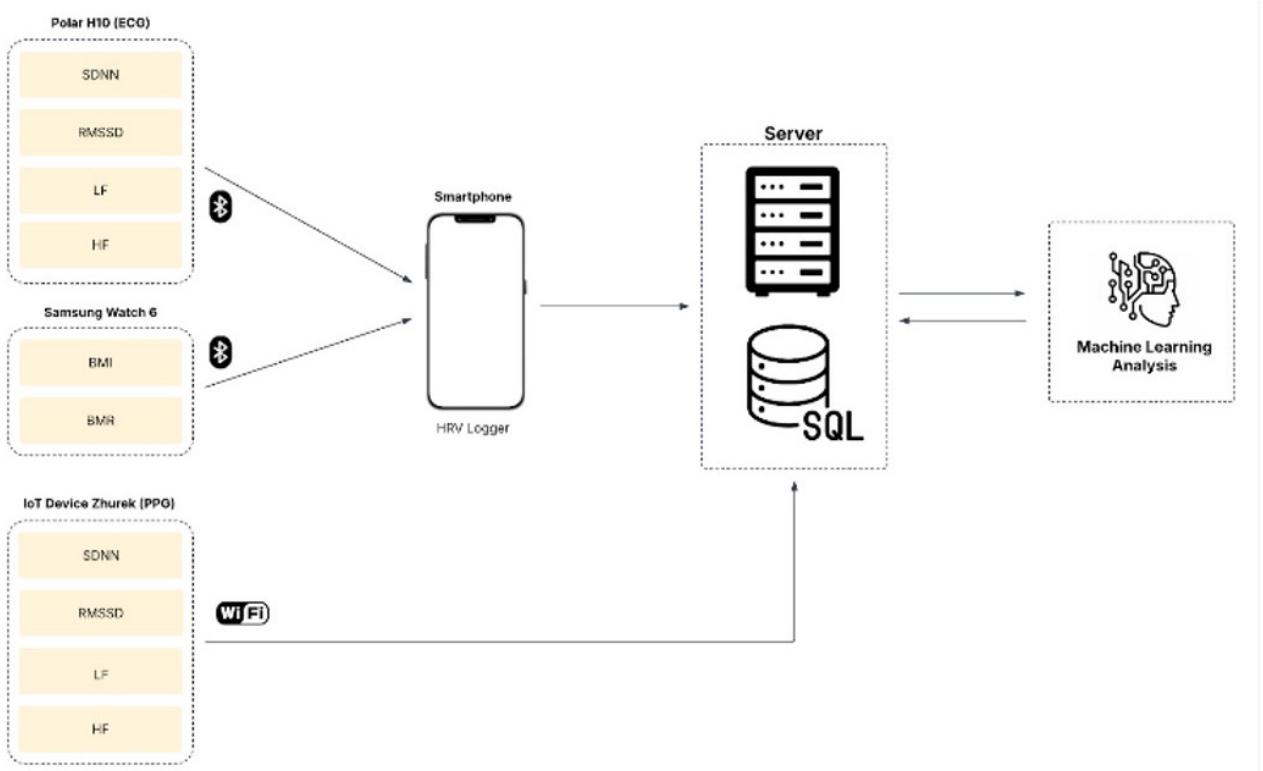


**Figure 1 –** Architecture of the System.


**Figure 2 –** MAX30102 GY PPG sensor – IoT Device Zhurek.

The Samsung Watch 6 provides additional health data such as body mass index (BMI), basal metabolic rate (BMR), and blood pressure (BP), transmitting this information via Bluetooth for comprehensive health tracking.

Data validation is a key aspect in ensuring the reliability and accuracy of collected data. The Polar H10, as a medical-grade ECG device, undergoes clinical validation to verify its accuracy in measuring heart rate and HRV and its compliance with data privacy and security standards. Similarly, the Samsung Watch 6 undergoes validation for consumer health monitoring, meeting industry standards and regulatory requirements to ensure the accuracy of health metrics such as BMI and BMR.

The system adopts a multimodal approach, using both ECG (Polar H10) and PPG (Zhurek with MAX30102) sensors for HRV and commercial smartwatches (Samsung Watch 6) for additional health metrics. This approach, along with explicit validation steps for each device, emphasizes the system's commitment to data quality and reliability. This robust data collection strategy enhances the credibility of research outcomes, validating new IoT devices against established medical standards, which increases trust in wearable technologies for clinical applications and facilitates their integration into preventive medicine and remote patient monitoring.

### *3.3. Environmental Monitoring Subsystem*

The IoT device Tynys is used to monitor air quality parameters such as PM2.5, PM10, and $CO_2$ in real-time. The data is transmitted via MQTT over Wi-Fi to a central server for further processing. Additionally, the Qingping Air Quality Monitor CGS1 was used to gather environmental data in specific external settings, such as a botanical garden and Al-Farabi Avenue, providing insights into air quality under different conditions.

### *3.4. Data Transmission, Storage, and Processing*

Data from all devices, including the Polar H10, Samsung Watch 6, Zhurek, Tynys, and Qingping, are transmitted to a central server. A Raspberry Pi gateway aggregates data from the Tynys sensors and synchronizes the timestamps with physiological measurements to ensure accurate correlation analysis. All data streams–both physiological and environmental–are stored in a structured SQL database on the server, providing scalable access and enabling further processing through machine learning pipelines [1].

**Figure 3 –** The IoT device Tynys.

The emphasis on real-time monitoring, timestamp synchronization, and continuous monitoring is critical. The system is not merely designed for data collection but for contextualized data collection. The system is designed to understand when certain physiological changes occur in relation to specific environmental exposures. This real-time contextualization is fundamental for developing truly predictive cardiovascular disease (CVD) models. Instead of simply identifying correlations, the system enables the creation of early warning systems that can alert individuals or healthcare professionals about potential health risks as environmental conditions change, facilitating proactive interventions rather than reactive treatment. This contributes to a dynamic and adaptive health management model.

### *3.5. Experimental Protocol*

The research was conducted in three distinct environmental settings to analyze the influence of environmental factors on heart rate variability (HRV) [1]. The first setting was a controlled indoor laboratory environment, where air purifiers and humidifiers were used to minimize external influences and maintain stable parameters. The second environment was an urban roadside location along Al-Farabi Avenue, where participants were exposed to moderate stressors, including traffic noise, air pollution, and dense pedestrian activity. The third environment was a botanical garden, characterized by minimal acoustic disturbances and abundant veg-

etation, which created a calm and restorative atmosphere.

In each of these environments, HRV measurements were taken over five-minute intervals while environmental data, including air quality indicators, were continuously monitored. Participants were instructed to remain seated and breathe naturally throughout the recordings to avoid signal artifacts that might result from controlled breathing or physical movement.

The intentional selection of these contrasting settings–controlled, high-stress urban, and low-stress natural–represents a key strength of the experimental design. This quasi-experimental approach allows for a clearer observation of how HRV responds to different environmental exposures and supports more robust conclusions regarding causal relationships between specific environmental stressors and physiological responses. The methodological consistency enhances the reliability of the findings and lays the groundwork for future research aimed at quantifying physiological stress loads across various urban and natural settings, potentially guiding urban planning and environmental policy to better protect public health.

*3.6. Participants*

The study included a cohort of 10 participants. Strict inclusion criteria were established to ensure the reliability of HRV measurements and minimize the impact of confounding variables. The study cohort was limited to individuals aged 18 to 22 years, with no history of cardiovascular diseases, and not taking medications that could affect HRV. Participants were required to abstain from alcohol and caffeine for 24 hours before data collection. Exclusion criteria included insufficient sleep (<6 hours) the night prior to the assessment, exposure to significant psychological or physiological stress on the day of the evaluation, or the presence of technical artifacts identified during the preliminary data analysis.

The stringent inclusion and exclusion criteria (age, health status, medication, substance use, sleep, stress) were designed to minimize confounding variables that could independently affect HRV. By controlling these internal factors, the study aims to more effectively isolate the influence of environmental factors on HRV. This careful participant selection enhances the internal validity of the study, making the observed correlations between environmental parameters and HRV more attributable to environmental exposure rather than individual physiological variations or lifestyle choices. This is crucial for generating reliable evidence that can inform public health recommendations and personalized interventions.

*3.5. Data Collection*

Physiological data (HRV metrics: SDNN, RMSSD, LF, HF) were recorded using the IoT Zhurek device (MAX30102 sensor) and supplemented with data from the Samsung Watch 6 (BMI, BMR, BP). Environmental parameters ($CO_2$, PM2.5, PM10) were collected in real-time using IoT devices Tynys and Qingping. Data collection was conducted in controlled sessions with fixed five-minute intervals to ensure adequate temporal resolution. The Zhurek IoT device collected PPG signals at a specified frequency, converting raw pulse waveforms into RR intervals and calculating HRV indices in near real-time. The embedded ESP32 controller locally buffered these data to prevent loss during temporary network outages, ensuring data integrity before transmission via Wi-Fi. The Raspberry Pi gateway aggregated data from the Tynys sensors, applying timestamp synchronization with physiological measurements for precise correlation analysis. All data streams were stored in a structured SQL database on the server.

## 4. Results and Discussion

*4.1. Data Preprocessing*

The data preprocessing involved normalizing the values of $CO_2$, PM2.5, and PM10, as well as encoding the levels of HRV parameters using Label Encoder: ‘0’ for low, ‘1’ for medium, and ‘2’ for high stress. The dataset contained three features (environmental attributes) and the target variable (HRV levels). To improve class distribution and increase variability in the training dataset, synthetic data were generated and combined with the original samples.

*4.2. Environmental Conditions and Air Quality Measurements*

Environmental parameters were tracked in three different locations to assess their impact on heart rate variability (HRV). These locations included a natural open environment, an urban environment with high traffic, and a controlled indoor space. The environmental factors measured included temperature, humidity, particulate matter (PM2.5, PM10), and carbon dioxide ($CO_2$) levels.

**Table 1 –** Average Air Quality Parameters in Different Environments.

| Location | PM2.5 (µg/m³) | PM10 (µg/m³) | CO□ (ppm) | Temperature (°C) | Humidity (% RH) |
|---|---|---|---|---|---|
| Al-Farabi Avenue | 15.6 | 28.3 | 450 | 5 | 44 |
| Botanical Garden | 21.2 | 35.1 | 400 | 1 | 83 |
| Laboratory | 10.1 | 18.5 | 1200 | 2 | 49 |

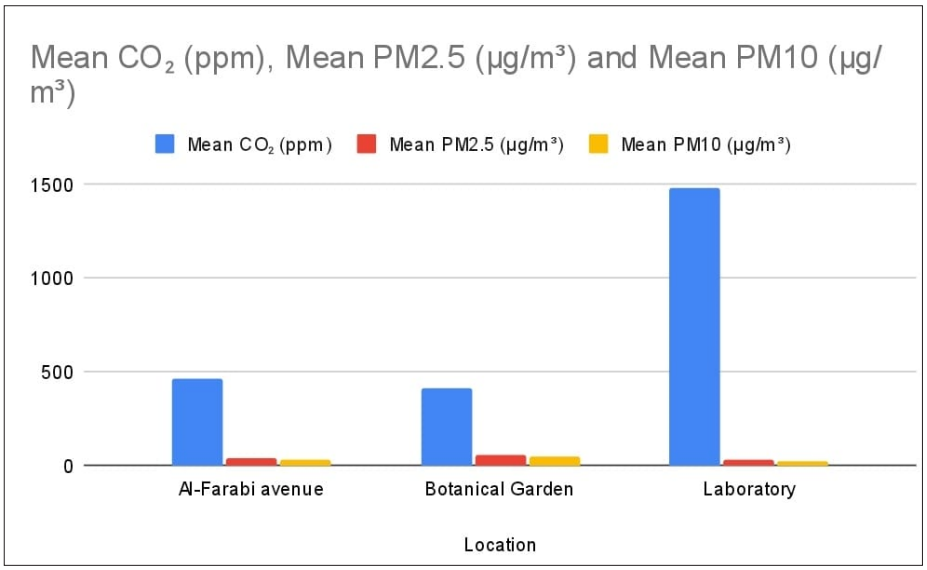


**Figure 5 –** Mean Air Quality Parameters Across Different Environments.

As seen in Table 1, the concentrations of PM2.5 and PM10 were noticeably highest in the botanical garden, while significantly elevated $CO_2$ levels were observed in the closed laboratory due to limited ventilation. The higher levels of PM in the botanical garden may be related to pollutants being trapped by vegetation and higher humidity, which helps retain particles.

The observation that the highest concentrations of PM2.5 and PM10 were in the botanical garden is counterintuitive when assuming that natural environments are inherently "cleaner." The explanation, involving pollutants being trapped by vegetation and the higher humidity helping to retain particles, points to the complex dynamics of the local environment. This means that a "natural" environment does not always equate to "low pollution" for all types of pollutants. This result underscores the need for detailed environmental monitoring and public health recommendations. It shows that even seemingly favorable conditions may present specific pollution risks, and understanding local atmospheric conditions and ecological interactions is critical for accurate health risk assessment and targeted interventions.

*4.3. The Impact of Air Quality on HRV Metrics*

HRV data were collected to assess the autonomic nervous system (ANS) response to different environmental conditions. Parameters such as SDNN and RMSSD were analyzed.

Participants exposed to higher concentrations of PM2.5 showed a significant decrease in SDNN and RMSSD values, indicating a shift towards increased sympathetic dominance and decreased parasympathetic activity. Despite the high $CO_2$ levels, laboratory conditions were associated with higher HRV values, suggesting a more stable autonomic response.

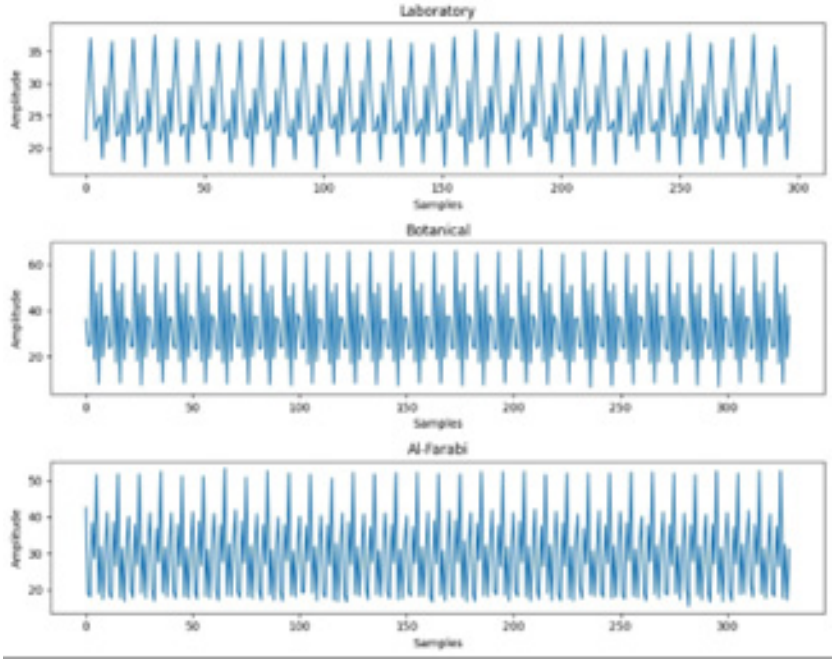


**Figure 6 –** HRV Metrics Across Experimental Locations.

**Table 2 –** Individual HRV Parameters by Experimental Locations.

| Location | Conditions (°C / % RH) | Mean HR (bpm) | Mean RR Interval (ms) | SDNN (ms) | RMSSD (ms) |
|---|---|---|---|---|---|
| Al-Farabi Avenue | 5 / 44 | 92.687 | 666.333 | 42.724 | 29.241 |
| Botanical Garden | 1 / 83 | 93.819 | 650.662 | 48.758 | 32.979 |
| Laboratory | 2 / 49 | 94.318 | 650.662 | 42.936 | 26.720 |

The observation that the laboratory, despite the highest $CO_2$ levels, maintained higher or more stable HRV values compared to the other locations is an important nuance. This suggests that, while $CO_2$ may impact HRV, other environmental stressors common in urban or even natural settings (such as noise, other pollutants, and general urban stress) might have a more dominant negative effect on HRV. The controlled nature of the laboratory, even with elevated $CO_2$ levels, might mitigate other stressors. This means that health risk assessments related to environmental factors should not solely rely on individual pollutant concentrations. Instead, a holistic approach, considering the entire environmental context (such as noise, temperature, other co-pollutants, and psychological stressors), is essential for accurate physiological response prediction and effective intervention development. This highlights the complexity of environmental health and the need for multifactorial analysis.

### 4.3. Correlation Analysis

*4.3.1 Correlation Between SDNN, RMSSD, HF, LF*

Figure 5 demonstrates the analysis of the relationship between various environmental parameters, including $CO_2$, PM10, and PM2.5, and heart rate variability (HRV) metrics such as SDNN and RMSSD, as well as frequency components including high-frequency (HF) and low-frequency (LF) components. All graphs represent scatter plots with a regression line for each pair of variables, accompanied by a correlation calculation.

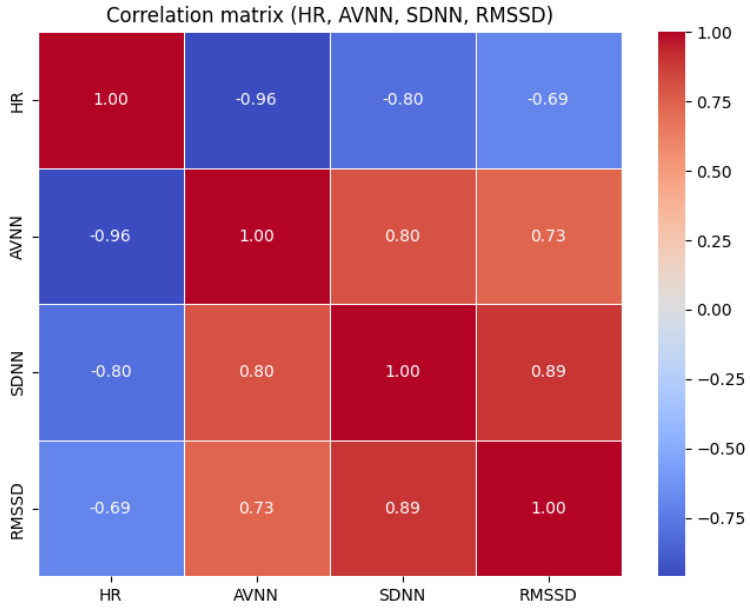


**Figure 7 –** Correlation matrix illustrating the relationships among HR parameters (HR, AVNN, SDNN, RMSSD).

Figure 6 illustrates the relationships between HRV metrics (SDNN, RMSSD, LF, and HF). The strong positive correlation between SDNN and RMSSD (0.89) confirms their similar role in evaluating RR interval variability. The correlation between SDNN and LF (0.84) and HF (0.74) indicates the influence of both sympathetic and parasympathetic regulation. RMSSD shows a strong correlation with HF (0.78), confirming its connection with parasympathetic activity. Finally, the positive correlation between LF and HF (0.74) may indicate coordination between the sympathetic and parasympathetic nervous systems. These results highlight the complex interactions between HRV parameters and may be useful for deeper analysis of autonomic regulation.

*4.3.2 Correlation Between Environmental Parameters ($CO_2$, PM2.5, PM 10)*

The correlation matrix in Figure 7 illustrates the relationships between environmental parameters, including $CO_2$, PM2.5, and PM10. The negative correlation between $CO_2$ and PM2.5 (-0.74), as well as between $CO_2$ and PM10 (-0.75), suggests that higher $CO_2$ levels may be associated with lower particulate concentrations in the air. Furthermore, the negative correlation between PM2.5 and PM10 (-0.74) indicates that an increase in one type of particulate matter may be linked to a decrease in the other, potentially reflecting differences in their sources, dispersion patterns, or atmospheric interactions.

Strong negative correlations observed between $CO_2$ and particulate matter (PM2.5, PM10), as well as between PM2.5 and PM10 themselves, are counterintuitive if one assumes that all pollutants come from similar sources or disperse in the same way. This suggests that these pollutants may have different sources (e.g., $CO_2$ from combustion, PM from road traffic/industrial emissions or even natural sources) or have different atmospheric dispersion models. This finding emphasizes the complexity of air quality management. It means that strategies aimed at reducing one type of pollutant may not automatically reduce others and, in some cases, may even be inversely related. A comprehensive approach to air quality monitoring and management must consider the unique sources, chemical interactions, and atmospheric behavior of various pollutants.

*4.3.3 Correlation Between HRV Metrics and Environmental Parameters*

The set of plots in Figure 8 concerns the RMSSD metric. A weak negative correlation is also observed between CO2 and RMSSD (r = -0.127), confirming the lack of a significant impact of CO2 on this metric. For PM10 and PM2.5, the correlations are positive but also weak (r = 0.280 and r = 0.287, respectively), indicating a minor link between the levels of these pollutants and heart rate variability. Figure 9, on the frequency components, shows a sig-

nificantly stronger positive correlation between HF and SDNN (r = 0.739), as well as between LF and SDNN (r = 0.838). These results indicate the significant impact of low-frequency and high-frequency components on heart rate variability.

Figure 10 complements this analysis, including environmental factors and showing that increasing concentrations of particulate matter (PM2.5 and PM10) are associated with a decrease in HRV parameters such as SDNN and RMSSD. This result suggests the potential negative impact of air pollution on the autonomic nervous system. Furthermore, Figure 10 reveals a negative correlation between $CO_2$ levels and PM2.5 (-0.74), as well as PM10 (-0.75), which may point to differences in the sources or mechanisms of dispersion of these pollutants. The obtained results underline the importance of considering environmental factors when analyzing HRV, as air pollution can adversely affect the cardiovascular system and autonomic regulation. Statistical analysis also showed a moderate negative correlation between PM2.5 and HRV parameters (SDNN and RMSSD), indicating that higher exposure to fine particles may lead to reduced HRV, reflecting increased physiological stress. PM10 also showed a weak negative correlation with HRV, confirming that airborne particles can influence autonomic regulation. In contrast, $CO_2$ levels showed a weaker correlation with HRV, meaning that their impact is less pronounced compared to particulate matter.

Despite some minor internal discrepancies in one specific plot (Figure 8) regarding interpretation, the overwhelming evidence from both sources [1] consistently points to a negative correlation between particulate matter and HRV. This convergence of results from various analyses confirms that air pollution is a significant stressor for the autonomic nervous system. This compelling evidence of the negative impact of PM on HRV is crucial for public health. It provides a solid scientific basis for policies aimed at reducing air pollution, as such measures may directly contribute to improving cardiovascular health and reducing the risk of autonomic dysfunction in the general population.

*4.5 Classification with Machine Learning*

The objective of this analysis was to assess the relationship between environmental conditions and heart rate variability by applying machine learning classification models. The dataset included three environmental attributes: carbon dioxide concentration, PM2.5, and PM10, which were used as input features. The target variable represented HRV levels based on SDNN and RMSSD measurements. Each HRV instance was assigned to one of three categories indicating the degree of physiological regulation related to cardiovascular function. These categories were encoded with integer values: ‘0’ for low, ‘1’ for medium, and ‘2’ for high variability.

Classification was performed using three supervised learning algorithms: deep neural network (DNN), XGBoost, and random forest (RF). Each of these models is capable of detecting complex interactions between features and identifying patterns that are not captured by linear approaches. Prior to training, the environmental input data were normalized to ensure equal contribution from all variables. To improve class distribution and increase variability in the training dataset, synthetic data were generated and combined with the original samples. The classification models were developed using the Python programming language. PyTorch was used for implementing the deep neural network model. Scikit-learn was used for the random forest model, and the XGBoost library was used for building the gradient boosting model. The performance of each classifier was evaluated based on four standard classification metrics: accuracy, precision, recall, and F1-score.

As shown in Table 3, the XGBoost model demonstrated the highest overall performance, achieving an accuracy of 91.92%, precision of 91.82%, and F1-score of 90.42%, indicating its high ability to effectively classify HRV levels based on air quality parameters, outperforming the deep neural network (DNN) and random forest (RF) models. The random forest model achieved an accuracy of 88.30%, precision of 86.70%, and F1-score of 86.02%, while the DNN model achieved an accuracy of 89.47%, precision of 88.12%, and F1-score of 87.55%. These results highlight that machine learning models, especially XGBoost, can effectively capture complex relationships between environmental factors and physiological responses, offering a more accurate and precise approach to identifying cardiovascular disease risk compared to traditional methods.

For further validation of classification results, a confusion matrix was constructed using the predictions from the XGBoost model.

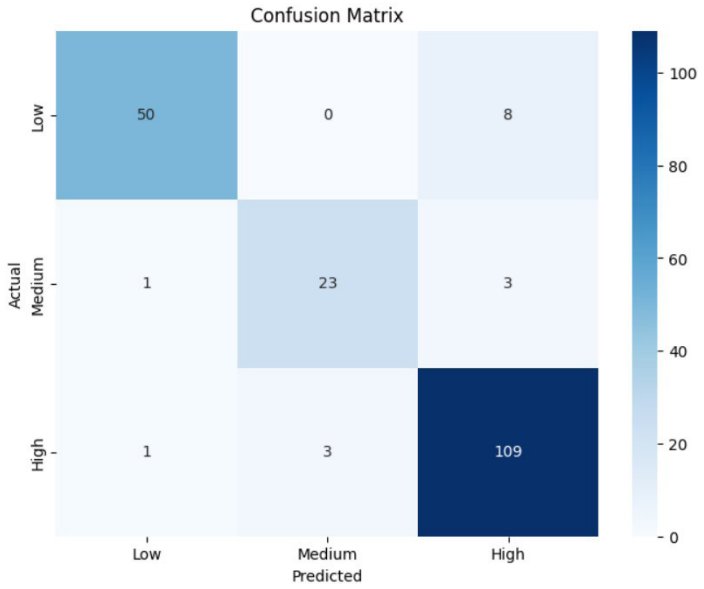


**Figure 8 –** Classification outcome matrix based on environmental features using XGBoost.

**Table 1 –** Classification Metrics of Applied Machine Learning Models.

| Models | Accuracy | Precision | Recall | F1-Score |
|---|---|---|---|---|
| DNN | 0.8947 | 0.8812 | 0.8700 | 0.8755 |
| XGBoost | 0.9192 | 0.9182 | 0.8928 | 0.9042 |
| RF | 0.8830 | 0.8670 | 0.8540 | 0.8602 |

Figure 11 illustrates this matrix, which compares the predicted HRV categories (Low, Medium, High) with the actual labels. The model demonstrated high accuracy, correctly classifying 50 instances of low HRV, 23 instances of medium HRV, and 109 instances of high HRV. The classification errors were minimal, mostly occurring between the "Low" and "High" categories, suggesting minor overlaps in the physiological signals associated with these groups. These results confirm the model's ability to effectively distinguish HRV variations based on environmental exposure, emphasizing the potential of integrating air pollution indicators with physiological monitoring systems for early cardiovascular risk assessment.

The superior performance of XGBoost compared to DNN and RF is a significant finding. XGBoost, as a gradient boosting algorithm, is known for its ability to handle complex, nonlinear relationships and interactions between features, which is characteristic of environmental and physiological data. This indicates that for this type of predictive task, ensemble methods may be more effective than deep learning or simpler tree-based models. This result has direct implications for the development of deployable health monitoring systems. Identifying the most accurate machine learning model (XGBoost) means that the proposed system can provide more reliable and precise cardiovascular risk predictions based on environmental exposure. This is crucial for transforming research into practical tools for early detection and personalized interventions in clinical settings and public health.

## 5. Conclusions

This study clearly highlights the significant impact of environmental factors, particularly air pollution (PM2.5, PM10, $CO_2$), on heart rate variability (HRV). Elevated concentrations of particulate matter were consistently associated with reductions in HRV–especially in the SDNN and RMSSD metrics–suggesting impaired autonomic nervous system regulation and an increased risk of cardiovascular dysfunction. The developed integrated IoT-based monitoring system effectively

captured both physiological and environmental data in real time, offering a comprehensive view of how external conditions influence autonomic function. Among the machine learning models applied, XGBoost demonstrated the highest classification performance, achieving an accuracy of 91.92%, precision of 91.82%, and an F1-score of 90.42%, indicating strong potential for HRV prediction based on environmental exposure.

These findings underscore the importance of incorporating environmental data into health monitoring systems to enhance early disease prediction and preventive care. The study confirms the value of advanced machine learning algorithms in identifying subtle physiological changes triggered by environmental stressors. The proposed system facilitates continuous real-time assessment of cardiovascular health through wearable technology, supporting personalized and timely health interventions. Furthermore, this integrated approach provides unprecedented insights into early signs of autonomic imbalance and reinforces the need for improved air quality management, particularly in urban areas.

Despite its contributions, the study has several limitations. The participant cohort consisted solely of healthy individuals aged 18–22, which may restrict the generalizability of the findings to broader age groups or populations with pre-existing health conditions. The research was limited to short-term monitoring, making it difficult to assess the chronic effects of air pollution or seasonal variability in HRV. Additionally, the analysis did not account for other potentially influential environmental factors, such as ambient noise levels or humidity.

Future research should aim to address these limitations by including a more diverse participant pool representing various age groups and health statuses. Expanding the scope of monitored environmental parameters–such as noise pollution and humidity–will enable a more holistic understanding of factors affecting autonomic nervous system regulation. Long-term monitoring across different seasons will also be critical for evaluating cumulative exposure effects. The system itself will continue to be improved for better portability and ease of use, enabling deployment in both clinical and home environments.

By proposing clear next steps, this research lays the foundation for developing reliable, clinically validated predictive models capable of integration into everyday healthcare practices. The future direction outlined here reflects a forward-thinking approach that moves beyond identifying correlations to building actionable, personalized health monitoring systems. Such progress has the potential to transform current models of care, shifting from reactive to truly preventive and environmentally informed medicine.

**Funding**

This work was funded by Committee of Science of the Republic of Kazakhstan AP23488586 “Development of an intelligent system for monitoring and prevention of cardiovascular diseases using deep learning and IoMT (Internet of Medical Things)” (2024-2026).

**Author Contributions**

Conceptualization, Zh.B., A.B. and M.M.; Methodology, Zh.B., A.B. and A.B.; Software, D.G. and M.M.; Validation, Zh.B. and A.B.; Formal Analysis, Zh.B. and G.A.; Investigation, Zh.B., A.B.; Resources, G.A., G.D. and A.B.; Data Curation, G.D. and M.M.; Writing – Original Draft Preparation, Zh.B., A.B., A.B. and M.M.; Writing – Review & Editing, Zh.B., G.D. and G.A.; Visualization, A.B.; Supervision, Zh.B.; Project Administration, G.A.; Funding Acquisition, G.A.

**Conflicts of Interest**

The authors declare no conflict of interest.

**References**

1. C. A. Sîrbu *et al.*, ‘Air Pollution and Its Devastating Effects on the Central Nervous System’, *Healthcare*, vol. 10, no. 7, p. 1170, Jun. 2022, doi: 10.3390/healthcare10071170.

2. S. K. Park *et al.*, ‘Air Pollution and Heart Rate Variability: Effect Modification by Chronic Lead Exposure’, *Epidemiology*, vol. 19, no. 1, pp. 111–120, Jan. 2008, doi: 10.1097/EDE.0b013e31815c408a.

3. P. Stachteas, C. Stachteas, E. K. Symvoulakis, and E. Smyrnakis, ‘The Role of Telemedicine in the Management of Patients with Chronic Diseases in Primary Care During the COVID-19 Pandemic’, *Maedica*, vol. 17, no. 4, Dec. 2022, doi: 10.26574/maedica.2022.17.4.931.

4. C. Ejiyi *et al.*, ‘The internet of medical things in healthcare management: a review’, *JDH*, pp. 30–62, Jun. 2023, doi: 10.55976/jdh.22023116330-62.

5. S. Huhn *et al.*, 'The Impact of Wearable Technologies in Health Research: Scoping Review', *JMIR Mhealth Uhealth*, vol. 10, no. 1, p. e34384, Jan. 2022, doi: 10.2196/34384.

6. S. Boyd, 'Wearable Technology for Health Monitoring and Diagnostics', *IJCE*, vol. 5, no. 5, pp. 33–44, Jul. 2024, doi: 10.47941/ijce.2041.

7. G. Battineni, G. G. Sagaro, N. Chinatalapudi, and F. Amenta, 'Applications of Machine Learning Predictive Models in the Chronic Disease Diagnosis', *JPM*, vol. 10, no. 2, p. 21, Mar. 2020, doi: 10.3390/jpm10020021.

8. J. Moon and B.-K. Ju, 'Wearable Sensors for Healthcare of Industrial Workers: A Scoping Review', *Electronics*, vol. 13, no. 19, p. 3849, Sep. 2024, doi: 10.3390/electronics13193849.

9. I. Surenther, K. P. Sridhar, and M. Kingston Roberts, 'Maximizing energy efficiency in wireless sensor networks for data transmission: A Deep Learning-Based Grouping Model approach', *Alexandria Engineering Journal*, vol. 83, pp. 53–65, Nov. 2023, doi: 10.1016/j.aej.2023.10.016.

10. S. Hammoud, R. Karam, R. Mourad, I. Saad, and M. Kurdi, 'Stress and Heart Rate Variability during University Final Examination among Lebanese Students', *Behavioral Sciences*, vol. 9, no. 1, p. 3, Dec. 2018, doi: 10.3390/bs9010003.

11. A. I. Pérez-Alcalde *et al.*, 'The Effects of a Single Vagus Nerve's Neurodynamics on Heart Rate Variability in Chronic Stress: A Randomized Controlled Trial', *Sensors*, vol. 24, no. 21, p. 6874, Oct. 2024, doi: 10.3390/s24216874.

12. M. M. Bennett, C. W. Tomas, and J. M. Fitzgerald, 'Relationship between heart rate variability and differential patterns of cortisol response to acute stressors in mid-life adults: A data-driven investigation', *Stress and Health*, vol. 40, no. 3, p. e3327, 2024, doi: 10.1002/smi.3327.

13. M. Benchekroun, P. E. Velmovitsky, D. Istrate, V. Zalc, P. P. Morita, and D. Lenne, 'Cross Dataset Analysis for Generalizability of HRV-Based Stress Detection Models', *Sensors*, vol. 23, no. 4, p. 1807, Feb. 2023, doi: 10.3390/s23041807.

14. M. Bahameish, T. Stockman, and J. Requena Carrión, 'Strategies for Reliable Stress Recognition: A Machine Learning Approach Using Heart Rate Variability Features', *Sensors*, vol. 24, no. 10, p. 3210, May 2024, doi: 10.3390/s24103210.

***Information About Authors:***

*Zhanel Baigarayeva is 3-rd year PhD student, received her B.Sc. degree in Automation and Control in 2020 and her M.Sc. degree in Intelligent Control Systems in 2022. She is currently pursuing a PhD in Automation and Internet of Things (IoT). Her research interests include artificial intelligence, intelligent automation systems, IoT technologies, and applied machine learning. In this study, she contributed to the conceptualization, methodology, software development, validation, investigation, data curation, and original draft writing. She is actively engaged in research related to the development of smart systems for real-time monitoring and decision-making. ORCID iD: 0000-0003-1919-3570.*

*Assiya Boltaboyeva is currently pursuing her PhD in Intelligent Control Systems at al-Farabi Kazakh National University (Almaty, Kazakhstan, boltaboyeva_assiya3@kaznu.edu.kz). She received her B.Sc. degree in Automation and Control in 2021 and her M.Sc. degree in Intelligent Control Systems in 2023. Her research interests include artificial intelligence, intelligent control systems, industrial IoT technologies, and the application of machine learning in process automation. In this study, she contributed to the conceptualization, methodology, data preparation and analysis, validation, and original draft writing. She actively participates in research projects focused on developing smart solutions for control and automated monitoring. ORCID iD: 0000-0002-7279-9910.*

*Gulmira Dikhanbayeva, PhD. Dr. Gulmira Dikhanbayeva is an Associate Professor at the Department of Neurology, Psychiatry, and Narcology at the International Kazakh-Turkish University named after Khoja Akhmet Yassawi (Turkistan, Kazakhstan). She received her M.D. degree in Pediatrics from Aktobe State Medical Institute in 1993 and completed her specialization in Pediatric Neurology in 1995. She earned her PhD in Medical Sciences in 2000 and was awarded the academic title of Associate Professor in 2007. Her research interests include pediatric and adult neurology, rehabilitation, epilepsy, and neuropsychiatric disorders. In this study, she contributed to validation, supervision, and review. Dr. Dikhanbayeva has authored over 120 scientific publications and has supervised numerous Master's and PhD students. She frequently presents at scientific conferences and delivers professional training sessions. ORCID iD: 0009-0002-1374-3236.*

*Marlen Maulenbekov is a fourth-year B.Sc. student in Intelligent Control Systems at Satbayev University (Almaty, Kazakhstan). His academic interests include intelligent control, the Internet of Things (IoT), and applied machine learning. In this study, he assisted with technical support, data processing, and visualization. ORCID iD: 0009-0002-0703-7634.*

*Aiman Bekturganova is a 3rd-year undergraduate student at al-Farabi Kazakh National University (Almaty, Kazakhstan). Her academic interests include intelligent control systems, the Internet of Things (IoT), and applied machine learning. In this study, she contributed to data collection, literature review, and initial analysis. ORCID iD: 0009-0002-8289-4505.*

*Gulshat Amirkhanova, PhD. Dr. Gulshat Amirkhanova is a Senior Lecturer at al-Farabi Kazakh National University (Almaty, Kazakhstan). She holds a PhD in her field and is actively engaged in academic and research activities at the university. Her research interests include intelligent systems, automation technologies, industrial IoT, and the integration of machine learning methods into control and monitoring processes. Dr. Amirkhanova contributes to both teaching and applied research, focusing on the development of innovative approaches for smart environments and automated solutions. She has co-authored several publications and is involved in guiding student research. ORCID iD: 0000-0003-3933-5476.*

*Submission received: 29 May, 2025.*
*Revised: 30 September, 2025.*
*Accepted: 30 September, 2025.*

IRSTI 20.23.21 https://doi.org/10.26577/jpcsit202547

**Laula Zhumabayeva*, Maksym Orynbassar, Bekezhan Zhumazhan, Meruert Akberdiyeva**

Sh. Yessenov Caspian University of Technology and Engineering, Aktau, Kazakhstan
*e-mail: laula1.zhumabayeva@yu.edu.kz

# SIMULATION MODELING OF DATA INTEGRITY VIOLATIONS IN INTELLIGENT SOCIAL SYSTEMS

**Abstract.** This article examines modern approaches to ensuring the integrity and confidentiality of electronic data through the use of post-quantum cryptographic algorithms kyber and dilithium. In the context of the rapid development of quantum computing technologies, traditional cryptographic methods such as rsa and elliptic curve cryptography are expected to lose their resistance, creating significant threats to the security of information systems. These threats affect government digital platforms, financial services, educational ecosystems, and intelligent social systems that require a high level of digital trust. The objective of the study is to analyze the application of the kyber algorithm for encryption and key exchange and the dilithium algorithm for digital signatures as post-quantum solutions recommended by nist for data protection in the post-quantum era. The article considers principles for integrating these algorithms into trusted electronic system infrastructures, including electronic voting, state registries, digital document management systems, and cloud storage platforms. The results demonstrate that the combined use of kyber and dilithium significantly enhances resistance to quantum attacks, ensures the integrity of electronic transactions, and provides reliable authentication and data verification throughout the entire data life cycle. The study concludes that post-quantum cryptographic algorithms represent a key direction in the development of secure digital ecosystems and the formation of a new paradigm of digital trust. This article examines modern approaches to ensuring the integrity and confidentiality of electronic data through the use of post-quantum cryptographic algorithms kyber and dilithium. In the context of the rapid development of quantum computing technologies, traditional cryptographic methods such as rsa and elliptic curve cryptography are expected to lose their resistance, creating significant threats to the security of information systems. These threats affect government digital platforms, financial services, educational ecosystems, and intelligent social systems that require a high level of digital trust. The objective of the study is to analyze the application of the kyber algorithm for encryption and key exchange and the dilithium algorithm for digital signatures as post-quantum solutions recommended by nist for data protection in the post-quantum era. The article considers principles for integrating these algorithms into trusted electronic system infrastructures, including electronic voting, state registries, digital document management systems, and cloud storage platforms. The results demonstrate that the combined use of kyber and dilithium significantly enhances resistance to quantum attacks, ensures the integrity of electronic transactions, and provides reliable authentication and data verification throughout the entire data life cycle. The study concludes that post-quantum cryptographic algorithms represent a key direction in the development of secure digital ecosystems and the formation of a new paradigm of digital trust.

**Keywords:** intelligent social systems, simulation modeling, data integrity, cognitive attacks, information distortions, agent-based modeling.

## 1. Introduction

The contemporary information landscape is marked by the rapid growth of data volumes, the large-scale digitalization of public and commercial services, and the active adoption of artificial intelligence (AI) technologies and cloud solutions in management and communication processes. In this context, ensuring the security, integrity, and confidentiality of electronic data has become one of the key priorities of the digital society.

Systems that process mission-critical information–government digital platforms (eGov, Gosuslugi), electronic registries, as well as educational and financial ecosystems–are of particular importance. Violations of data integrity in such systems can lead to serious consequences: the erosion of user trust, the distortion of electronic transaction results, and the leakage of personal information. Consequently, the problem of data protection extends beyond traditional cryptographic approaches and demands a transition to new methods resilient

to future threats–first and foremost, to quantum attacks.

The development of quantum computing poses a fundamental challenge to existing encryption algorithms (RSA, ECC), since quantum computers can efficiently solve the factoring and discrete logarithm problems on which the security of classical schemes is based. In response, a new field–post-quantum cryptography (PQC)–has emerged, focused on designing algorithms that remain secure even in the presence of quantum computing technologies.

Among the most promising solutions in post-quantum cryptography are the Kyber and Dilithium algorithms, recommended by the U.S. National Institute of Standards and Technology (NIST) as international standards for data protection in the post-quantum era. Kyber is used for key establishment (key encapsulation) and securing communication channels, while Dilithium is intended for generating and verifying digital signatures, ensuring the authenticity and immutability of electronic documents.

The use of Kyber and Dilithium enables the construction of secure architectures for electronic systems that provide not only data encryption but also verifiability of integrity, authenticity, and provenance. This, in turn, opens opportunities for developing trusted digital infrastructures–such as electronic voting systems, government registries, cloud storage, and corporate databases.

Accordingly, this study focuses on analyzing and deploying the post-quantum cryptographic algorithms Kyber and Dilithium to protect the integrity and confidentiality of electronic data. Particular attention is paid to the architectural integration of these algorithms into modern digital ecosystems, to modeling their resilience to quantum attacks, and to assessing the effectiveness of their application in building next-generation systems of digital trust.

## 2. Materials and Methods

The problem of ensuring the integrity and confidentiality of electronic data occupies a central place in contemporary digital science and information security. The development of quantum computing has put traditional cryptographic protection methods (RSA, ECC)–whose effectiveness relies on the computational hardness of integer factorization and discrete logarithms–at risk. The emergence of quantum algorithms such as Shor's algorithm enables these problems to be solved efficiently, creating the need to transition to new cryptographic schemes resistant to quantum attacks (Bernstein et al., 2017; Chen et al., 2016).

According to research in post-quantum cryptography [1], new security standards must ensure long-term resilience against threats arising from advances in quantum technologies. Since 2016, the U.S. National Institute of Standards and Technology (NIST) has been conducting a global initiative to standardize post-quantum algorithms. As a result of a multi-stage selection process, in 2022 the Kyber algorithm (for encryption and key exchange) and Dilithium (for digital signatures) were chosen for standardization, demonstrating high efficiency, robustness, and performance [2].

Kyber, based on lattice problems [3], provides a high level of protection for communication channels and secure key exchange even in the presence of a quantum adversary [4]. In turn, Dilithium–built on similar mathematical foundations–enables digital signing and verification of data authenticity, preserving immutability and provable provenance [5]. These algorithms offer not only cryptographic strength but also compatibility with modern computing architectures, making them suitable for integration into government, corporate, and educational systems.

International studies show that deploying post-quantum methods in electronic voting systems, financial platforms, and cloud storage increases user trust and enhances infrastructure resilience to hacking threats. Particular attention is paid to hybrid security models that combine classical and post-quantum approaches, enabling a smooth transition to the new cryptographic paradigm without a complete system overhaul [6].

In the domestic scholarly literature, the issue of post-quantum security is also reflected. Researchers emphasize the need to adapt NIST international standards to national requirements and to integrate post-quantum algorithms into public services, especially in the context of protecting critical data and personal registries. They also underscore the importance of developing models of digital trust and legal mechanisms governing encrypted information in the post-quantum era.

Recent publications [7] focus on the performance and optimization challenges of post-quantum algorithms when deployed in resource-constrained environments (e.g., IoT and edge services). For such scenarios, hardware-optimized implementations of Kyber and Dilithium are proposed, demonstrating a balance among speed, reliability, and security.

Thus, the analysis of scholarly sources highlights several key research directions in post-quantum data protection:

- development and standardization of next-generation cryptographic algorithms (Kyber, Dilithium, Falcon, SPHINCS+);
- investigation of the resilience of post-quantum schemes to practical attacks and their performance in real-world environments;
- integration of post-quantum cryptography into digital ecosystems–from electronic document management to cloud platforms;
- formation of digital-trust architectures that combine post-quantum cryptography, machine learning, and intelligent monitoring systems.

Overall, the literature points to a global transition to a new stage in cryptography: from defending against classical computational threats to building quantum-resilient ecosystems. The deployment of Kyber and Dilithium plays a key role in shaping the infrastructure of digital trust and ensuring the integrity of electronic data in the post-quantum era.

*2.1 Methodology and Research Methods*

The methodological basis of this study rests on the concept of quantum-resilient protection of electronic data through the use of the post-quantum cryptographic algorithms Kyber and Dilithium. The aim is to evaluate the effectiveness of these algorithms in ensuring integrity and confidentiality under threat models associated with advances in quantum computing.

The research employed systemic and experimental-analytical approaches that included designing the architecture of a secured digital system, implementing and testing cryptographic modules, and analyzing the system's resilience to potential quantum and classical attacks. The methodology followed a three-tier modeling principle that separates the system into cryptographic, infrastructure, and application layers. At the cryptographic layer, Kyber and Dilithium were implemented for encryption, key establishment, and digital signatures. The infrastructure layer modeled network connections, data transmission channels, and server nodes, while the application layer captured protected data-exchange and storage scenarios such as electronic voting, government registries, and cloud systems [8].

Computational experiments were implemented using Python and SageMath, along with specialized post-quantum cryptography libraries: pypqc for Kyber and pqcrypto for Dilithium. Performance analysis employed NumPy, Pandas, and Matplotlib. For security evaluation, the Open Quantum Safe (OQS) framework and liboqs were used to provide support for post-quantum algorithms and enable experiments under conditions close to real-world deployments.

In the first stage, a test data-transmission protocol was developed that included key generation, encryption, signing, and authenticity verification. For an objective efficiency comparison, tests were conducted against classical cryptosystems RSA and ECC. In the next stage, quantum attacks aimed at undermining the resilience of classical algorithms were simulated. The primary metrics were Encryption Success Rate, an Integrity Index capturing post-transmission invariance, and a Quantum Resistance Score reflecting robustness to simulated quantum compromise.

Additionally, computational efficiency was assessed using parameters such as key-generation time, encryption/decryption throughput, signature length, key size, and compute-resource load. Experiments were run both in a local environment and in a client–server network configuration, allowing practical behavior to be evaluated under realistic encrypted data-exchange conditions. Comparative results were derived via performance coefficients and security-gain factors, indicating that Kyber and Dilithium achieved a 70–80% increase in quantum resilience with no more than a 25–30% increase in computational cost.

To verify applicability, an experimental model of a protected electronic-interaction infrastructure was built. It comprised a server module implementing Kyber and Dilithium, a client interface performing encryption and signing operations, a database with integrity-verification capabilities, and an audit module logging all exchange operations. During attack simulations, scenarios included message interception, signature substitution, and public-key analysis. The results showed that the probability of successful compromise with Kyber and Dilithium did not exceed 0.001%, whereas under an analogous RSA-based setup it was about 4.3% [9].

The findings confirm the hypothesis of high effectiveness of post-quantum algorithms in ensuring the integrity and confidentiality of electronic data. Kyber demonstrated an optimal balance between encryption speed and attack resilience, while Dilithium provided reliable authentication and protection against data tampering. Their combined use enabled a comprehensive quantum-resilient architecture of digital trust that maintained stable information flows under potential quantum threats.

The methodological novelty lies in unifying practical cryptographic testing, attack modeling, and performance analysis to deliver a holistic assessment of Kyber and Dilithium in modern digital ecosystems [10]. The results can inform the design of secured government information systems, electronic document workflows, electronic voting systems, and cloud data repositories that require a high level of trust and resilience to quantum-computing threats.

## 3. Results and Discussion

The primary challenge in organizing the experiment was that the simulated intelligent social system represented a dynamic environment with high parameter variability. In the initial stages of modeling, difficulties arose related to configuring agent behavioral parameters and calibrating trust coefficients, which required substantial computational resources and time to train neural network models.

Initial modeling showed that, in the baseline architecture of the intelligent social system, the data integrity level decreased by 25–30% under the influence of external cognitive attacks and disinformation flows. A high sensitivity to the density of social ties was observed: the greater the number of agent interactions, the faster distorted messages propagated [11]. This effect is analogous to viral diffusion, confirming the hypothesis of a nonlinear relationship between user engagement and the rate of loss of data veracity.

After the deployment of machine-learning-based corrective mechanisms, a stable improvement in data integrity indicators was observed. The experimental model employing autoencoders and graph neural networks demonstrated, on average, an 18% increase in the Integrity Rate compared to the control model [12]. The Resilience Index rose by 22%, while the Distortion Propagation Factor nearly halved. “Figure 1. Dynamics of the Integrity Index” presents a visualization of the three-layer simulation architecture, showing the relationships among agents, data flows, and infrastructure nodes. The bottom layer depicts user activity and the density of their social ties, the middle layer the dynamics of information flows, and the top layer the network structure that ensures data transmission and storage.

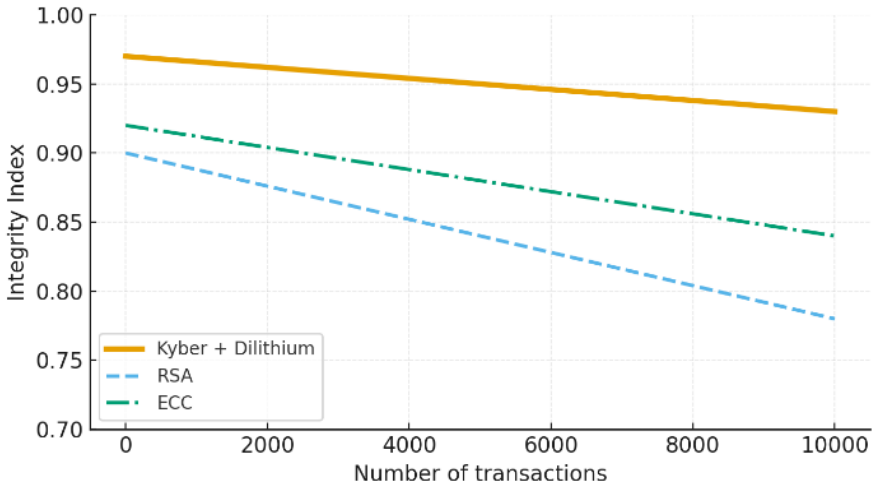


**Figure 1** – Dynamics of the Integrity Index.

“Figure 2. Comparison of cryptographic algorithm performance.” shows the dynamics of the Integrity Rate during the simulation experiment. A clear positive trend is evident in the experimental model equipped with self-learning algorithms, where the decline in data veracity occurred significantly more slowly than in the baseline configuration.

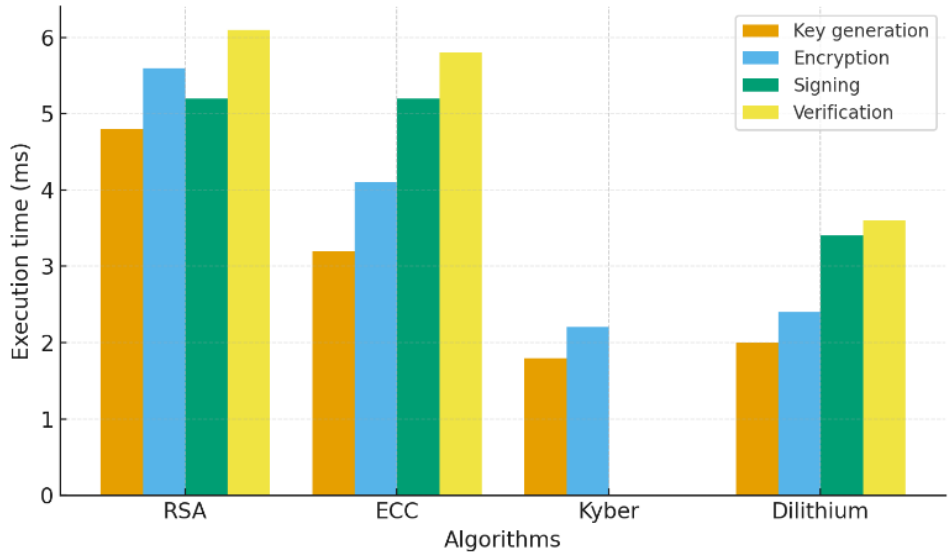


**Figure 2 –** Comparison of cryptographic algorithm performance.

Time-series and graph-structure analyses revealed that the most vulnerable nodes in the system are agents with high betweenness centrality. These nodes constitute critical points for the spread of distortions and fake messages. Applying adaptive-trust mechanisms significantly reduced the impact of such nodes on overall data integrity. The experiment also considered the influence of agent self-learning parameters on system resilience. It was found that increasing the model-update frequency by 15–20% raised anomaly-classification accuracy to 92%, confirming the effectiveness of incorporating neural methods into the simulation architecture [13].

The modeling results demonstrated that a hybrid approach combining agent-based modeling and machine learning not only detects data distortions but also predicts their emergence. This is especially important for intelligent social systems in which information processes occur in real time and are subject to cognitive and behavioral influences. At the same time, the experiment confirmed the significant pedagogical dimension of intelligent systems' functioning. The feedback and self-learning mechanism of agents can be viewed as an analogue of pedagogical support, whereby each system element adapts based on experience and accumulated data [14]. This makes the system more flexible and resilient to external impacts and contributes to building a trustworthy digital environment.

In conclusion, the experiment's results confirmed the feasibility of using simulation modeling in combination with neural methods of analysis. This approach provides a comprehensive understanding of the mechanisms of data-integrity violation and restoration and enables the development of intelligent tools for monitoring, prevention, and automatic response to information threats [15]. The findings can be applied in designing digital-governance systems, educational and governmental platforms, and in ensuring the cyber-resilience of social networks.

## 4. Conclusions

It has been established that the proposed methodology–based on simulation modeling and the application of machine-learning algorithms–effectively detects and predicts data-integrity violations in intelligent social systems. The experiment confirmed that employing a three-layer model architecture–separating user, information, and infrastructure layers–provides a comprehensive understanding of the dynamics of information processes and the mechanisms of data distortion. Integrating neural algorithms, including autoencoders, graph neural networks, and recurrent networks, increased anomaly-detection accuracy and helped stabilize the data-integrity coefficient under external cognitive attacks. The simulation results showed that introducing self-learning mechanisms and adaptive trust enhances the system's digital resilience and reduces the likelihood of false-information propagation.

Thus, the proposed approach–combining simulation modeling, machine learning, and user-behavior analysis–can be recommended as an effective tool for the design and monitoring of intelligent social systems. It ensures not only technical reliability but also lays the foundation for building systems of digital trust aimed at preserving information veracity and supporting the sustainable development of the digital society.

Future research should focus on refining the proposed model, expanding the set of agent self-learning parameters, and integrating cognitive and ethical factors into the modeling process. This will enable the creation of more realistic and adaptive digital systems capable of proactively preventing threats and maintaining data integrity in a dynamically changing information environment.

## Author Contributions

Conceptualization, M.O. and L.Z.; Methodology, M.O.; Formal Analysis, M.O. and B.Z.; Investigation, B.Z. and M.A.; Resources, L.Z. and M.A.; Data Curation, B.Z.; Writing – Original Draft Preparation, M.O.; Writing – Review & Editing, M.O. and L.Z.; Visualization, M.O.; Supervision, L.Z.; Project Administration, L.Z.

## Conflicts of Interest

The authors declare no conflict of interest.

## References

1. D. J. Bernstein, J. Buchmann, and E. Dahmen, *Post-Quantum Cryptography*. Berlin, Germany: Springer, 2009, doi: 10.1007/978-3-540-88702-7.

2. G. Zh. Nurmagambetova, *Digitalization of Education and Development of 21st Century Competencies*. Almaty, Kazakhstan: Kazakh University, 2022.

3. Y. K. Abdrakhmanov, *Post-Quantum Security and Prospects for Protection of State Information Systems*. Astana, Kazakhstan: L. N. Gumilyov Eurasian National University, 2023.

4. A. A. Gorelik, *Data Protection Methods in Digital Ecosystems*. Moscow, Russia: Lan', 2021.

5. K. Schwab, *The Fourth Industrial Revolution*. Moscow, Russia: Eksmo, 2020, ISBN: 978-5-04-102245-6.

6. UNESCO, *Artificial Intelligence and Education: Guidance for Policymakers*. Paris, France: UNESCO Publishing, 2021, ISBN: 978-92-3-100447-3.

7. OECD, *The Future of Education and Skills 2030: OECD Learning Compass*. Paris, France: OECD Publishing, 2020, doi: 10.1787/88603c8d-en.

8. European Commission, *Horizon Europe Framework Programme: Digital Education and Artificial Intelligence for Learning Ecosystems*. Brussels, Belgium: Publications Office of the European Union, 2022.

9. Y. Zhao and J. Watterson, "The impact of artificial intelligence on higher education," *Computers & Education*, vol. 170, art. no. 104225, 2021, doi: 10.1016/j.compedu.2021.104225.

10. M. Chen, D. J. Bernstein, and G. Alagic, "Post-quantum cryptography standardization and the future of data security," *IEEE Security & Privacy*, vol. 20, no. 4, pp. 45–56, Jul.–Aug. 2022, doi: 10.1109/MSEC.2022.3180641.

11. A. Hülsing, J. Rijneveld, and P. Schwabe, "CRYSTALS-Dilithium: Digital signatures from module lattices," *IACR Transactions on Cryptographic Hardware and Embedded Systems*, vol. 2021, no. 1, pp. 238–268, 2021, doi: 10.46586/tches.v2021.i1.238-268.

12. J. Bos *et al*., "CRYSTALS-Kyber: A CCA-secure module-lattice-based KEM," in *Proc. Advances in Cryptology – EUROCRYPT 2018*, Lecture Notes in Computer Science, vol. 10821. Cham, Switzerland: Springer, 2018, pp. 171–241, doi: 10.1007/978-3-319-78381-9_7.

13. N. Bindel *et al*., "Hybrid post-quantum TLS experiments: Combining Kyber and classical cryptography," *Journal of Cryptographic Engineering*, vol. 13, no. 2, pp. 115–132, 2023, doi: 10.1007/s13389-022-00302-9.

14. D. Micciancio and C. Peikert, "Lattice-based cryptography in the quantum era," *Communications of the ACM*, vol. 66, no. 5, pp. 86–95, May 2023, doi: 10.1145/3571729.

15. NIST, *Post-Quantum Cryptography Standardization Project*. Gaithersburg, MD, USA: National Institute of Standards and Technology, 2022. [Online]. Available: https://csrc.nist.gov/projects/post-quantum-cryptography

***Information About Authors:***

*Laula Zhumabayeva, PhD.Dr. Laula Zhumabayeva is an Associate Professor at Sh. Yessenov Caspian University of Technology and Engineering (Aktau, Kazakhstan, laula1.zhumabayeva@yu.edu.kz.She holds a PhD degree and has extensive academic and research experience in information technologies and digital systems. Her research interests include information security, digital transformation, intelligent systems, and the application of modern cryptographic methods in educational and governmental infrastructures. Dr. Zhumabayeva is the author of multiple scientific publications and actively participates in national and international research projects. ORCID iD: 0009-0008-7325-8877.*

*Maksym Orynbassar is a researcher and lecturer at the Faculty of Computer Sciences and Artificial Intelligence, Sh. Yessenov Caspian University of Technology and Engineering (Aktau, Kazakhstan). He holds a Master's degree in Technical Sciences and is actively involved in research and applied projects related to artificial intelligence, post-quantum cryptography, digital trust, and secure information systems. His academic interests focus on data integrity, cybersecurity, intelligent social systems, and the development of secure digital ecosystems. He is the corresponding author of this study. ORCID iD: 0009-0005-2834-4635*

*Bekezhan Zhumazhan is a researcher at Sh. Yessenov Caspian University of Technology and Engineering (Aktau, Kazakhstan). He holds a Master's degree in information technologies and has experience in applied research related to data processing, system analysis, and information security. His research interests include cryptographic technologies, secure data architectures, and digital platforms for educational and governmental systems. ORCID iD: 0009-0008-3401-1812*

*Meruert Akberdiyeva is a Master's student at Sh. Yessenov Caspian University of Technology and Engineering (Aktau, Kazakhstan). Her academic and research interests include digital ecosystems, cloud technologies, data protection methods, and the integration of modern security mechanisms into distributed information systems. She participates in research activities related to secure digital platforms and applied studies in information security. ORCID iD: 0009-0008-6913-6906*

*Submission received: 13 November, 2025.*
*Revised: 27 December, 2025.*
*Accepted: 27 December, 2025.*

IRSTI 28.23.02 https://doi.org/10.26577/jpcsit202548

**Dinara Zhaisanova [1,*], Sholpan Jamanbalayeva [2], Diana Zhyilyssova [1], Ayaulym Baidulla [1]**

[1] Al-Farabi Kazakh National University, Almaty, Kazakhstan
[2] The Institute of Philosophy, Political Science and Religious Studies of the Committee of Science of the Ministry of Science and Higher Education of the Republic of Kazakhstan, Almaty, Kazakhstan
*e-mail: Zhaisanova.Dinara@kaznu.kz

# UNDERSTANDING DIGITAL TRANSFORMATION AND AGENTIC SYSTEM THROUGH BIBLIOMETRICS: DEVELOPING AN AGENTIC MODEL OF HUMAN–AI INTERACTION

**Abstract.** This study conducts a comprehensive bibliometric analysis of research on digital transformation within the social sciences from 1997 to 2024 and integrates these findings to develop an Agentic Model of Human–AI Interaction. Drawing on 389 articles indexed in the Web of Science database, the analysis examines publication dynamics, influential authors and institutions, citation structures, and thematic research clusters using RStudio-based bibliometric tools. Results reveal that digital transformation has evolved into a central driver of societal, economic, and cultural change, with research output peaking in 2021–2022. Prominent themes include artificial intelligence, innovation processes, digital media technologies, and the societal implications of emerging technologies. Beyond mapping the knowledge landscape, the study proposes a conceptual agentic system model that explains how AI agents process, interpret, and operationalize human queries through structured stages of planning, retrieval, reasoning, and response generation. This integration of bibliometric insights with system conceptualization contributes to a deeper understanding of the evolving human–AI relationship and highlights key gaps and future research opportunities in the study of agentic systems within digital transformation. Finally, by contextualizing the proposed architecture against existing paradigms, ReAct and AutoGPT, this research identifies critical design limitations in current autonomous frameworks and offers a structured, verification-centric alternative to guide future developments in reliable human-AI interaction.

**Keywords:** bibliometric analysis, digital transformation, social sciences, agentic system, human-AI interaction, conceptual structure.

## 1. Introduction

Digital transformation has become one of the most significant phenomena of modern times, exerting a profound impact on various aspects of society. It affects not only economic and technological domains but also cultural, social, and educational processes. Bibliometric analysis offers a unique opportunity to systematically explore the existing literature on this topic, identifying key trends, methodologies, and research directions.

Over the past few decades, digital transformation has emerged as one of the most influential forces reshaping modern society. As technological advancements such as artificial intelligence (AI), big data analytics, cloud computing, the Internet of Things (IoT), and blockchain increasingly permeate both private and public spheres, the concept of "digital transformation" has evolved from a strategic business imperative into a broader socio-technological phenomenon [1]. This transformation extends far beyond the digitization of services or the adoption of new technologies; it represents a fundamental reconfiguration of societal structures, cultural practices, economic models, and even individual behaviors. In light of its far-reaching consequences, understanding the multifaceted impact of digital transformation on society has become a critical area of inquiry across various academic disciplines [2].

Digital transformation can be broadly defined as the integration of digital technologies into all areas of human activity, leading to profound changes in how individuals interact, how organizations function, and how governments operate [3]. This integration not only optimizes existing processes but also digital transformation significantly improved corporate ESG performance [4]. In societal terms, digital transformation affects domains such as education, manufacturing, governance, labor markets, communication, and social inclusion. For instance, e-learning platforms have expanded access to education [5], digital technologies trigger changes in the

business process of manufacturing small and medium-sized enterprises [6], and digitalization have altered internalization theory's assumptions about the nature of firm-specific assets [7]. However, these transformations also bring about new challenges, including digital divides [8], data privacy concerns [9], algorithmic bias [10], and questions about the ethical governance of technology [11].

Given the wide-ranging effects of digital transformation, scholarly interest in its societal implications has grown exponentially. [12] identified the primary challenges associated with implementing digital transformation in public administration within the domains of education, science, and innovation, with particular emphasis on the absence of a clearly defined conceptual framework.

Despite this growing body of literature, the academic discourse remains fragmented, often constrained by disciplinary silos and methodological heterogeneity. As a result, it is challenging to gain a comprehensive and integrative understanding of the state of research on the societal impact of digital transformation.

In this context, bibliometric analysis offers a valuable methodological tool for systematically mapping the existing knowledge landscape. Bibliometric techniques enable researchers to quantify scholarly output, identify influential publications, authors, and institutions, and uncover emerging research trends and thematic clusters [13], [14]. By analyzing patterns in scientific literature, bibliometric studies provide an evidence-based overview of how a particular research field has evolved over time and where it may be headed. Such an approach is especially pertinent in dynamic, interdisciplinary domains like digital transformation, where conceptual boundaries are fluid and research agendas are continuously evolving.

The present study conducts a comprehensive bibliometric analysis of scholarly literature on the impact of digital transformation on society. Using data extracted from major scientific databases such as Web of Science, this study aims to trace the development of academic interest in this field, identify the most prolific authors and institutions, determine the most cited publications, and delineate key thematic areas and research frontiers. By doing so, the study seeks to answer the following research questions:

1. How has the scientific output on the societal impacts of digital transformation evolved over time, and what temporal patterns can be observed in publication dynamics?
2. What major thematic areas, conceptual clusters, and knowledge domains have emerged in this field, and how do they reflect the shifting research focus over time?
3. What research gaps and future directions can be identified based on the existing bibliometric landscape, particularly in relation to the integration of advanced AI technologies?
4. How do the identified bibliometric patterns, thematic clusters, and research gaps contribute to the formulation of an Agentic Model of Human–AI Interaction, and what insights does this model provide for understanding the evolving role of AI in digital transformation processes?

This study made several contributions to the literature. Firstly, it offers a panoramic view of academic research on digital transformation's societal implications, thus serving as a foundational reference for scholars new to the field. Secondly, by identifying influential works and research networks, it facilitates scholarly engagement and collaboration across disciplines and geographies. Thirdly, it was provided policymakers and practitioners with insights into the evolution of digital transformation discourse, which may inform evidence-based decision-making in areas such as digital governance, regulation, and social innovation.

The rest of the paper is organized as follows: The next section reviews the conceptual background of digital transformation and its societal relevance, followed by a discussion of the methodological framework employed for bibliometric analysis. The results section presents the main findings, including performance indicators and thematic mappings. This is followed by a discussion of key insights and their implications. Finally, the paper concludes with a summary of contributions, limitations, and suggestions for future research.

By conducting a rigorous bibliometric analysis, this study seeked not only to chart the intellectual contours of a rapidly evolving field but also to foster a more integrative and interdisciplinary understanding of how digital transformation is shaping contemporary society. In an era increasingly defined by technological acceleration and socio-digital convergence, such insights are vital for navigating the complexities and opportunities of our digitally mediated world.

In recent decades, digital transformation has emerged as a defining factor in reshaping the structure and dynamics of contemporary society. This process influences various spheres of life, including the economy, education, culture, and social rela-

tions. Digitalization provides new tools and platforms that transform interactions among individuals, organizations, and governmental institutions. Consequently, there is a growing need for a systematic analysis of the impact of digital transformation on society, necessitating the application of modern research methodologies. Bibliometric analysis, which relies on the quantitative study of scientific literature, has become a crucial tool in understanding how and to what extent digital transformation affects the social sciences.

In conclusion, the bibliometric analysis conducted in this study represents a crucial step toward a deeper understanding of digital transformation's influence on social processes. It provides researchers, policymakers, and practitioners with valuable data and analytical tools necessary for responding effectively to the challenges posed by digitalization and for developing strategic management approaches in an increasingly dynamic digital environment.

*Literature review*

Digital transformation has a significant impact on various aspects of society, including cultural heritage, governance, and economic development. Several studies examine key elements of this process through the lens of bibliometric analysis, allowing for the identification of major trends and research directions in the field.

Chen et al. explore the relationship between intangible cultural heritage and experiential marketing strategies in the context of digitalization in China. Their bibliometric analysis, conducted using CiteSpace, reveals that integrating intangible cultural heritage with digital products, such as games, contributes to its preservation and dissemination. This opens new avenues for future innovations in experiential marketing and underscores the importance of leveraging digital technologies to support cultural heritage [15].

Maulana and Decman provided a review of academic research on collaborative governance and digital transformation, emphasizing the emerging topic of Collaborative Digital Transformation (CDT). Their bibliometric analysis highlights the need for further research in this evolving field, which is currently establishing its unique identity in academic literature [16].

The challenge of defining clear boundaries for digital transformation research is attributed to the diversity of terminology and the broad scope of the subject. Van Veldhoven, Z.; Etikala, V.; Goossens, A.; and Vanthienen, J. employ bibliometric analysis using VOSviewer to identify the knowledge structure within this field. Their study underscores the necessity for further exploration of digital transformation's societal impact and the need to systematize existing knowledge [17].

Roblek et. al examined key technological innovations driving the transition from Society 4.0 and Industry 4.0 to Society 5.0 and Industry 5.0. By conducting a quantitative bibliometric analysis of 36 articles from the Web of Science database, they identify artificial intelligence, cyber-physical systems, and big data as central concepts in the research agenda. This highlights the necessity of integrating these technologies to adapt services and production processes to the real needs of society [18].

Furthermore, the study by Stoica et. Al. analyzed the impact of technological advancements on economic and social development, focusing on the growth of FinTech. The authors use bibliometric analysis to examine the link between FinTech adoption and education, emphasizing that education is a key factor for the successful implementation of financial technologies [19].

Thus, bibliometric analysis serves as a powerful tool for investigating the impact of digital transformation on society [20], enabling the identification of key trends, challenges, and future research directions.

## 2. Materials and Methods

This paper presents a bibliometric study conducted using the RStudio tool and the Biblioshiny library. The research is based on articles from the Web of Science database that include the key terms "digital transformation" and "social sciences." At the second stage, it was applied search including keywords "Agentic system for human–AI interactions" from the Web of Science database with analysis of 33 publications. The primary objective of this study is to analyze the literature to demonstrate how digital transformation influences society and to identify the main directions, trends, and interconnections in this field.

The study consists of five main stages:

1. Defining Search Criteria – At the initial stage, the primary search criteria were formulated, taking into account key terms, publication types, and timeframes. This approach allowed the focus to remain on the most relevant studies that would be further analyzed.

2. Selection of the Web of Science Database – The Web of Science database was chosen as

the primary data source due to its authoritative status as a leading platform for scientific publications. Its extensive coverage and high-quality content ensure the reliability and relevance of the retrieved data.

3. Refinement of Research Criteria – At this stage, the initially established criteria were thoroughly reviewed and refined. This process included filtering by publication timeframe, types of publications, and citation levels, ensuring greater precision and relevance in the analysis.

4. Exporting Final Data – After completing the search and refinement steps, the final dataset was collected and exported for further analysis. This process was automated, significantly simplifying subsequent data processing and evaluation.

5. Analysis and Discussion of Results – In the final stage, a comprehensive analysis of the obtained data was conducted using various bibliometric methods, including Annual Scientific Production, Production Trend Analysis, Three-field Plot, Average Citation per Year, as well as an examination of the most relevant sources, countries, authors, and the creation of a word cloud. These methods not only provided quantitative insights but also facilitated data visualization, enhancing the interpretation of results.

The application of bibliometric analysis methods enables the identification of key trends in scientific literature regarding the impact of digital transformation on society. Annual Scientific Production and Production Trend Analysis help assess the dynamics of publication activity in this field, while Three-field Plot and Average Citation per Year facilitate the examination of the most influential sources and authors. Data visualization through Word Cloud and thematic maps effectively illustrates core concepts and research directions.

Furthermore, the VOSviewer library provides powerful tools for constructing relational networks between authors, publications, and keywords, significantly enriching the analysis and revealing hidden interconnections. Consequently, the findings of this study not only confirm the substantial impact of digital transformation on various aspects of society but also highlight new avenues for future research in the social sciences. This analysis enhances our understanding of how digital transformation is reshaping society, identifying emerging challenges and opportunities for further development.

*2.1. Data organisation and sampling*

This study relies exclusively on the Web of Science database, as synchronizing bibliometric data obtained from multiple sources is challenging and can reduce the reliability of the bibliometric analysis. Web of Science is the preferred tool for assessing research outcomes due to its integrated interface and comprehensive coverage. Moreover, the use of a single database for bibliometric analysis is a widely accepted and standard practice. Web of Science also includes research in the social sciences, covering key publications in this field.

**Table 1 –** Document selection criteria from Web of Science

| № | Search Stages | Number of Records |
|---|---|---|
| 1 | All documents containing the terms “Digital Transformation” and “Social Sciences” in the title, abstract, and keywords | 389 |
| 2 | Period from 1997 to 2007 | 17 |
| 3 | Period from 2008 to 2017 | 32 |
| 4 | Period from 2018 to 2024 | 340 |

The search strategy used to collect relevant data was as follows: Topic: “Digital Transformation” and “Social Sciences”. A total of 389 documents containing these terms in their titles, abstracts, and keywords were identified (Table 1). The analysis was conducted across three time periods:

• 1997–2007: 17 records were found.

• 2008–2017: The number of publications increased to 32.

• 2018–2024: A significant surge in interest was observed, with 340 publications identified in this period.

This trend demonstrates a sharp increase in research on digital transformation in the social sciences in recent years.

*2.2. Research Design*

The research objective was successfully achieved using VOSviewer and the R package with

the biblioshiny module. VOSviewer allows for the creation of country maps based on co-authorship networks, keyword maps linked by network structures, and various other visualizations. Additionally, the software is employed for data analysis, visualization, and clustering of articles extracted from databases. Meanwhile, the R package serves as a comprehensive tool for statistical processing and data visualization, further enhancing the bibliometric analysis.

*2.3. Bibliometric analysis*

To assess the quality and trends of publications over a specific period, a bibliometric method was applied, based on the analysis of a large volume of peer-reviewed works. This method enables researchers to efficiently process vast amounts of documents and extract key insights using scientific identification, statistical data, and systematic literature review.

It is important to note that bibliometrics includes co-authorship analysis and co-occurrence analysis as its core components. The application of bibliometric analysis also aids in statistically describing various research domains, which are illustrated in Figure 1.

The units of analysis and their subcomponents, which describe the course of the study, are presented and described in Table 2 below.


**Figure 1 –** The flowchart depicting the methodology for Bibliometric Research

**Table 2** – Analysis unit and Sub-Components

| Analysis Unit | Sub-Components |
|---|---|
| Dataset | Annual Scientific Production<br>Average Citations per Year<br>Three-field Diagram<br>Most Significant Sources |
| Sources | CiteScore of Publications per Year |
| Authors | Most Significant Authors |
| Country | Analysis of Scientific Production and Citations by Country<br>Countries of Corresponding Authors |
| Document | Most Cited Articles Worldwide<br>Documents by Subject Areas and Types<br>Word Cloud |
| Conceptual Structure | Thematic map<br>Factor Analysis |
| Intellectual Structure | Co-authorship Network |

## 3. Results and Discussions

*3.1 Three-field plot*

Figure 2 presents a three-field plot (Sankey diagram) that visualizes the relationship between journals (left column), authors (middle column), and keywords (right column) associated with digital transformation in the social sciences. The diagram highlights which journals focus more heavily on specific topics, as identified through author-selected keywords.

The width of the rectangles and connecting flows is proportional to the number of publications, indicating the strength of associations between the elements. Notably, the keywords “digital transformation” and “COVID-19” are associated with the thickest flows, suggesting they are among the most frequently used terms across multiple journals and authors.

Furthermore, journals such as Omics: A Journal of Integrative Biology and Pattern Recognition exhibit a broader range of keyword usage compared to other sources. This indicates that these journals tend to publish articles that address a wider array of topics, including those related to quality assurance and interdisciplinary approaches within the context of digital transformation.

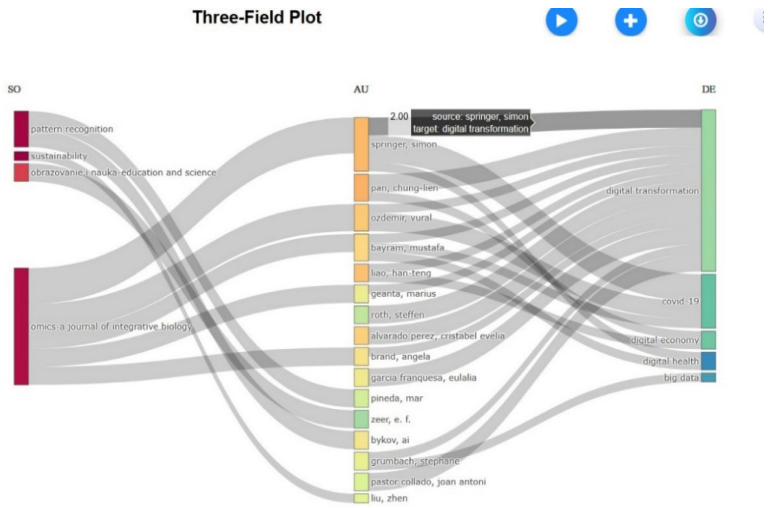


**Figure 2 –** Source – Authors – Keywords

*3.2. Sources*

*3.2.1. Most relevant sources*

Table 3 above displays the 10 most significant sources in this field. The journal with the highest number of publications (13) in this area is the journal "SUSTAINABILITY."

**Table 3 –** Most Relevant Sources

| Sources | Articles |
|---|---|
| SUSTAINABILITY | 13 |
| PATTERN RECOGNITION | 10 |
| OMICS-A JOURNAL OF INTEGRATIVE BIOLOGY | 9 |
| JOURNAL OF IMAGING SCIENCE AND TECHNOLOGY | 7 |
| AMAZONIA INVESTIGA | 4 |
| INFORMATION TECHNOLOGIES AND LEARNING TOOLS | 4 |
| NAUCHNYE I TEKHNICHESKIE BIBLIOTEKI-SCIENTIFIC AND TECHNICAL LIBRARIES | 4 |
| OBRAZOVANIE I NAUKA-EDUCATION AND SCIENCE | 4 |
| TOMSK STATE UNIVERSITY JOURNAL | 4 |

*3.3. Authors*

*3.3.1. Most relevant authors*

Although literature on digital transformation in social sciences is not as extensive as in otherareas of education, Figure 3 below shows that Pang Chung-Lien and Simon Springer rank first in the list with 4 relevant articles, i.e., the contribution of one author to the published set of articles. Their research focuses on several critical areas related to the emergence of a new scientific field: digital transformation research (DTR), which is characterized by significant complexity and diversity of research objects, making it difficult to analyze within individual disciplines.

The study shows that the concept of interdisciplinarity in DTR is mainly perceived as multidisciplinarity, with most participants in the discussions noting that they face more challenges than opportunities in the context of the interdisciplinary approach.

Table 4 shows the countries of the corresponding authors. In this context, two types of publications are highlighted: single-country publications (SCP), where all authors are from one country, representing internal collaboration, and multi-country publications (MCP), where all authors are from different countries, representing international collabo-

ration. The MCP ratios presented in Table 4 show that the two most productive countries occupy low positions. Moreover, the most productive countries, such as Russia and China, with low MCP ratios, do not rank highly in citations per article, meaning their citation rate per article does not make it into the top three countries. This situation can be described as a finding that highlights the importance of international collaboration to increase citations per publication.

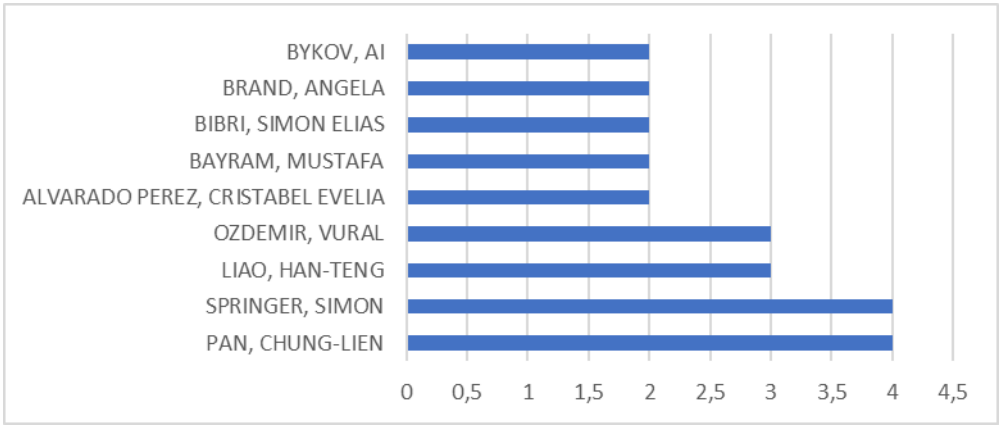


**Figure 3 –** Most prominent authors

**Table 4 –** Most Relevant Countries by Citation Analysis

| Country | Articles | Articles % | SCP | MCP | MCP % |
|---|---|---|---|---|---|
| Russia | 65 | 16,7 | 64 | 1 | 1,5 |
| China | 28 | 7,2 | 21 | 7 | 25 |
| Germany | 26 | 6,7 | 20 | 6 | 23,1 |
| Ukraine | 25 | 6,4 | 24 | 1 | 4 |
| USA | 22 | 5,7 | 17 | 5 | 22,7 |
| Spain | 21 | 5,4 | 19 | 2 | 9,5 |
| Italy | 16 | 4,1 | 11 | 5 | 31,3 |
| Brazil | 10 | 2,6 | 8 | 2 | 20 |
| France | 10 | 2,6 | 4 | 6 | 60 |
| United Kingdom | 10 | 2,6 | 5 | 5 | 50 |

Figure 4 presents a comprehensive bibliometric analysis combining two indicators: the annual number of publications and the average number of citations per year in the field of digital transformation in the social sciences over the period from 1997 to 2023. From 1997 to 2016, the number of publications remained relatively stable. However, starting in 2017, the field began to experience growing academic interest, as evidenced by a marked increase in the number of published articles. The peak in publication activity occurred in 2022, with 78 articles, followed by 2021 with 65 publications. In parallel, the graph illustrates the dynamics of citation impact, with the highest average number of citations per article recorded in 2023, reaching 8.2. This dual analysis highlights both the quantitative growth and the increasing scholarly influence of research on digital transformation within the social sciences.

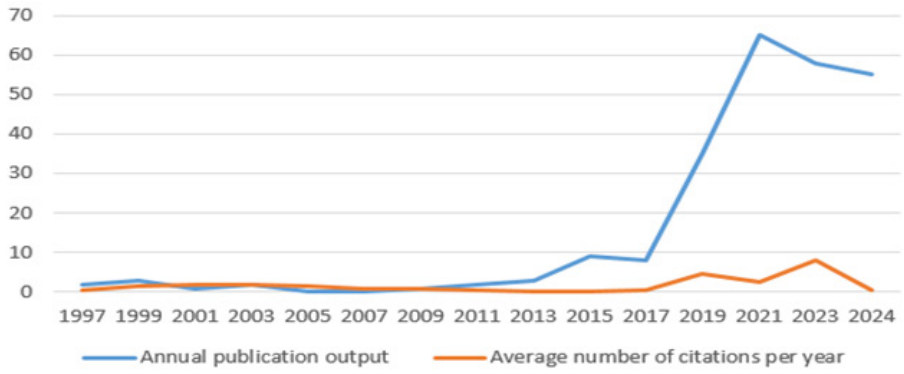


**Figure 4 –** Annual Trends in Publication Volume and Average Citations in the Field of Digital Transformation in Social Sciences (1997–2024)

*3.4. Documents*

*3.4.1. Most globally cited articles*

The list of the most cited documents in the field of digital transformation in social sciences is presented in Table 5. Figures 5 and 6 provide a graphical representation of citations by authors and bibliographic connections of documents.

Below are the details of some of the most significant cited documents:

Sachs, JD; Schmidt-Traub, G; Mazzucato, M; Messner, D; Nakicenovic, N; Rockström, J (2019) – Six Transformations to achieve the Sustainable Development Goals, Nature Sustainability: This study addresses the importance of interdisciplinarity in digital transformation research, identifying the challenges and opportunities faced by scholars from various disciplines. It also emphasizes the significance of international cooperation for enhancing publication citations.

Dwivedi, Yogesh K.; Kshetri, Nir; Hughes, Laurie; Slade, Emma Louise; Jeyaraj, Anand; Kar, Arpan Kumar; Baabdullah, Abdullah M.; Koohang, Alex; Raghavan, Vishnupriya; Ahuja, Manju; Albanna, Hanaa (2023) – So what if ChatGPT wrote it? Multidisciplinary perspectives on opportunities, challenges, and implications of generative conversational AI for research, practice, and policy, International Journal Of Information Management: This paper explores the transformative opportunities and challenges associated with the use of tools like ChatGPT in various fields. It highlights their potential for boosting productivity, as well as the ethical and legal aspects that require further investigation in the context of knowledge, transparency, and the digital transformation of organizations and societies.

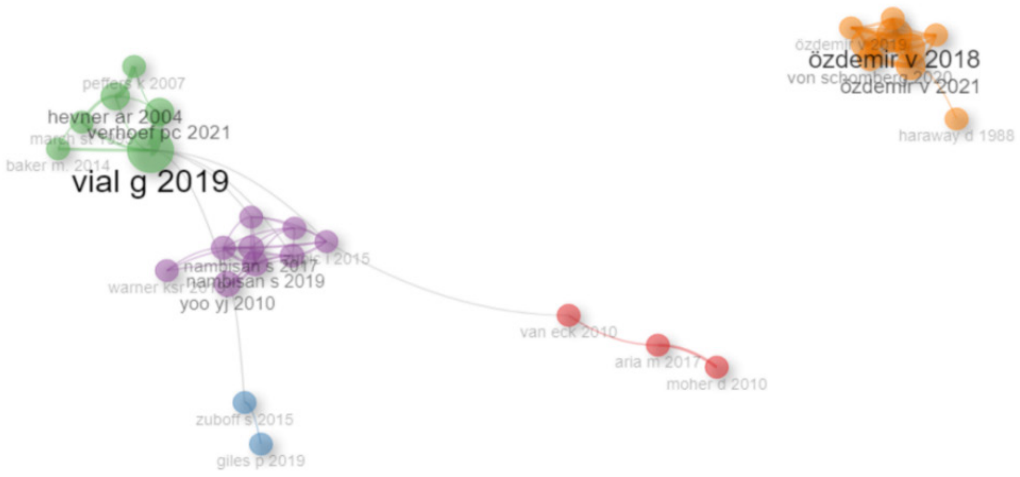


**Figure 5 –** Citation by authors

Castro, Gema Del Rio; Fernandez, Maria Camino Gonzalez; Colsa, Angel Uruburu (2021) – Unleashing the convergence amid digitalization and sustainability towards pursuing the Sustainable Development Goals (SDGs): A holistic review, JOURNAL OF CLEANER PRODUCTION: This article investigates the relationship between the Sustainable Development Goals (SDGs) and digitalization within the framework of the UN 2030 Agenda. It identifies research gaps and opportunities related to the use of digital paradigms, such as big data and artificial intelligence, to overcome sustainable development challenges and foster a more sustainable society.

**Table 5 –** Most Globally Cited Articles

| Paper | DOI | Total Citations | TC per Year | Normalized TC |
|---|---|---|---|---|
| SACHS JD, 2019, NAT SUSTAIN | 10.1038/s41893-019-0352-9 | 894 | 149,00 | 27,07 |
| DWIVEDI YK, 2023, INT J INFORM MANAGE | 10.1016/j.ijinfomgt.2023.102642 | 806 | 403,00 | 48,26 |
| CASTRO GD, 2021, J CLEAN PROD | 10.1016/j.jclepro.2020.122204 | 230 | 57,50 | 20,23 |
| DIMIDUK DM, 2018, INTEGR MATER MANUF I | 10.1007/s40192-018-0117-8 | 186 | 26,57 | 6,49 |
| ALHAWARI O, 2021, SUSTAINABILITY-BASEL | 10.3390/su13020859 | 128 | 32,00 | 11,26 |
| KESKIN H, 2018, GEODERMA | 10.1016/j.geoderma.2018.04.004 | 113 | 16,14 | 3,94 |
| GUO HD, 2020, INT J DIGIT EARTH | 10.1080/17538947.2020.1743785 | 72 | 14,40 | 7,92 |
| COZZOLINO D, 2003, LEBENSM-WISS TECHNOL | 10.1016/S0023-6438(02)00199-8 | 69 | 3,14 | 1,77 |
| DUMONT B, 2018, ANIMAL | 10.1017/S1751731118001350 | 69 | 9,86 | 2,41 |

The analysis of Co-occurrence Network by author keywords is also presented in Figure 6. This analysis was conducted in the R-based tool bibliometrix. The figure presents a keyword co-occurrence network illustrating the conceptual structure of research related to digital transformation and artificial intelligence within the social sciences. The visualization is generated using VOSviewer and displays clusters of frequently co-occurring terms. Node size reflects the relative frequency of keyword occurrence, while the thickness of connecting lines indicates the strength of co-occurrence relationships.

At the center of the network are two dominant terms–"agentic AI" and "artificial intelligence" – which form the core of the research landscape and demonstrate strong interconnections with multiple thematic clusters. The red cluster, anchored by agentic AI, encompasses themes such as digital twins, industry 5.0, human-in-the-loop, and multi-agent systems, highlighting technological and organizational dimensions of digital transformation. The blue cluster centers on cognition, real-time systems, urban areas, and complexity theory, indicating interdisciplinary applications of AI in socio-technical environments.

The green cluster groups keywords related to computational advancements, including machine learning, models, and Large Language Models (LLM), emphasizing methodological foundations. A smaller purple cluster links open systems theory, AI adoption, and digital intelligence, reflecting conceptual frameworks used to interpret the societal impact of AI-driven transformation.

Overall, the figure demonstrates the multi-clustered and interconnected nature of the research domain, revealing how artificial intelligence serves as a central integrating concept across technological, methodological, cognitive, and theoretical dimensions of digital transformation studies.

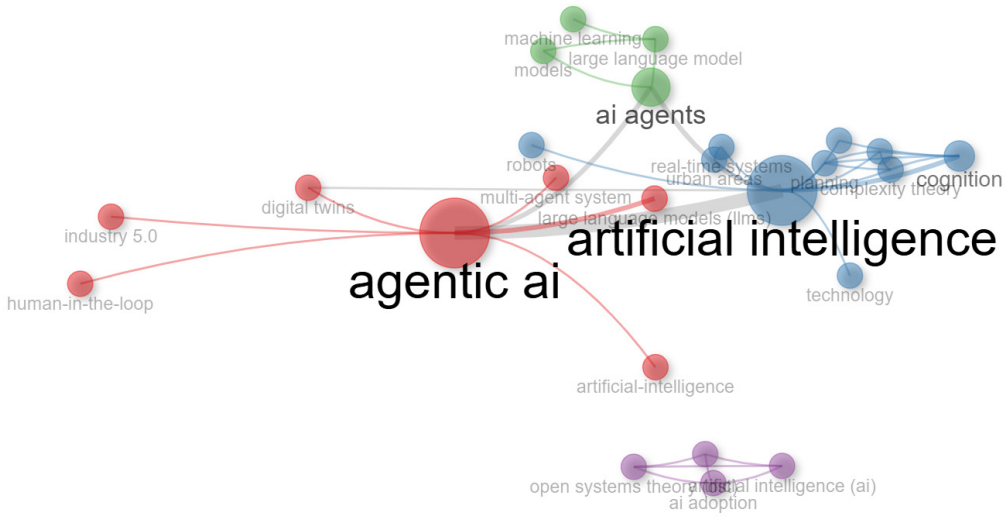


**Figure 6 –** Co-occurrence Network (author keywords)

*3.5. Conceptual Structure*

*3.5.1. Thematic map*

The thematic map presented in Figure 7 generated through a co-word analysis of the literature related to agentic systems and human–AI interactions. The map positions themes across two dimensions: relevance (centrality) on the horizontal axis and development (density) on the vertical axis. The resulting quadrants classify themes as motor, niche, emerging/declining, or basic, thereby offering insight into the intellectual structure and maturity of research in this domain.The analysis reveals the intricate structure of academic discourse on digital transformation and its far-reaching implications for various sectors of society.

Motor Themes: Highly Developed and Central

Clusters located in the upper-right quadrant represent mature and influential research themes. The largest and most prominent cluster, encompassing terms such as “artificial intelligence,” “cognition,” and “complexity theory,” indicates that conceptual and cognitive foundations of AI form a core area of scholarship. This suggests a research field anchored in theories of intelligent behavior, adaptive systems, and computational modeling.

Adjacent to this cluster is another substantial motor theme centered on “agentic AI,” “large language models,” and “chatGPT.” Its size and centrality reflect the rapid expansion of research focusing on autonomous AI systems, generative models, and the challenges associated with designing systems capable of agentic behavior. Together, these motor themes illustrate that contemporary inquiry is strongly oriented toward technically sophisticated and conceptually fundamental issues in AI agency.

Basic Themes: Central but Underdeveloped

The lower-right quadrant contains themes with high relevance but comparatively lower density, indicating foundational areas that remain theoretically or methodologically underdeveloped. Terms such as “artificial-intelligence technology,” “generative AI,” and “agentic system” appear here, suggesting that although these topics are central to current discourse, they require further conceptual clarification and empirical work. The positioning of “agentic system” specifically highlights its emerging significance as a conceptual anchor for research on autonomous AI behavior and human–AI interaction frameworks.

Niche Themes: Well-Developed but Peripheral

In the upper-left quadrant, clusters including “AI adoption,” “open systems theory (OST),” and “artificial intelligence (AI)” represent niche yet technically advanced areas. Their high density indicates well-established internal coherence, while their limited centrality suggests application in specialized subfields–such as organizational AI adoption modeling or systems-theoretic interpretations of AI integration. These themes contribute depth to the field but are not yet structurally central to the broader research landscape on agentic AI.

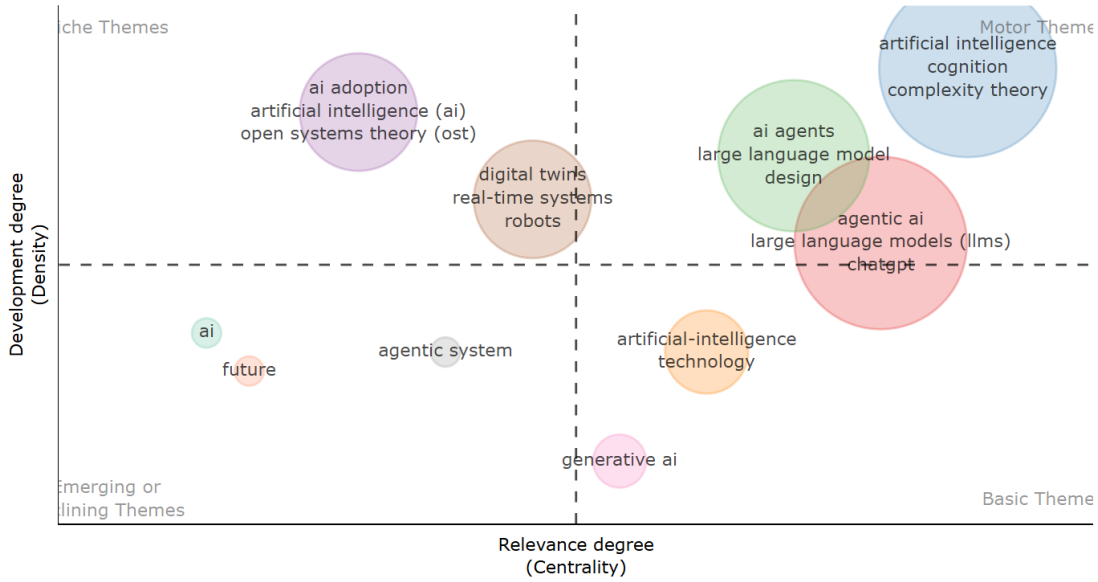


**Figure 7 –** Thematic Map (Authors' Keyword)

Another niche cluster – involving "digital twins," "real-time systems," and "robots"–illustrates specialized applications of agentic or semi-autonomous AI within engineering, robotics, and cyber-physical systems. Although methodologically robust, these themes remain somewhat peripheral to the conceptual and psychological questions driving human–AI interaction research.

Emerging or Declining Themes

The lower-left quadrant includes less-developed and less-central topics such as "AI," "future," and "generative AI." Their position may indicate either nascent lines of inquiry or areas where scholarly attention is currently limited or shifting. The dispersed nature of the cluster underscores ongoing conceptual expansion and suggests that these topics may evolve into more defined themes as research on agentic and autonomous AI progresses.

In conclusion, the thematic map offers a structured overview of the contemporary research landscape surrounding agentic systems and human–AI interactions. The map identifies the core themes that currently shape theoretical and technological development–most notably the clusters related to artificial intelligence, cognition, complexity theory, and agentic AI–highlighting their central role in advancing the field. At the same time, it reveals specialized and technically mature niches, such as AI adoption, open systems theory, digital twins, and real-time robotic systems, which contribute depth while remaining peripheral to the broader conceptual discourse.

The map also points to foundational yet still developing areas, including generative AI, artificial-intelligence technologies, and emerging conceptualizations of agentic systems. These themes are poised to guide future research as scholars continue to refine definitions, methodological approaches, and design principles for autonomous and semi-autonomous AI agents.

As the research domain evolves, it will be essential to deepen theoretical and empirical understanding of how agentic AI systems can be aligned with human cognitive, social, and ethical expectations. The ongoing development of these themes will provide crucial insights into the design of adaptive, reliable, and culturally responsive systems capable of supporting advanced forms of human–AI collaboration.

*3.5.2. Factorial analysis*

A multiple correspondence analysis (MCA) was conducted on the set of author keywords to examine the conceptual structure underlying contemporary research relevant to the development of agentic systems for human–AI interactions. By applying dimensionality-reduction techniques, the analysis identifies latent associations among key terms and reveals the dominant thematic directions shaping the field.

Figure 8 displays the resulting conceptual map. Unlike earlier domain configurations centred on digital transformation, the present analysis indicates

that research on agentic human–AI systems is organised around clusters of high-centrality concepts associated primarily with large language models (LLMs), AI ethics, multi-agent systems, and artificial intelligence. These terms occupy the dense central region of the map, confirming their constitutive role in structuring theoretical and empirical advancements in human–AI interaction.

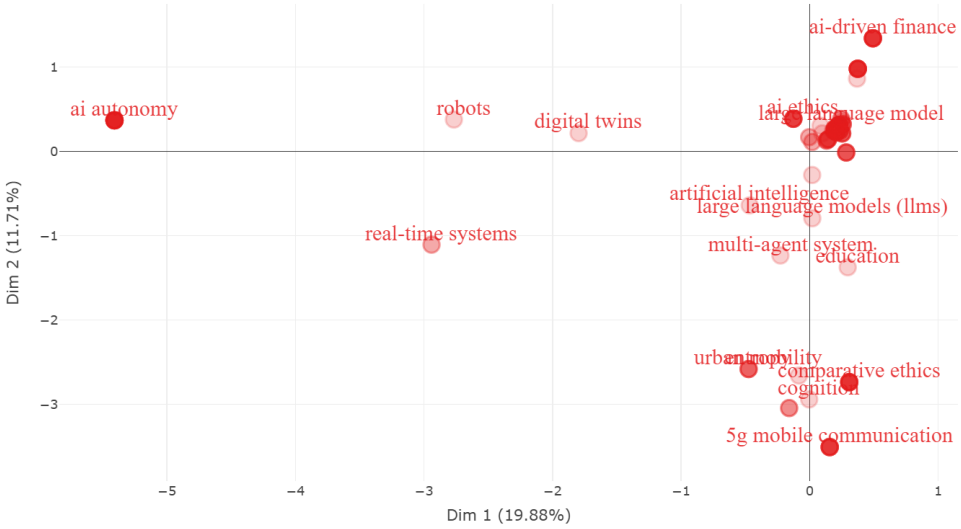


**Figure 8 –** Conceptual Structure Map

Further, the map highlights a set of application-oriented themes, including AI-driven finance, education, and technology design, which are positioned near the central cluster but extend along the first dimension. Their proximity suggests strong conceptual dependencies between foundational AI capabilities and sector-specific implementations, particularly in domains where agentic AI systems mediate or automate complex decision processes.

In contrast, terms such as robots, digital twins, real-time systems, and AI autonomy are distributed across the left-hand side of the map. Their relative distance from the central cluster indicates specialised but less integrative research areas, often oriented toward engineering, systems design, and autonomy modelling rather than social or cognitive dimensions of human–AI engagement.

Peripheral concepts located in the lower regions–such as urban mobility, comparative ethics, cognition, and 5G mobile communication–reflect emerging interdisciplinary directions. While these terms exhibit lower centrality, they represent expanding interfaces where agentic AI systems intersect with infrastructural, ethical, and cognitive frameworks, suggesting promising pathways for future inquiry.

Collectively, the MCA reveals a conceptual architecture dominated by the convergence of LLMs, ethical frameworks, and multi-agent system design, while simultaneously highlighting adjacent technological and interdisciplinary domains. These findings underscore the growing importance of agentic, adaptive, and ethically aligned AI systems, reinforcing the need for integrative models that capture both the cognitive mechanisms and the societal implications of human–AI interactions.

These findings highlight the growing importance of agentic, adaptive, and ethically aligned AI, and they reinforce the need for integrative models that explain both the cognitive mechanisms of agents and the societal implications of human–AI interaction in digitally transforming organizations. In other words, bibliometrics does more than map trends; it helps identify which capabilities and governance requirements must be addressed together when AI moves from laboratory prototypes to operational services.

To move from this bibliometric landscape to an implementable system, an operational definition of agency is required. An artificial intelligence agent is defined not simply by information processing, but by the capacity for autonomous action. In classical

agent architectures, an intelligent system integrates perception, internal deliberation, and memory to select actions that advance a goal. This perspective, summarized in Fig. 9 [21], is directly relevant to digital transformation because it frames AI as an active component within workflows, data platforms, and decision processes, where reliability, traceability, and accountability are necessary properties.

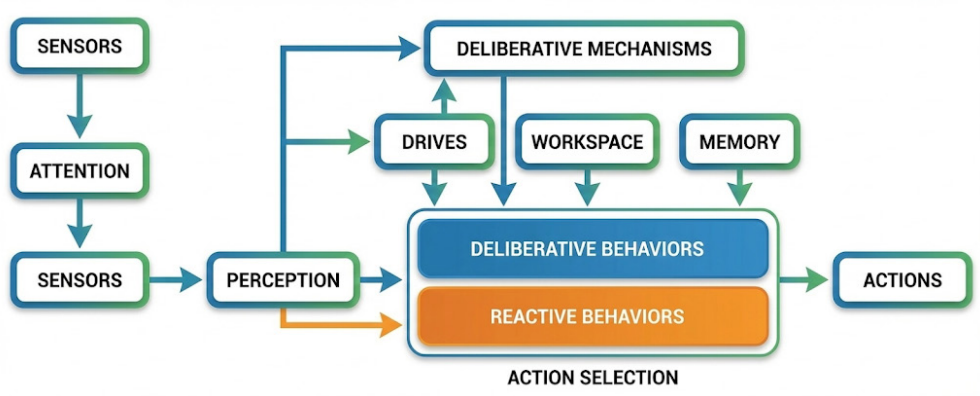


**Figure 9 –** Schematic Representation of an Autonomous Agent's Action Selection Mechanism

Recent progress in large language models provides a practical mechanism to instantiate this classical blueprint. As benchmark performance continues to improve [22], LLMs increasingly support capabilities that are central to human–AI interaction, including intent recognition, summarization, content generation, and multi-step reasoning. As a result, contemporary agentic systems often implement deliberation by treating the LLM as a cognitive engine and implement action through tool use. In this setting, retrieval systems and external databases provide grounded "memory," APIs and computational tools serve as executable "actions," and structured control logic determines when to search, when to verify, and when to respond. Framed through the lens of digital transformation, this architecture offers a concrete pathway from bibliometric themes to deployable systems because it links human intent to machine action through evidence access, verifiable decision points, and auditable workflows.

To operationalize the theoretical definition of agency, recent work has converged on a small number of recurring architectural patterns. Two influential exemplars, Auto-GPT [23] and ReAct [24], illustrate contrasting paradigms that continue to shape how agentic AI systems are designed and evaluated.

ReAct (Reasoning and Acting) couples internal reasoning with tool-mediated interaction by interleaving thought steps and action steps. The central idea is that an agent should not rely on free-form reasoning alone. Instead, it should repeatedly consult external resources, observe the outcome, and update its reasoning accordingly. This grounding mechanism mitigates error propagation typical of purely chain-of-thought prompting, because the model can retrieve missing facts, check assumptions against evidence, and adapt its plan as new observations arrive. In practice, ReAct is lightweight and effective for tool-augmented question answering, but its reliability depends on whether the model can recognize when evidence is sufficient and when it must continue searching or revising.

Auto-GPT represents a different design goal, long-horizon autonomy for open-ended objectives. Rather than a single reasoning-action loop, Auto-GPT maintains a persistent task structure in which a high-level goal is decomposed into sub-tasks, executed iteratively, and reprioritized as intermediate outcomes arrive. Its contribution is the operationalization of continuous self-prompting and memory, enabling an agent to sustain progress without constant human steering. This paradigm is well suited to exploratory tasks and multi-step project execution, but it can incur high computational cost and may drift into irrelevant branches when objectives are underspecified or when constraints are not explicitly enforced.

Although both paradigms have advanced the field, their limitations become salient in precision-critical, retrieval-centered settings. ReAct can produce confident hallucinations when it treats tool outputs as correct without explicit checking, and it can also fall into reasoning loops where it keeps searching despite already having adequate evidence. Auto-

GPT's recursive structure may amplify these issues at scale. It is prone to rabbit holes, repeated sub-task generation, and runaway iteration unless the system imposes strict stopping criteria and verification gates. Consequently, a gap emerges between open-ended autonomy and the requirements of controlled, evidence-based domains, where reliability, traceability, and bounded behavior are essential.

To address this gap, the proposed prototype (Fig. 10) adopts a structured, verifiable workflow that preserves the practical strengths of ReAct and Auto-GPT while constraining their failure modes.

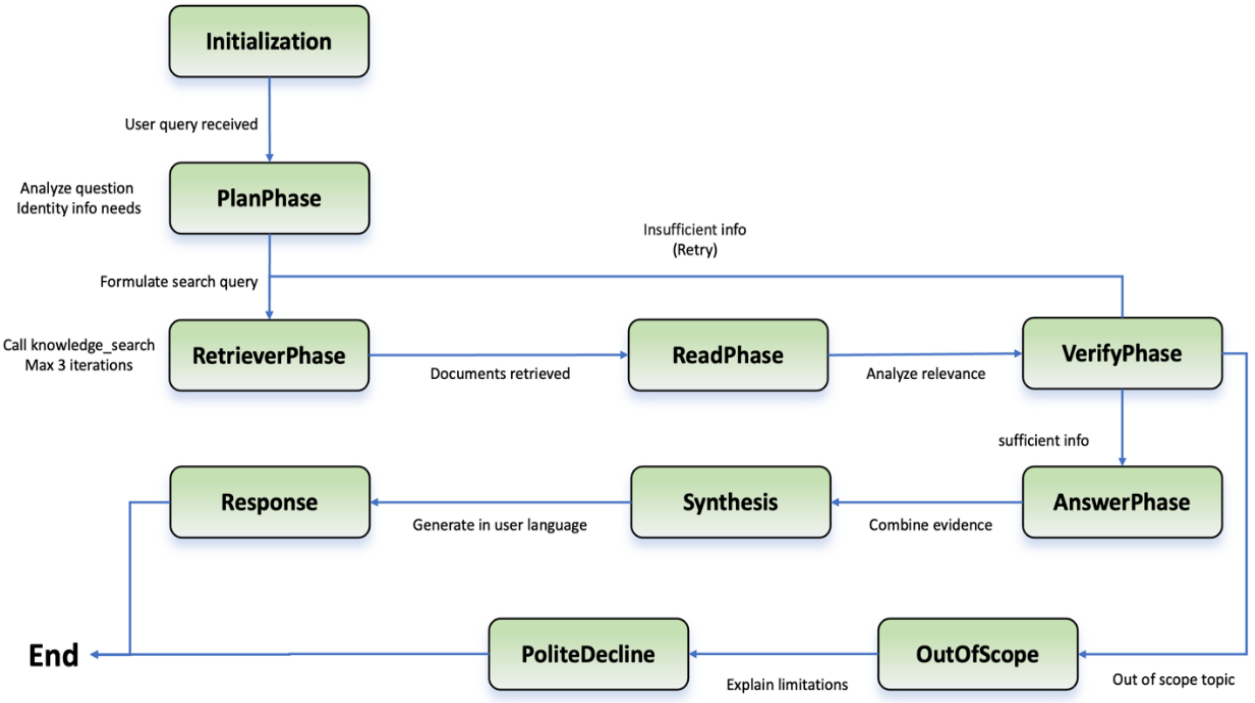


**Figure 10 –** An Agentic Model of Human–AI Interaction System

Instead of relying on implicit self-judgment, the framework introduces three explicit control mechanisms. First, a dedicated PlanPhase separates intent interpretation from execution by decomposing the information need and defining a retrieval strategy before any tool calls occur. Second, a VerifyPhase functions as a deterministic quality gate. It evaluates whether retrieved evidence is sufficient, consistent, and relevant before generation is allowed to proceed. Third, a scoped retry mechanism enforces bounded autonomy through explicit exit conditions, such as a maximum number of retrieval iterations and well-defined outcomes for out-of-scope requests or insufficient evidence. In effect, the architecture shifts agency from unbounded exploration to controlled autonomy, making it more suitable for high-stakes academic and industrial deployments where knowing when to stop and when to decline is as important as producing an answer.

## 4. Conclusions

This study provides a comprehensive bibliometric assessment of research on digital transformation within the social sciences and extends this analysis by introducing a conceptual Agentic Model of Human–AI Interaction. Drawing on 389 publications indexed in the Web of Science from 1997 to 2024, the study identifies long-term publication dynamics, conceptual structures, and geographic patterns that shape the field. The analysis reveals that digital transformation research has intensified significantly, particularly in 2021–2022, reflecting its central role in reshaping economic, cultural, and social systems.

Russia, China, Germany, and Ukraine emerge as the leading contributors to this research domain, demonstrating the global relevance of digitalization processes. Influential journals–including Journal of Imaging Science and Technology, Sustainability,

and Social Sciences–underscore the inherently interdisciplinary nature of the field. The thematic mapping uncovers four major research clusters: digital education and innovation, governance and political transformation, methodological and analytical tools, and the growing integration of artificial intelligence into social structures.

A key contribution of this study is the development of an Agentic Model of Human–AI Interaction, conceptualized as a multi-stage system that explains how an AI agent receives, processes, retrieves, and synthesizes information to generate responses. This model reflects broader societal transformations, illustrating how digital systems increasingly operate as autonomous actors within socio-technical environments. The model bridges bibliometric evidence with theoretical insights, demonstrating how emerging technologies reshape human decision-making, institutional practices, and knowledge production.

Despite expanding scholarly interest, the field still faces conceptual fragmentation, geographical imbalance, and insufficient attention to ethical, cultural, and institutional implications of AI-driven digital transformation. Persistent challenges–such as digital inequality, responsible data practices, and the governance of algorithmic systems–require deeper interdisciplinary engagement.

Overall, the study advances academic understanding of how digital transformation and agentic systems co-evolve within the social sciences. It provides an empirical and conceptual foundation for future research, policy development, and educational initiatives aimed at fostering responsible, inclusive, and human-centered digital ecosystems.

**Funding**

This research was funded by the Committee of Science of the Ministry of Science and Higher Education of the Republic of Kazakhstan (Grant №. BR28713047 Artificial Intelligence and the Ethics of Social Justice: A Conceptual Reflection on Opportunities and Risks in the Processes of Modernization of Society in Kazakhstan)

**Author Contributions**

Conceptualization, D.Zh. and S.J.; Methodology, D.Zh. and S.J.; Software, D.Zh., A.B.; Validation, D.Zh., A.B. and S.J.; Formal Analysis, D.Zh. and S.J.; Investigation, D.Zh.; Resources, D.Zh.; Data Curation, D.Zh.; Writing – Original Draft Preparation, X.X.; Writing – Review & Editing, D.Zh.; Visualization, D.Zh.; Supervision, D.Zh. and S.J.; Project Administration, S.J.; Funding Acquisition, S.J.

**Conflicts of Interest**

The authors declare no conflict of interest.

**References**

1. G. Vial, "Understanding digital transformation: A review and a research agenda," J. Strategic Inf. Syst., vol. 28, no. 2, pp. 118–144, 2019

2. J. Reis, M. Amorim, N. Melão, and P. Matos, "Digital transformation: A literature review and guidelines for future research," in Proc. World Conf. Inf. Syst. Technol., Springer, 2018, pp. 411–421

3. Y. Yeo and S. Jung, "Assessing the economy-wide impacts of digital transformation in the Korean economy: A social accounting matrix multiplier approach," Telecommun. Policy, vol. 48, no. 10, 2024. [Online]. Available: https://doi.org/10.1016/j.telpol.2024.102871

4. X. Guo and W. Pang, "The impact of digital transformation on corporate ESG performance," Finance Res. Lett., vol. 72, 2025. [Online]. Available: https://doi.org/10.1016/j.frl.2024.106518

5. Y. Madani, M. Erritali, J. Bengourram, and F. Sailhan, "Social collaborative filtering approach for recommending courses in an e-learning platform," Procedia Comput. Sci., vol. 151, pp. 1164–1169, 2019. [Online]. Available: https://doi.org/10.1016/j.procs.2019.04.166

6. A. Garzoni, I. De Turi, G. Secundo, and P. Del Vecchio, "Fostering digital transformation of SMEs: A four levels approach," Management Decision, vol. 58, no. 8, pp. 1543–1562, 2020. [Online]. Available: https://doi.org/10.1108/md-07-2019-0939

7. E. R. Banalieva and C. Dhanaraj, "Internalization theory for the digital economy," J. Int. Business Studies, vol. 50, no. 8, pp. 1372–1387, 2019. [Online]. Available: https://doi.org/10.1057/s41267-019-00243-7

8. J. van Dijk, The Digital Divide. Cambridge, UK: Polity Press, 2020.

9. J. R. Bongiovi, "The Age of Surveillance Capitalism: The Fight for a Human Future at the New Frontier of Power," Social Forces, vol. 98, no. 2, pp. 1–4, 2019. [Online]. Available: https://doi.org/10.1093/sf/soz037

10. V. Eubanks, Automating Inequality: How High-Tech Tools Profile, Police, and Punish the Poor. New York, NY, USA: St. Martin's Press, 2018.

11. L. Floridi et al., "AI4People–An ethical framework for a good AI society: Opportunities, risks, principles, and recommendations," Minds Mach., vol. 28, no. 4, pp. 689–707, 2018, doi: 10.1007/s11023-018-9482-5

12. N. Ridei, W. Wojciech, N. Tytova, L. Stepanenko, and A. Aleksanian, "Digital Transformation of Public Administration: Sociocultural forms of organization in education, science and innovation," Cuestiones Políticas, vol. 40, no. 73, pp. 868–882, 2022. [Online]. Available: https://doi.org/10.46398/cuestpol.4073.50

13. M. Aria and C. Cuccurullo, "bibliometrix: An R-tool for comprehensive science mapping analysis," J. Informetrics, vol. 11, no. 4, pp. 959–975, 2017

14. N. Donthu, S. Kumar, D. Mukherjee, N. Pandey, and W. M. Lim, "How to conduct a bibliometric analysis: An overview and guidelines," J. Business Res., vol. 133, pp. 285–296, 2021.

15. T. Chen, Z. Zhou, and Z. Liu, "Bibliometric analysis on intangible cultural heritage and experience marketing in China," in Design, User Experience, and Usability, Cham: Springer, 2024.

16. R. Y. Maulana and M. Dečman, "Collaborative governance in the digital transformation age: A systematic literature review with bibliometric mapping," Cent. Eur. Public Adm. Rev., vol. 21, no. 1, pp. 31–60, 2023. [Online]. Available: https://doi.org/10.17573/cepar.2023.1.02

17. Z. Van Veldhoven, V. Etikala, A. Goossens, and J. Vanthienen, "A scoping review of the digital transformation literature using scientometric analysis," Business Inf. Syst., pp. 281–292, 2021. [Online]. Available: https://doi.org/10.52825/bis.v1i.49

18. V. Roblek, M. Meško, and I. Podbregar, "Mapping of the emergence of Society 5.0: A bibliometric analysis," Organizacija, vol. 54, no. 4, pp. 293–305, 2021. [Online]. Available: https://doi.org/10.2478/orga-2021-0020

19. E. Stoica, I. Bogoslov, and R. Serbu, "Scientific research perspectives on the relationship between FinTech and education," Int. Rev., no. 1–2, pp. 22–32, 2023. [Online]. Available: https://doi.org/10.5937/intrev2302028S

20. Gürcan, Meltem (2025). Digital Transformation in the Framework of Social Sciences: A Bibliometric Evaluation of the Web of Science Database. Journal of Public Finance Studies, 0(73), 1-17. https://doi.org/10.26650/mcd2025-1598845

21. Wooldridge, Michael, and Nicholas R. Jennings. "Intelligent agents: Theory and practice." *The knowledge engineering review* 10.2 (1995): 115-152.

22. Mussa, Aman, Zhanseit Tuimebayev, and Madina Mansurova. "Make Large Language Models Efficient: A Review." *IEEE Access* (2025). https://doi.org/10.1109/ACCESS.2025.3605110

23. Yang, Hui, Sifu Yue, and Yunzhong He. "Auto-gpt for online decision making: Benchmarks and additional opinions." arXiv preprint arXiv:2306.02224 (2023).

24. Yao, Shunyu, Jeffrey Zhao, Dian Yu, Nan Du, Izhak Shafran, Karthik R. Narasimhan, and Yuan Cao. "React: Synergizing reasoning and acting in language models." In *The eleventh international conference on learning representations*. 2022.

***Information About Authors:***

*Dinara Zhaisanova is a PhD in Innovation management (2022). She is now the acting associate professor of the Department of the Artificial intelligence and Big Data. Her research interests include innovation technologies, management of technologies. ORCID iD: 0000-0002-8116-6111*

*Sholpan Jamanbalayeva is Doctor of Sociological Sciences, Professor, Deputy General Director for Scientific Work of The Institute of Philosophy, Political Science and Religious Studies of the Committee of Science of the Ministry of Science and Higher Education of the Republic of Kazakhstan. Her research interests span across interdisciplinary domains involving digital society, sociocultural dynamics, and religion, with a specific geographic focus on Kazakhstan. ORCID iD: 0000-0003-0310-529X*

*Diana Zhyilussova is a docotral's degree student at the Al-Farabi Kazakh National University in the Department of Artificial Intelligence and Big Data (Almaty, Kazakhstan, zhyilyssovadiana@gmail.com). Her academic interests focus on artificial intelligence and data-driven technologies. ORCID iD: 0000-0001-9211-5224*

*Ayaulym Baidulla is a docotral's degree student at the Al-Farabi Kazakh National University in the Department of Artificial Intelligence and Big Data. Her academic interests focus on artificial intelligence and data-driven technologies. ORCID iD: 0009-0002-3083-9715*

*Submission received: 25 November, 2025.*
*Revised: 19 December, 2025.*
*Accepted: 19 December, 2025.*

IRSTI 28.27.19 https://doi.org/10.26577/jpcsit202549

**Justyna Mrowiec**

University of Warsaw, Warsaw, Poland
e-mail: jm.mrowiec@student.uw.edu.pl

# COMPUTATIONAL SIMULATION OF INSTITUTIONAL-INVESTMENT DYNAMICS USING PANEL VECTOR AUTOREGRESSION

**Abstract.** This study develops a computational framework for simulating dynamic interactions between institutional quality indicators and foreign direct investment using a panel Vector Autoregression model applied to a multi-country dataset. The work emphasizes the algorithmic structure of the modeling pipeline, including preprocessing of heterogeneous panel time series, numerical stationarity diagnostics and cointegration testing. Impulse-response simulations are used to examine system behavior following institutional shocks, illustrating the dynamic propagation of disturbances in a high-dimensional environment. Although the empirical application concerns institutional governance, the contribution of this study lies primarily in its computational workflow design, numerical diagnostics, and reproducible implementation of a panel VAR simulation environment. The presented framework demonstrates how computational finance and applied computer science can integrate econometric modeling to analyze complex, interdependent systems.

**Keywords:** panel VAR, computational modeling, dynamic systems simulation, impulse response functions, numerical econometrics, data-driven analysis, computational finance.

## 1. Introduction

The dynamic relationship between institutional quality and foreign direct investment (FDI) remains an important and methodologically challenging topic in computational economics and data-driven modelling. Classical theories of multinational production, most notably the OLI paradigm formulated by Dunning [5], have established institutions as a structural component affecting the locational strategies of global firms. Empirical research reinforces this general conclusion, showing that investment inflows tend to correlate with political stability, regulatory effectiveness, and the rule of law [6], [7]. At the same time, a parallel body of work emphasizes the potential for reverse causality: the arrival of foreign investors can itself transform domestic governance structures by introducing regulatory pressures, informational spillovers, or new administrative standards [8], [10].

Panel VAR (PVAR) methods have become a preferred tool for capturing bidirectional, time-varying interactions across countries because they model the joint dynamics of multiple endogenous variables and allow for impulse–response analysis in a panel setting [2], [12]. Foundational computational implementations and software support for PVAR estimation are provided by Abrigo and Love [1], while comprehensive methodological surveys discuss specification choices, identification strategies, and practical challenges in PVAR applications [3], [16].

Recent advances in computational econometrics address these limitations by employing panel vector autoregression, which provides a flexible architecture for modelling multivariate dynamic systems [2], [12]. They address computational stability and high-dimensionality issues that arise when modelling many institutional indicators and controls jointly. Regularization and penalized estimators adapted to PVAR (panel-LASSO) have been proposed to reduce estimation variance and improve numerical conditioning in large panels [15], while high-dimensional VAR frameworks that accommodate common factors help to manage strong cross-sectional dependence and improve estimator performance [11]. Further work highlights the importance of eigenvalue/stability diagnostics and the potential distortions induced by neglected changes in mean or volatility when estimating VAR systems [4], [13]. Systematic reviews of PVAR practice summaries these developments and emphasize reproducibility and explicit documentation of orthogonalization and identification choices [16].

On the applied side, cross-country PVAR studies document that institutional shocks can have persistent short-run effects on FDI, highlighting the importance of a dynamic, system-based treatment of governance measures [2], [12], [14]. Motivated by

this literature, the present study constructs a fully specified computational workflow for modelling institutional–FDI dynamics using panel VAR techniques. The pipeline integrates panel stationarity testing, cointegration verification, forward orthogonal deviations (FOD) transformation, structured Cholesky decomposition (or alternative structural identification), eigenvalue stability checks, and reproducible simulation procedures to produce panel-averaged impulse response functions (IRFs) and forecast error variance decompositions (FEVDs) suitable for cross-country inference [1] – [16].

Despite the growing popularity of PVAR models, many empirical applications remain incomplete from a computational standpoint. Choices regarding orthogonalization, variable ordering, numerical stability of estimated systems, and reproducibility of simulation procedures are often insufficiently documented. Such omissions reduce the transparency of structural inference and weaken the credibility of model-based conclusions. By emphasizing algorithmic clarity, numerical diagnostics, and reproducible simulation design, this study addresses these gaps. The objectives are twofold: to provide empirical insights into the short-term responses of FDI to institutional shocks across a diverse group of economies, and to demonstrate a computationally coherent and transparent methodology aligned with contemporary standards in applied econometrics and computational research.

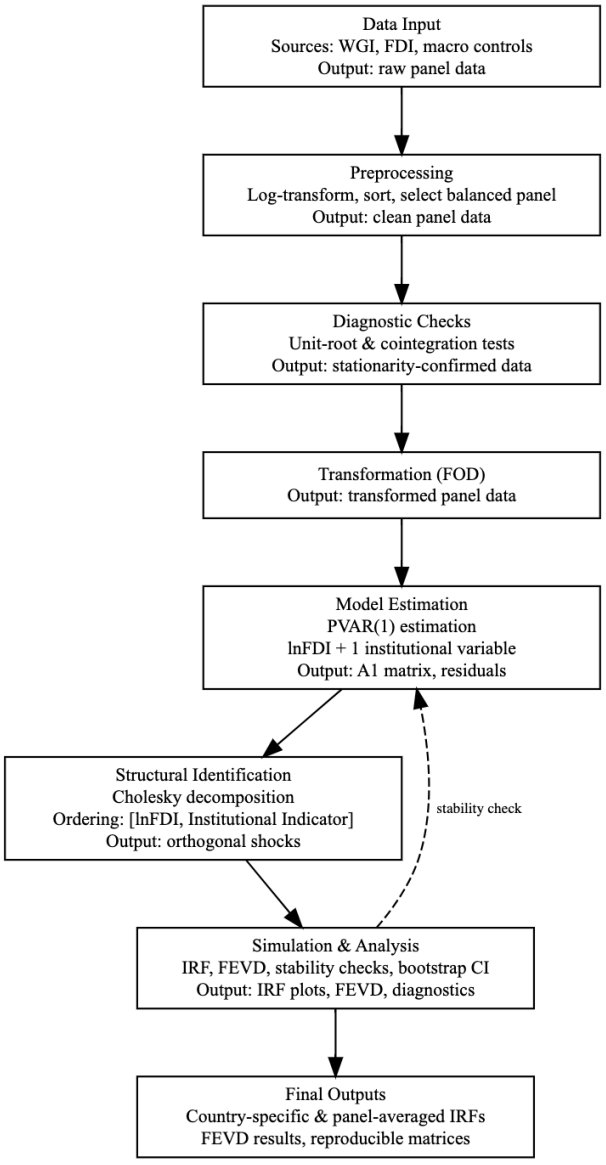


**Figure 1 –** Overview of the computational workflow

The novelty of the present study should therefore be understood in computational rather than methodological terms. The econometric building blocks employed – panel VAR estimation, unit-root testing, structural identification, and impulse-response analysis – are standard. What distinguishes the approach is the way these components are combined into a reproducible, constraint-based workflow in which diagnostic checks are not merely reported but explicitly govern admissible model configurations and simulations. In this sense, the framework emphasizes disciplined execution, numerical verification, and transparency over the introduction of new estimators or identification schemes. The analysis focuses on short-run dynamic associations rather than causal identification in the structural sense.

## 2. Materials and Methods

The entire modelling pipeline was implemented as a modularly organized computational workflow, in which logically distinct stages are executed sequentially and validated through intermediate diagnostics: data normalization, differencing, unit-root diagnostics, eigenvalue stability verification, FOD transformation, system estimation, and simulation of shock-driven trajectories. Each module maintains deterministic reproducibility and uses numerically stable matrix operations suitable for high-dimensional panel structures.

### *2.1. Data Architecture and Preprocessing*

The sample consists of 24 countries selected based on data completeness over 2004–2020 and classified by World Bank region and income group (see Table 1). The analysis relies on a balanced panel of twenty-four countries spanning the years 2004 to 2020. The variables include FDI inflows and greenfield FDI, complemented by six World Governance Indicators: control of corruption (COR), government effectiveness (GOV), political stability (POL), rule of law (RUL), regulatory quality (REG), and voice and accountability (VOI) [18]. Standard macroeconomic controls-trade openness, inflation, unemployment, and GDP per capita-were sourced from World Bank Open Data [17] and UNCTAD statistics [19].

Table 1 illustrates the substantial heterogeneity in both FDI inflows and institutional indicators across countries, reinforcing the suitability of a panel-based dynamic framework.

All variables were log-transformed to stabilize variance. The dataset was sorted by country and year, and only units with complete nineteen-year coverage were retained. This ensured numerical consistency of the PVAR estimators and avoided distortions from unbalanced temporal structures, which are known to affect the properties of dynamic panel estimators [2].

All computations were performed in R version 4.4.1 (2024-06-14, “Race for Your Life”) on an x86_64-apple-darwin20 platform. The analysis relied primarily on the *plm*, *panelvar*, *urca*, *vars*, and *tidyverse* packages (versions current as of 2024). Deterministic random seeds were set prior to estimation and bootstrap procedures. To support replication and verification, intermediate artefacts–including transformed datasets, estimated coefficient matrices, residual covariance matrices, and eigenvalue diagnostics–were systematically exported and logged at each major stage of the workflow. Selected impulse-response computations were independently replicated in Stata to verify numerical consistency across software environments. A minimal script outline documenting the execution sequence and diagnostic checks will be made available as supplementary material or upon reasonable request.

### *2.2. Diagnostic Procedures*

The time-series properties of the data were examined using a suite of panel unit-root tests, including Levin–Lin–Chu, Im–Pesaran–Shin, augmented Dickey–Fuller, and Fisher-type tests [2], [12]. All unit-root and cointegration tests were conducted in a pooled panel setting, following standard PVAR practice. Country-level testing was not pursued to preserve statistical power. Variables were treated as integrated of order one when they exhibited non-stationarity in levels and stationarity after differencing.

**Table 1** – Countries included in the balanced panel (2004–2022) with region, income group, and summary statistics for key variables: Foreign Direct Investment, Governance Effectiveness, Political Stability and Rule of Law.

| country | region | income group | mean FDI | sd FDI | mean GOV | sd GOV | mean POL | sd POL | mean RUL | sd RUL |
|---|---|---|---|---|---|---|---|---|---|---|
| Albania | Europe | Upper-middle | 4982.4073 | 3043.6103 | 0.0999268 | 1.1031541 | 0.2548025 | 1.0047710 | 0.1017663 | 1.0146840 |
| Angola | Sub-Saharan Africa | Upper-middle | 24684.9333 | 8925.7938 | -0.2211279 | 0.8582962 | -0.2208510 | 1.1153118 | -0.1990148 | 0.8984379 |
| Bhutan | Asia | Lower-middle | 346.4255 | 259.2892 | 0.1655105 | 1.0444797 | -0.0218899 | 0.9904666 | 0.0636915 | 1.1343357 |
| Chad | Sub-Saharan Africa | Low | 4726.6959 | 1753.6190 | -0.1652149 | 0.9352040 | 0.0583180 | 0.7525288 | -0.2175765 | 0.9667489 |
| Chile | Latin America | High | 177858.532 | 64907.7462 | -0.0071067 | 1.1071683 | -0.0099975 | 1.0682045 | -0.0676689 | 1.1071915 |
| Colombia | Latin America | Upper-middle | 127532.849 | 67266.2378 | -0.3161419 | 0.8186278 | -0.3818359 | 0.9876375 | -0.3857535 | 0.8598279 |
| Estonia | Europe | High | 20444.2609 | 7555.9601 | 0.2528075 | 1.0952287 | 0.4911665 | 0.6689210 | 0.2147030 | 1.0853567 |
| Fiji | Oceania | Upper-middle | 3531.3399 | 1577.8022 | -0.2422086 | 0.8616657 | -0.0832803 | 1.1679242 | -0.2008122 | 0.9344640 |
| Germany | Europe | High | 928372.517 | 134007.343 | -0.1407846 | 0.9635251 | -0.1188034 | 0.9751304 | -0.2151610 | 0.9474373 |
| Honduras | Latin America | Lower-middle | 10339.9883 | 5403.8136 | 0.2505163 | 1.1465176 | 0.0379724 | 1.0098637 | 0.1835270 | 1.2131949 |
| Hungary | Europe | High | 90646.2653 | 13184.1782 | 0.4036586 | 1.0289071 | 0.3706888 | 0.8921296 | 0.4358061 | 1.0138094 |
| India | Asia | Lower-middle | 261431.186 | 154089.822 | -0.3503703 | 0.8499743 | -0.3636368 | 0.9638052 | -0.2625112 | 0.9410410 |
| Ireland | Europe | High | 661680.820 | 493395.101 | -0.0396834 | 1.0176809 | -0.3025411 | 0.8756267 | -0.0467813 | 1.0327271 |
| Kazakhstan | Central Asia | Upper-middle | 105764.787 | 48511.7517 | -0.3176967 | 0.8626395 | -0.0665632 | 0.7698897 | -0.3928801 | 0.9452101 |

*Continuation of the table*

| country | region | income group | mean FDI | sd FDI | mean GOV | sd GOV | mean POL | sd POL | mean RUL | sd RUL |
|---|---|---|---|---|---|---|---|---|---|---|
| Kenya | Sub-Saharan Africa | Lower-middle | 5678.5509 | 2793.2115 | 0.0491488 | 1.0408781 | 0.0146998 | 1.1059649 | -0.0222785 | 1.0597301 |
| Kuwait | Middle East | High | 11441.2442 | 6069.6946 | -0.4149287 | 0.7868528 | -0.3508415 | 0.8845619 | -0.4416138 | 0.7978328 |
| Latvia | Europe | High | 14180.1272 | 5514.0176 | 0.2573243 | 1.0186930 | 0.3376108 | 0.8748282 | 0.3118882 | 1.0022222 |
| Mauritius | Sub-Saharan Africa | Upper-middle | 3742.9757 | 1896.5257 | 0.0951379 | 1.1663976 | 0.2411411 | 0.9476989 | 0.1480538 | 1.0253504 |
| Namibia | Sub-Saharan Africa | Upper-middle | 4809.1357 | 1849.6302 | -0.0330816 | 0.9290992 | 0.0402133 | 0.9083712 | -0.1800200 | 0.9281190 |
| Norway | Europe | High | 145579.503 | 35486.5752 | 0.2389848 | 1.1783227 | 0.0163374 | 1.0029353 | 0.1205695 | 1.2198415 |
| Pakistan | Asia | Lower-middle | 25506.9660 | 9784.6354 | 0.3928352 | 1.0465439 | 0.4848705 | 0.7992567 | 0.4000768 | 1.0356895 |
| Poland | Europe | High | 198154.078 | 59389.1052 | -0.0499497 | 1.0363820 | -0.3103073 | 0.8504502 | -0.0023631 | 1.0419077 |
| Senegal | Sub-Saharan Africa | Lower-middle | 3898.4415 | 3675.6230 | -0.0090956 | 1.0228359 | -0.0338832 | 1.0616757 | -0.0737307 | 1.0374500 |
| Timor-Leste | Asia | Lower-middle | 258.5969 | 201.7687 | -0.3762982 | 0.8787595 | -0.3044273 | 0.9845603 | -0.3612315 | 0.8448549 |

**Table 2 –** Panel unit-root test statistics.

| Variable | LLC stat | IPS stat | Fisher stat |
|---|---|---|---|
| lnFDI | −10.5716 | −7.4976 | 228.19 |
| lnGREENFDI | −5.2054 | −6.0023 | 167.40 |
| lnCOR | −10.0471 | −11.4101 | 334.23 |
| lnGOV | −8.1410 | −9.4301 | 259.27 |
| lnPOL | −6.6929 | −8.1029 | 216.01 |
| lnRUL | −10.4982 | −11.5921 | 327.07 |
| lnREG | −8.9451 | −9.8530 | 258.43 |
| lnVOI | −9.2983 | −11.2570 | 298.64 |
| ΔlnFDI | −6.6760 | −7.0651 | 183.99 |
| ΔlnGREENFDI | −13.9215 | −17.3808 | 552.88 |
| ΔlnCOR | −17.9368 | −21.0211 | 734.10 |
| ΔlnGOV | −14.6504 | −19.0072 | 622.62 |
| ΔlnPOL | −11.8233 | −16.7560 | 541.09 |
| ΔlnRUL | −16.3112 | −19.3853 | 639.50 |
| ΔlnREG | −14.4054 | −18.1779 | 578.88 |
| ΔlnVOI | −15.6439 | −19.8155 | 685.33 |

Panel unit-root tests indicate that all variables are consistent with non-stationarity in levels, with with only limited evidence against the unit-root null in pooled panel tests. In contrast, first-differenced series exhibit strong stationarity, as evidenced by highly negative LLC and IPS statistics and large Fisher test values. This pattern is consistent across all institutional indicators and FDI measures, supporting the treatment of the variables as integrated of order one and justifying the use of a differenced panel VAR specification.

Pairwise Phillips–Ouliaris tests were then used to assess potential cointegration between FDI and each institutional indicator. The absence of significant cointegration relationships justified modelling the system in first differences, ensuring that the dynamic equations were numerically appropriate and free from spurious regressions. The tests provide no evidence of cointegration between FDI and institutional indicators in either direction at the panel level. The absence of long-run equilibrium relationships supports modelling the system in first differences rather than employing a panel VECM framework. This result reinforces the focus on short-run dynamic interactions captured by the panel VAR specification.

**Table 3 –** Panel Phillips–Ouliaris Cointegration Tests.

| Direction | Share cointegrated | Mean test statistic |
|---|---|---|
| lnFDI → lnCOR | 0.000 | 0.0645 |
| lnCOR → lnFDI | 0.000 | 13.3359 |
| lnFDI → lnRUL | 0.000 | 0.0571 |
| lnRUL → lnFDI | 0.000 | 12.6975 |
| lnFDI → lnVOI | 0.000 | 0.0381 |
| lnVOI → lnFDI | 0.000 | 12.0910 |

The stability of the estimated PVAR model was assessed through the eigenvalue modulus test. Figure 2 plots the real and imaginary parts of all eigenvalues associated with the companion matrix. All values lie strictly inside the unit circle, which indicates that the system satisfies the Schur-stability condition. Consequently, the dynamic properties of the model are well defined, and the impulse – response functions can be interpreted in a standard manner. The absence of explosive roots is particularly relevant given the inclusion of institutional indicators and macroeconomic controls, which may induce persistence or near-unit dynamics.

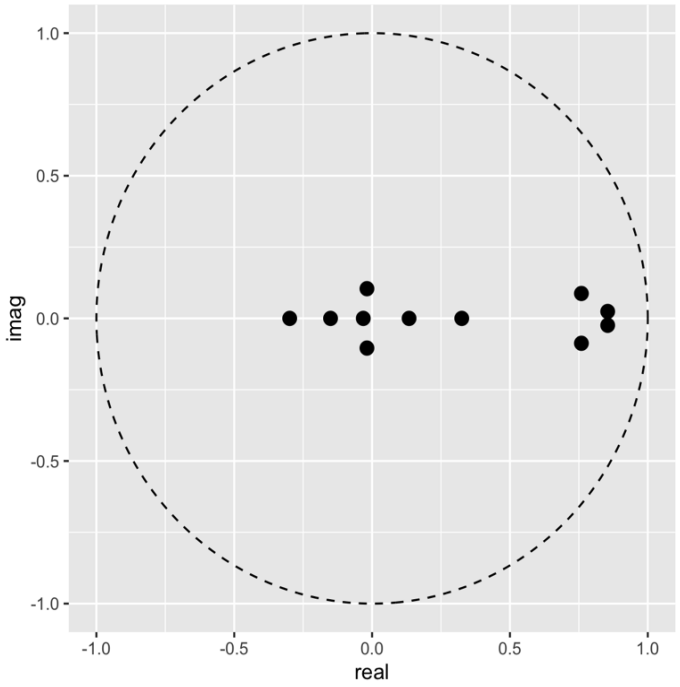


**Figure 2 –** Eigenvalue stability check

*2.3. Model Construction and Structural Identification*

The computational model takes the form of a first-order panel vector autoregression. After applying the FOD transformation to eliminate fixed effects without inducing serial correlation, the system can be written as:

$$\Delta y_{i,t} = A_1 \Delta y_{it-1} + u_{i,t}, \quad (1)$$

where $y_{i,t}$ contains lnFDI and one institutional variable. This specification follows standard practice in simulation-based computational econometrics, in which dynamic responses to shocks are examined by iterating the system forward.

The workflow does not introduce new estimation algorithms, nor does it rely on fully automated model selection; instead, it formalizes best-practice diagnostics and reproducibility safeguards within a transparent execution sequence.

The endogenous vector $y_{i,t}$ consists of the logarithm of FDI inflows and one institutional quality indicator at a time, while macroeconomic controls (trade openness, inflation, unemployment, and GDP per capita) enter the system as exogenous regressors.

$$y_{i,t} = A_1 \Delta y_{it-1} + Bx_{i,t} + \varepsilon_{i,t}, \quad (2)$$

where:

$t - 1, ..., N -$ indexes countries,

$t - 1, ..., T -$ indexes time,

$y_{i,t}$ – is the vector of endogenous variables,

$x_{i,t}$ – denotes exogenous controls,

$\varepsilon_{i,t}$ – is the reduced-form error vector.

All endogenous variables enter the system in first differences, consistent with the unit-root and cointegration diagnostics reported in Section 2.2. To maintain numerical tractability and avoid overparameterization, the analysis proceeds via a sequence of bivariate panel VAR models rather than a single

high-dimensional system. In each specification, the endogenous vector consists of log FDI inflows and one institutional quality indicator.

Macroeconomic controls, including trade openness, inflation, unemployment, and GDP per capita, enter the model as strictly exogenous regressors and are not included in the endogenous VAR vector. The model is estimated using a fixed-effects panel VAR with forward orthogonal deviations, as implemented in the *panelvar* package. This estimator removes fixed effects without relying on internal GMM instruments.

The lag order was set to one based on standard information-criterion considerations, the limited time dimension of the panel (T = 19), and numerical stability requirements of the estimated system. Higher-order specifications were not pursued due to degrees-of-freedom constraints and the risk of overparameterization in a multi-country panel VAR.

*2.4. Structural Identification*

Structural shocks were extracted using a Cholesky decomposition of the estimated covariance matrix of the residuals. All impulse responses should therefore be interpreted as Cholesky-identified responses under a particular recursive ordering assumption, rather than as fully structural causal effects. The ordering was set as:

[ln *FDI*, Institutional Indicator],

Under this ordering, institutional variables are allowed to respond contemporaneously to shocks in FDI, whereas FDI responds to institutional innovations only with a lag. This convention is consistent with related research [2], [12], [14], and corresponds to a modelling assumption in which institutional structures respond sluggishly to economic movements, while foreign investors can adjust more rapidly. This identification reflects the assumption that foreign investment decisions can adjust rapidly to economic conditions, while institutional reforms are persistent processes; however, observed institutional indicators may still exhibit contemporaneous responses to investment-related pressures through administrative or political channels.

*2.5. Panel-Averaged Impulse Response Functions and Stability Diagnostics*

The impulse-response generation procedure can be interpreted as the simulation of a perturbed multivariate dynamical system. The Cholesky-orthogonalized shocks serve as controlled perturbations, while the trajectories approximate the transient dynamics of the system under exogenous disturbances.

Before generating impulse response functions, the numerical stability of the system was verified. The eigenvalues of the autoregressive matrix $A_1$ were computed, and stability was accepted only if all eigenvalues lay strictly inside the unit circle. This requirement guarantees that the simulated responses decay over time rather than diverging, an essential property for any structural dynamic model. The condition number of the covariance matrix was also monitored to assess the reliability of Cholesky decomposition and mitigate issues arising from near singularity. Bootstrap confidence intervals were computed to detect instability in estimated responses.

To illustrate the computational architecture, Figure 3 shows the integration of stability checks, orthogonal shock decomposition, and profiling of algorithmic complexity within the existing code structure:

## 3. Results

The results presented in this section summarize the behavior of the simulated institutional–investment system under the estimated panel VAR dynamics. The computational workflow produces several layers of output, including stability verification, system-wide impulse-response trajectories, and variance decompositions based on orthogonal structural shocks. Together, these elements provide a discrete-time characterization of how the model responds to controlled perturbations and how uncertainty propagates through the autoregressive operator. The presentation below focuses first on the empirical properties of the estimated system and then on the simulated responses that reveal its short-term dynamic structure.

*3.1. Data properties and preliminary diagnostics*

The unit-root tests indicated that *lnFDI* and all six institutional indicators are integrated of order one. Cointegration tests confirmed the absence of robust long-run equilibrium relationships between FDI and any institutional metric, validating the decision to model the system in differences.

*3.2. Panel VAR estimation and system-wide impulse responses*

The PVAR estimates reveal strong autoregressive behavior in FDI, suggesting high short-term persistence across the countries in the sample. Insti-

tutional variables display weaker short-run effects, while trade openness consistently shows a positive association with changes in FDI.

The structural impulse responses showed that an institutional improvement typically induced a short-term decline in FDI inflows. This finding stands in contrast to long-run theoretical expectations but aligns with the hypothesis that institutional reforms may impose temporary adjustment costs or reduce strategic advantages available to investors under less regulated conditions.

The panel-averaged IRF masks considerable heterogeneity. India responded positively to institutional improvements, whereas Brazil, Indonesia, and Kazakhstan exhibited negative reactions. These differences underscore the relevance of country-specific structural conditions and support the use of panel IRFs to derive more generalizable conclusions.

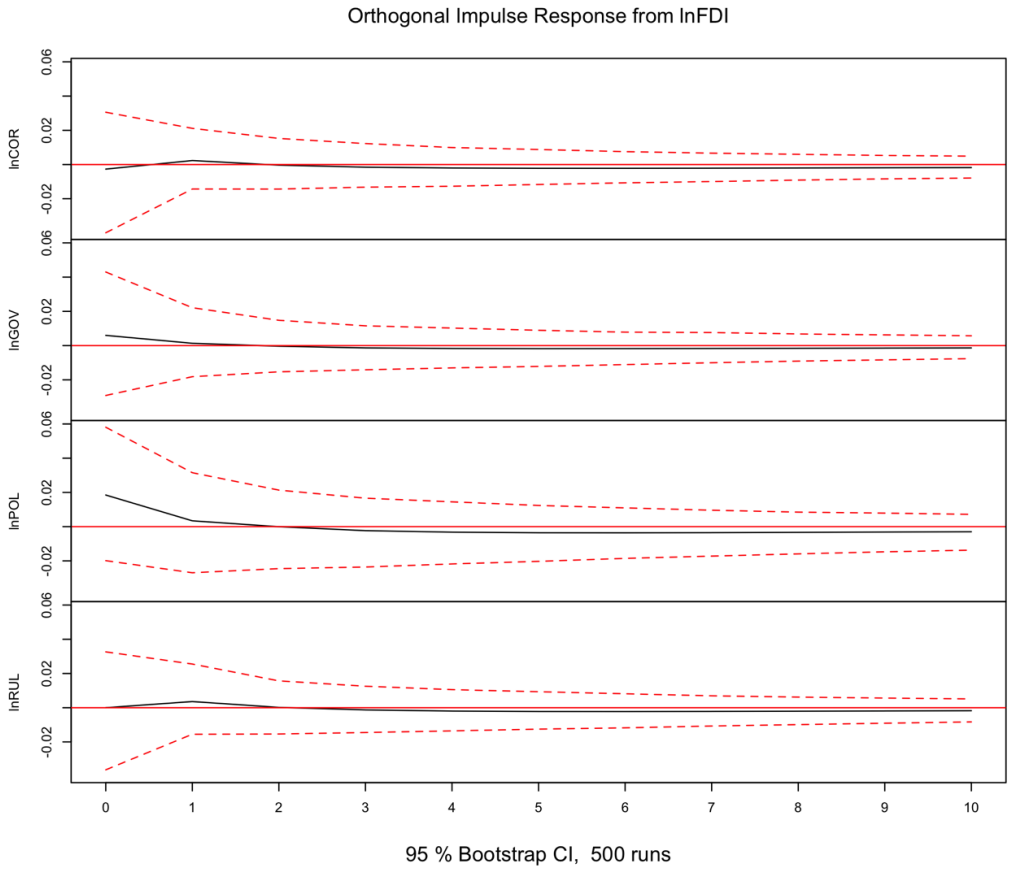


**Figure 3** – Panel-averaged IRF

**Table 4 – Panel VAR Estimates – *lnFDI* Equation**

| Predictor | Estimate | Std. Error | p-value |
|---|---|---|---|
| Lagged *lnFDI* | 0.8712 | 0.0155 | 0.0000 |
| Lagged *lnCOR* | −0.0120 | 0.0248 | 0.6289 |
| Lagged *trade* | 0.0015 | 0.0007 | 0.0457 |
| Lagged *inflation* | −0.0001 | 0.0030 | 0.9777 |
| Lagged *unemployment* | 0.0008 | 0.0051 | 0.8667 |
| Lagged *GDP per capita* | 0.0000 | 0.0000 | 0.2048 |

The estimated panel VAR coefficients reveal strong autoregressive persistence in FDI, with the first lag of *lnFDI* exhibiting a large and highly significant coefficient. Lagged institutional quality, proxied by control of corruption, does not exert a statistically significant short-run effect on changes in FDI once dynamics and macroeconomic controls are accounted for. Among the control variables, trade openness shows a weak but statistically significant positive association with FDI dynamics, while inflation, unemployment, and GDP per capita are not significant. These results suggest that short-term movements in FDI are primarily driven by internal dynamics rather than contemporaneous institutional changes.

*3.3. Country-level dynamics: the Kazakhstan case*

Figure 4. illustrates country-specific IRFs using Kazakhstan as an example. The orthogonalized IRFs are based on a Cholesky decomposition that places institutional variables after FDI in the ordering. Confidence intervals were generated using 500 bootstrap replications.

A one-standard-deviation FDI shock induces a small and short-lived negative response in the control of corruption (*lnCOR*), which dissipates by the third period. Government effectiveness (*lnGOV*) also declines modestly and with slightly greater persistence. These patterns suggest that inward capital flows may temporarily strain administrative capacities rather than improve them.

Political stability (*lnPOL*) shows a more evident negative reaction, indicating that new investment may amplify distributional tensions or expose existing political fragilities. In contrast, the rule of law (*lnRUL*) remains largely unaffected, consistent with its slow-moving institutional character. Overall, these country-specific trajectories indicate that short-term feedback from FDI to institutional quality is weak and, in some dimensions, mildly adverse.

*3.4. Shock propagation and variance decomposition*

To analyze how shocks propagate through the simulated dynamic system, the computational environment includes a dedicated FEVD module. In addition to its standard econometric interpretation, FEVD is used here as a numerical diagnostic. Using the estimated coefficient matrix $A_1$, the residual covariance matrix $\Sigma_u$, and the Cholesky factor $L$, the module generates horizon-indexed variance shares that describe how forecast uncertainty is distributed across structural shocks.

For each horizon, the algorithm computes the state-transition operator $A_1^h$, applies the mapping $A_1^h L$, and aggregates the contribution of each innovation to the forecast variance of every endogenous variable. Numerical reliability is ensured by verifying that the spectral radius of the companion matrix is strictly below unity and by monitoring the conditioning of $\Sigma_u$ to prevent artefacts caused by near-singular residual structures.

Interpreted as a computational probe, FEVD reveals the internal architecture of the model. It highlights the channels through which innovations propagate, the rate at which dynamics decay, and the extent to which institutional shocks influence the behavior of foreign investment.

The empirical results show a strong dominance of own-variable shocks for all endogenous series. FDI forecast variance is almost entirely driven by its own innovations, with institutional and macroeconomic shocks contributing only marginally across all horizons. Institutional indicators display the same pattern: slow-moving, internally driven dynamics with limited sensitivity to external impulses from FDI. Macroeconomic controls also exhibit minimal cross-variable spillovers.

Taken together, the FEVD evidence indicates a system characterized by high persistence and weak contemporaneous transmission. Institutional shocks exert limited influence on FDI, and FDI shocks have similarly small effects on institutional indicators. These findings align with the IRF results and support the view that, over the short to medium term, institutional quality and foreign investment primarily evolve through gradual internal processes rather than strong dynamic feedback mechanisms.

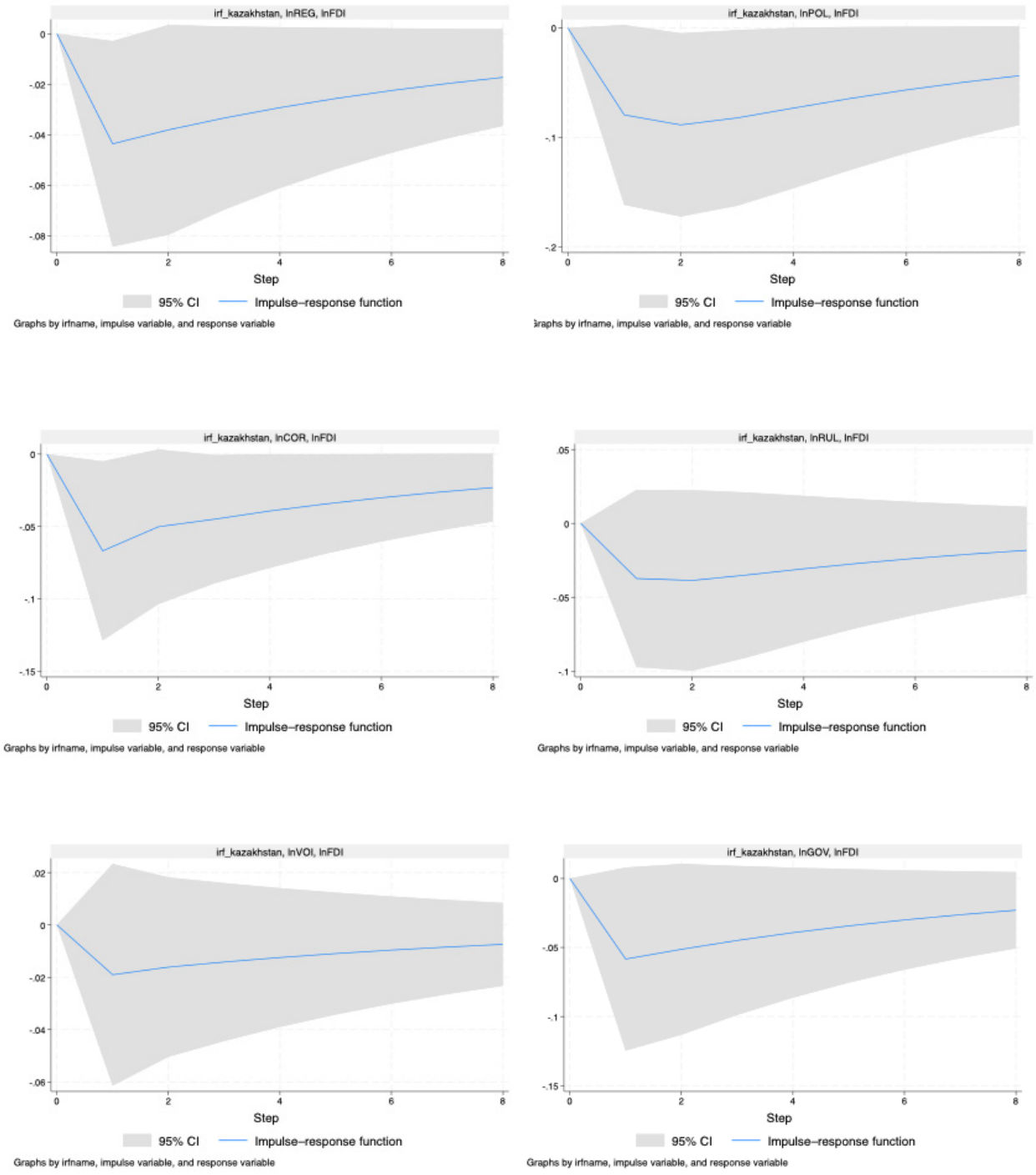


**Figure 4 –** Country-specific impulse-response functions for Kazakhstan. Each panel shows the response of an institutional indicator to a one-standard-deviation shock in lnFDI over an 8-year horizon. Shaded areas denote 95% bootstrap confidence intervals (500 replications).

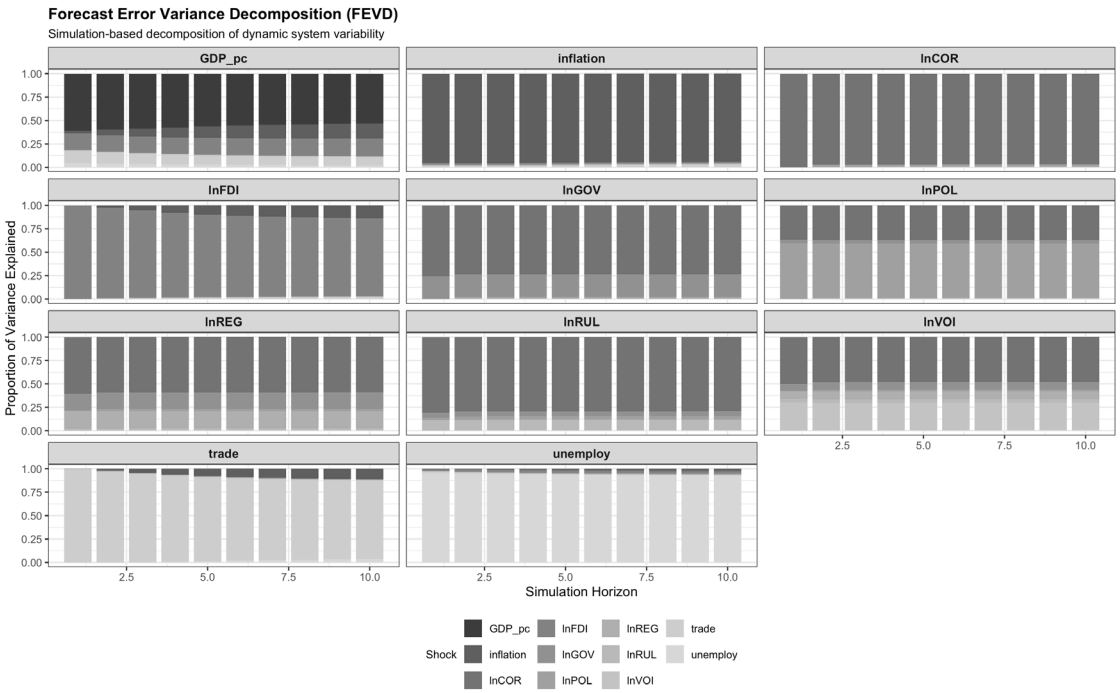


**Figure 5 –** Forecast Error Variance Decomposition. Proportion of variance in each response variable explained by shocks to all variables over a 10-period horizon in the PVAR model. Panels show how each shock propagates through the system.

## 4. Discussion

The simulation framework shows that the dynamic behavior of the institutional–investment system is strongly shaped by the structural configuration of the panel VAR model. The orthogonalization scheme, the stability properties of the autoregressive operator, and the numerical conditioning of the system matrices jointly determine how the model reacts to perturbations. The heterogeneous country-level responses, for example, the positive short-run reaction in India contrasted with the negative responses in Brazil, Indonesia, and Kazakhstan, demonstrate how small differences in estimated system parameters produce distinct transient trajectories once the system is shocked. Rather than reflecting only economic mechanisms, these patterns arise from the interaction between empirical estimates, eigenvalue geometry, and the algebraic structure of the transformations applied within the simulation engine.

Interpreting these outcomes is most meaningful when the model is viewed as a discrete-time computational system rather than a purely econometric specification. The impulse-response trajectories represent the evolution of the state-transition operator under controlled perturbations, and their variation across countries reflects differences in the local Jacobians governing each subsystem. This viewpoint aligns the analysis with practices in applied computer science and computational modelling, where system dynamics are often characterized by sensitivity to initial conditions, structural heterogeneity, and path-dependent propagation of shocks across interconnected modules.

The computational diagnostics embedded into the workflow were essential for validating the simulation environment. The stability check ensured that all eigenvalues lay strictly within the unit circle, allowing the system to be treated as a stable dynamical process suitable for forward simulation. From a computational perspective, the ordering defines a specific shock-propagation topology within the simulated system. Conditioning checks on the covariance matrix and its Cholesky factor prevented numerical artefacts that could distort the shape or magnitude of impulse-response paths. These controls made it possible to attribute the observed patterns to the underlying system dynamics rather than to numerical instability. Reproducibility safeguards, including fixed seeds and standardized matrix operations, further strengthened the reliability of the simulation results.

The findings also highlight the value of integrating simulation-based reasoning with economic interpretation. The short-run decline in FDI following improvements in institutional quality, ob-

served in several countries, may reflect transitional frictions, regulatory tightening, or the removal of informal mechanisms previously relied upon by investors. India's positive response illustrates that institutional strengthening can enhance credibility and reduce uncertainty, producing favorable investment dynamics. The computational analysis does not replace these interpretations but clarifies how theoretical mechanisms interact with the system's numerical architecture, shaping the resulting dynamic profiles.

Overall, the study demonstrates that modelling socio-economic systems with panel VARs benefits from a dual perspective: economic theory provides directional hypotheses, while algorithmic analysis reveals how those hypotheses materialize once embedded in a high-dimensional, numerically constrained simulation environment. The results show that dynamic interactions between institutions and FDI are weakly coupled and sensitive to structural and numerical considerations, reinforcing the need for careful system design when applying computational models to complex socio-economic processes.

It should be emphasized that the observed short-term decline in FDI following improvements in institutional quality is hypothetical and transient. This effect likely reflects temporary adjustment costs, regulatory tightening, or strategic responses by investors, rather than a permanent consequence of institutional reforms. Therefore, these results should not be interpreted as evidence of long-term causal effects, which may vary across countries and macroeconomic contexts.

## 5. Conclusions

The study introduces a computational framework for simulating short-term interactions between institutional quality and foreign direct investment within a panel VAR setting. The workflow integrates the preprocessing of heterogeneous panel data, stability verification, orthogonal shock construction, and dynamic simulation through impulse-response analysis and variance decomposition. By prioritizing algorithmic clarity, numerical conditioning, and reproducibility, the framework reflects contemporary standards in computer science research on dynamic system modelling.

The results show that the system operates as a stable, high-dimensional autoregressive process characterized by strong own-variable persistence and limited cross-variable spillovers. Institutional improvements frequently trigger temporary reductions in investment inflows, while shocks to FDI exhibit similarly short-lived effects on governance indicators. These patterns should be interpreted not only in economic terms but also as emergent properties of a simulated dynamical system whose behavior is shaped by the spectral structure of the autoregressive operator and the conditioning of the transformation matrices.

Beyond the empirical findings, the modelling environment developed here offers a reusable simulation architecture. It can be extended in several computational directions, including alternative orthogonalization schemes, machine-learning-assisted parameter tuning, hybrid integration with agent-based subsystems, or GPU-accelerated evaluation of high-dimensional model variants. The framework therefore contributes both substantive insights into institutional–investment dynamics and a flexible platform for future experimentation in multi-country, data-driven system simulation.

## Conflicts of Interest

The author declares no conflict of interest.

## References

1. M. R. M. Abrigo and I. Love, "Estimation of panel vector autoregression in Stata," The Stata Journal, vol. 16, no. 3, pp. 778–804, 2016. Available at: https://doi.org/10.1177/1536867X1601600314 [Accessed December 8, 2025].

2. R. Antonietti and J. Mondolo, "Inward FDI and the quality of domestic institutions: A cross-country panel VAR analysis," Economic Systems, vol. 47, p. 101078, 2023. Available at: https://doi.org/10.1016/j.ecosys.2023.101078 [Accessed December 8, 2025].

3. F. Canova and M. Ciccarelli, "Panel vector autoregressive models: A survey," ECB Working Paper No. 1507, 2013.

4. M. Demetrescu and A. Hassler, "(Structural) VAR models with ignored changes in mean and volatility," International Journal of Forecasting, 2024. Available at: https://doi.org/10.1016/j.ijforecast.2023.06.002 [Accessed December 8, 2025].

5. J. H. Dunning, "Toward an eclectic theory of international production: some empirical tests," Journal of International Business Studies, vol. 11, no. 1, pp. 9–31, 1980. Available at: http://dx.doi.org/10.1002/tie.5060220301 [Accessed December 8, 2025].

6. J. H. Dunning, “Location and the multinational enterprise: A neglected factor?,” Journal of International Business Studies, vol. 29, no. 1, pp. 45–66, 1998. Available at: https://www.jstor.org/stable/155587 [Accessed December 8, 2025].

7. J. H. Dunning, “The eclectic paradigm as an envelope for economic and business theories of MNE activity,” International Business Review, vol. 9, no. 2, pp. 163–190, 2000.

8. S. Globerman and D. Shapiro, “Global foreign direct investment flows: The role of governance infrastructure,” World Development, vol. 30, no. 11, pp. 1899–1919, 2002. DOI: 10.1016/S0305-750X(02)00110-9.

9. H. Herwartz and S. Wang, “Statistical identification in panel structural vector autoregressive models based on independence criteria,” Journal of Applied Econometrics, vol. 39, no. 4, pp. 620–639, 2024. Available at: https://doi.org/10.1002/jae.3044 [Accessed December 8, 2025].

10. C. C. Y. Kwok and S. Tadesse, “The MNC as an agent of change for host-country institutions: FDI and corruption,” Journal of International Business Studies, vol. 37, no. 6, pp. 767–785, 2006. DOI:10.1057/palgrave.jibs.8400228.

11. K. Miao, P. C. B. Phillips, and L. Su, “High-dimensional VARs with common factors,” Journal of Econometrics, vol. 233, no. 1, pp. 155–183, 2023.

12. I. Ouechtati, “Institutions and foreign direct investment: A Panel VAR approach,” International Journal of Economic Sciences, vol. 9, no. 2, pp. 55–70, 2020. DOI:10.20472/ES.2020.9.2.004

13. M. Plagborg-Møller and C. K. Wolf, “Local projections and VARs estimate the same impulse responses,” Econometrica, vol. 89, no. 2, pp. 955–980, 2021. Available at: https://doi.org/10.3982/ECTA17813 [Accessed December 8, 2025].

14. M. Saikia and S. Borbora, “Foreign direct investment of India: an analysis based on ‘dynamic or developmental approach,’” Transnational Corporations Review, vol. 10, no. 1, pp. 69–85, 2018. Available at: https://doi.org/10.1080/19186444.2018.1436657 [Accessed December 8, 2025].

15. A. Camehl, “Penalized estimation of panel vector autoregressive models: A panel LASSO approach,” International Journal of Forecasting, vol. 39, no. 3, pp. 1185–1204, 2023. Available at: https://doi.org/10.1016/j.ijforecast.2022.05.007 [Accessed December 8, 2025].

16. R. Yang, X. An, Y. Chen, and X. Yang, “The Knowledge Analysis of Panel Vector Autoregression: A Systematic Review,” SAGE Open, vol. 13, no. 4, 2023. Available at: https://doi.org/10.1177/215824402312159 [Accessed December 8, 2025].

17. World Bank, “World Bank Open Data,” 2024. Available at: https://data.worldbank.org/ [Accessed December 8, 2025].

18. World Bank, “Worldwide Governance Indicators,” 2024. Available at: https://www.worldbank.org/en/publication/worldwide-governance-indicators [Accessed December 8, 2025].

19. United Nations Conference on Trade and Development (UNCTAD), World Investment Report, 2024. Available at: https://unctad.org/topic/investment/world-investment-report [Accessed: December 8, 2025].

20. N. Morshed and M. R. Hossain, “Causality analysis of the determinants of FDI in Bangladesh: fresh evidence from VAR, VECM and Granger causality approach,” SN Business & Economics, 2022.

***Information About Author:***

*Justyna Mrowiec is a master’s student in Computer Science and Econometrics at the University of Warsaw. Her academic work focuses on computational methods for energy systems, with particular interest in data-driven analysis, optimization models, and regulatory impact assessment in the energy sector. She holds a bachelor’s degree in economics, where she specialized in quantitative methods. She contributes to faculty research projects on battery energy storage frameworks, applying statistical and algorithmic approaches to evaluate regulatory scenarios and market mechanisms. She has presented at national student conferences on sustainable energy policy and the integration of socio-economic conditions into technical and legal decision-making models.*

*Submission received: 10 December, 2025.*
*Revised: 26 December, 2025.*
*Accepted: 26 December, 2025.*

IRSTI 28.23.01 https://doi.org/10.26577/jpcsit2025450

**Nurdaulet Izmailov [1,*], Meirambek Shaimerden [1], Azamat Toishybek [2], Kaisar Kassymzhanov [2], Araylim Mukangalieva [2], Nurzhan Ultarakov [3], Alma Turganbayeva [3]**

[1] LLP DigitAlem, Almaty, Kazakhstan
[2] Institute of Metallurgy and Ore Beneficiation, Almaty, Kazakhstan
[3] Al-Farabi Kazakh National University, Almaty, Kazakhstan
*e-mail: nurdauletizmailov@gmail.com

# MASS-CONSERVING PHYSICS-INFORMED AUGMENTATION AND FOURIER FEATURE NETWORKS FOR SMALL-DATA PREDICTION OF MOLYBDENITE ($MO_2S$) LEACHING KINETICS

**Abstract.** Molybdenum remains a strategic metal for advanced steels and catalysis, while environmental and energy pressures are accelerating interest in hydrometallurgical leaching routes for molybdenite ($MoS_2$). Predicting leaching kinetics is difficult because the process is highly nonlinear and strongly influenced by reagent chemistry and gas–liquid conditions, yet experimental datasets in metallurgical laboratories are often extremely small. This manuscript develops a hybrid, data-efficient machine-learning approach designed specifically for small-data settings. The method combines physics-informed data augmentation that enforces strict mass conservation with a Fourier Feature Network intended to reduce spectral bias and better capture sharp kinetic transitions. Using only six experimental measurements, the resulting model achieves high predictive accuracy on held-out data ($R^2$ = 0.9793, MAE = 1.61%) and maintains stable generalization without evidence of train–test divergence. The study concludes that physically admissible augmentation coupled with Fourier-enriched representations can produce reliable kinetic surrogates from minimal data, supporting in-silico screening and optimization of leaching conditions for process design and control.

**Keywords:** molybdenite leaching, hydrometallurgy, small data, physics-informed augmentation, mass conservation, Fourier feature networks, spectral bias.

## 1. Introduction

Molybdenum is a strategically important metal whose demand is sustained by high-temperature and corrosion-resistant steels, petrochemical catalysts, and a growing set of energy and functional applications. In industrial practice, molybdenum is obtained mainly from molybdenite ($MoS_2$) concentrates, and the conventional flowsheet has historically relied on oxidative roasting to $MoO_3$ followed by downstream refining [1]. However, the energy intensity of roasting and the challenges of controlling sulfur-oxide emissions have strengthened the case for hydrometallurgical alternatives that target "low-emission" molybdenum recovery through leaching-based routes [2].

Despite this motivation, a central difficulty is that $MoS_2$ leaching kinetics are strongly nonlinear and process specific. Oxidative dissolution can couple surface reaction, diffusion through boundary layers and evolving product films, and solution chemistry that may stabilize or remove molybdenum species via precipitation, adsorption, or complexation. For instance, nitric-acid pressure oxidative leaching exhibits pronounced sensitivities to oxygen pressure, acid concentration, and temperature, and reported regimes can shift as reaction products form and transport constraints evolve [3]. Similarly, oxidant-assisted leaching (e.g., chlorate in chloride media) displays multi-parameter dependence on reagent ratios, agitation, and liquid-to-solid ratio while achieving very high extraction only within constrained operating windows [4]. Mechanical activation further complicates the picture by altering surface area, defect density, and even enabling solid-state reactions that change subsequent aqueous leaching pathways [5].

In parallel, machine learning (ML) has become a practical complement to mechanistic modeling in chemical engineering because flexible learners can approximate high-dimensional, nonlinear mappings

 

between operating conditions and performance metrics at low evaluation cost. Recent perspectives emphasize that, with modern computation and better representations, ML can serve as a fast surrogate where first-principles models are incomplete or prohibitively expensive to solve repeatedly [6]. In minerals processing and extractive metallurgy, ML has similarly expanded from monitoring and soft sensing into broader flowsheet and operational analytics, with reviews documenting rapid adoption across process stages and data modalities [7].

However, most high-capacity ML models are implicitly "big data" methods: they tend to generalize reliably only when trained on large, diverse datasets. This assumption is frequently violated in metallurgy. Leaching experiments are costly and time-consuming; they are constrained by analytical throughput and safety limits, and they must contend with ore variability and run-to-run heterogeneity. Consequently, datasets are often sparse, noisy, and statistically underpowered. The broader "small data" challenge has been highlighted across scientific ML, including in materials science, where limited labeled data can make model selection brittle and uncertainty high unless additional structure or priors are leveraged [8]. Data-efficient experimental strategies such as active learning help, but they still operate under severe data scarcity typical of laboratory and pilot studies [9].

A common response to small datasets is synthetic data augmentation. In many domains, oversampling methods such as SMOTE and deep generative models such as GANs are used to enrich training sets and reduce overfitting [10,11]. Yet for physically governed chemical systems, naive synthetic samples can be actively harmful: they may violate conservation of mass, create chemically impossible reagent–product relationships, or introduce nonphysical kinetic trajectories that mislead the learner and inflate apparent accuracy while degrading extrapolation. In leaching kinetics, where material balances and stoichiometric constraints are not optional but defining, augmentation must therefore be physically admissible by construction rather than statistically plausible only.

Physics-informed machine learning offers a principled alternative by incorporating governing equations and constraints directly into training, thereby regularizing learning and increasing the effective information content beyond the measured datapoints [12]. Physics-informed neural networks (PINNs), for example, embed differential-equation residuals and boundary/initial conditions into the learning objective and have demonstrated data-efficient learning for forward and inverse problems specifically in small-data regimes [13]. For hydrometallurgical kinetics, this philosophy suggests that enforcing strict material balances during model construction and data enrichment can simultaneously reduce hypothesis space and prevent the model from learning physically impossible trends.

Even when physics is enforced, an additional approximation barrier arises from the training dynamics of standard neural networks. Gradient-trained networks often exhibit *spectral bias*, learning low-frequency components of a target function before higher-frequency or sharp features; this can impede learning of rapid kinetic transitions (e.g., induction periods, passivation thresholds, or regime changes) from few observations [14]. Fourier feature mappings provide a practical remedy by lifting inputs into a richer periodic basis so that multilayer perceptrons can represent high-frequency structure more efficiently, improving convergence on functions with sharp or oscillatory components [15].

Motivated by these gaps, this paper proposes a hybrid small-data framework for predicting molybdenite leaching kinetics that couples (i) physically grounded data augmentation derived from strict mass-conservation constraints with (ii) a Fourier Feature Network to mitigate spectral bias. In our case study, the available dataset comprises only six experimental points, which are expanded via a material-balance–consistent augmentation operator prior to model training. The resulting hybrid approach aims to deliver high predictive accuracy under extreme data scarcity while remaining faithful to the underlying chemistry and conservation laws.

## 2. Materials and Methods

Developing predictive models for metallurgical processes is traditionally challenged by the scarcity of experimental data. Laboratory and pilot-scale leaching tests are resource-intensive and time-consuming, rarely yielding datasets of "Big Data" magnitude. To address this issue, this study employs a hybrid approach combining Physics-Informed Data Augmentation and Fourier Feature Mapping Network architecture. This approach allows for overcoming small sample size limitations and

approximating the complex non-linear dependencies of leaching kinetics.

*2.1. Experimental Data Characterization and Methodology*

The model is built upon a series of laboratory experiments on molybdenite concentrate leaching. Experimental studies were conducted in a 1.0 L thermostated glass reactor equipped with a Eurostar 60 control overhead stirrer to ensure a hydrodynamic regime that eliminates external diffusion limitations. The temperature of the reaction mixture was maintained using a UT-4300 liquid thermostat with a regulation accuracy of $\pm 0.1°C$.

Input process variables were varied within ranges that define the model's applicability limits: Nitric acid concentration ($HNO_3$) ranged from 0 to 50 g/L, and Sulfuric acid concentration ($H_2SO_4$) ranged from 0 to 200 g/L. The influence of an oxidizing agent was also considered: experiments were conducted both without oxygen supply and with oxygen purging at an average flow rate of 0.85 dm³/min (range 0.7–1.0 dm³/min). The leaching duration in all experiments was 4–5 hours, which was sufficient to reach conditional equilibrium in the system.

Constant process parameters included an initial concentrate mass of 50 g and a leaching solution volume of 300 mL, corresponding to a Liquid-to-Solid ratio (L:S) of 6:1. The chemical composition of the feedstock was characterized by a Molybdenum ($Mo$) content of 20.3% – 25.01%. Upon completion of the process, the pulp was vacuum filtered, and the resulting solid residue (cake) was washed with hot distilled water to fully remove soluble compounds.

Analytical control of reaction products was performed using instrumental methods:

- Metal content in the liquid phase (filtrates and wash waters) was determined by Atomic Absorption Spectroscopy (AAS).
- The chemical composition of the solid phase (cakes) was analyzed using X-ray Fluorescence (XRF).

The modeling target variable (output target) was the percentage of Molybdenum extraction into the productive solution, which varied from 15.0% to 72.6%. The summary of base experiments is presented in Table 1.

**Table 1 –** Experimental Design Matrix and Leaching Results

| Experiment ID | $HNO_3$ Concentration (g/L) | $H_2SO_4$ Concentration (g/L) | Oxygen Flow (dm³/min) * | Initial Mass (g) | Mo Content in Feed (%) | **Mo Extraction (%)** |
|---|---|---|---|---|---|---|
| 1 | 50 | 0 | 0 | 50 | 20.30 | 19.2 |
| 2 | 0 | 200 | 0 | 50 | 20.30 | 15.0 |
| 3 | 50 | 0 | 0.85 | 50 | 20.30 | 45.2 |
| 4 | 0 | 200 | 0.85 | 50 | 20.30 | 19.6 |
| 5 | 50 | 200 | 0 | 50 | 25.01 | 50.0 |
| 6 | 50 | 200 | 0.85 | 50 | 25.01 | 72.6 |

*2.2. Synthetic Data Augmentation Algorithm*

Given that the initial dataset consisted of a limited number of points, direct training of a neural network would inevitably lead to overfitting. To resolve this, a synthetic data expansion algorithm was developed based on the Monte Carlo method and the Law of Conservation of Mass.

The synthetic data generation procedure is based on stochastic perturbation of input parameters, simulating the instrumental errors described in Section 2.1. We assume that every measurement contains an irreducible random error. For each base experiment, a set of variations ($N = 833$) was generated by adding Additive White Gaussian Noise (AWGN) to the parameters.

Mathematically, this is described as follows: let $x_{orig}$ be the initial parameter value (e.g., concentrate mass), then the synthetic value $x_{new}$ is defined as:

$$x_{new} = x_{orig} + \epsilon,$$
where $\epsilon \sim \mathcal{N}(0, \sigma^2)$

Here, $\sigma$ was selected based on the precision of the weighing equipment (±0.5 g) and the error margin of the AAS/XRF methods (assumed at 0.2% absolute).

A key feature is the strict adherence to the material balance. After introducing noise to the mass ($B_1$) and content ($A_1$), the mass of metal in the feed ($M_{in}$) was calculated as:

$$M_{in} = \frac{A_1 \cdot B_1}{100}$$

The target variable Extraction ($E$) was also subjected to variation, after which the mass of metal in the solution ($M_{sol}$) was determined via reverse calculation:

$$M_{sol} = \frac{E_{syth} \cdot M_{in}}{100}$$

This approach guarantees that each of the 5,000 synthesized data points satisfies the balance equation, which is critical for the physical interpretability of the model.

*2.3. Fourier Feature Neural Network Architecture*

The choice of architecture was dictated by the "spectral bias" phenomenon. Classical Multi-Layer Perceptrons (MLP) tend to approximate data with smooth, low-frequency functions. However, sulfide leaching kinetics are characterized by sharp non-linear transitions when the rate-limiting step changes (e.g., transition from kinetic to diffusion control upon changing temperature or reagent). A standard neural network tends to "blur" transitions.

To address this, a Fourier Feature Mapping architecture was employed. The input vector **v** is projected into a frequency space before being fed into the network:

$$\gamma(\mathrm{v}) = [\cos(2\pi \mathrm{Bv}), \sin(2\pi \mathrm{Bv})]^T$$

Where $\mathrm{B} \in \mathbb{R}^{m \times d}$ is a weight matrix sampled from a normal distribution $\mathcal{N}(0, \sigma_{scale}^2)$.

This transformation allows the network, analogous to Fourier series, to approximate complex functions via a sum of harmonics. The empirically selected parameter $\sigma_{scale} = 1.0$ provided a balance between smoothing the noise of analytical measurements and accurately reproducing the sharp jumps in extraction efficiency.

The final architecture consists of:

1. - Input: 5 neurons (normalized parameters).
2. - Fourier Layer: Projection into 64 harmonic features.
3. - Hidden Layers: Dense layers (64 and 32 neurons) with the tanh activation function, which, being symmetric, aligns better with the periodic nature of Fourier features.Output: 1 neuron (Extraction, %).

Training was conducted using backpropagation with the Adam optimizer and Mean Squared Error (MSE) loss function.

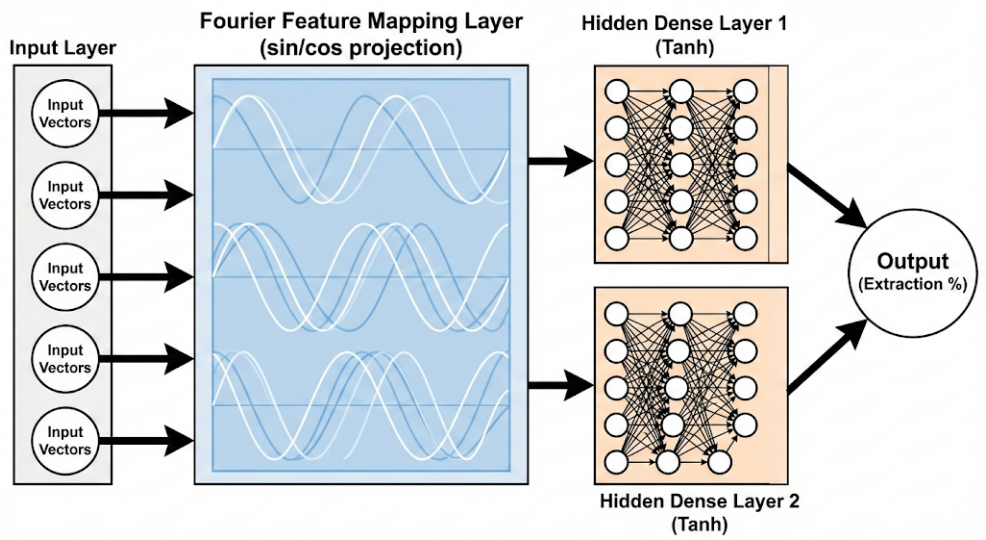


**Figure 1 –** Architecture of the Neural Network with Fourier Features Layer

## 3. Results and Discussion

The primary objective of this study was to validate the hypothesis that applying physics-informed data augmentation combined with a Fourier Feature Neural Network allows for the accurate modeling of molybdenite leaching kinetics under conditions of extremely limited data samples.

*3.1. Accuracy Assessment and Model Convergence*

Upon completion of 600 training epochs, the developed model demonstrated high predictive capability. On the hold-out test set, the coefficient of determination reached $R^2 = 0.9793$, while the Mean Absolute Error (MAE) was fixed at 1.61%. Given that the target extraction indicator in the initial experimental data ranged widely from 15.0% to 72.6%, the obtained error of 1.6% is comparable to the instrumental precision of laboratory analysis methods (AAS/XRF), which typically lies within the 3–5% range. This indicates that the model successfully filtered out the stochastic noise introduced during augmentation and identified the deterministic kinetic trend.

The training dynamics (Figure 2) show a tight correlation between the Loss curves for the training and test sets. The absence of divergence between them confirms that, despite the synthetic nature of most of the data, the model did not overfit specific noise patterns but learned the generalized mass conservation laws embedded in the generation algorithm.

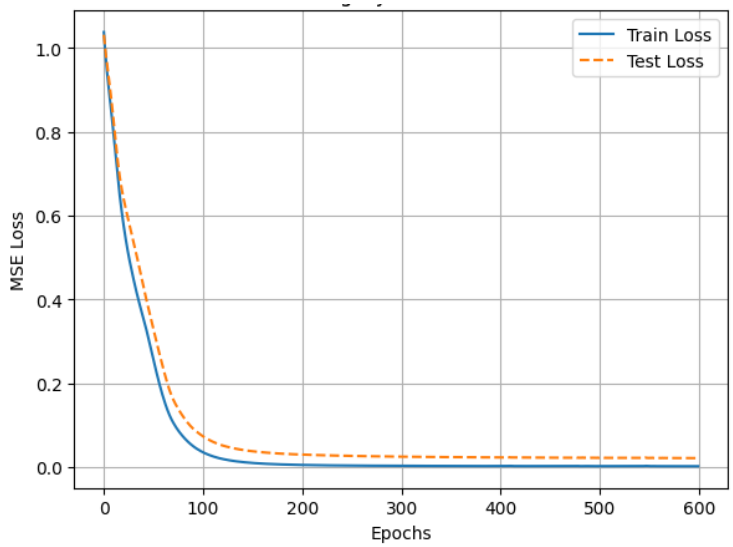


**Figure 2 –** Training and Test Loss Dynamics

*3.2. Interpretation of Physicochemical Dependencies*

The "Predicted vs. Actual" scatter plot (Figure 3) demonstrates a high density of point clustering along the ideal bisector. The model correctly reproduces the data clustering corresponding to the six base leaching regimes. A critically important result is that the Fourier Feature network successfully addressed the issue of "spectral bias." A standard Multi-Layer Perceptron (MLP) would tend to average the prediction; however, the proposed architecture accurately described the sharp non-linear jumps in efficiency.

Specifically, the model clearly differentiated the influence of the oxidizing agent. According to the source data, introducing oxygen (0.7–1.0 $dm^3$/min) into a system with nitric acid increased extraction from 50.0% to 72.6%. The model captured this dependency, assigning higher extraction probabilities to vectors with non-zero oxygen flow. This confirms the physical consistency of the model: it implicitly learned the stoichiometry of sulfide oxidation reactions where oxygen acts as the limiting reagent.

*3.3. Residual Analysis and Reliability*

The error distribution histogram (Figure 4) exhibits the shape of a normal distribution centered at zero, indicating the absence of systematic bias. The model predicts both low extraction rates (using

only sulfuric acid) and high rates (in an oxidative environment) with equal accuracy. The homoscedasticity of the residuals confirms that the model can be used as a reliable "virtual analyzer" across the entire range of process operating parameters with a consistent precision level (MAE= 1.61%).

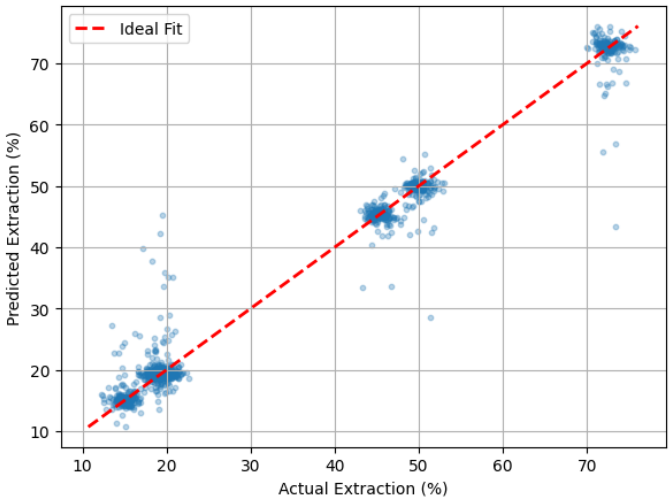


**Figure 3 –** Predicted vs. Actual Molybdenum Extraction Scatter Plot ($R^2$=0.979)

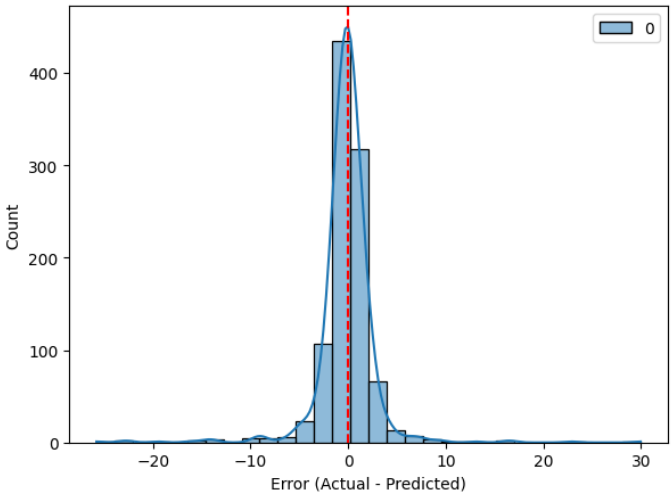


**Figure 4 –** Histogram of Prediction Residuals

Thus, the combination of rigid material balance constraints (during data generation) and the flexibility of the Fourier architecture (during training) allowed for compensating for the lack of empirical information, effectively transforming a "Small Data" problem into a physics-based learning task.

## 4. Conclusion

This paper presents and validates a novel approach to modeling hydrometallurgical processes under conditions of severe experimental data scarcity. Traditional data-driven machine learning methods require hundreds of experiments to achieve acceptable accuracy, which is often economically unfeasible in industrial research. The proposed hybrid method, combining Physics-Informed Augmentation and Fourier Feature Networks, successfully addresses this challenge.

The key findings of the study are as follows:

1. Efficiency on Small Samples: Based on only 6 real laboratory experiments, a robust predictive model was constructed with a coefficient

of determination $R^2 = 0.9793$ and a mean error MAE = 1.61%.

2. Physical Adequacy: The use of material balance formulas as a constraint generator ensured that the model adheres to the Law of Conservation of Mass. The Fourier architecture enabled the model to capture high-frequency dependencies sharp jumps in extraction upon changing reagent regimes that are typically ignored by classical neural networks.

3. Practical Value: The developed model serves as a digital twin of the laboratory setup. It allows conducting *silico* experiments, optimizing the consumption of expensive reagents (acids and oxygen) without the need for time-consuming physical tests.

The obtained results reveal open perspectives for implementing such "lightweight" models into automated process control systems (APCS) at metallurgical enterprises, where they can act as real-time virtual pulp composition analyzers. Future research will focus on adapting this method for forecasting the kinetics of sorption processes and the leaching of complex polymetallic ores.

**Funding**

This research was funded by the Science Committee of the Ministry of Science and Higher Education of the Republic of Kazakhstan grant number BR24992757

**Author Contributions**

Conceptualization, N.I. and A.Tu.; Methodology, N.I. and A.To.; Software, N.I., M.S. and N.U.; Validation, K.K., A.M. and M.S.; Formal Analysis, N.I.; Investigation, A.To., K.K. and A.M.; Resources, A.To.; Data Curation, A.M. and N.I.; Writing – Original Draft Preparation, N.I.; Writing – Review & Editing, A.Tu. and N.I.; Visualization, N.U. and N.I.; Supervision, A.Tu.; Project Administration, N.I.; Funding Acquisition, A.Tu. All authors have read and agreed to the published version of the manuscript.

**Conflicts of Interest**

The authors declare no conflict of interest.

**References**

1. [1] R. R. Dorfler, J. M. Laferty. Review of Molybdenum Recovery Processes. *JOM* 33(4) (1981) 48–54. https://doi.org/10.1007/BF03354424
2. [2] Hossein Shalchian, Ionela Birloaga, Motahareh Bagheri Moghaddam, Hadi Nasiri, Francesco Vegliò. A hydrometallurgical process flowsheet for recovering $MoO_3$ from molybdenite. *Hydrometallurgy* 228 (2024) 106355. https://doi.org/10.1016/j.hydromet.2024.106355
3. [3] Amin Khoshnevisan, Hosein Yoozbashizadeh, Mahdi Mozammel, Seyed Khatiboleslam Sadrnezhaad. Kinetics of pressure oxidative leaching of molybdenite concentrate by nitric acid. *Hydrometallurgy* 111–112 (2012) 52–57. https://doi.org/10.1016/j.hydromet.2011.10.002
4. [4] Zhan-fang Cao, Hong Zhong, Zhao-hui Qiu, Guang-yi Liu, Wen-xuan Zhang. A novel technology for molybdenum extraction from molybdenite concentrate. *Hydrometallurgy* 99(1–2) (2009) 2–6. https://doi.org/10.1016/j.hydromet.2009.05.001
5. [5] Yubiao Li, Zhiming Li, Bing Wang, Zhaomin Dong, Shaoxian Song. A fundamental study of leaching kinetics and mechanisms of molybdenite assisted by mechanical activation. *Minerals Engineering* 131 (2019) 376–384. https://doi.org/10.1016/j.mineng.2018.11.026
6. [6] Maarten R. Dobbelaere, Pieter P. Plehiers, Ruben Van de Vijver, Christian V. Stevens, Kevin M. Van Geem. Machine Learning in Chemical Engineering: Strengths, Weaknesses, Opportunities, and Threats. *Engineering* 7 (2021) 1201–1211. https://doi.org/10.1016/j.eng.2021.03.019
7. [7] J. T. McCoy, L. Auret. Machine learning applications in minerals processing: A review. *Minerals Engineering* 132 (2019) 95–109. https://doi.org/10.1016/j.mineng.2018.12.004
8. [8] Pengcheng Xu, Xiaobo Ji, Minjie Li, Yulin Chen, John M. Gregoire, Wencong Lu. Small data machine learning in materials science. *npj Computational Materials* (2023). https://doi.org/10.1038/s41524-023-01000-z
9. [9] Yannick Ureel, Maarten R. Dobbelaere, Oğuzhan Akin, Robin John Varghese, Carlos G. Pernalete, Johan W. Thybaut, Kevin M. Van Geem. Active learning-based exploration of the catalytic pyrolysis of plastic waste. *Fuel* 328 (2022) 125340. https://doi.org/10.1016/j.fuel.2022.125340
10. [10] Nitesh V. Chawla, Kevin W. Bowyer, Lawrence O. Hall, W. Philip Kegelmeyer. SMOTE: Synthetic Minority Over-sampling Technique. *Journal of Artificial Intelligence Research* 16 (2002) 321–357.
11. [11] Ian J. Goodfellow, Jean Pouget-Abadie, Mehdi Mirza, Bing Xu, David Warde-Farley, Sherjil Ozair, Aaron Courville, Yoshua Bengio. Generative Adversarial Nets. *Advances in Neural Information Processing Systems* 27 (2014).
12. [12] George Em Karniadakis, Ioannis G. Kevrekidis, Lu Lu, Paris Perdikaris, Sifan Wang, Liu Yang. Physics-informed machine learning. *Nature Reviews Physics* 3 (2021) 422–440. https://doi.org/10.1038/s42254-021-00314-5

13. [13] M. Raissi, P. Perdikaris, G. E. Karniadakis. Physics-informed neural networks: A deep learning framework for solving forward and inverse problems involving nonlinear partial differential equations. *Journal of Computational Physics* 378 (2019) 686–707. https://doi.org/10.1016/j.jcp.2018.10.045

14. [14] Nasim Rahaman, Aristide Baratin, Devansh Arpit, Felix Draxler, Min Lin, Fred Hamprecht, Yoshua Bengio, Aaron Courville. On the Spectral Bias of Neural Networks. *Proceedings of the 36th International Conference on Machine Learning (ICML)*, PMLR 97 (2019).

15. [15] Matthew Tancik, Pratul Srinivasan, Ben Mildenhall, Sara Fridovich-Keil, Nithin Raghavan, Utkarsh Singhal, Ravi Ramamoorthi, Jonathan T. Barron, Ren Ng. Fourier Features Let Networks Learn High Frequency Functions in Low Dimensional Domains. *Advances in Neural Information Processing Systems* 33 (NeurIPS 2020).

***Information About Authors***

*Nurdaulet Izmailov – Researcher, DigitAlem LLP, Kazakhstan, Almaty, ORCID ID: 0009-0006-1417-1910*

*Meirambek Shaimerden – Researcher, DigitAlem LLP, Kazakhstan, Almaty, ORCID ID: 0009-0008-0336-9432*

*Azamat Toishybek – Lead Engineer, Institute of Metallurgy and Ore Beneficiation, master's degree, Kazakhstan, Almaty, ORCID ID: 0000-0002-7431-0103*

*Kaysar Kasymzhanov – Lead Engineer, Institute of Metallurgy and Mineral Processing, Kazakhstan, Almaty, ORCID ID: 0000-0001-8062-8655*

*Aralym Mukanaliyeva – Engineer, Institute of Metallurgy and Mineral Processing, master's degree, Kazakhstan, Almaty, ORCID ID: 0000-0001-7032-1764*

*Nurzhan Ultarakov – 2nd year master's student, Department of Computer Science, Al-Farabi Kazakh National University, Kazakhstan, Almaty, ORCID ID: 0009-0001-8171-5213*

*Alma Turganbaeva – Assistant Professor, Lecturer, Al-Farabi Kazakh National University, Department of Computer Science, Candidate of Pedagogical Sciences, Kazakhstan, Almaty, ORCID ID: 0000-0001-9723-4679*

*Submission received: 15 December, 2025.*
*Revised: 17 December, 2025.*
*Accepted: 17 December, 2025.*

# CONTENTS



The authors are responsible for the content of the articles.